NASA/CR-20205006102

Characterization of the NASA Glenn Research Center 8- by 6-Foot Supersonic Wind Tunnel (2019 Test)

Aaron M. Johnson
Jacobs Technology, Brook Park, Ohio

David A. Rinehart
HX5 Sierra, LLC, Brook Park, Ohio

April 2021

NASA STI Program . . . in Profile

Since its founding, NASA has been dedicated to the advancement of aeronautics and space science. The NASA Scientific and Technical Information (STI) Program plays a key part in helping NASA maintain this important role.

The NASA STI Program operates under the auspices of the Agency Chief Information Officer. It collects, organizes, provides for archiving, and disseminates NASA's STI. The NASA STI Program provides access to the NASA Technical Report Server—Registered (NTRS Reg) and NASA Technical Report Server—Public (NTRS) thus providing one of the largest collections of aeronautical and space science STI in the world. Results are published in both non-NASA channels and by NASA in the NASA STI Report Series, which includes the following report types:

- TECHNICAL PUBLICATION. Reports of completed research or a major significant phase of research that present the results of NASA programs and include extensive data or theoretical analysis. Includes compilations of significant scientific and technical data and information deemed to be of continuing reference value. NASA counter-part of peer-reviewed formal professional papers, but has less stringent limitations on manuscript length and extent of graphic presentations.

- TECHNICAL MEMORANDUM. Scientific and technical findings that are preliminary or of specialized interest, e.g., "quick-release" reports, working papers, and bibliographies that contain minimal annotation. Does not contain extensive analysis.

- CONTRACTOR REPORT. Scientific and technical findings by NASA-sponsored contractors and grantees.

- CONFERENCE PUBLICATION. Collected papers from scientific and technical conferences, symposia, seminars, or other meetings sponsored or co-sponsored by NASA.

- SPECIAL PUBLICATION. Scientific, technical, or historical information from NASA programs, projects, and missions, often concerned with subjects having substantial public interest.

- TECHNICAL TRANSLATION. English-language translations of foreign scientific and technical material pertinent to NASA's mission.

For more information about the NASA STI program, see the following:

- Access the NASA STI program home page at http://www.sti.nasa.gov

- E-mail your question to help@sti.nasa.gov

- Fax your question to the NASA STI Information Desk at 757-864-6500

- Telephone the NASA STI Information Desk at 757-864-9658

- Write to:
  NASA STI Program
  Mail Stop 148
  NASA Langley Research Center
  Hampton, VA 23681-2199

NASA/CR-20205006102

Characterization of the NASA Glenn Research Center 8- by 6-Foot Supersonic Wind Tunnel (2019 Test)

Aaron M. Johnson
Jacobs Technology, Brook Park, Ohio

David A. Rinehart
HX5 Sierra, LLC, Brook Park, Ohio

Prepared under Contract NNC15BA02B

National Aeronautics and
Space Administration

Glenn Research Center
Cleveland, Ohio 44135

April 2021

Acknowledgments

The NASA Aeronautics Evaluation and Test Capabilities project funded the full characterization study. The test would not have been possible without the immense support from 8- by 6-Foot Supersonic Wind Tunnel facility engineering and technician staff.

Level of Review: This material has been technically reviewed by expert reviewer(s).

Available from

NASA STI Program
Mail Stop 148
NASA Langley Research Center
Hampton, VA 23681-2199

National Technical Information Service
5285 Port Royal Road
Springfield, VA 22161
703-605-6000

This report is available in electronic form at http://www.sti.nasa.gov/ and http://ntrs.nasa.gov/

Characterization of the NASA Glenn Research Center 8- by 6-Foot Supersonic Wind Tunnel (2019 Test)

Aaron M. Johnson
Jacobs Technology
Brook Park, Ohio 44142

David A. Rinehart
HX5 Sierra, LLC
Brook Park, Ohio 44142

Summary

There were several major modifications made to the NASA Glenn Research Center 8- by 6-Foot Supersonic Wind Tunnel (8×6 SWT) between 2016 and 2019, including the 9- by 15-Foot Low-Speed Wind Tunnel acoustic improvement modifications. Following completion of these facility modifications, a characterization test was conducted in the 8×6 SWT test section. This test entry collected data for a single test section porosity configuration across the entire operating range of the facility. Flow field data were collected at a cross-sectional plane and axially along test section centerline for use in quantifying the test section flow quality. Off-nominal supersonic conditions were surveyed through variation of balance chamber pressure at each of the discrete flexible wall nozzle settings. Additionally, a baseline check calibration dataset was acquired during this entry.

Symbols

A_0 to A_2	coefficient for computing test section static pressure (subsonic)
$A_{S,0}$ to $A_{S,3}$	coefficient for computing test section static pressure (supersonic)
$A_{SX,0}$ to $A_{SX,2}$	coefficient for computing test section static pressure using a local calibration relationship (supersonic)
B_0 to B_2	coefficient for computing test section total pressure (subsonic)
$B_{S,0}$ to $B_{S,3}$	coefficient for computing test section total pressure behind a normal shock (supersonic)
$B_{SX,0}$ to $B_{SX,1}$	coefficient for computing test section total pressure behind a normal shock using a local calibration relationship (supersonic)
C_0 to C_2	coefficient for computing test section total temperature (subsonic)
$C_{S,0}$ to $C_{S,2}$	coefficient for computing test section total temperature (supersonic)
$C_{SX,0}$ to $C_{SX,1}$	coefficient for computing test section total temperature using a local calibration relationship (supersonic)
i	index used to denote an item in an array of values (i.e., variable(i), i = 1 to 10)
M	Mach number
P	pressure
R	gas constant of air, R = 1,716.59 lb-ft/slug·°R
Re	Reynolds number
$R_{S,\mathrm{aft},bal}$	ratio of test section aft static to balance chamber static pressure
$R_{S,bal,bm}$	ratio of average balance chamber static to bellmouth total pressure

T	temperature
V	velocity
x	generic variable used to abbreviate equations, value of x defined near equation
α	pitch flow angle
β	yaw flow angle
γ	ratio of specific heats, γ = 1.4
Δ	difference between two values
σ	standard deviation

Subscripts

2	flow downstream of a normal shock
array	related to a flow parameter measured on the transonic array (i.e., $P_{T,\text{array}}$)
avg	average value
aft	denotes the static pressures on the aft end of the cone cylinder
bal	balance chamber parameter
bm	bellmouth rake parameter (i.e., bellmouth total pressure, $P_{T,bm}$)
corr	corrected value, referring to pitch and yaw flow angles
cyl	related to measurements from the cylinder portion of the cone-cylinder model
model	measurements on the surface of the cone-cylinder model
nom	nominal (i.e., nominal Mach number setting M_{nom})
post	after construction
pre	prior to construction
QCR	transonic quick-check rake measurement
S	static condition of a flow parameter (i.e., static pressure, P_S)
T	stagntation condition of a flow parameter (i.e., total or stagnation pressure, P_T)
ts	calibrated or calculated test section condition (i.e., M_{ts})

1.0 Introduction

The 8- by 6-Foot Supersonic Wind Tunnel (8×6 SWT) tunnel loop underwent major structural modifications as part of the 9- by 15-Foot Low-Speed Wind Tunnel (9×15 LSWT) acoustic improvement modifications (2016 to 2019). Additionally, upgrades to the facility's data and control systems occurred during the same time period. A test section characterization was conducted in 2019 following the completion of all planned facility improvements, an integrated systems test, and a flow quality validation test entry.[1] Details of the 2019 characterization test entry, including descriptions of the test hardware and procedures, data reduction, resulting calibration routines, and flow quality information, are described in this report.

[1]See Reference 1 for flow quality survey information conducted prior to the 9×15 LSWT acoustic improvement modifications. Results of the flow quality surveys conducted at the dryer bed inlet following the acoustic improvement modifications are shown in Appendix A.

1.1 Background

As a matter of record and to give the reader a better understanding of the changes made to the 8×6 SWT facility, the following summary of facility modifications is given.

1.1.1 9- by 15-Foot Low-Speed Wind Tunnel Acoustic Improvement Modifications

In an effort to lower the background noise level in the 9×15 LSWT, significant modifications were made throughout the return leg of the 8×6 SWT, including a full reconstruction of the 9×15 LSWT test section. Some of the larger structures, which likely have a significant impact on the tunnel loop performance, are the turning vanes installed in turns 2 and 3 (upstream and downstream of the 9×15 LSWT test section), serpentine baffles downstream of the tunnel heat exchanger (cooler), and a more gradual 9×15 LSWT diffuser section. A more thorough description of the facility structural modifications from this effort is shown in Appendix B.

1.1.2 Data and Control Systems Improvements

During the construction period in which the 9×15 LSWT acoustic improvement modifications occurred, several modifications were made to the facility data and control systems. The following list details the changes made to the 8×6 SWT data and control systems:

1. The facility data acquisition system was converted from Escort to COBRA (Collect, Observe, Broadcast, Record, and Analyze). The COBRA data system was developed in-house at NASA Glenn Research Center and is being standardized across the large ground test facilities at Glenn.
2. The pressure measurement system was upgraded from the 8400 ESP (electronically scanned pressure) System (TE Connectivity) to the Optimus Pressure Scanning System (TE Connectivity). The 8×6 SWT typically utilizes a series of 15-psid miniature pressure scanners to measure all facility and test-specific pressures.
3. An upgrade to the facility control system, Ovation™ (Emerson Electric Co.), was completed.

1.2 Test Objectives

The primary objective of the 2019 test entry was to provide calibration relationships for the 8×6 SWT test section following the 9×15 LSWT acoustic improvement modifications and changes to the facility data and control systems. Due to the breadth of the 8×6 SWT operating envelope and the number of potential test section porosity configurations, a true full calibration requires months of test time, therefore, a single test section porosity configuration was selected (14-ft test section, 5.8-percent porosity) to reduce the length of the 2019 test entry. The selected porosity configuration was to be used by the upcoming 8×6 SWT customer and is historically the most popular porosity configuration among customers. Specific test objectives are as follows:

1. Provide an empty test section calibration over the entire Mach number range of the 8×6 SWT for test section porosity configuration 1 (14-ft test section, 5.8-percent porosity).
2. Provide detailed flow quality surveys in terms of streamwise centerline static pressure distributions and total pressure, total temperature, and flow angularity at a cross-sectional plane at the 14-ft test section measurement plane (centerline of downstream schlieren windows).
3. Investigate off-nominal supersonic operation through variation of balance chamber pressure levels at a given flexible-wall nozzle (flexwall) setting.

4. Acquire repeat measurements across the Mach number range of the 8×6 SWT to aid in uncertainty estimates of calibrated freestream conditions.
5. Collect a baseline check calibration dataset for the 8×6 SWT to allow for development of statistical process control charts for test section calibration relationship health monitoring.

Data were collected to support each of these objectives. The results of all of the test objectives are discussed in this report. Item number 4 is discussed predominantly in a separate report documenting the updated uncertainty analysis of the 8×6 SWT freestream conditions (Ref. 2). Item number 5 is discussed briefly, however, it is related to a long-term effort.

2.0 Description of Facility[2]

The 8×6 SWT and 9×15 LSWT complex, shown in Figure 1, is an atmospheric pressure, continuous flow propulsion wind tunnel. The airflow is driven through the facility by a seven-stage axial compressor (18-ft inlet diameter) that is powered by three 29,000-hp electric motors. The 8- by 6-ft test section is a porous-wall, transonic test section with a Mach number range of 0.25 to 2.0. By using all three drive

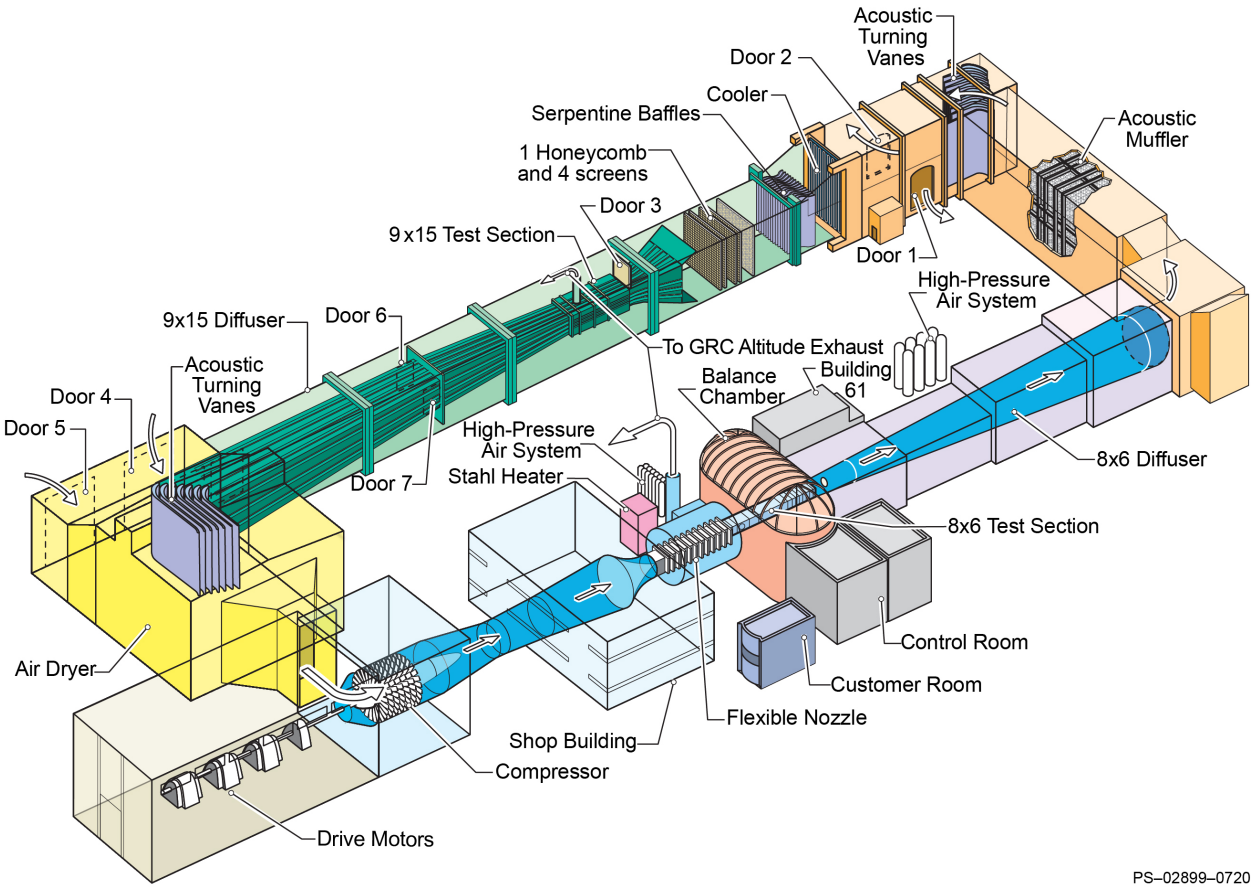

Figure 1.—Overview of 8- by 6-Foot Supersonic Wind Tunnel and 9- by 15-Foot Low-Speed Wind Tunnel complex following 9- by 15-Foot Low-Speed Wind Tunnel acoustic improvement modifications.

[2]Adapted from Reference 3.

motors, the Mach number range in the transonic test section is 0.36 to 2.0; one-drive-motor operation is required to reach the lower Mach numbers, Mach 0.25 to 0.50. The 9- by 15-ft test section is located in the return leg of the 8×6 SWT loop. The 8- by 6-ft test section walls, floor, and ceiling have no divergence over the 23-ft, 6-in. length of the test section. The test section consists of a solid wall supersonic flow region (9-ft, 1-in. length) followed by a porous wall transonic region (14 ft, 5 in.). There are six configurations for the transonic test section based on the length of the porous area used and the open area of the test section surfaces; a seventh configuration exists for testing within the solid-wall, supersonic test section with the transonic test section porosity configured as defined here:

1. 14-ft, 5.8-percent porosity
2. 8-ft, 6.2-percent porosity
3. 8-ft, 3.1-percent porosity
4. 8-ft, 6.2-percent porosity modified
5. 8-ft, 3.1-percent porosity modified
6. 14-ft, schlieren windows installed
7. Supersonic test section (transonic test section configured to 8-ft, 6.2-percent porosity)

The 14-ft transonic test section uses the entire length of the porous area; the 8-ft test section is the aft 8 ft of the porous test section with the first 6 ft of the 14 ft of porosity plugged (Figure 2). The tunnel can be operated in either an aerodynamic (closed-loop) or propulsion (open-loop) cycle (for propulsion cycle, flow control doors 1 and 2 are open so that the airflow is exhausted from the tunnel with air entering through facility doors 4 and 5 in turn 3).

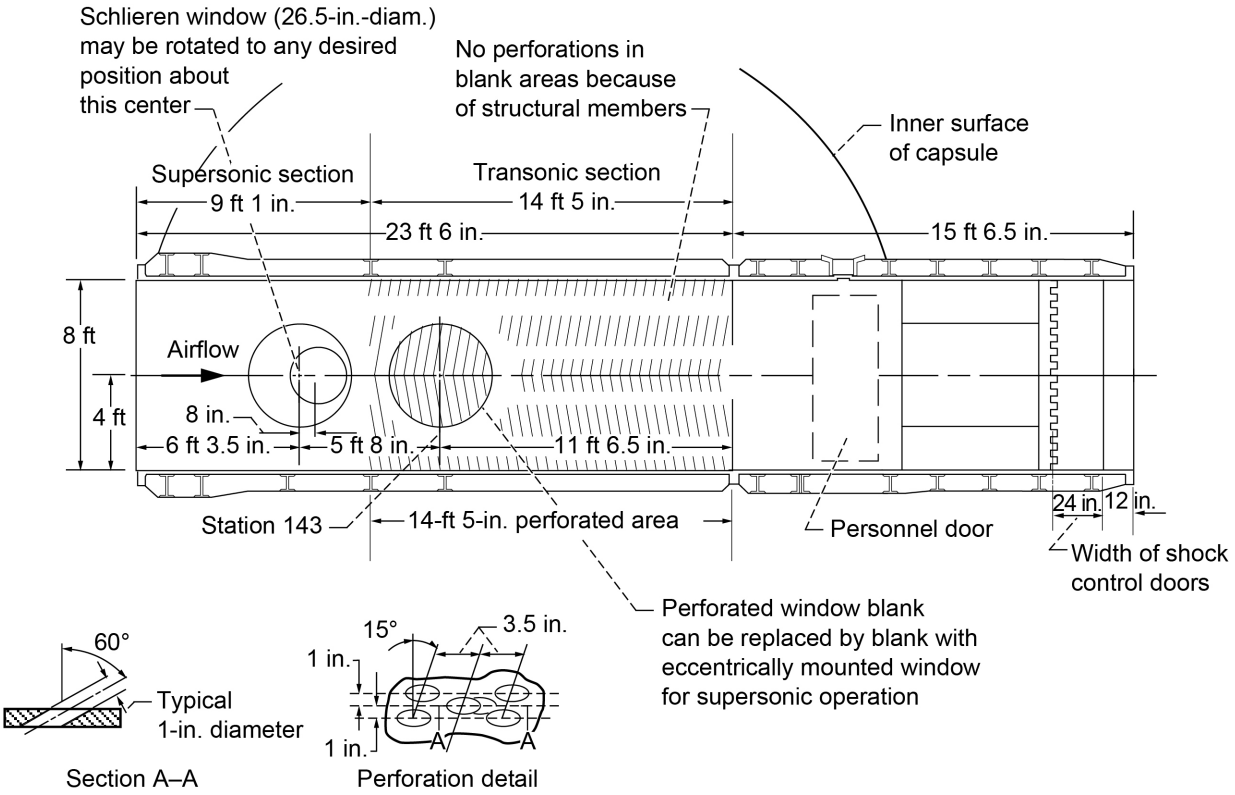

Figure 2.—Elevation view of 8- by 6-ft test section. Dimensions are in inches unless otherwise noted.

The conditions in the 8- by 6-ft test section are set by controlling compressor speed, flexwall position, balance chamber pressure (test section bleed), and shock door (second throat) position. Very low speed conditions (below Mach 0.1) can be achieved in the 8- by 6-ft test section by using only the air dryer building air circulation fans (the eight fans are used to pull air through the air dryer building to cool the desiccant beds; by properly configuring the tunnel and air dryer flow control doors, the fans will push air through the 8- by 6-ft test section).

Flow quality improvements were installed in the facility in 1992. The improvements that affect the 8- by 6-ft test section were a flow straightening honeycomb and three 10-mesh turbulence reduction screens in the settling chamber upstream of the test section and an aerodynamically contoured compressor exit tailcone fairing. Between 2016 and 2019, the 9×15 LSWT acoustic improvement modifications project was completed, which introduced several large flow-manipulating structures into the tunnel loop, including turning vane structures in both turns 2 and 3, upstream and downstream of the 9- by 15-ft test section, respectively. Appendix B discusses these facility modification more thoroughly. A more complete description of the 8×6 SWT is found in Reference 4.

3.0 Instrumentation and Test Hardware[3]

Existing test hardware and instrumentation were used in the 2019 test entry. New facility data systems implemented during the 9×15 LSWT acoustic improvement modifications were also used for this entry. The 4-inch-diameter cone cylinder and transonic array models have been used in previous 8×6 SWT characterization test entries (Ref. 3). Each of these instruments, their associated support systems, and their locations are described in the following sections.

3.1 4-Inch-Diameter Cone Cylinder

The 4-inch-diameter cone cylinder was used to measure the axial static pressure distribution in the test section for each Mach number setting. The 4-in. cone cylinder was chosen for this test entry from the family of cone-cylinder models available for use in the 8×6 SWT. The family of cone-cylinder models consists of a 4-, 8-, 12-, 16-, and 20-in.-diameter model. The 4-in.-diameter model is typically used to provide empty test section calibration data while the larger diameter models provide blockage effect data. The 4-in. model (0.18-percent blockage) is approximately 86-in. long and has a total of 132 static pressure taps. See Figure 3 for details on the 4-in. cone cylinder and instrumentation layout.

Each cone-cylinder model consists of a 10° half-angle cone with a base diameter as listed previously in the model names that extends into a constant diameter cylinder. Each model is instrumented with static taps arranged in four axial rows spaced 90° apart. The cone-cylinder models are typically sting mounted into the 8×6 SWT transonic strut. Axial position changes of the 4-in. cone-cylinder model in the tunnel are accomplished by means of a split sting section that can be added to or removed from the model assembly without disconnecting the instrumentation lines. The split sting section allows for an axial position change of 34 in. The tip of the cone cylinders can be positioned at either the inlet of the 8-ft test section or at the centerline of the schlieren window blanks in the 14-ft test section (referred to as the "14-ft test section measurement plane"). See Figure 4 showing the 4-inch-diameter cone cylinder installed during the 2019 test entry with the 4-in.-diameter cone tip at test section station (TSTA) 144.375.

[3]Section and subsections adapted from Reference 3.

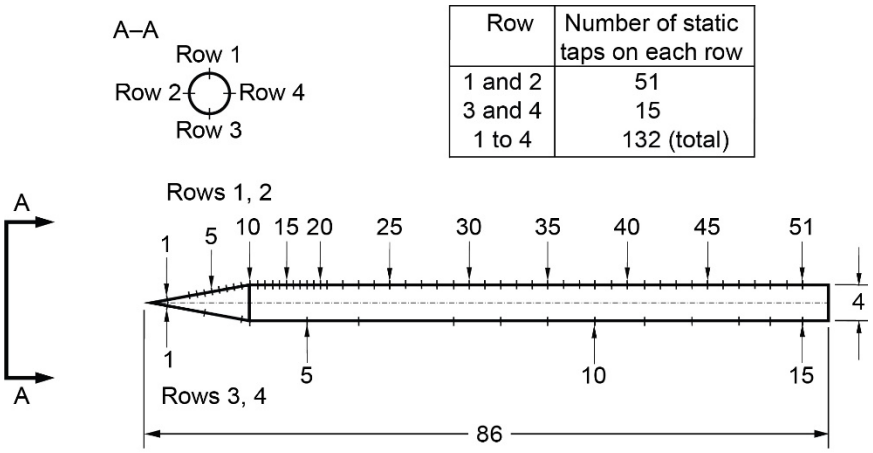

Figure 3.—Instrumentation layout of 4-inch-diameter cone cylinder. All dimensions in inches.

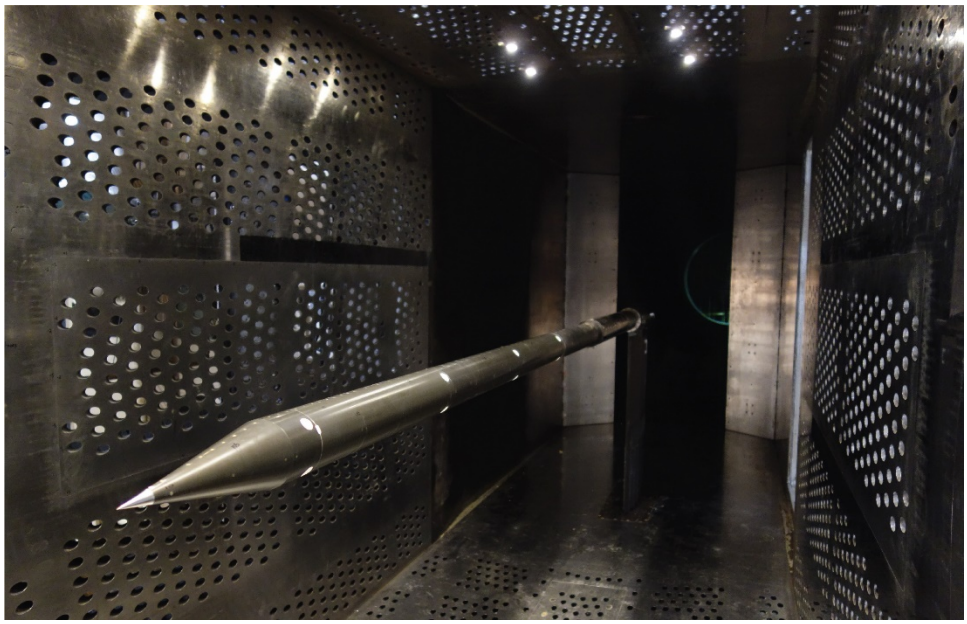

Figure 4.—Installation of 4-inch-diameter cone cylinder in 8- by 6-ft test section during 2019 test section characterization test entry. Model is shown with cone tip at test section station (TSTA) 144.375.

3.2 Transonic Array

The transonic array was used to survey the test section flow field to provide information on the total and static pressure, total temperature, and flow angle within a plane. The array instrumentation layout is shown in Figure 5. The standard array instrumentation comprises 5 flow angularity probes, 6 pitot-static pressure probes, 11 thermocouples, and 2 hot-film anemometry probes.[4] The array is typically sting mounted in the transonic strut and further supported by wall plates attached to both ends of the array body and by a vertical support downstream of the array body. All the surfaces of the array have a 10° taper to minimize aerodynamic interference. The array body is made of 304 stainless steel, the sting of 4340 steel, and the wall plates of 6061–T6 aluminum. During the 2019 test entry, the array was positioned axially such that the tips of the flow angle probes were at the 14-ft test section measurement plane. The array was tested at three vertical positions at this station (tunnel centerline and 1 ft above and below tunnel centerline). Figure 6 shows a typical installation of the array in the transonic test section and Figure 7 shows the array installed at the three vertical heights surveyed during the 2019 test entry. The wall plates (which are not shown in Figure 6) are attached to the tunnel walls by bolts that pass through the test section porosity holes. The floor plate for the vertical support is also attached to the tunnel using T-nuts through the porosity holes. There is a set of five vertical supports (one for each potential vertical position). The vertical support is bolted to the floor plate and to a collar that clamps around the sting just aft of the array body. The sting, through which the instrumentation lines pass, is supported in the transonic strut cradle.[5] One of the sting joints is also an expansion joint to compensate for thermal growth. Figure 8 shows the measurement locations of the transonic array (and other test hardware) within the 8- by 6-ft test section during the 2019 test entry.

The flow angle probes have a five-hole, hemispherical-head design, which allow resolution of two flow-angle components (pitch and yaw). The flow-angle probes were calibrated for a Mach number range of 0.5 to 2.0. The Mach number range of the 8×6 SWT is 0.36 to 2.0 for three-drive-motor operation while the operating range of the probe calibration facility at Sandia National Laboratories (Albuquerque, New Mexico) was 0.5 to 4.0 so probe flow-angle calibration data were extrapolated at the low Mach number conditions in the 8×6 SWT. These probes, as well as the pitot-static probes, extend 21.5 in. from the leading edge of the array.

The thermocouple probes (type-E, “special-limit-of-error” wire) are mounted to the bottom of the array body, with the heads of the thermocouples about even with the array leading edge and 2.25 in. below rake centerline. All thermocouples are terminated to the temperature reference junctions without any intermediate connections (commonly referred to as “home-run” length thermocouples). Due to space constraints within the array body and the size of the thermocouple wire chosen, 10 of the 11 wires were routed on the exterior of model. Except for the thermocouple at centerline, the wires exit the array through notches in the instrumentation cover plates in the top of the array body, are nichrom-strapped along the top of the array body and sting, and are routed into the transonic strut alongside the pressure tubing out of the test section. The thermocouple probes on the transonic array were modified prior to a customer-specific characterization test entry in 2016.

---

[4]Hot-film anemometry probes were not used during the 2019 entry. The NASA Glenn free-jet probe calibration facility (CE-12) was not available prior to testing to allow for the hot films to be adequately characterized and prepared for the entry. The upper hot-film probe support was removed and replaced with a cover plate for the 2019 test entry.

[5]In 2016, an upgrade to the transonic array thermocouples occurred that prevented the wires from being routed within the array’s sting. The wires, save for the wire of the centerline thermocouple, are routed atop and nichrom-strapped to the array body and sting before passing into the transonic strut and out of the test section.

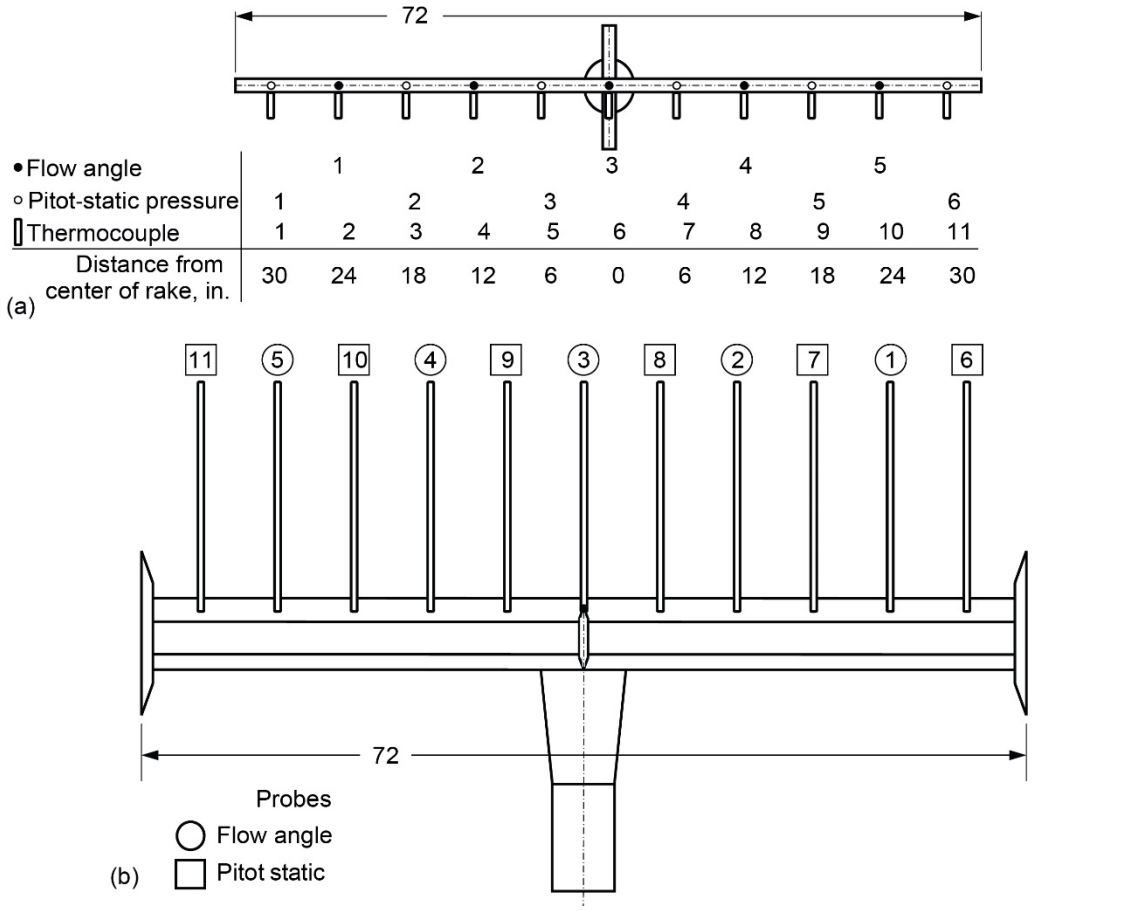

Figure 5.—Instrumentation layout of transonic array. (a) Upstream looking aft view. (b) Top-down view. All dimensions are in inches.

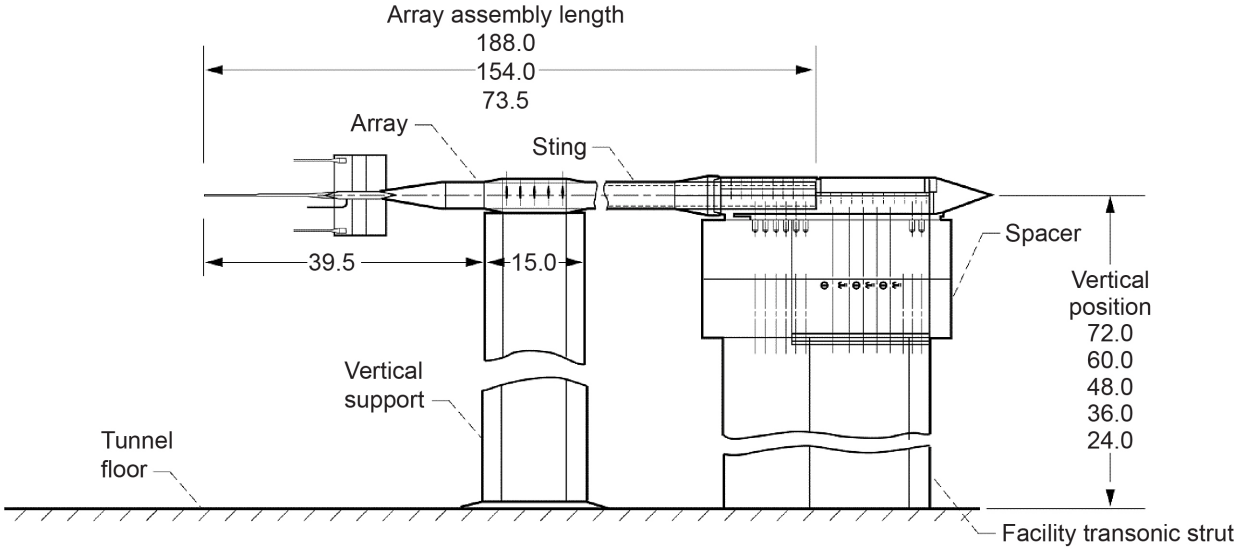

Figure 6.—Typical installation of transonic array in 8- by 6-ft test section (elevation view). Array can be stationed axially in three positions. At each axial station, array can be positioned at five vertical heights. All dimensions are in inches.

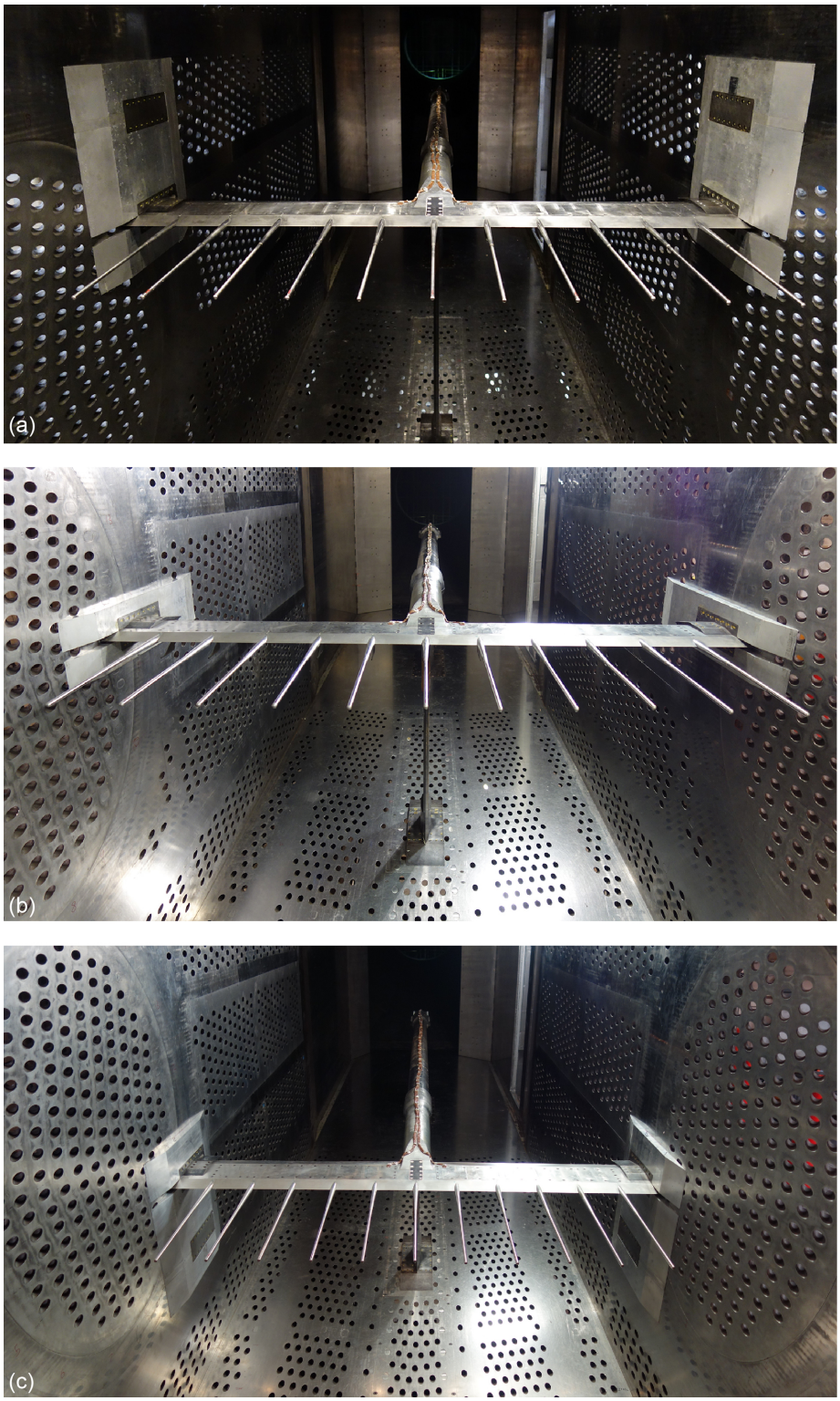

Figure 7.—Transonic array installed in 8- by 6-ft supersonic test section during 2019 test entry with pressure probe tips at 14-ft test section measurement plane. Array was positioned (a) 1 ft above centerline, (b) at centerline, and (c) 1 ft below centerline during this test entry.

Test section station (TSTA) of hardware locations in the 8×6 SWT (2019 test)		
Model		TSTA
4-in.-diam. cone cylinder		144.375
Transonic array	Centerline (CL)	137.531
	CL + 1 ft	137.766
	CL – 1 ft	137.563
Transonic quick-check rake		139.875

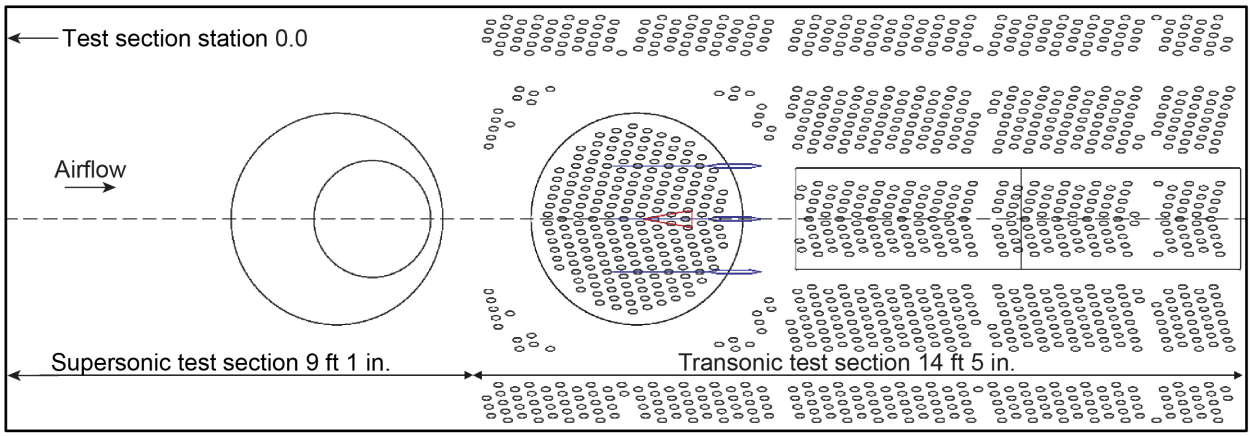

Figure 8.—Measurement locations of 4-inch-diameter cone cylinder and transonic array during 2019 test section characterization. Airflow is from left to right. Measurement locations are defined as cone tip for cone cylinder models and pressure probe tips for transonic array.

3.3 Transonic Quick-Check Rake

The transonic quick-check rake was designed to allow for efficient check calibrations of the 8×6 SWT test section calibration relationships. Figure 9 shows the transonic quick-check rake installed in the 8- by 6-ft test section with probe tips near the centerline of the downstream schlieren window blanks (also referred to as the "14-ft test section measurement plane"). The rake is vertically oriented, attached securely to its base plate via 17 ½-20 bolts, and the base plate attaches to the test section floor using 18 ½-20 bolts that pass through the test section porosity holes. The rake was designed to support a variety of flow sensing probes. The standard 8×6 SWT check calibration instrumentation layout includes the following: a pitot probe, conical static pressure probe, a five-hole hemispherical flow-angle probe (same as those used in the transonic array), and three type-E aspirated-tip thermocouples are used. In order from topmost to bottommost probe, the following was the probe order in 2019:

1. Static pressure probe
2. Thermocouple 1
3. Five-hole flow-angle probe
4. Thermocouple 2
5. Pitot probe
6. Thermocouple 3

Probes are 6 in. apart with the third probe location from the top being at test section centerline (48 in. from the test section floor). A folded sheet-metal cover plate protects the instrumentation cables as they travel down the trailing edge of the rake body to exit the test section through a porosity hole.

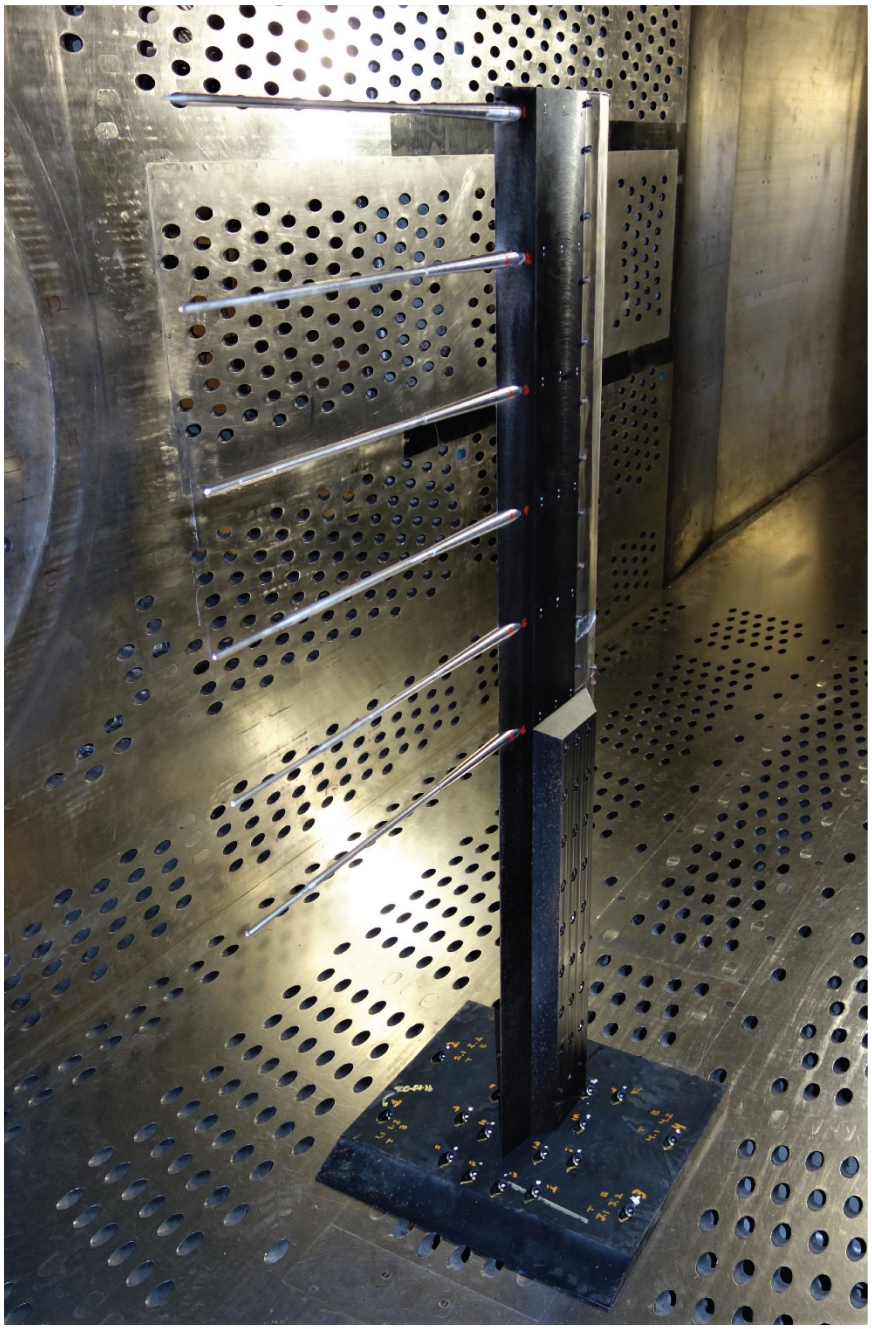

Figure 9.—Transonic quick-check rake installed in 8- by 6-ft test section during 2019 characterization test entry with probe tips at test section station 139.875 (near 14-ft test section measurement plane).

3.4 Facility Instrumentation

The following permanent instrumentation was used during the test section characterization test entry in 2019:

- Bellmouth rakes—two wall-mounted rakes are located near the exit of the bellmouth upstream of the test section. One rake is mounted to the north tunnel wall and the other to the south tunnel wall at approximately the tunnel centerline (the rakes are designated “north” and “south,” see

Figure 10). The instrumentation mounted on each rake consists of four total pressure and two total temperature probes. Each rake has a fifth pitot tube devoted to the tunnel control system, and one of the four total temperature probes is devoted to the tunnel control system. Similar to the transonic array, the thermocouples on the bellmouth rakes were modified in 2016. The thermocouples are the same type-E, "special-limit-of-error" wire as used on the transonic array with aspirated probe tips.[6]

- Balance chamber pressure—four pressures are measured within the balance chamber. These pressure taps are distributed around the balance chamber.
- Facility static pressures—Figure 11 shows the location of all static pressure taps located on the ceiling of the 8- by 6-ft test section and high-speed diffuser section.
- Flexible-wall nozzle camshaft encoder—an encoder on the flexible-wall nozzle's camshaft measures the rotational angle of the shaft. There are known orientations of the camshaft to achieve the appropriate contour for Mach 1.1 to 2.0 in 0.1 Mach increments. Calibrations of the walls' contours have been performed to verify this relationship.[7]

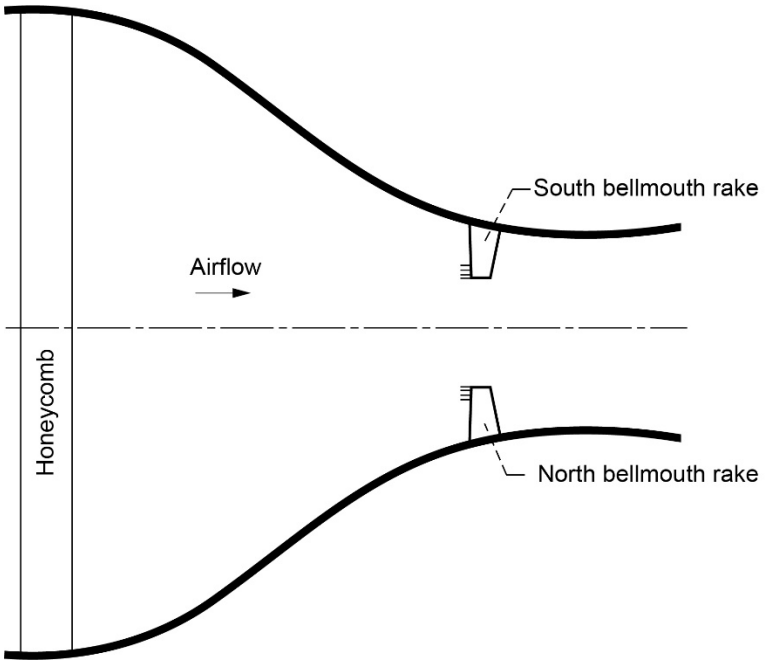

Figure 10.—Installation of bellmouth rakes upstream of the 8- by 6-ft test section as viewed from above the tunnel. Bellmouth rakes measure both total pressure and temperature.

[6]Thermal recovery correction are not applied to the bellmouth rake thermocouple measurements as these are reference measurements and not representative of freestream flow in the test section. Repeatability is more important than accuracy for reference instrumentation measurements.

[7]The most recent flexwall calibration was performed prior to the 2019 test entry at flexwall settings of Mach 1.0, 1.4, and 2.0. Typical variations from contour measurements taken in 2005 were less than 0.015 in. at each of the 14 measurement locations along the walls length.

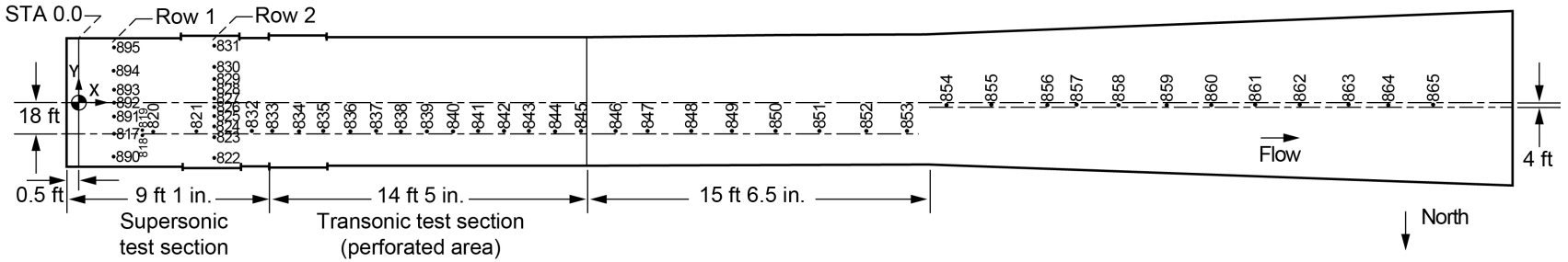

Static tap location	Axial station, X, in.	Distance from centerline, Y, in.	Static tap location	Axial station, X, in.	Distance from centerline, Y, in.
817	17.00	–18.00	838	169.25	–18.00
890	17.00	–30.63	839	183.25	–18.00
891	17.00	–7.50	840	197.50	–18.00
892	17.00	0.00	841	211.50	–18.00
893	17.00	7.56	842	225.50	–18.00
894	17.00	18.06	843	239.50	–18.00
895	17.00	25.78	844	253.38	–18.00
818	32.88	–19.56	845	267.63	–18.00
819	32.88	–16.56	846	286.50	–18.00
820	39.31	–18.00	847	303.75	–18.00
821	63.31	–18.00	848	327.50	–18.00
822	72.25	–31.50	849	350.50	–18.00
823	72.25	–19.50	850	374.06	–18.00
824	72.25	–13.50	851	398.75	–18.00
825	72.25	–7.50	852	422.63	–18.00
826	72.25	–2.50	853	446.00	–18.00
827	72.25	2.50	854	473.38	–4.00
828	72.25	7.50	855	497.44	–4.00
829	72.25	13.50	856	528.19	–4.00
830	72.25	19.50	857	543.31	–4.00
831	72.25	31.50	858	567.19	–4.00
832	87.50	–18.00	859	593.25	–4.00
833	99.25	–18.00	860	617.31	–4.00
834	113.25	–18.00	861	641.25	–4.00
835	127.25	–18.00	862	665.25	–4.00
836	141.38	–18.00	863	692.31	–4.00
837	155.75	–18.00	864	713.25	–4.00
			865	736.94	–4.00

Figure 11.—Facility static tap locations in 8- by 6-ft test section ceiling and diffuser.

3.5 Data Systems

The tunnel data system used during this test entry in the 8×6 SWT was COBRA, which was implemented during the 9×15 LSWT acoustic improvement modifications project construction period (2016 to 2019). Real-time data acquisition and display was provided by the COBRA data system. This system accommodates the ESP inputs, plus all steady-state analog and digital signals used including thermocouples and pertinent tunnel control parameters such as compressor speed, shock door positions, and positions of flow control doors 1 and 2. Data acquisition, engineering unit conversions, and calculations are performed by the data system at selected frequencies. All data during the 2019 test entry were acquired at 12.5 Hz.[8] For this test, unless noted otherwise, each collected data reading was 60 s in length. Data can be filtered and batched several ways following data collection through the COBRA data system. All data shown in this report, unless otherwise noted, is averaged across the length of the reading.

Steady-state pressure data were acquired with the Optimus Data System and 32-channel, 15-psid electronic pressure scanners (ESP–32HD digital temperature compensation (DTC) Gen-1 and Gen-2). The pressure scanners are miniature electronic differential pressure measurement units with an individual piezoresistive pressure sensor for each channel. This model of pressure scanner allows for digitial temperature compensation and in situ calibrations. An in situ calibration consists of setting five pressures, as measured by a high-accuracy 30-psia pressure calibration unit, across the span of the pressure scanner then making a span and zero adjustment for each channel. In situ calibrations are typically performed every 2 hours or more frequently per data engineer and test conductor judgment. Calibrations of the ESP system during this test entry were typically conducted at each flexwall setting for supersonic conditions and approximately every 30 to 60 min for subsonic operation. The reference pressure for the differential pressures sensed by the pressure scanners were measured by a 15-psia Mensor LP pressure transducer (Model CPT6180).

The thermocouples on the transonic array, bellmouth rakes, and transonic quick-check rake were terminated to the same Kaye Uniform Temperature Reference (UTR) where the thermocouples were junctioned to copper. Two resistance temperature detectors (RTDs) in each reference measured the temperature of the junction using a Fluke Calibration 2562 module (Fluke Corporation). Copper wires connect the Kaye UTR to COBRA.

4.0 Operational Considerations[9]

Descriptions of test setup, operational procedures, and test matrices used during the 2019 test entry are contained in this section. In general, the test setup and operational procedures are similar to those used in previous entries (Ref. 3).

4.1 Test Setup and Procedures

The test procedures specific to each piece of characterization hardware are described in the following sections.

4.1.1 4-Inch-Diameter Cone Cylinder

Prior to installation, the 4-inch-diameter cone cylinder was inspected by instrumentation technicians to ensure static tap quality. During the inspection, all static taps were cleaned, all orifices were imaged using a handheld digital microscope at × 50 and × 200 magnification to document defects that could

[8]The Mensor LP pressure transducer used for the ESP reference pressure provided samples to the data system at 10 Hz.
[9]Section and subsections adapted from Reference 3.

impact data quality, and pressure lines were vacuum checked. Examples of the orifice imaging at × 50 and × 200 magnification are shown in Figure 12. No static taps were identified as significantly damaged following inspection of the magnified images.

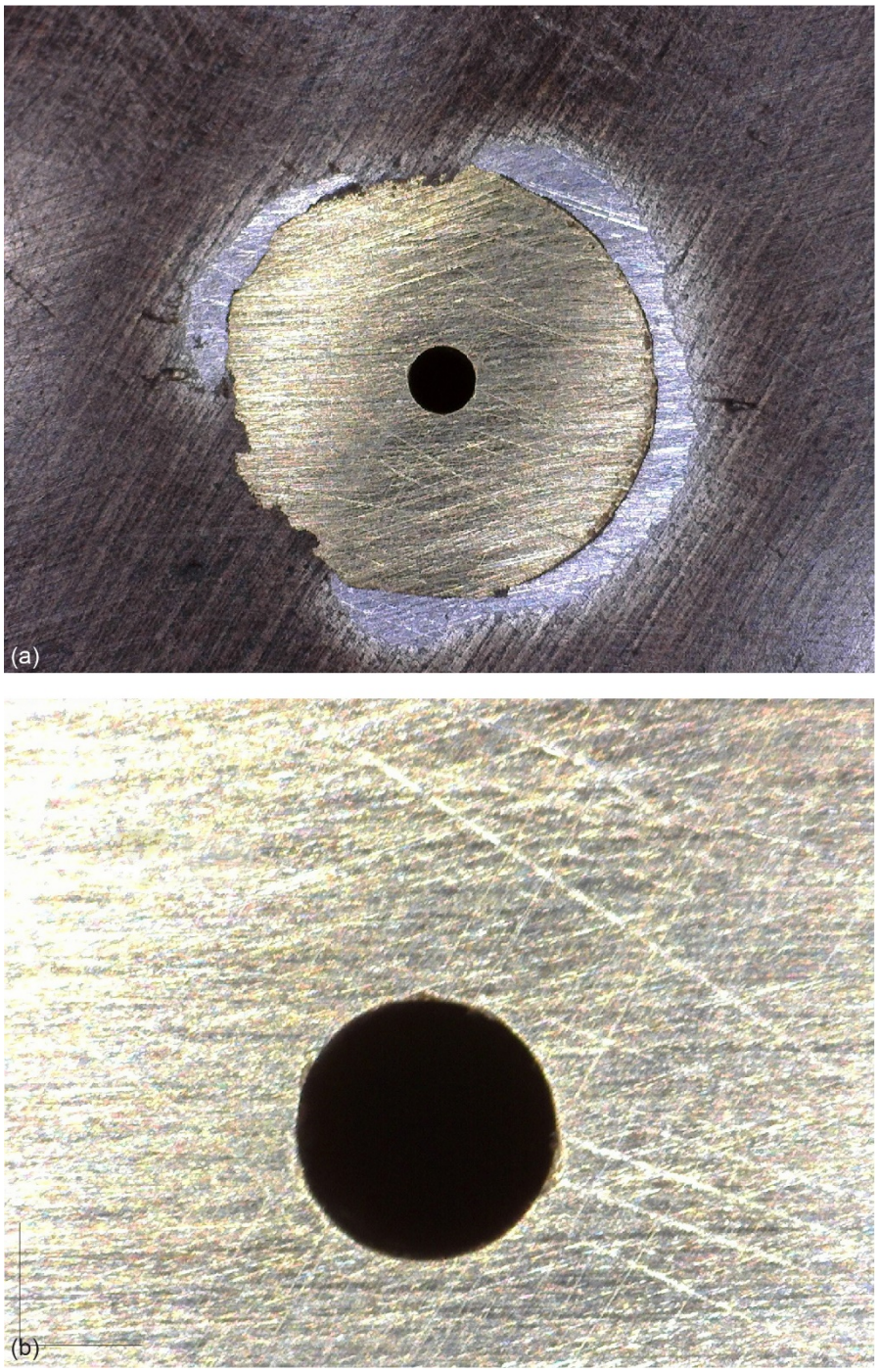

Figure 12.—Images captured of port 12 in row 1 of 4-inch-diameter cone cylinder's static pressure orifices prior to installation for 2019 characterization test entry in 8- by 6-Foot Supersonic Wind Tunnel. Images were captured at (a) × 50 and (b) × 200 magnification using Dino-Lite Digital Microscope (SKU#: AM4815ZT) (AnMo Electronics Corporation).

Following installation of the model, end-to-end checks of all instrumentation lines were conducted to ensure data quality. Any issues were resolved prior to testing and noted in the test log. Prior to each run, the cone cylinder was positioned such that the tip of the cone was at the test section centerline and leveled in pitch using a handheld digital inclinometer placed just downstream of the shoulder of the cone cylinder. The model pitch angle was monitored during the run by an electrolytic inclinometer within the forward portion of the cone-cylinder model. If required, the model was adjusted back to 0° during the test using the transonic strut pitch controls.

During a typical tunnel run, the highest Mach number conditions were set first to preserve air dryer capacity, and then the Mach number was reduced incrementally to cover the entire operating range of the facility. Off-nominal supersonic conditions were surveyed during this entry through balance chamber pressure variation; only the 10 defined physical positions of the flexwall for supersonic operation were surveyed during the 2019 test entry. By reducing the balance chamber pressure further than the nominal set point, the average static pressure in the transonic test section decreases, thus increasing the average Mach number in the porous test section. This is commonly referred to in this report as overspeeding the test section. The reverse is also true; increasing balance chamber pressure results in a lowering of the Mach number, which is commonly referred to in this report as "underspeeding the test section." At a given flexwall setting, the nominal ratio of balance chamber static to bellmouth total pressure, $R_{S,bal,bm}$, was surveyed followed by the highest planned overspeed condition with all other off-nominal set points surveyed in descending order. Typically, two overspeed and two underspeed conditions were set at each supersonic flexwall setting, however, overspeed or underspeed conditions were removed from the test matrix at the discretion of the test engineer for poor flow quality observed on the model, model stability concerns, and/or risk of unstarting the transonic test section.

4.1.2 Transonic Array

Prior to installation in the 8×6 SWT test section, the transonic array was thoroughly inspected by instrumentation technicians. The two thermocouple probes nearest the left side of the rake when upstream looking aft (near south test section wall) were replaced after being damaged at the end of a 2016 test entry. The braze joints at the base of the flow angle and pitot-static probes were repaired. Additionally, all pressure lines were vacuum checked and repaired, as needed. As hot-film measurements were not taken during the 2019 test entry, the hot-film probe support on the top surface of the rake body was removed and a cover plate installed.

Following the initial installation of the array in the test section, the flow-angle probe pitch and yaw alignment offsets were measured using a portable FaroArm® coordinate measuring machine (CMM) from Faro Technologies, Inc., and the baseline rake pitch and yaw angles were measured using a digital inclinometer and tape measure. The CMM used the tunnel floor for a reference plane in the pitch axis and a centerline plane created from both tunnel walls for a reference in the yaw axis. For each rake height change, the rake pitch and yaw angles were measured and compared to the baseline values. The differences from the baseline values were used to correct the measured flow angles for rake misalignment. End-to-end instrumentation checks were also made following the array installation. The same Mach number schedule (flexwall settings and balance chamber pressure variations) described for the cone cylinder was used for the array surveys. Vertical position changes for the array were made manually, so there was no translation of the hardware while the tunnel was running.

4.1.3 Transonic Quick-Check Rake

Following installation of the transonic quick-check rake, the flow angle probe pitch and yaw alignment offsets were measured using the same portable CMM used for the transonic array. These values were used to correct the measured flow angles. End-to-end instrumentation checks were also made, and a similar Mach number schedule described for the cone cylinder was used for the transonic quick-check rake, however, the off-nominal supersonic conditions using balance chamber pressure variations were not surveyed.

4.2 Test Matrix

All characterization hardware used in this test entry was stationed with its tip or pressure probe tips near the centerline of the downstream schlieren window blanks (14-ft test section measurement plane). All testing in support of this tunnel characterization was conducted in the closed-loop (aerodynamic cycle) operating mode for test section porosity configuration 1: 14-ft, 5.8-percent porosity. Operating the facility in the closed- versus open-loop (propulsion cycle) operation historically does not have any effect on the test section conditions in terms of flow quality or calibration, but there is the potential for reduced operating time when operating in open-loop due to a lack of dry air or, in other words, an insufficiently low dew point. Several Mach numbers (0.5, 0.9, 1.4, 1.5, and 1.9) were surveyed in open-loop operating mode with the 4-inch-diameter cone cylinder to validate this historical assumption. The test matrix for the 2019 test entry's supersonic conditions is shown in Table 1. The $R_{S,bal,bm}$ for nominal and overspeed and underspeed conditions at each flexwall setting are shown in Table 2.

TABLE 1.—TEST MATRIX OF SUPERSONIC CONDITIONS SURVEYED WITH 4-INCH-DIAMETER CONE CYLINDER AND TRANSONIC ARRAY DURING 8- BY 6-FOOT SUPERSONIC WIND TUNNEL TEST SECTION CHARACTERIZATION (2019 TEST)

[(A) surveyed with the 4-inch-diameter cone cylinder. (B) surveyed with transonic array at centerline (CL). (C) surveyed with transonic quick-check rake. (NA) data not acquired. (+) surveyed with transonic array at 1 ft above CL. (–) surveyed with transonic array at 1 ft below CL.]

Flexwall Mach number setting	Second overspeed	First overspeed	Nominal	First underspeed	Second underspeed
2.0	NA	A, B–	A, B±, C	A, B–	A, –
1.9	NA	A, B–	A, B±, C	A, B–	A, B–
1.8	A, B–	A, B–	A, B±, C	A, B–	A, B–
1.7	A, B±	A, B±	A, B±, C	A, B±	NA
1.6	A, B±	A, B±	A, B±, C	A, B±	NA
1.5	A, B±	A, B±	A, B±, C	A, B±	A, B±
1.4	A, B±	A, B±	A, B±, C	A, B±	A, B±
1.3	A, B±	A, B±	A, B±, C	A, B±	A, B±
1.2	NA	A, B±	A, B±, C	A, B–	NA
1.1	NA	A, B±	A, B±, C	NA	NA

TABLE 2.—RATIOS OF BALANCE CHAMBER TO BELLMOUTH TOTAL PRESSURE SURVEYED AT EACH FLEXWALL SETTING DURING 2019 TEST SECTION CHARACTERIZATION OF 8- BY 6-FOOT SUPERSONIC WIND TUNNEL

Flexwall Mach number setting	Second overspeed	First overspeed	Nominal	First underspeed	Second underspeed
2.0	---------	0.1361	0.1410	0.1462	0.1510
1.9	---------	.1575	.1641	.1701	.1761
1.8	0.1781	.1840	.1912	.1982	.2050
1.7	.2090	.2159	.2240	.2320	---------
1.6	.2421	.2500	.2591	.2679	---------
1.5	.2781	.2872	.2971	.3021	.3070
1.4	.3205	.3312	.3421	.3470	.3528
1.3	.3780	.3663	.3901	.3962	.4022
1.2	---------	.4141	.4270	.4347	---------
1.1	---------	.4779	.4932	---------	---------

Subsonic surveys were conducted with the 4-inch-diameter cone cylinder and transonic array at its three heights (centerline and ±1 ft from centerline) at the following Mach numbers:

- Three-motor operation: Mach 0.95 to 0.40 in 0.05 Mach increments and Mach 0.36
- One-motor operation: Mach 0.50 to 0.25 in 0.05 Mach increments

The transonic quick-check rake performed subsonic surveys at the following subset of Mach numbers:

- Three-motor operation: Mach 0.90, 0.80, 0.70, 0.60, 0.50, 0.40, and 0.36
- One-motor operation: Mach 0.50, 0.40, 0.30, and 0.25

Repeat conditions were acquired with the 4-inch-diameter cone cylinder and transonic array at test section centerline at each nominal supersonic Mach number setting (Mach 2.0 to 1.1 in 0.1 Mach increments), Mach 0.90, 0.70, and 0.50 for three-drive-motor operation, and Mach 0.45 and 0.30 for one-drive-motor operation. The transonic quick-check rake performed all of the repeat conditions listed previously, except for Mach 0.45. A total of three readings at each of the repeated conditions were acquired while ensuring the facility was brought off-condition between repeats.

The original characterization plan for this entry included additional surveys with the 4-inch-diameter cone cylinder and transonic array at the inlet of the 8-ft test section and surveys with the transonic array at five vertical heights at each survey station. Due to schedule constraints, the characterization plan was reduced and portions have been deferred to a future test entry.

At each test condition, one 60-s reading was recorded. During the 2019 test entry, the pressure scanning modules were calibrated at each supersonic flexwall setting and approximately every 30 to 60 min while testing at subsonic conditions. As previously mentioned, the highest Mach numbers were typically set first to conserve air dryer bed capacity. For all testing, a detailed log was maintained to track

test points, collected data reading numbers, hardware and instrumentation problems, etc. On line data monitoring was used to ensure data quality.

5.0 Data Reduction[10]

The data analysis methodology used for each part of the characterization test entry is described in the following sections. The information presented here applies to the general treatment of the data; for some specific applications, details of the data reduction are included in the discussion section.

The first step of the data reduction and analysis was a thorough review of the data to ensure data quality. While most instrumentation and data problems were detected and resolved either prior to or during the testing, there were instances where bad or questionable data was collected and further investigation was required (i.e., bad data points were flagged and therefore not used in subsequent steps of the analysis). Notes taken during the testing as part of the test engineers' log were used to troubleshoot problems with data channels.

At the completion of the test entry, the data were reprocessed using programs that simulated the online data reduction process. This step corrected any errors in the data from instrumentation problems or test setup errors. The posttest analyses were performed by custom scripts in MATLAB® (The MathWorks, Inc.).

5.1 4-Inch-Diameter Cone Cylinder

A detailed description of the development of the cone cylinder data analysis methodology is contained in Reference 5, but an abbreviated explanation is included here. The average static pressure on the cone portion of the model can be used to estimate the local freestream Mach number and static pressure for supersonic conditions; a theoretical relationship between a cone-cylinder model's cone surface static pressure and the freestream Mach number exists for supersonic conditions (see Ref. 5 for details). The average static pressure over the aft portion of the cylinder, $P_{S,cyl,avg}$, provides a direct measurement of the freestream static pressure for all Mach number settings. The static pressure measurements on the model are first averaged circumferentially at each axial station before averaging in the streamwise direction.

5.2 Transonic Array

A detailed description of the transonic array data reduction methodology is contained in Reference 3 with some high-level descriptions included in this section. The local freestream total pressure at the pitot-static and five-hole hemispherical head flow angularity probes is measured at subsonic test section conditions. The local total pressure downstream of a normal shock ($P_{T,2}$) is measured by each of these probes at supersonic test section conditions. The calibrated test section static pressure generated from the aft portion of the 4-inch-diameter cone cylinder was used to compute local Mach number at each pressure probe on the transonic array. It is believed that the cone cylinder is a more accurate measurement of freestream static pressure, particularly at supersonic conditions between Mach 1.0 and 1.5 where probe-to-probe interference on the array is apparent. Two components of flow angle are computed at each of the five-hole flow angularity probes per data reduction method in Reference 3. Data acquired in the Sandia National Laboratory Trisonic Wind Tunnel were used to calibrate the flow-angle probes (Ref. 8 and 9 from Ref. 3).

[10]Adapted from Reference 3.

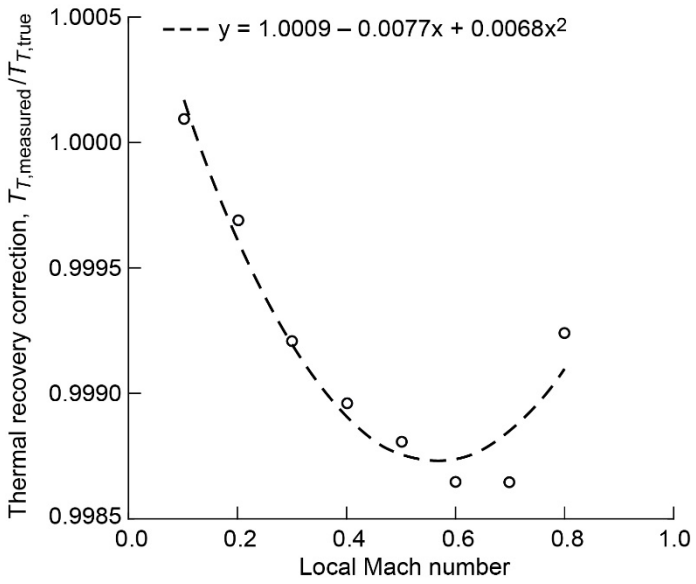

Figure 13.—Thermal recovery correction data and regression model for transonic array thermocouple design. Data acquired in NASA Glenn Research Center Engine Research Building free-jet calibration facility (CE–12).

In 2016, a model of the centerline thermocouple probe on the transonic array was created, instrumented using the same type and length of wire used in the array, and the thermal recovery characteristics of the probe were determined. Data were acquired between Mach 0.1 and 0.8 in 0.1 Mach increments at ambient temperature in a 3.5-in.-diameter free-jet calibration facility (CE–12) in the NASA Glenn Research Center Engine Research Building (ERB). The measured thermocouple temperature (in Rankine) was divided by the freestream total temperature (in Rankine) of the facility's free jet to generate a correction factor. The correction factor was found to be a second-order polynomial function of local Mach number; Figure 13 shows the thermal recovery correction data acquired from the free-jet characterization test and the regression model fit through the data. On the transonic array, the local Mach number at each pressure probe is used to determine the correction factor and the thermocouple measurement at the same lateral location along the array is divided by the correction factor to produce the true local freestream total temperature. If the local Mach number is greater than Mach 0.8 or less than Mach 0.1, no correction is applied.

6.0 Discussion of Results

All results discussed and data presented in the following sections are from the 2019 test section characterization test entry.

TABLE 3.—SUMMARY OF TEST SECTION FLOW QUALITY GOALS
FOR NASA GLENN RESEARCH CENTER WIND TUNNELS

Flow quality parameter	Aeropropulsion tunnels[a]	Icing Research Tunnel
Mach number variation	0.005	0.005
Flow angularity, degree	±0.25	±0.25
Turbulence intensity, percent	0.25	0.50
Total temperature variation, °F	4	2

[a]Aeropropulsion tunnels at NASA Glenn are 9- by 15-Foot Low-Speed, 8- by 6-Foot Supersonic, and 10- by 10-Foot Supersonic Wind Tunnels.

6.1 Flow Quality Goals[11]

Flow quality goals for the NASA Glenn wind tunnels have been defined and are listed in Table 3. These flow quality goals are based on information and recommendations from the Wind Tunnel Calibration Workshop held at NASA Langley Research Center (Ref. 10 from Ref. 3) and modified for the specific missions of the propulsion wind tunnel facilities at NASA Glenn.

6.2 4-Inch-Diameter Cone Cylinder

The static pressure distributions along the 4-inch-diameter cone-cylinder model are shown in Figure 14 to Figure 27. The model static pressure, $P_{S,\text{model}}$, data is normalized by the average bellmouth total pressure, $P_{T,bm}$, to remove potential temporal variation between datasets. Each data point in the cone-cylinder model's dataset is an average of either two or four static pressure measurements around the circumference of the model at that axial station. If repeat points were acquired with the cone cylinder at a given condition, the data displayed in the figure is an average of the repeat readings. For a given flexwall setting, the pressure distributions on the cone cylinder are shown at the nominal condition and each overspeed and underspeed condition surveyed.

The average static pressure along the cylinder, $P_{S,cyl,avg}$, is displayed downstream of the cone cylinder data for each balance chamber pressure setting in Figure 14 to Figure 27. The average static pressure along the cylinder is the average, first circumferentially then axially, at all pressure port stations 40 in. or more downstream of the cone tip. The aft portion of the cylinder covered the distance between TSTAs 184.715 and 228.715 during the 2019 characterization test entry. Also plotted is the theoretical pressure ratio along a 10° half-angle cone-cylinder model at the average cylinder Mach number for the nominal supersonic conditions (Ref. 5). The theoretical freestream Mach number and static pressure estimates from cone surface pressures were not used in these figures or further analyses of this test entry's data. The average cylinder static pressure is a more direct measurement of freestream flow and was therefore chosen to be the primary representation of freestream static pressure in the 8×6 SWT test section.

Several customers in recent history have preferred the 8×6 SWT tunnel operators to set the average test section Mach number to a certain value that was not the nominal calibrated condition (i.e., nominal pressure ratio, $R_{S,bal,bm}$, and flexwall position). It has typically been the practice to allow this by overspeeding or underspeeding a nominal Mach number setting with the understanding that the flow quality was not well understood at these off-nominal conditions. The investigations performed during the 2019 characterization test entry were, in part, to justify the facility engineers' and wind tunnel

[11]Adapted from Reference 3.

characterization engineers' warnings to customers of poor flow quality when venturing away from the facility's calibrated regions.

A further analysis of the static pressure distributions aft of 40 in. from the cone tip was needed to convey not only the average conditions along the cylinder under nominal and off-nominal facility settings but also the streamwise gradient (or slope) and variation about the average (or standard deviation). The standard deviation of the cylinder data was needed in addition to the gradient data to convey the poor axial pressure distribution flow quality observed at many of the off-nominal balance chamber pressure settings (e.g., the slope of a sine wave can still be zero). The static pressure measured along the cylinder was also converted to a Mach number using the calibrated test section total pressure, $P_{T,ts}$, and isentropic relations (Ref. 6). Note that streamwise static pressure and Mach number gradients were considered to be zero if the linear fit was insignificant (i.e., p value > $\alpha = 0.05$). Table 4 and Table 5 tabulate the following information for the nominal and off-nominal balance pressure settings for each nominal flexwall setting:

- Average Mach number on the cylinder, $M_{cyl,avg}$
- The static pressure streamwise gradient (positive being an increase in static pressure with distance downstream), $\Delta P_{S,cyl,\text{aft}}$/ft
- The standard deviation of static pressure along the aft portion of the cylinder, $\sigma(P_{S,cyl,\text{aft}})$
- The Mach number streamwise gradient (positive being an increase in Mach number with distance downstream), $\Delta M_{cyl,\text{aft}}$/ft
- The standard deviation of Mach number along the aft portion of the cylinder, $\sigma(M_{cyl,\text{aft}})$

Many observations and trends can be drawn from investigating Table 4 or Table 5 and Figure 14 to Figure 27. The data collected at a nominal flexwall Mach number, M_{nom}, of Mach 1.8, for example, shows a less severe static pressure gradient along the aft end of the cylinder for the first overspeed condition when compared to nominal despite having a 50 percent higher standard deviation. This is a good representative case as to why both values are needed to numerically judge and understand the streamwise pressure distribution on the cylinder. In most cases, these two values can be used to show that the historically used nominal pressure ratio of balance chamber to bellmouth total pressure is the appropriate choice for optimal flow quality. There are a couple cases, $M_{nom} = 1.9$ and 2.0, where the nominal pressure ratio setting created both a steeper streamwise pressure gradient and higher standard deviation of cylinder static pressure than the first underspeed condition. In other words, while the average test section Mach number was lower (further from the M_{nom} of 1.9 and 2.0), the streamwise static pressure distribution was relatively better at flexwall settings of Mach 1.9 and 2.0 for the first underspeed condition than the nominal. The presence of reflected shocks (or other flow features) produced by the model tip and/or shoulder at lower supersonic Mach numbers tend to significantly influence the pressure measurements on the model thus increasing the values of $\sigma(M_{cyl,\text{aft}})$ at nominal Mach 1.4 and below. For supersonic operation, the choice was made to maintain the nominal pressure ratios as the recommended pressure ratio to which the facility should be controlled at a given flexwall setting.

TABLE 4.—TEST SECTION MACH NUMBER AND STREAMWISE STATIC PRESSURE GRADIENTS AND STANDARD DEVIATIONS AT NOMINAL, OVERSPEED, AND UNDERSPEED SUPERSONIC CONDITIONS IN 8- BY 6-FT TEST SECTION AS MEASURED BY 4-INCH-DIAMETER CONE CYLINDER DURING 2019 CHARACTERIZATION TEST ENTRY

[All data is for test section porosity configuration 1 (14-ft test section, 5.8-percent porosity). The aft portion of the cylinder is considered to be all pressure ports aft of 40 in. downstream of the cone tip: test section station (TSTA) 184.715 to 228.715 during the 2019 characterization test entry. Test section Mach number is therefore the average Mach number at TSTA 206.715. Static pressure gradients were set to 0.0 for insignificant first-order polynomial fits ($\alpha = 0.05$).]

Parameter	Flexwall nominal Mach number	Second overspeed	First overspeed	Nominal	First underspeed	Second underspeed
Test section Mach number, M_{ts}	2.0	---	2.027	1.989	1.929	1.856
	1.9	---	1.936	1.891	1.830	1.751
	1.8	1.870	1.842	1.792	1.724	1.651
	1.7	1.744	1.713	1.663	1.600	---
	1.6	1.626	1.596	1.553	1.509	---
	1.5	1.516	1.488	1.457	1.442	1.426
	1.4	1.413	1.385	1.355	1.344	1.329
	1.3	1.310	1.279	1.252	1.243	1.234
	1.2	---	1.208	1.184	1.173	---
	1.1	---	1.102	1.073	---	---
Static pressure gradient along cylinder, $\Delta P_{S,cyl,\mathrm{aft}}$/ft, psia/ft	2.0	---	0.0823	0.0568	0	0
	1.9	---	.1293	.0799	0	–0.1215
	1.8	0.1804	.1471	.0805	0	–.1463
	1.7	.1888	.1372	.0577	0	---
	1.6	.1079	.0715	.0426	0	---
	1.5	0	0	0	0	0
	1.4	–.0821	0	0	0	0
	1.3	0	0	0	–0.1101	–.1164
	1.2	---	0	0	0	---
	1.1	---	0	.1059	---	---
Standard deviation of cylinder static pressure, $\sigma(P_{S,cyl,\mathrm{aft}})$, psia	2.0	---	0.1896	0.1134	0.0484	0.1790
	1.9	---	.2165	.1205	.0693	.2524
	1.8	0.2701	.2079	.1009	.1605	.3907
	1.7	.2988	.1983	.0835	.2132	---
	1.6	.2891	.1771	.0810	.1688	---
	1.5	.2603	.1648	.0974	.0963	.1131
	1.4	.1909	.1294	.1770	.2184	.2530
	1.3	.1364	.1674	.2055	.2060	.2447
	1.2	---	.2076	.3258	.3838	---
	1.1	---	.2770	.2452	---	---

TABLE 5.—TEST SECTION MACH NUMBER AND STREAMWISE MACH NUMBER GRADIENTS AND STANDARD DEVIATIONS AT NOMINAL, OVERSPEED, AND UNDERSPEED SUPERSONIC CONDITIONS IN 8- BY 6-ft TEST SECTION AS MEASURED BY 4-INCH-DIAMETER CONE CYLINDER DURING 2019 CHARACTERIZATION TEST ENTRY

[All data is for test section porosity configuration 1 (14-ft test section, 5.8-percent porosity). The aft portion of the cylinder is considered to be all pressure ports aft of 40 in. downstream of the cone tip: test section station (TSTA) 184.715 to 228.715 during the 2019 characterization test entry. Test section Mach number is therefore the average Mach number at TSTA 206.715. Mach number gradients were set to 0.0 for insignificant first-order polynomial fits ($\alpha = 0.05$).]

Parameter	Flexwall nominal Mach number	Second overspeed	First overspeed	Nominal	First underspeed	Second underspeed
Test section Mach number, M_{ts}	2.0	----------	2.027	1.989	1.929	1.856
	1.9	----------	1.936	1.891	1.830	1.751
	1.8	1.870	1.842	1.792	1.724	1.651
	1.7	1.744	1.713	1.663	1.600	---------
	1.6	1.626	1.596	1.553	1.509	---------
	1.5	1.516	1.488	1.457	1.442	1.426
	1.4	1.413	1.385	1.355	1.344	1.329
	1.3	1.310	1.279	1.252	1.243	1.234
	1.2	----------	1.208	1.184	1.173	---------
	1.1	----------	1.102	1.073	---------	---------
Mach number gradient along cylinder, $\Delta M_{cyl,aft}$/ft	2.0	----------	–0.0166	–0.0113	0	0
	1.9	----------	–.0236	–.0142	0	0.0194
	1.8	–0.0320	–.0255	–.0132	0	0
	1.7	–.0312	–.0219	–.0085	0	---------
	1.6	–.0166	–.0105	–.0058	0	---------
	1.5	0	0	0	0	0
	1.4	.0103	0	0	0	0
	1.3	0	0	0	0.0123	.0129
	1.2	----------	0	0	0	---------
	1.1	----------	0	–.0104	---------	---------
Standard deviation of cylinder Mach, no., $\sigma(M_{cyl,aft})$	2.0	----------	0.0390	0.0228	0.0093	0.0327
	1.9	----------	.0399	.0214	.0118	.0406
	1.8	0.0475	.0359	.0166	.0254	.0590
	1.7	.0485	.0314	.0124	.0312	---------
	1.6	.0429	.0257	.0110	.0227	---------
	1.5	.0354	.0219	.0123	.0123	.0142
	1.4	.0238	.0159	.0210	.0258	.0296
	1.3	.0162	.0195	.0230	.0230	.0272
	1.2	----------	.0218	.0339	.0391	---------
	1.1	----------	.0274	.0240	---------	---------

Table 6 contains the same information as Table 4 and Table 5 for only nominal supersonic conditions and all subsonic test section Mach numbers surveyed during the test entry. The pressure distribution is much "flatter" and easier to interpret in realtime for subsonic conditions than during supersonic operation, as shown in Figure 14 to Figure 27 and Table 6. During the 2019 test entry, facility subsonic operational pressure ratios ($R_{S,bal,bm}$ and the ratio of test section aft static to balance chamber pressure, $R_{S,\mathrm{aft},bal}$) were adjusted slightly to improve the measured pressure gradient while maintaining the desired Mach number set point.

The streamwise Mach number gradient is typically slightly negative (decrease in Mach number with movement downstream) for nominal supersonic conditions. The most severe pressure gradient of –0.014 Mach per foot occurs at Mach 1.9. The Mach number gradients for all subsonic conditions are between –0.0003 and 0.0002 Mach per foot at Mach 0.95.

6.3 Transonic Array

The following sections discuss the results for several different flow parameters suveryed by the transonic array during the 2019 test entry.

6.3.1 Total Pressure

The total pressure ratio distributions across the 8- by 6-ft test section at the pressure probe tips (14-ft test section measurement plane) at centerline and 1 ft above and below centerline are shown in Figure 28 to Figure 56. The freestream total pressure at each pressure probe, $P_{T,\mathrm{array}}$, is normalized by the calibrated test section total pressure, $P_{T,ts}$, to remove temporal variation. For supersonic conditions, the freestream local Mach number at each pressure probe on the array is calculated using the Rayleigh pitot formula, the measured total pressure behind a normal shock at each probe, $P_{T,2}$, and the calibrated test section static pressure, $P_{S,ts,}$ as discussed in the data reduction section. The freestream total pressure at each probe is calculated using isentropic relations, the local Mach number, and $P_{S,ts}$ (Ref. 6). Data were not acquired at all off-nominal balance chamber pressures at all array heights thus resulting in varying amounts of data in each of the plots for supersonic conditions. Subsonic total pressure ratio data are also shown in Figure 38 to Figure 56, however, the local array total pressure is simply the measured pitot pressure.

There is typically a very uniform flow field in the test section across the nominal operating range of the facility, however, as seen in previous characterization tests, Mach 2.0 and 1.9 total pressure profiles have a deficit near the center of the test section. The deficit at these higher Mach numbers, per suggestions from Reference 3, is likely due to separation off the compressor exit tailcone. The total pressure deficit in the center of the test section, when compared to total pressures measured nearer the test section walls, is approximately 0.4 psi at Mach 2.0 and 0.7 psi at Mach 1.9.[12]

[12]The deficit values shown are only considering data acquired at centerline, not 1 ft above or below centerline.

TABLE 6.—TEST SECTION MACH NUMBER AND STREAMWISE GRADIENTS AND STANDARD DEVIATIONS OF STATIC PRESSURE AND MACH NUMBER AT NOMINAL SUPERSONIC AND SUBSONIC CONDITION IN 8- BY 6-ft TEST SECTION AS MEASURED BY 4-INCH-DIAMETER CONE CYLINDER DURING 2019 CHARACTERIZATION TEST ENTRY

[All data is for test section porosity configuration 1 (14-ft test section, 5.8-percent porosity). The aft portion of the cylinder is considered to be all pressure ports aft of 40 in. downstream of the cone tip: test section station (TSTA) 184.715 to 228.715 during the 2019 characterization test entry. Test section Mach number is therefore the average Mach number at TSTA 206.715. Static pressure and Mach number gradients were set to 0.0 for insignificant first-order polynomial fits ($\alpha = 0.05$).]

Nominal Mach number	Test section Mach number, M_{ts}	Static pressure gradient on cylinder, $\Delta P_{S,cyl,\mathrm{aft}}$/ft psia/ft	Standard deviation of cylinder static pressure, $\sigma(P_{S,cyl,\mathrm{aft}})$ psia	Mach number gradient on cylinder, $\Delta M_{cyl,\mathrm{aft}}$/ft	Standard deviation of cylinder Mach number, $\sigma(M_{cyl,\mathrm{aft}})$
Three-drive-motor operation					
2.0	1.989	0.05677	0.1134	–0.0113	0.0228
1.9	1.891	.07988	.1205	–.0142	.0214
1.8	1.792	.08054	.1009	–.0132	.0166
1.7	1.663	.05768	.0835	–.0085	.0124
1.6	1.553	.04256	.0810	–.0058	.0110
1.5	1.457	0	.0974	0	.0123
1.4	1.355	0	.1770	0	.0210
1.3	1.252	0	.2055	0	.0230
1.2	1.184	0	.3258	0	.0339
1.1	1.073	.10589	.2452	–.0104	.0240
.95	.951	0	.0115	0	.0011
.90	.901	0	.0099	0	.0009
.85	.850	0	.0083	0	.0008
.80	.800	0	.0069	0	.0006
.75	.750	0	.0068	0	.0006
.70	.700	0	.0064	0	.0006
.65	.650	–.00218	.0059	.0002	.0005
.60	.600	–.00216	.0053	.0002	.0005
.55	.551	–.00191	.0045	.0002	.0004
.50	.500	–.00188	.0040	.0002	.0004
.45	.450	–.00137	.0031	.0002	.0004
.40	.400	0	.0022	0	.0003
.36	.368	0	.0018	0	.0002
One-drive-motor operation					
0.50	0.501	–0.00128	0.00338	0.0001	0.0004
.45	.451	–.00112	.00283	.0001	.0003
.40	.401	0	.00211	0	.0003
.35	.350	0	.00145	0	.0002
.30	.301	.00057	.00125	–.0001	.0002
.25	.250	.00149	.00190	–.0003	.0004

Overspeed and underspeed conditions typically exhibit the most influence on the pressure probes located 6 and 12 in. away from the test section walls. The core of the test section, for the purpose of analyzing the flow-field uniformity in this report, is defined as the data collected by the center 7 (out of 11) probe locations on the array at centerline and 1 ft above and below centerline.[13] The spatial variation of the supersonic nominal and off-nominal total pressure distributions are summarized in Table 7. Subsonic total pressure variation, as well as Mach number, total temperature, and flow-angle variation, is similarly summarized in Table 8. A standard deviation was used to convey uniformity of the flow parameters in the test section as it can be statistically useful for researchers and customers, as opposed to a range value. At least 14 data points (2 array heights) were available for each supersonic condition's standard deviation calculation (save for the second underspeed condition at Mach 2.0; see test matrix in Table 1). The total pressure variation shown at nominal supersonic conditions in Table 7 are either better or on par with the variation seen at off-nominal conditions, lending additional evidence to the choice to not alter the historical nominal pressure ratio ($R_{S,bal,bm}$) settings for supersonic operation.

TABLE 7.—SPATIAL VARIATION OF FREESTREAM TOTAL PRESSURE, $P_{T,\text{array}}$, AS MEASURED BY TRANSONIC ARRAY AT 14-FT TEST SECTION MEASUREMENT PLANE IN 8- BY 6-FT TEST SECTION DURING 2019 CHARACTERIZATION TEST ENTRY

[Data were extracted from the center seven probes on the array at centerline and 1 ft above and below centerline.]

Parameter	Flexwall nominal Mach number	Second overspeed	First overspeed	Nominal	First underspeed	Second underspeed
Standard deviation of $P_{T,\text{array}}$, psia	2.0	--------	0.154	0.191	0.190	0.386
	1.9	--------	.291	.268	.292	.293
	1.8	0.086	.083	.072	.075	.074
	1.7	.107	.102	.093	.085	--------
	1.6	.102	.080	.059	.057	--------
	1.5	.037	.035	.033	.031	.032
	1.4	.065	.051	.039	.038	.044
	1.3	.046	.035	.030	.033	.034
	1.2	--------	.010	.018	.017	--------
	1.1	--------	.003	.005	--------	--------

[13]The center seven probe locations, whether pressure or temperature, on the array with the array positioned at centerline are used in creation of past (Ref. 3) and current calibration relationships.

TABLE 8.—STANDARD DEVIATION OF FREESTREAM TOTAL PRESSURE, $P_{T,\text{array}}$, MACH NUMBER, M_{array}, AND TOTAL TEMPERATURE, $T_{T,\text{array}}$, AND STANDARD DEVIATION AND MEAN VALUE OF PITCH AND YAW FLOW ANGLES, α AND β, AS MEASURED BY TRANSONIC ARRAY AT 14-FT TEST SECTION MEASUREMENT PLANE IN 8- BY 6-FT TEST SECTION DURING 2019 CHARACTERIZATION TEST ENTRY

[Data were extracted from the center seven probes on the array at centerline and 1 ft above and below centerline.]

Nominal Mach number	Standard deviation					Mean	
	Total pressure, $P_{T,\text{array}}$, psia	Mach number, M_{array}	Total temperature, $T_{T,\text{array}}$, R	Pitch flow angle, α, degree	Yaw flow angle, β, degree	Pitch flow angle, α, degree	Yaw flow angle, β, degree
Three-drive-motor operation							
0.95	0.0039	0.00021	1.13	0.09	0.14	0.01	–0.02
.90	.0038	.00021	1.12	.10	.15	.02	–.04
.85	.0037	.00021	1.12	.11	.13	.00	–.03
.80	.0037	.00022	1.16	.16	.17	–.03	–.03
.75	.0036	.00022	1.13	.16	.13	.02	–.07
.70	.0035	.00023	1.07	.16	.09	–.02	–.06
.65	.0033	.00022	1.12	.15	.09	–.01	.00
.60	.0031	.00022	1.13	.17	.12	–.01	.05
.55	.0026	.00021	1.06	.13	.10	.01	.05
.50	.0022	.00020	1.06	.12	.14	–.06	.12
.45	.0018	.00018	1.00	.23	.16	.03	.14
.40	.0014	.00015	1.06	.26	.10	–.06	–.05
.36	.0012	.00014	1.13	.16	.10	–.02	–.08
One-drive-motor operation							
0.50	0.0019	0.00018	1.06	0.14	0.15	–0.02	0.12
.45	.0015	.00016	1.08	.22	.16	.03	.13
.40	.0012	.00014	1.12	.26	.11	–.06	–.05
.35	.0009	.00013	1.16	.14	.11	.00	–.04
.30	.0007	.00011	1.28	.13	.10	.01	–.02
.25	.0005	.00009	1.48	.13	.11	–.01	.03

6.3.2 Mach Number

The freestream Mach number distributions across the 8- by 6-ft test section are shown in Figure 57 to Figure 85 where the local freestream Mach number at each probe, M_{array}, is normalized by the calibrated test section Mach number, M_{ts}. For subsonic Mach number ratio data in Figure 67 to Figure 85, the local array Mach number is computed using isentropic relations, measured pitot pressure, and calibrated test section static pressure, $P_{S,ts}$ (Ref. 6). Because a constant static pressure is used to compute the local freestream total pressure and Mach number at the array probes, the trends are very similar between Figure 28 to Figure 56 and Figure 57 to Figure 85. Similar to Table 7 for total pressure, Table 9 was created to display the Mach number standard deviations across the core of the test section. Table 9 displays similar trends to those seen in the supersonic total pressure variation. The deficit seen near centerline at Mach 2.0 and 1.9 produces a decrease in Mach number of 0.010 and 0.018, respectively, relative to M_{array} values observed nearer the test section walls. The spatial variation tends to decrease with decreasing Mach number. Subsonic Mach number variation is approximately 0.0007 at Mach 0.95 and 0.0003 at Mach 0.25.

TABLE 9.—SPATIAL VARIATION OF FREESTREAM MACH NUMBER, M_{array}, AS MEASURED BY TRANSONIC ARRAY AT 14-FT TEST SECTION MEASUREMENT PLANE IN 8- BY 6-FT TEST SECTION DURING 2019 CHARACTERIZATION TEST ENTRY

[Data were extracted from the center seven probes on the array at centerline and 1 ft above and below centerline.]

Parameter	Flexwall nominal Mach number	Second overspeed	First overspeed	Nominal	First underspeed	Second underspeed
Standard deviation of M_{array}	2.0	---------	0.0039	0.0049	0.0050	0.0106
	1.9	---------	.0077	.0073	.0082	.0087
	1.8	0.0023	.0023	.0021	.0022	.0023
	1.7	.0032	.0031	.0029	.0028	---------
	1.6	.0032	.0026	.0020	.0020	---------
	1.5	.0013	.0012	.0012	.0011	.0012
	1.4	.0024	.0019	.0015	.0015	.0018
	1.3	.0018	.0014	.0013	.0014	.0015
	1.2	---------	.0004	.0008	.0008	---------
	1.1	---------	.0001	.0002	--------	---------

6.3.3 Total Temperature

The total temperature ratio distributions across the 8- by 6-ft test section are shown in Figure 86 to Figure 114 where the local total temperature, $T_{T,\text{array}}$, is normalized by the calibrated test section total temperature, $T_{T,ts}$. The array thermocouple measurements are corrected for thermal recovery at local array Mach numbers, M_{array}, less than Mach 0.8. At supersonic conditions, there is an arching of the temperature ratio distribution (warmer in the center, cooler near the tunnel walls) that becomes gradually more pronounced with decreasing Mach number. This trend reverses at subsonic conditions; Mach 0.95 shows a similar rainbow-shaped distribution of temperature that gradually flattens out with decreasing Mach number. At approximately Mach 0.40 and below, a slight lateral gradient in total temperature appears in the test section with higher temperatures near the inner wall of the tunnel loop. The relatively large lateral gradients observed at the higher supersonic Mach numbers in the 1996 and 1997 characterization test entries (Ref. 3) were not as significant in this entry. For example, at Mach 2.0 on centerline, there is only a 0.5 °F difference from left to right (upstream, looking aft in the test section) in the core of the test section and only 1.5 °F difference when considering all 11 thermocouple measurements across the array. The severity of the gradient value varies with array height. This can likely be attributed in part to the addition of turning vanes in corners 2 and 3 of the tunnel loop (upstream and downstream of the 9- by 15-ft test section) and other flow manipulators during the 9×15 LSWT acoustic improvement modifications project.

Table 10 shows the standard deviation of total temperature for supersonic conditions across the core of the test section, similar to those for total pressure and Mach number. Additionally, Table 10 includes the range of the temperature data in the core of the test section and using all 11 thermocouple probes. Table 8 includes the standard deviation of total temperature for the subsonic conditions across the core of the test section, and Table 11 adds the temperature range information described previously for the subsonic conditions. The temperature range tends to grow with decreasing Mach number at supersonic conditions, grow with increasing Mach number at subsonic conditions for three-drive-motor operation, and grow with decreasing Mach number for one-drive-motor operation. Counterintuitively, the temperature data collected at 1 ft above centerline tends to be lower (cooler) than that at centerline and 1 ft below centerline. Data collected at low subsonic speeds show this trend continuing with temperatures

at 1 ft below centerline becoming warmer than the other two array heights. This, along with data to be discussed from the transonic quick-check rake, leads to the conclusion that this counterintuitive temperature trend is not an instrumentation bias at one configuration of the array.

TABLE 10.—SPATIAL VARIATION OF TOTAL TEMPERATURE, $T_{T,\text{array}}$, AS MEASURED BY TRANSONIC ARRAY AT 14-FT TEST SECTION MEASUREMENT PLANE IN 8- BY 6-FT TEST SECTION DURING 2019 CHARACTERIZATION TEST ENTRY

[Data were extracted from the center seven probes on the array at centerline (CL) and 1 ft above and below CL.]

Parameter	Flexwall nominal Mach number	Second overspeed	First overspeed	Nominal	First underspeed	Second underspeed
Standard deviation of $T_{T,\text{array}}$, R	2.0	------	0.67	1.07	0.70	0.51
	1.9	------	.70	1.12	.73	.74
	1.8	0.39	.40	1.14	.44	.49
	1.7	1.13	1.16	1.14	1.17	------
	1.6	.82	.89	.65	.98	------
	1.5	1.40	1.44	1.29	1.46	1.47
	1.4	1.35	1.34	1.40	1.36	1.43
	1.3	1.29	1.27	1.17	1.16	1.16
	1.2	------	1.17	1.17	.54	------
	1.1	------	1.16	1.14	------	------
Range of $T_{T,\text{array}}$ across core of test section, R	2.0	------	2.23	3.36	2.29	1.34
	1.9	------	1.94	3.36	2.01	2.05
	1.8	1.29	1.34	3.51	1.42	1.55
	1.7	3.43	3.48	3.35	3.44	------
	1.6	2.69	2.86	2.18	3.12	------
	1.5	4.64	4.72	4.28	4.85	4.95
	1.4	4.84	4.83	5.12	4.88	5.20
	1.3	4.77	4.76	4.44	4.39	4.36
	1.2	------	4.49	4.45	1.67	------
	1.1	------	4.42	4.38	------	------
Range of $T_{T,\text{array}}$ across all array probes,[a] R	2.0	------	2.35	3.52	2.62	1.64
	1.9	------	1.95	3.48	2.14	2.05
	1.8	1.55	1.51	3.51	1.57	1.84
	1.7	4.24	4.38	4.18	4.58	------
	1.6	3.85	4.04	3.51	4.32	------
	1.5	5.56	5.66	5.22	5.82	5.90
	1.4	6.06	6.03	6.34	6.13	6.34
	1.3	6.20	6.18	6.03	5.91	5.84
	1.2	------	6.15	6.07	4.56	------
	1.1	------	6.33	6.28	------	------

[a]All array probes refers to the 11 probes on the array at CL and 1 ft above and below CL.

TABLE 11.—RANGE OF TOTAL TEMPERATURE, $T_{T,\text{array}}$, AS MEASURED BY TRANSONIC ARRAY AT 14-FT TEST SECTION MEASUREMENT PLANE IN 8- BY 6-FT TEST SECTION DURING 2019 CHARACTERIZATION TEST ENTRY

[Data used to compute the range values were extracted from the "core" of the test section (center seven probes on the array) and all 11 thermocouple probes on the array at centerline and 1 ft above and below centerline.]

Nominal Mach number	Range of total temperature, $T_{T,\text{array}}$, R	
	Range across core of test section	Range across all transonic array thermocouple probes
Three-drive-motor operation		
0.95	4.39	6.34
.90	4.35	6.22
.85	4.30	6.03
.80	4.50	5.54
.75	4.33	5.62
.70	4.11	5.19
.65	4.22	4.94
.60	4.12	4.52
.55	3.94	4.28
.50	3.79	4.01
.45	3.38	3.51
.40	3.51	3.54
.36	3.49	3.49
One-drive-motor operation		
0.50	3.93	4.34
.45	3.92	4.22
.40	3.99	4.21
.35	3.97	4.10
.30	4.17	4.20
.25	4.51	4.97

6.3.4 Flow Angle

The flow-angle distributions in the 8- by 6-ft test section are shown in Figure 115 to Figure 129 in the form of quiver plots. The corrected pitch, α_{corr}, and yaw, β_{corr}, flow angles at the array five-hole flow-angle probes were corrected by prerun measurements of the array and pretest probe misalignment measurements, as discussed in Section 4.1. The magntitude of the flow angles, pitch and yaw, in the core of the test section is typically less than 0.25° for subsonic conditions and less than 0.50° for supersonic conditions, but, in many cases, the flow angularity is much less. Table 12 and Table 13 show the mean and standard deviation of the pitch and yaw flow angles, respectively, in the core of the test section at

supersonic conditions, including nominal and off-nominal balance chamber pressure settings. In most cases, as could be expected, the increase or decrease in balance chamber pressure from the nominal setting affects the outermost pressure probes (as mentioned in the total pressure distribution discussion). For example, a decrease in balance chamber pressure pulls the flow towards the tunnel surfaces. The flow-angle distributions at a flexwall setting of Mach 1.3 in Figure 122 exemplify this well. The mean flow angles and their variation across the core of the test section for subsonic conditions are shown in Table 8. The mean pitch or yaw flow angle is less than 0.15° across the subsonic operating range with lower flow angularity typically near transonic conditions. Appendix C contains figures of flow angle distributions that resemble the distribution plots for the other flow parameters.

TABLE 12.—MEAN AND STANDARD DEVIATION OF PITCH FLOW ANGLE, α, AS MEASURED BY TRANSONIC ARRAY AT 14-FT TEST SECTION MEASUREMENT PLANE IN 8- BY 6-FT TEST SECTION DURING 2019 CHARACTERIZATION TEST ENTRY

[Data were extracted from the center three flow angle probes on the array at centerline and 1 ft above and below centerline.]

Parameter	Flexwall Mach number	Second overspeed	First overspeed	Nominal	First underspeed	Second underspeed
Mean of α, degree	2.0	------	0.08	0.06	0.10	0.29
	1.9	------	.07	.06	.07	.07
	1.8	0.06	.05	.02	.04	.05
	1.7	–.02	–.02	–.02	–.01	------
	1.6	.00	.00	.01	.03	------
	1.5	.12	.13	.13	.13	.12
	1.4	.18	.18	.17	.17	.17
	1.3	–.25	–.20	–.11	–.02	.05
	1.2	------	.04	.14	.28	------
	1.1	------	–.01	–.02	------	------
Standard deviation of α, degree	2.0	------	0.35	.31	0.34	0.16
	1.9	------	.23	.19	.23	.23
	1.8	0.45	.45	.42	.48	.48
	1.7	.19	.19	.19	.20	------
	1.6	.25	.24	.19	.18	------
	1.5	.22	.21	.18	.17	.17
	1.4	.23	.24	.26	.26	.29
	1.3	.26	.16	.13	.21	.31
	1.2	------	.23	.48	.78	------
	1.1	------	.25	.40	------	------

TABLE 13.—MEAN AND STANDARD DEVIATION OF YAW FLOW ANGLE, β, AS MEASURED BY TRANSONIC ARRAY AT 14-FT TEST SECTION MEASUREMENT PLANE IN 8- BY 6-FT TEST SECTION DURING 2019 CHARACTERIZATION TEST ENTRY

[Data were extracted from the center three flow angle probes on the array at centerline and 1 ft above and below centerline.]

Parameter	Flexwall Mach number	Second overspeed	First overspeed	Nominal	First underspeed	Second underspeed
Mean of β, degree	2.0	-------	–0.10	–0.05	–0.05	–0.03
	1.9	-------	–.08	–.04	–.09	–.10
	1.8	–0.14	–.15	–.12	–.17	–.18
	1.7	–.11	–.11	–.12	–.12	--------
	1.6	–.05	–.05	–.05	–.05	--------
	1.5	.11	.10	.08	.08	.07
	1.4	.11	.10	.09	.09	.08
	1.3	–.26	–.25	–.21	–.19	–.18
	1.2	-------	–.01	–.10	–.13	--------
	1.1	-------	.00	–.16	--------	--------
Standard deviation of β, degree	2.0	-------	0.35	0.31	0.34	0.36
	1.9	-------	.13	.14	.13	.13
	1.8	0.52	.51	.46	.51	.51
	1.7	.17	.17	.16	.17	--------
	1.6	.32	.30	.22	.14	--------
	1.5	.22	.20	.16	.14	.13
	1.4	.27	.27	.28	.27	.29
	1.3	.34	.22	.13	.17	.25
	1.2	-------	.24	.40	.60	--------
	1.1	-------	.26	.45	--------	--------

6.4 Calibration Models for Determining Test Section Operating Conditions

One of the primary objectives of the 2019 test section characterization test entry was to provide calibration relationships for determining test section operating conditions. These calibration relationships relate the measured test section flow parameters during the characterization test entry to facility instrumentation measurements. Only calibration relationships for test section porosity configuration 1 (14-ft test section, 5.8-percent porosity) are discussed in this report. The test section calibration relationships, generated only from 2019 test entry data, cover three-drive-motor operation (Mach 0.36 to 2.0) and one-drive-motor operation (Mach 0.25 to 0.50) in the 8×6 SWT. This section will describe the required inputs, calibration routines and outputs, and additional test section flow parameter calculations. The information in this section was used to modify the facility data system's subroutine (CAL8X6) used in all data collection programs to compute test section conditions.

The inputs to the calibration relationships are listed below:

- Bellmouth total pressure (psia), $P_{T,bm}$: average of eight bellmouth total pressure measurements, $P_{T,bm}(i)$, i = 1 to 8; there are four pressures on the north and four on the south bellmouth rakes.

- Bellmouth total temperature (R), $T_{T,bm}$: average of four bellmouth total temperature measurements, $T_{T,bm}(i)$, i = 1 to 4; there are two thermocouple probes (type-E, "special-limit-of-error" wire) per bellmouth rake.[14]
- Balance chamber static pressure (psia), $P_{S,bal}$: average of four balance chamber static pressures, $P_{S,bal}(i)$, i = 1 to 4.
- Flexwall camshaft angle (degree), FLEX: rotational angle of the camshaft that controls the flexible-wall nozzle contour upstream of the 8- by 6-ft test section.
- Test section configuration, TSCFG:
  - TSCFG = 1 for the 14-ft, 5.8-percent porosity
  - TSCFG = 2 for the 8-ft, 6.2-percent porosity
  - TSCFG = 3 for the 8-ft, 3.1-percent porosity
  - TSCFG = 4 for the 8-ft, 6.2-percent modified porosity
  - TSCFG = 5 for the 8-ft, 3.1-percent modified porosity
  - TSCFG = 6 for the 14-ft schlieren windows installed
  - TSCFG = 7 for the supersonic test section with the transonic test section configured for an 8-ft, 6.2-percent porosity

The calibration relationships were based on data collected with the 4-inch-diameter cone cylinder and transonic array. The average cylinder static pressure on the 4-inch-diameter cone cylinder, $P_{S,cyl,avg}$, was chosen to represent the calibrated test section static pressure, $P_{S,ts}$. Data acquired at tunnel centerline with the transonic array were used to create the test section total pressure ($P_{T,ts}$ or $P_{T,2}$) and total temperature ($T_{T,ts}$) calibration relationships. Stagnation pressure and temperature data were averaged across the center seven probe locations on the array to obtain average test section conditions, $P_{T,avg}$ and $T_{T,avg}$, respectively, for use in the regression models. At supersonic conditions, the array produces the average total pressure behind a normal shock, $P_{T,2,avg}$.

In the transonic test section, a ratio of $P_{S,bal}$ to $P_{T,bm}$ is used as a key parameter in determining all calibrated test section conditions (Ref. 3):

$$R_{S,bal,bm} = \frac{P_{S,bal}}{P_{T,bm}} \tag{1}$$

The simplest approach to the regression models was taken initially using forms of the regression models similar to those presented in Reference 3. In the following subsections, each flow parameter's regression models will be discussed.

6.4.1 Static Pressure

Regression models for $P_{S,cyl,avg}$ normalized by $P_{T,bm}$ as a function of the $R_{S,bal,bm}$ were generated for both subsonic and supersonic conditions. For subsonic conditions, repeats were not used in the regression models to avoid unevenly weighting the model. For supersonic conditions, only the three repeated nominal conditions at each flexwall setting were used in the regression model. Figure 130 shows both of the static pressure calibration relationships and the following equations are used to compute test section static pressure for subsonic ($R_{S,bal,bm} > 0.5330$) and supersonic operation, respectively:

[14]One of the four thermocouple measurements on the bellmouth rakes is used for the facility control system and is "coded-out" in the facility data system.

$$P_{S,ts} = P_{T,bm}\left(A_0 + A_1 x + A_2 x^2\right), \quad \text{where } x = R_{S,bal,bm} \tag{2}$$

$$P_{S,ts} = P_{T,bm}\left(A_{S,0} + A_{S,1} x + A_{S,2} x^2 + A_{S,3} x^3\right), \quad \text{where } x = R_{S,bal,bm} \tag{3}$$

Coefficients, A_0 to A_2 and $A_{S,0}$ to $A_{S,3}$, are defined in Table 14. The residuals for the regression models are shown, as well, in Figure 130. Note that the residuals were multiplied by the appropriate $P_{T,bm}$ values at each operating condition to obtain residuals in engineering units. Across the subsonic operating range, residuals were less than 0.005 psia.

TABLE 14.—CALIBRATION COEFFICIENTS FOR TEST SECTION FLOW PARAMETER REGRESSION MODELS IN 8- BY 6-FOOT SUPERSONIC WIND TUNNEL

[All coefficients are only for computing freestream conditions in the 8- by 6-ft test section when in test section porosity configuration 1 (14-ft test section, 5.8-percent porosity). These coefficients are related to Revision 7 of the computing requirements for the CAL8X6 subroutine, dated August 4, 2020.]

Flow parameter (speed regime)	Coefficient	Value
$P_{S,ts}$ (subsonic)	A_0	0.0210731306593265
	A_1	.8939625640329290
	A_2	.0856971907990224
$P_{S,ts}$ (supersonic)	$A_{S,0}$	.0055384188445698
	$A_{S,1}$	.7815845356552070
	$A_{S,2}$	.8642546593023140
	$A_{S,3}$	–.9788245110324170
$P_{T,ts}$ (subsonic)	B_0	1.0039661682427900
	B_1	–.0176607401147288
	B_2	.0244157594206177
	B_3	–.0107212911857357
$P_{T,2}$ (supersonic)	$B_{S,0}$	.3249458525036050
	$B_{S,1}$	3.8396656489135100
	$B_{S,2}$	–7.3998483105078400
	$B_{S,3}$	4.8438968326437300
$T_{T,ts}$ (subsonic)	C_0	.9815588913655010
	C_1	.0756619044993195
	C_2	–.0583828856188405
$T_{T,ts}$ (supersonic)	$C_{S,0}$	.9898146863091240
	$C_{S,1}$	.0632892416212709
	$C_{S,2}$	–.0630669746069085

Another objective of the test entry was to investigate the off-nominal balance chamber pressure settings for supersonic conditions and, if possible, incorporate them into the calibration relationships. All data acquired at each flexwall setting, nominal and off-nominal, were fit to quadratic or linear relationships in the same form as shown in the previous equations. Repeated conditions at nominal balance chamber pressure settings were averaged to prevent uneven weighting of the regression models. The regression models for each flexwall setting, referred to as the "local static pressure calibration relationships", and their associated residuals are shown in Figure 131. The equations are as follows:

$$P_{S,ts} = P_{T,bm}\left(A_{SX,0} + A_{SX,1}x + A_{SX,2}x^2\right), \quad \text{where } x = R_{S,bal,bm} \tag{4}$$

The coefficients, $A_{SX,0}$ to $A_{SX,2}$, are defined in Table 15 for each flexwall setting. Once again, the residuals were multiplied by the appropriate bellmouth total pressure values at each operating condition to obtain residuals in engineering units. The residuals for the local calibration relationships are typically lower than those for the curve spanning the supersonic operating range of the 8×6 SWT. As seen in Figure 130 and Figure 131, the residuals of the nominal conditions are typically clustered together with smaller scatter amongst themselves than the residual values, thus indicating the mean of the sets of repeat data points more accurately represent the true conditions than the regression models. For this reason, a correction factor was desired to adjust the static pressure ratio ($P_{S,cyl,avg}$ /$P_{T,bm}$) to the mean of the three repeated nominal data points; these repeated data points are deemed more accurate than the regression model. With the correction factor, the equation for determining $P_{S,ts}$ becomes

$$P_{S,ts} = P_{T,bm}\left(A_{SX,0} + A_{SX,1}x + A_{SX,2}x^2 + \text{Correction}\right), \quad \text{where } x = R_{S,bal,bm} \tag{5}$$

The static pressure ratio corrections are shown in Table 16. The correction factor is unique to each flexwall setting and is to only be applied when at a given flexwall setting and within ±0.0005 of the nominal $R_{S,bal,bm}$. The range in which the correction is applied was chosen upon inspection of the range of values of $R_{S,bal,bm}$ over which the repeated nominal conditions were surveyed.

In practice, it is expected that the operator will set the facility flexwall to the desired nominal setting, achieve the proper nominal $R_{S,bal,bm}$, and the correction factor will be applied to the static pressure ratio, thus achieving the most accurate estimation of $P_{S,ts}$. If the value of $R_{S,bal,bm}$ falls outside the range specified in Table 16, then the local static pressure calibration model (Figure 131) for the given flexwall setting is found in Table 15. The tunnel operator should not operate beyond the values in Table 15 of $R_{S,bal,bm}$ for a given flexwall setting as that would cause extrapolation of the calibration relationships. Additionally, the flexwall camshaft angle should be within a certain range of the nominal values shown in Table 15 to allow for the local regression models to be used. The current range of flexwall camshaft angle is ±2.0° for allowing usage of the local calibration relationships, however, this value can be adjusted by facility and/or data engineers for operational reasons. The flexwall camshaft angle repeats the nominal positions much more tightly than this acceptable range suggests, and there are flats machined into the cams for almost all of the nominal flexwall settings, which extend ±1.0° to ±1.5° about the nominal camshaft angles in Table 15.[15] To maintain continuity of conditions when changing between nominal flexwall conditions, the regression model for static pressure, which spans the supersonic operating range of the facility (Figure 130) shall be used when neither the flexwall or pressure ratio criteria discussed previously are met.

[15]The Mach 1.3 flat on the flexwall cam is a 3.0° arc, the flats at Mach 1.4, 1.5, and 1.6 are 2.5° arcs, and the flats at Mach 1.7, 1.8, 1.9, and 2.0 are 2.0° arcs. There are no flats at a nominal flexwall Mach number setting of Mach 1.1 and 1.2.

TABLE 15.—CALIBRATION COEFFICIENTS FOR LOCAL FREESTREAM STATIC PRESSURE REGRESSION MODELS IN 8- BY 6-FOOT SUPERSONIC WIND TUNNEL AT EACH NOMINAL FLEXWALL SETTING

[Table includes the approximate flexwall camshaft angle setting and range of balance chamber to bellmouth total pressure ratios, $R_{S,bal,bm}$, over which the local calibration models are applicable. All coefficients are only applicable to the 8- by 6-ft test section porosity configuration 1 (14-ft test section, 5.8-percent porosity). These coefficients are related to Revision 7 of the computing requirements for the CAL8X6 subroutine, dated August 4, 2020.]

Flexwall camshaft angle, FLEX, degree	Flexwall Mach number setting	$A_{SX,0}$	$A_{SX,1}$	$A_{SX,2}$	Lower limit on $R_{S,bal,bm}$	Upper limit on $R_{S,bal,bm}$
190.4	2.0	1.162808	–15.802475	60.157207	0.13606	0.15095
180.0	1.9	1.347328	–15.833591	52.110139	.15754	.17608
167.7	1.8	1.195391	–12.119588	35.569588	.17811	.20496
154.3	1.7	1.337626	–11.628510	29.517690	.20901	.23195
138.8	1.6	.753219	–5.215561	12.630958	.24210	.26789
121.3	1.5	.197290	–.414459	2.427207	.27806	.30697
101.3	1.4	.112155	.267087	1.111141	.32049	.35283
80.3	1.3	–1.154710	6.985912	–7.798756	.36626	.40216
67.6	1.2	–1.486869	8.032373	–8.349540	.41412	.43474
48.1	1.1	–.045947	1.074214	.000000	.47787	.49453

TABLE 16.—CORRECTION FACTOR TO RATIO OF TEST SECTION STATIC TO BELLMOUTH TOTAL PRESSURE ($P_{S,ts}/P_{T,bm}$) WHEN WITHIN SPECIFIED RANGE OF NOMINAL RATIO OF BALANCE CHAMBER TO BELLMOUTH TOTAL PRESSURE ($R_{S,bal,bm}$) SETTING FOR EACH FLEXWALL SETTING

[All coefficients are only applicable to the 8- by 6-ft test section porosity configuration 1 (14-ft test section, 5.8-percent porosity). These correction factors are related to Revision 7 of the computing requirements for the CAL8X6 subroutine, dated August 4, 2020.]

Flexwall camshaft angle, FLEX, degree	Flexwall Mach number setting	Nominal $R_{S,bal,bm}$	Correction to ratio of test section static to bellmouth total pressure	Range (±) of $R_{S,bal,bm}$ over which correction is applied
190.4	2.0	0.14098	0.00017069	0.00050
180.0	1.9	.16411	.00021817	.00050
167.7	1.8	.19123	–.00032185	.00050
154.3	1.7	.22403	–.00030523	.00050
138.8	1.6	.25909	.00025663	.00050
121.3	1.5	.29712	.00003518	.00050
101.3	1.4	.34206	.00044235	.00050
80.3	1.3	.39010	.00045441	.00050
67.6	1.2	.42699	0	NA
48.1	1.1	.49316	0	NA

6.4.2 Total Pressure

The calibration relationships for $P_{T,ts}$ (subsonic) and $P_{T,2}$ (supersonic) have a similar form to those decided upon for static pressure as a similar process was followed in choosing the appropriate regression models. For subsonic conditions, repeats were not used in the regression models to avoid unevenly weighting the model. A regression model for $P_{T,avg}$ normalized by $P_{T,bm}$ as a function of $R_{S,bal,bm}$ was generated for subsonic conditions (Figure 132). The following equation computes $P_{T,ts}$ for subsonic conditions ($R_{S,bal,bm} > 0.5330$):

$$P_{T,ts} = P_{T,bm}\left(B_0 + B_1 x + B_2 x^2\right), \quad \text{where } x = R_{S,bal,bm} \tag{6}$$

Coefficients, B_0 to B_2, are defined in Table 14. The subsonic total pressure in the bellmouth has nearly a 1:1 relationship with that in the test section, however, a correction is still beneficial upon closer inspection of the differences in $P_{T,avg}$ and $P_{T,bm}$. The maximum residual for the subsonic total pressure regression model is less than 0.0005 psia.

For supersonic conditions, a model using the average transonic array total pressure behind a normal shock ($P_{T,2,avg}$) normalized by $P_{T,bm}$ was generated as a function of $R_{S,bal,bm}$ (Figure 132). Only the three repeated nominal conditions at each flexwall setting were used in this regression model. The following equation computes the test section total pressure behind a normal shock:

$$P_{T,2} = P_{T,bm}\left(B_{S,0} + B_{S,1} x + B_{S,2} x^2 + B_{S,3} x^3\right), \quad \text{where } x = R_{S,bal,bm} \tag{7}$$

Coefficients, $B_{S,0}$ to $B_{S,3}$, are defined in Table 14. Similar to the static pressure supersonic calibration model, the residuals in Figure 132 show that the scatter among the residuals is much smaller than the actual value of the residuals. To incorporate the off-nominal balance chamber pressure settings into the calibration relationship for $P_{T,2}$, local calibration relationships at each flexwall setting were generated in Figure 133. The three repeat data points at the nominal settings of $R_{S,bal,bm}$ at each flexwall setting were averaged prior to forming the local regression models to avoid unevenly weighting the calibration relationships. The residuals in Figure 133 are much less than those in Figure 132, both of which have been converted into engineering units by multiplying by the appropriate value of $P_{T,bm}$ at each condition. The following is the equation for the local calibration relationships for $P_{T,2}$:

$$P_{T,2} = P_{T,bm}\left(B_{SX,0} + B_{SX,1} x\right), \quad \text{where } x = R_{S,bal,bm} \tag{8}$$

The coefficients $B_{SX,0}$ and $B_{SX,1}$ are defined in Table 17 as well as the range of $R_{S,bal,bm}$ over which the local calibration relationships are defined. An investigation of a potential correction to $P_{T,2}$ at each of the nominal balance chamber pressure settings was performed, but a correction was not applied due to the insignificance of such a correction. The scatter of the repeat points at several of the nominal balance chamber pressure settings is greater than or equal to the value of the potential correction. In practice, the total pressure calibration relationships are to be used in the same manner as described in Section 6.4.1.

TABLE 17.—CALIBRATION COEFFICIENTS FOR LOCAL TOTAL PRESSURE BEHIND NORMAL SHOCK REGRESSION MODELS IN 8- BY 6-FOOT SUPERSONIC WIND TUNNEL AT EACH NOMINAL FLEXWALL SETTING

[Table includes the approximate flexwall camshaft angle setting and range of balance chamber to bellmouth total pressure ratios, $R_{S,bal,bm}$, over which the local calibration models are applicable. All coefficients are only applicable to the 8- by 6-ft test section porosity configuration 1 (14-ft test section, 5.8-percent porosity). These coefficients are related to Revision 7 of the computing requirements for the CAL8X6 subroutine, dated August 4, 2020.]

Flexwall camshaft angle, FLEX, degree	Flexwall setting, M	$B_{SX,0}$	$B_{SX,1}$	Lower limit on $R_{S,bal,bm}$	Upper limit on $R_{S,bal,bm}$
190.4	2.0	0.73108612	–0.00559828	0.13588	0.14610
180.0	1.9	.77797437	–.00042005	.15728	.17595
167.7	1.8	.82509995	.00132309	.17810	.20515
154.3	1.7	.86171489	.03095261	.20899	.23199
138.8	1.6	.88562297	.07336468	.24180	.26783
121.3	1.5	.92164113	.05668395	.27815	.30707
101.3	1.4	.94082822	.07725645	.32019	.35277
80.3	1.3	.93914468	.11757274	.36584	.40232
67.6	1.2	.90199101	.21362504	.41402	.43579
48.1	1.1	1.01406980	–.03081111	.47788	.49018

6.4.3 Total Temperature

The calibration relationship for estimating $T_{T,ts}$ has a similar form to that of static and total pressure. The average transonic array total temperature ($T_{T,avg}$) normalized by the $T_{T,bm}$ as a function of $R_{S,bal,bm}$ is shown in Figure 134 for both subsonic and supersonic conditions. All temperatures must be in absolute units. Repeat data points for subsonic conditions were not used to create the subsonic regression model to prevent uneven weighting of the model. Only the three repeat data points acquired at the nominal supersonic conditions were used in creating the supersonic calibration relationship. The equations for the $T_{T,ts}$ regression models in Figure 134 for subsonic and supersonic operation, respectively, are

$$T_{T,ts} = T_{T,bm}\left(C_0 + C_1 x + C_2 x^2\right), \quad \text{where } x = R_{S,bal,bm} \tag{9}$$

$$T_{T,ts} = T_{T,bm}\left(C_{S,0} + C_{S,1} x + C_{S,2} x^2\right), \quad \text{where } x = R_{S,bal,bm} \tag{10}$$

The coefficients, C_0 to C_2 and $C_{S,0}$ to $C_{S,2}$, are defined in Table 14. Residuals were multiplied by the value of $T_{T,bm}$ at the corresponding condition in order to convert them to engineering units. This form of the equation was desirable as it accounts for day-to-day temperature variation through the normalization to $T_{T,bm}$ and also reflects the differences in thermal recovery from bellmouth to test section at varying airspeeds in the tunnel. This form is believed to be an improvement from the previous regression model where $T_{T,ts}$ was purely a function of $T_{T,bm}$.

The off-nominal balance chamber pressure settings at supersonic speeds were incorporated into the $T_{T,ts}$ calibration as shown in the local calibration relationships in Figure 135. The three repeat data points at the nominal settings of $R_{S,bal,bm}$ at each flexwall setting were averaged prior to forming the local

regression models to avoid unevenly weighting the local calibration relationship. The following equation is used to calculate $T_{T,ts}$ using the local relationships:

$$T_{T,ts} = T_{T,bm}\left(C_{SX,0} + C_{SX,1}x\right), \quad \text{where } x = R_{S,bal,bm} \tag{11}$$

The coefficients $C_{SX,0}$ and $C_{SX,1}$ are defined in Table 18 as well as the range of $R_{S,bal,bm}$ over which the local calibration relationships are defined. The residuals in Figure 135, also converted to engineering units, are noticeably lower at the higher supersonic Mach numbers than those in Figure 134. A correction to the nominal supersonic conditions, as done with the static pressure regression models, would be on the order of 0.1 °F. Because thermocouples were used to make these measurements, it is not believed that this scale of a correction would be significant relative to instrumentation accuracies. Additionally, there is relatively more scatter seen in the total temperature residuals than with the residuals for either static or total pressure. These $T_{T,ts}$ regression models are applied in the same manner described in Section 6.4.2.

The calculations for test section Mach number, freestream total pressure at supersonic conditions, and all other pertinent flow parameters of interest (i.e., test section dynamic pressure, Reynolds number, etc.) are shown in Reference 3. A summary of the inputs and outputs for the computing requirements described in this section is shown in Table 19 (some different inputs and outputs are used for solid-wall, supersonic test section configuration but not listed in Table 19, see Ref. 7 for omitted variables). A table of the typical operating conditions in the 8- by 6-ft test section for test section porosity configuration 1 (14-ft test section, 5.8-percent porosity), as computed using the data reduction process discussed in this section, is included in Table 20.

TABLE 18.—CALIBRATION COEFFICIENTS FOR LOCAL TOTAL TEMPERATURE REGRESSION MODELS IN 8- BY 6-FOOT SUPERSONIC WIND TUNNEL AT EACH NOMINAL FLEXWALL SETTING

[Table includes the approximate flexwall camshaft angle setting and range of balance chamber to bellmouth total pressure ratios, $R_{S,bal,bm}$, over which the local calibration models are applicable. All coefficients are only applicable to the 8- by 6-ft test section porosity configuration 1 (14-ft test section, 5.8-percent porosity). These coefficients are related to Revision 7 of the computing requirements for the CAL8X6 subroutine, dated August 4, 2020.]

Flexwall camshaft angle, FLEX, degree	Flexwall setting, M	$C_{SX,0}$	$C_{SX,1}$	Lower limit on $R_{S,bal,bm}$	Upper limit on $R_{S,bal,bm}$
190.4	2.0	0.998415131	–0.004307385	0.13588	0.14610
180.0	1.9	.998322539	–.000607545	.15728	.17595
167.7	1.8	1.001078785	–.008072632	.17810	.20515
154.3	1.7	.999985621	.003217682	.20899	.23199
138.8	1.6	1.001071385	.003259345	.24180	.26783
121.3	1.5	1.006312344	–.011136227	.27815	.30707
101.3	1.4	1.003447817	.001980710	.32019	.35277
80.3	1.3	.998173710	.016862145	.36584	.40232
67.6	1.2	1.003477817	.004161122	.41402	.43579
48.1	1.1	1.005697304	.000039983	.47788	.49018

TABLE 19.—SUMMARY OF PARAMETERS USED TO DETERMINE TRANSONIC TEST SECTION AEROTHERMAL CONDITIONS IN 8- BY 6-FOOT SUPERSONIC WIND TUNNEL SUPERSONIC TEST SECTION

Parameter	Data system program name	Description	Units	Source
Inputs—facility measurements and operational settings				
$P_{T,bm}$	APTBM	Bellmouth total pressure	psia	Input
$P_{S,bal}$	APSBAL	Balance chamber static pressure	psia	Input
$T_{T.bm}$	ATTBM	Bellmouth total temperature	R	Input
FLEX	FLEX	Flexwall camshaft angle	Degree	Input
TSCFG	TSCFG	Test section configuration	None	Input
Test section conditions—calculated prior to calibrated flow parameters				
$R_{S,bal,bm}$	RSBALBM	Ratio of balance chamber static to bellmouth total pressure	Dimensionless	Calculation
Test section conditions—calibrated flow parameters—subsonic				
$P_{S,ts}$	PSTS	Test section static pressure	psia	Calibration
$P_{T,ts}$	PTTS	Test section total pressure	psia	Calibration
$T_{T,ts}$	TTTS	Test section total temperature	R	Calibration
Test section conditions—calibrated flow parameters—supersonic				
$P_{S,ts}$	PSTS	Test section static pressure	psia	Calibration
$P_{T,2}$	PTTS2	Test section total pressure downstream of a normal shock	psia	Calibration
$T_{T,ts}$	TTTS	Test section total temperature	R	Calibration
Test section conditions—calculations for supersonic flow only				
$P_{T,ts}$	PTTS	Test section total pressure	psia	Calculation
Test section condition—calculated flow parameters				
M_{ts}	MTS	Test section Mach number	Dimensionless	Calculation
$T_{S,ts}$	TSTS	Test section static temperature	R	Calculation
V_{ts}	VTS	Test section airspeed	ft/s	Calculation
ρ_{ts}	RHOTS	Test section air density	slug/ft^3	Calculation
μ_{ts}	MUTS	Test section air viscosity	slug/(ft·sec)	Calculation
Re_{ts}	REFT	Test section Reynolds number per ft	10^6/ft	Calculation
q_{ts}	QTS	Test section dynamic pressure	psia	Calculation
Constants and coefficients				
γ	GAMMA	Ratio of specific heats = 1.4	Dimensionless	Constant
R	R	Gas constant = 1,716.49	lbf-ft/(slug·R)	Constant
A_0 to A_2	A0–A2	Subsonic static pressure calibration	Dimensionless	Calibration coefficients/ corrections
$A_{S,0}$ to $A_{S,3}$	AS0–AS3	Supersonic static pressure calibration		
$A_{SX,0}$ to $A_{SX,2}$	ASX0–ASX2	Supersonic local static pressure calibration		
Correction	Correction	Supersonic local static pressure correction		
B_0 to B_3	B0–B3	Subsonic total pressure calibration		
$B_{S,0}$ to $B_{S,3}$	BS0–BS3	Supersonic total pressure calibration		
$B_{SX,0}$ to $B_{SX,1}$	BSX0–BSX1	Supersonic local total pressure calibration		
C_0 to C_2	C0–C2	Subsonic total temperature calibration		
$C_{S,0}$ to $C_{S,2}$	CS0–CS2	Supersonic total temperature calibration		
$C_{SX,0}$ to $C_{SX,1}$	CSX0–CSX1	Supersonic local total temperature calibration		

TABLE 20.—TYPICAL TEST SECTION CONDITIONS IN 8- BY 6-FOOT SUPERSONIC WIND TUNNEL FOR TEST SECTION CONFIGURATION 1 (14-ft TEST SECTION, 5.8-PERCENT POROSITY)

[All values computed from facility measurements acquired during 4-in.-diameter cone cylinder runs during the 2019 test entry.]

Nominal Mach number	Test section Mach number, M_{ts}	Test section total pressure, $P_{T,ts}$		Test section static pressure, $P_{S,ts}$		Test section dynamic pressure, q_{ts}		Test section total temperature, $T_{T,ts}$, R	Test section static temperature, $T_{S,ts}$, R	Reynolds number per unit length, 10^6/ft
		psia	psfa	psia	psfa	psia	psfa			
Three-drive-motor operation										
2.0	1.989	24.444	3,519.9	3.178	457.7	8.801	1,267.3	646.6	361.0	4.918
1.9	1.891	23.956	3,449.7	3.623	521.8	9.073	1,306.5	646.1	376.6	5.035
1.8	1.792	22.563	3,249.0	3.976	572.6	8.936	1,286.8	638.0	388.5	5.021
1.7	1.663	20.951	3,016.9	4.488	646.2	8.687	1,250.9	629.6	405.4	4.969
1.6	1.553	19.771	2,847.1	4.985	717.8	8.417	1,212.0	622.0	419.6	4.925
1.5	1.457	18.984	2,733.7	5.501	792.2	8.175	1,177.3	615.0	431.7	4.912
1.4	1.355	18.133	2,611.1	6.064	873.2	7.799	1,123.1	607.9	444.6	4.847
1.3	1.252	17.382	2,503.0	6.689	963.2	7.344	1,057.6	601.8	458.1	4.750
1.2	1.184	17.518	2,522.6	7.375	1,062.1	7.238	1,042.3	598.1	467.1	4.827
1.1	1.073	17.299	2,491.1	8.375	1,206.0	6.751	972.1	597.5	485.7	4.723
.95	.951	16.569	2,385.9	9.256	1,332.9	5.863	844.3	590.1	499.7	4.461
.90	.901	16.677	2,401.5	9.855	1,419.1	5.594	805.6	591.6	509.0	4.391
.85	.850	16.700	2,404.8	10.415	1,499.7	5.265	758.1	590.4	515.9	4.305
.80	.800	17.002	2,448.3	11.151	1,605.7	4.999	719.8	591.8	524.6	4.248
.75	.750	17.171	2,472.6	11.820	1,702.1	4.658	670.7	593.5	533.4	4.133
.70	.700	17.390	2,504.2	12.534	1,804.9	4.302	619.6	593.2	540.2	4.026
.65	.650	17.496	2,519.5	13.170	1,896.4	3.897	561.2	592.0	545.8	3.876
.60	.600	17.340	2,497.0	13.594	1,957.5	3.427	493.5	589.1	549.5	3.662
.55	.551	17.038	2,453.5	13.866	1,996.6	2.943	423.7	582.9	549.6	3.426
.50	.500	16.817	2,421.7	14.174	2,041.1	2.484	357.7	577.5	549.9	3.180
.45	.450	16.643	2,396.6	14.480	2,085.1	2.057	296.2	572.9	550.6	2.920
.40	.400	16.516	2,378.2	14.790	2,129.7	1.659	238.8	569.9	552.2	2.641
.36	.368	16.388	2,359.8	14.921	2,148.7	1.418	204.2	567.0	552.0	2.454
One-drive-motor operation										
0.50	0.501	15.692	2,259.6	13.220	1,903.7	2.322	334.4	564.6	537.6	3.056
.45	.451	15.498	2,231.7	13.481	1,941.3	1.917	276.1	560.4	538.5	2.798
.40	.401	15.152	2,181.8	13.562	1,953.0	1.527	219.9	554.8	537.5	2.511
.35	.350	15.021	2,163.0	13.800	1,987.1	1.185	170.6	550.9	537.7	2.230
.30	.300	15.093	2,173.4	14.177	2,041.4	.896	129.0	549.3	539.6	1.956
.25	.250	15.203	2,189.2	14.558	2,096.3	.635	91.4	548.4	541.6	1.661

6.5 Transonic Quick-Check Rake

The check calibration program for the 8×6 SWT was initiated through collection of data across the operating envelope of the facility during the 2019 characterization test entry. This is expected to be the

first of many entries with the transonic quick-check rake with the same probe configuration and test processes to monitor stability of the calibration relationships established during this entry for test section configuration 1 (14-ft test section, 5.8-percent porosity). The assumption inherent in only checking the calibration of a single porosity configuration is that a deviation in the calibration in one configuration would be evident in the other porosity configurations, as well.[16]

As the goal of the check calibrations is to monitor calibration relationship health, the three calibrated flow parameters, static and total pressure and total temperature, were analyzed. The residuals (difference is measured from computed calibrated test section flow parameter) and the range of these residuals for repeated conditions are shown for static and total pressure and total temperature in Figure 136 to Figure 138, respectively, for supersonic and subsonic operation. It is beneficial to attempt to understand the reason for the trends present in the check calibration data, however, the repeatability of the measurements within test and test to test is more beneficial to the goals of the entry. The range of the residuals at repeated conditions aims to answer the question of within-test variation. Expected test-to-test variation will not be available until additional entries are completed in the future.

For static pressure (Figure 136), the residuals are typically larger near Mach 1.0. For low supersonic Mach numbers, this could be expected as the steeper shock angles at these conditions and instrumentation proximity (6-in. probe separation) could affect static pressure measurements. Recall that the transonic array static pressures showed signs of probe-to-probe interference at similar low supersonic speeds. The relatively higher residuals at Mach 0.80 and 0.90 could be due to probe-to-probe interference or back pressure from the rake body. At subsonic conditions, the residuals approach zero as the Mach number decreases. Similarly, the variation of repeated subsonic conditions is larger at transonic conditions. Mach 1.2 showed a much larger range of residuals likely due to the presence of shocks from adjacent probes impacting near the static pressure ports on the flow angle and static probes.

Residuals of the measured postnormal shock total pressure by the transonic quick-check rake's flow-angle and pitot probes (Figure 137) were significantly larger at Mach 1.9 and 2.0 due to the separation at the compressor exit tailcone, as discussed in the transonic array's total pressure survey results. The transonic array's off-centerline pressure probes dampen the effect of this separation in the value of $P_{T,2,avg}$. Comparison of the total pressure data acquired at the centerline probe on the array would likely agree more closely with that of the quick-check rake. At subsonic conditions, the residuals for total pressure typically decrease with decreasing Mach number. The range of these residuals (within-test variation) are less than or equal to 0.001 psia at all subsonic conditions.

The total temperature residuals, as measured by the three thermocouple probes on the transonic quick-check rake (Figure 138), show the same counterintuitive trend in the total temperature vertical distribution in the test section. The topmost thermocouple on the quick-check rake shows a relatively lower total temperature than that measured at the middle and bottom probe across the facility operating range. This observation is evidence against an installation bias causing the vertical variation observed in the transonic array's temperature data. As this spatial temperature variation may be of interest as a variable to track over time, the range of the measured total temperature on the three thermocouple probes at each reading is shown in Figure 139. This figure gives the spatial variation in temperature between 6 in. above and 18 in. below centerline in the test section. The quick-check rake total temperature, $T_{T,QCR,}$ spatial variation decreases from Mach 2.0 to 1.4 and is then relatively constant below Mach 1.4.

[16]The exception to this assumption potentially being the supersonic test section configuration (configuration 7) as it is further removed from the tunnel porosity and uses static pressure measured in the solid-wall test section as opposed to balance chamber pressure in the calibration relationships.

Despite not being a calibrated parameter, flow angle is also a potentially valuable variable to track as part of the check calibration program. Figure 140 shows the pitch and yaw flow angles as a function of the balance chamber static to bellmouth total pressure ratio. This figure also shows the within-test variation of the flow angles as measured across repeated conditions. The pitch flow angles are approximately between 0° and 0.25° at supersonic conditions and between 0.4° and 0.7° at subsonic conditions. The yaw flow angles at supersonic conditions are more varied (between –0.2° and 0.5°) and between 0.2° and 0.5° at subsonic conditions. An in situ ESP calibration occurred between collection of data at Mach 1.4 and 1.3 during the first sweep of supersonic conditions that caused a bias on one or more of the pressures used to determine yaw flow angle. These data points were removed from Figure 140; there are only two repeat conditions for flow angles measured between Mach 2.0 and 1.4 (inclusive). For supersonic and subsonic conditions, variations of pitch and yaw across repeats are 0.06° or less except for Mach 1.1 and 1.2 flexwall settings. The lack of a flat on the flexwall cams at these two supersonic Mach number settings could be the cause of the slightly increased flow angle variation observed at Mach 1.1 and 1.2.

In looking forward to the creation of statistical process control charts, one approach would be to track the residuals of each flow parameter, the flow angles, and variation across repeats at each facility setting surveyed. Another potential method, as used with instrumentation and balances (Ref. 8), would be to create regression models of the three calibrated flow parameters, similar in form to those presented in this report, and track the coefficients across check calibration test entries. As additional check calibration datasets are collected, this second method's usefulness will be assessed while the first method is primarily used.

7.0 Summary of Results

The following is a summary of the primary results from this test entry specifically related to the objectives stated in this report:

1. The 14-ft, 5.8-percent porosity configuration of the 8×6 SWT test section was calibrated across the facility's operating range. This includes calibration relationships for test section static pressure, total pressure (subsonic), total pressure aft of a normal shock (supersonic), and total temperature. Off-nominal supersonic conditions were characterized and incorporated into the relationships, as well. The subroutine for calculating test section conditions in the porous test section has been modified with the regression models defined in this report.
2. Data were acquired with the 4-in. cone cylinder to characterize the streamwise static pressure in the porous test section, and transonic array data were acquired at centerline and 1 ft above and below centerline to characterize the flow quality in this region of the tunnel, including total pressure, total temperature, and flow angularity.
    a. The static pressure and Mach number streamwsie gradients were surveyed by the aft portion of the 4-in. cone cylinder at nominal and off-nominal supersonic operating conditions and over the full range of subsonic conditions. The streamwise gradients are typically worse at off-nominal conditions when compared to nominal supersonic data.
    b. Total pressure and Mach number variation, as measured by the transonic array, show very similar trends as static pressure is assumed constant across the array. Mach number variation (standard deviation) in the core of the test section is about 0.025 Mach at a flexwall setting of 1.9. Variation levels are typically between 0.003 and 0.010 Mach at other nominal supersonic operating conditions surveyed. Subsonic Mach number spatial variation across the core of the test section is between 0.0007 and 0.0003 Mach.

c. Total temperature variation across the core of the test section, as measured by the transonic array, is between 2 and 5 °F at nominal supersonic and subsonic conditions. The temperature at the center of the test section is typically higher than the temperature nearer the tunnel walls across the operating range of the facility with the profile gradually flattening at the lower subsonic conditions.
d. The pitch and yaw flow angles measured by the transonic array across the core of the test section are typically ±0.50° or less for nominal supersonic operation and ±0.25° or less for subsonic operation.

3. The nominal and off-nominal ratios of balance chamber static to bellmouth total pressure at each supersonic flexwall setting were surveyed with the 4-in. cone cylinder and transonic array. Data from these surveys were used to generate local calibration relationships for test section static pressure, postnormal shock total pressure, and total temperature for a given flexwall setting. The flow quality in the porous test section, as measured by the cone cylinder and transonic array during this test entry, was degraded in multiple aspects by increasing or decreasing the balance chamber pressure away from the nominal settings. The wind tunnel characterization team suggests that customers continue to utilize the nominal supersonic operational settings; the nominal supersonic facility settings, not altered from historically determined values, were chosen for their relatively superior flow quality. Data from the 2019 test entry supports this choice. Risks of venturing away from the nominal supersonic facility settings include increased uncertainty in calibrated test section conditions and a less uniform flow field.
4. At each flexwall setting (Mach 1.1 to 2.0 in 0.1 increments), three data points were acquired with the 4-inch-diameter cone cylinder and transonic array at the nominal balance chamber pressure setting for that flexwall position to increase fidelity of the calibration relationships and decrease uncertainty. Three data points were acquired at several subsonic conditions (Mach 0.90, 0.70, and 0.50 for three-drive-motor operation; Mach 0.45 and 0.30 for one-drive-motor operation), as well, to aid in estimation of random uncertainty across the subsonic operating range. The facility was brought off-condition before returning to a condition to acquire repeat data. A thorough uncertainty analysis using results from the 2019 test entry will update the estimates in Reference 2 for 8×6 SWT flow parameter uncertainties and contributions from various sources.
5. A check calibration test entry was completed with the transonic quick-check rake across the operating range of the facility, including acquisition of repeat data at each nominal supersonic flexwall setting and several subsonic conditions (Mach 0.90, 0.70, and 0.50 for three-drive-motor operation; Mach 0.30 for one-drive-motor operation). Creation of statistical process control charts will commence following the collection of additional datasets from future check calibration test entries.

8.0 Concluding Remarks

A characterization test entry in the NASA Glenn Research Center 8- by 6-Foot Supersonic Wind Tunnel (8×6 SWT) porous test section was completed in 2019. This was the first characterization of the test section since the completion of the 9- by 15-Foot Low-Speed Wind Tunnel acoustic improvement modifications project. This entry provided data used to create calibration relationships for facility operation, as well as an understanding of the flow field in the transonic test section. The following are recommendations for future work or operational considerations per results of this test entry:

1. There is a general lack of turbulence data for the 8- by 6-ft test section (porous and solid-wall). The importance of this type of information to future facility customers should be investigated and, if

appropriate, this measurement should be an objective and priority of a future characterization test entry of the 8×6 SWT.

2. Supersonic operation at off-nominal ratios of balance chamber to bellmouth total pressure is characterized to a certain degree through the results of this test entry but still not a preferred method of operating the facility. Operation at the nominal supersonic operational settings achieves relatively superior flow quality in multiple aspects and should be the suggested method of supersonic operation for future customer tests to ensure data fidelity.
3. Gathering axial pressure profile data is plagued by the reflected oblique shock waves generated from the 4-inch-diameter cone cylinder's cone tip, primarily at the lower supersonic Mach numbers. It is suggested that a new static pressure profile characterization tool be designed and fabricated for any future characterization of the 8×6 SWT.
4. The aerothermal characterization testing in the 8×6 SWT should be a recurring activity with periodic checks of the calibration to ensure a stable and repeatable flow field for future customer testing.
5. Test customers for the 8×6 SWT should be briefed on tunnel operation and test section flow quality to make them aware of nuances of testing in this facility. For example, a nominal flexwall Mach number setting of Mach 1.5 produces an average transonic test section Mach number of 1.457. This trend of actual Mach number being less than nominal is present in both the porous and solid-wall test sections and across the supersonic operating range for each test section.

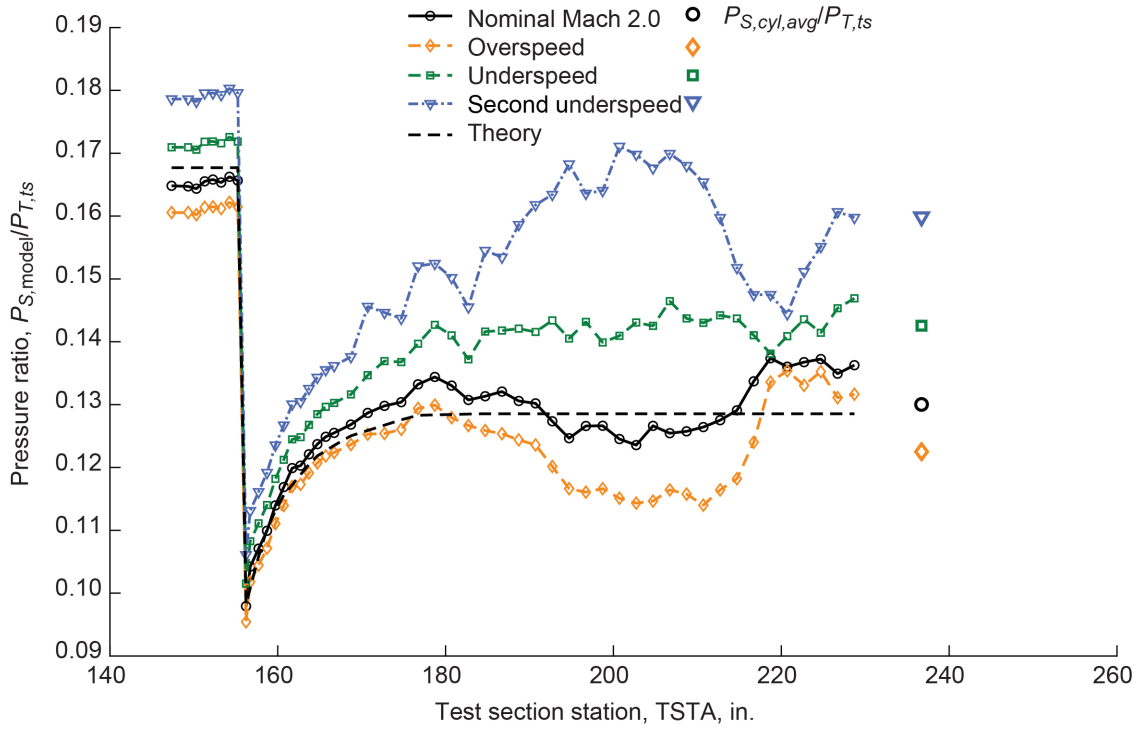

Figure 14.—Axial static pressure distributions along 4-inch-diameter cone cylinder with cone tip at test section station 144.375 in 8- by 6-ft test section. Data acquired during 2019 test section characterization entry at flexwall setting of Mach 2.0.

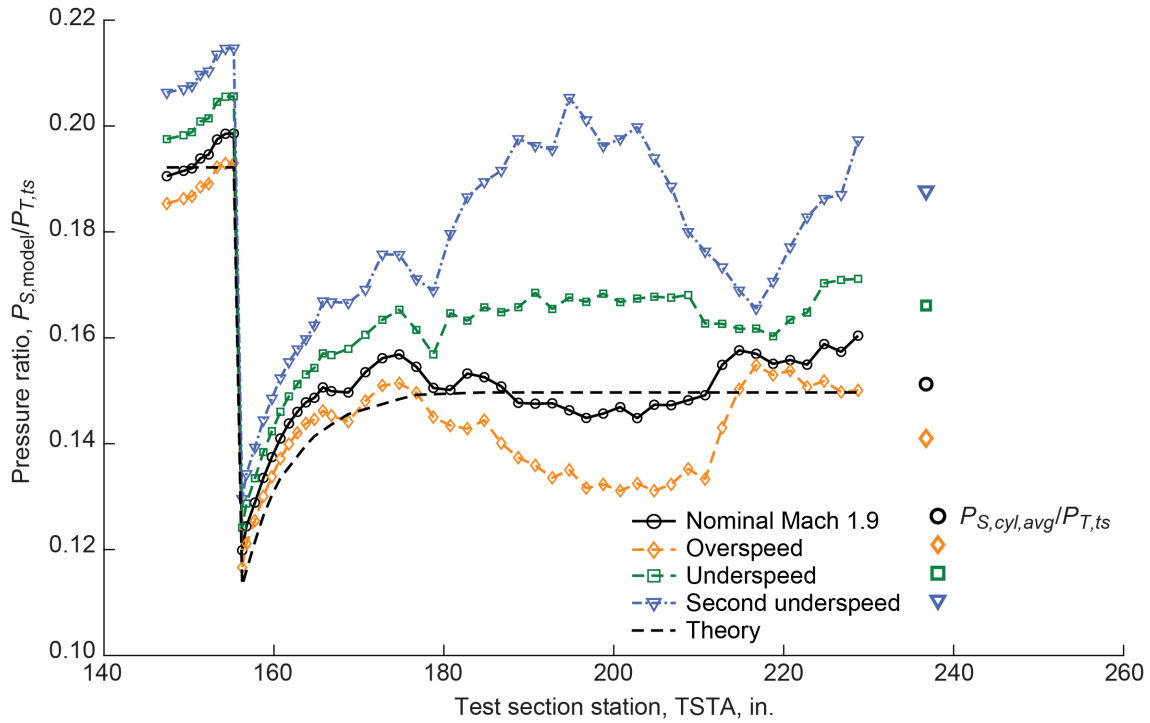

Figure 15.—Axial static pressure distributions along 4-inch-diameter cone cylinder with cone tip at test section station 144.375 in 8- by 6-ft test section. Data acquired during 2019 test section characterization entry at flexwall setting of Mach 1.9.

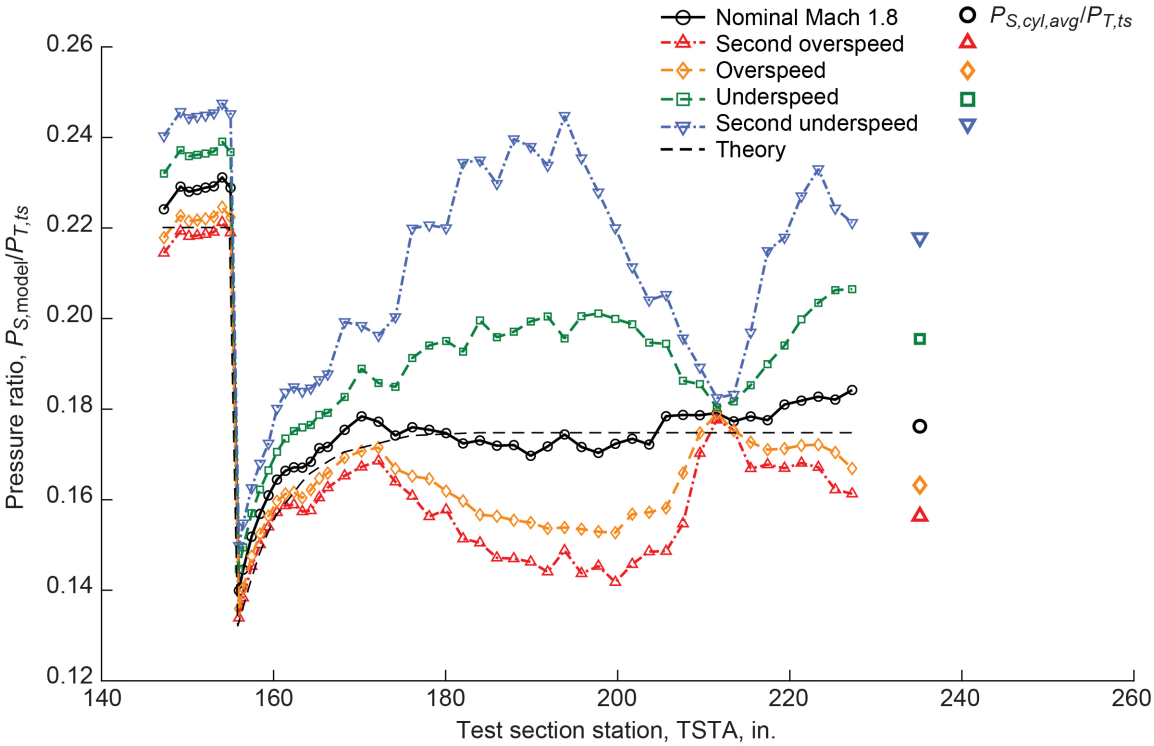

Figure 16.—Axial static pressure distributions along 4-inch-diameter cone cylinder with cone tip at test section station 144.375 in 8- by 6-ft test section. Data acquired during 2019 test section characterization entry at flexwall setting of Mach 1.8.

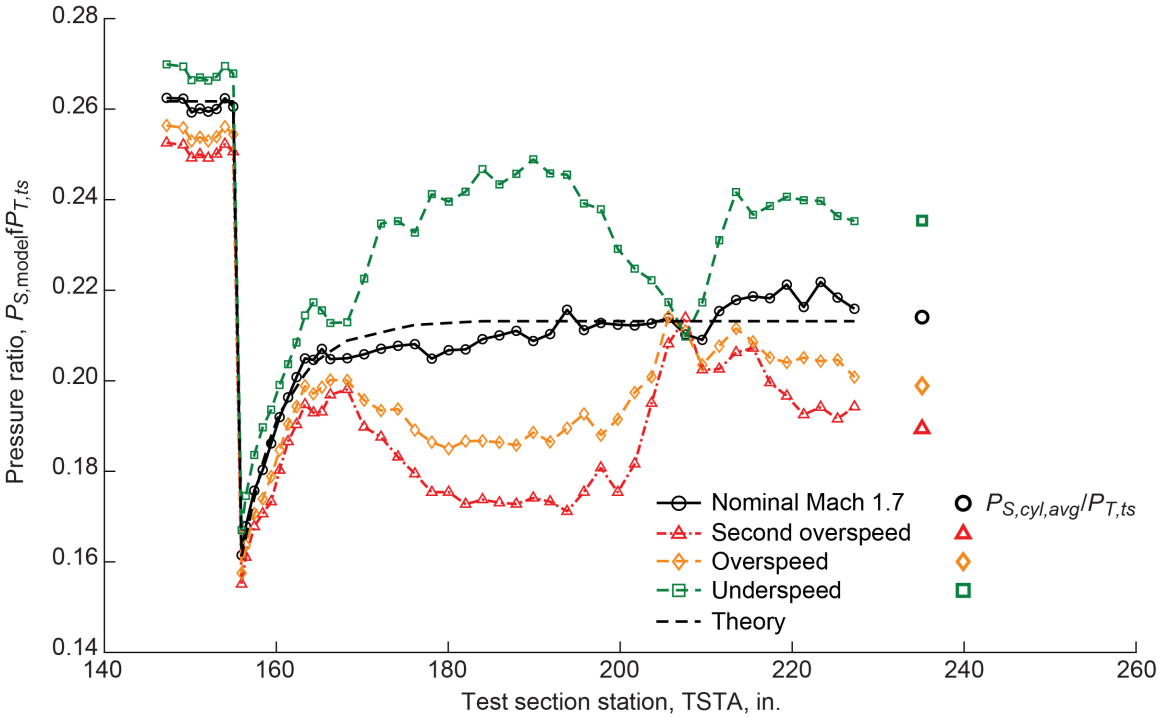

Figure 17.—Axial static pressure distributions along 4-inch-diameter cone cylinder with cone tip at test section station 144.375 in 8- by 6-ft test section. Data acquired during 2019 test section characterization entry at flexwall setting of Mach 1.7.

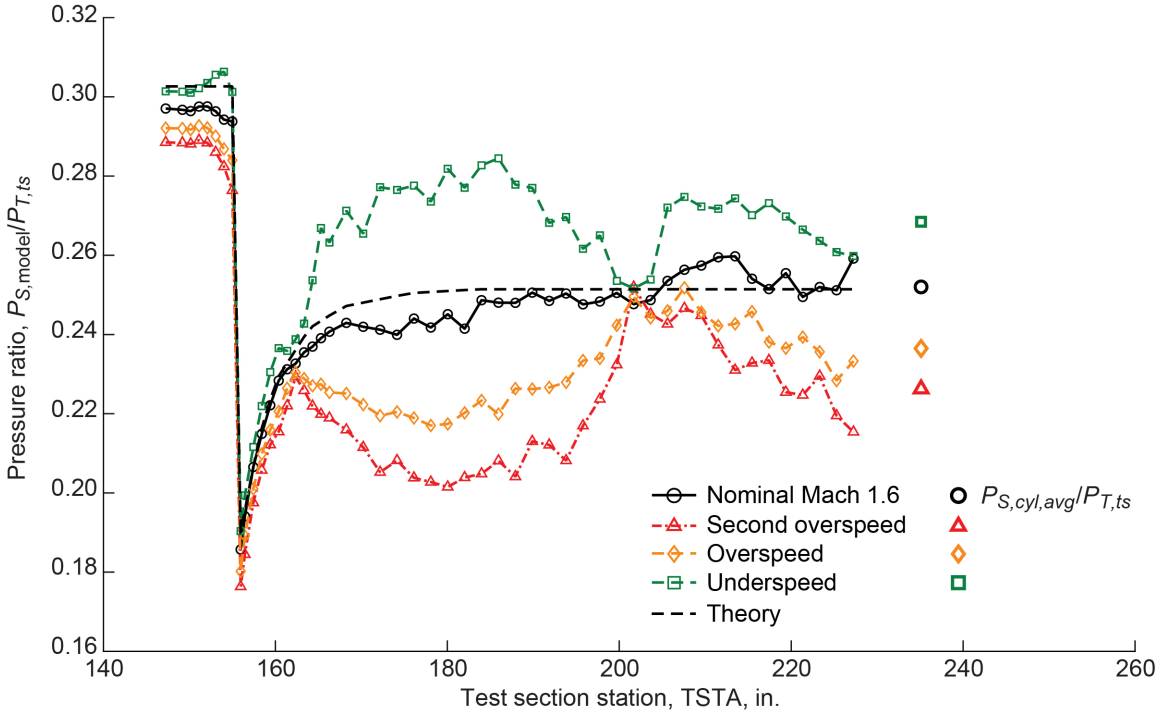

Figure 18.—Axial static pressure distributions along 4-inch-diameter cone cylinder with cone tip at test section station 144.375 in 8- by 6-ft test section. Data acquired during 2019 test section characterization entry at flexwall setting of Mach 1.6.

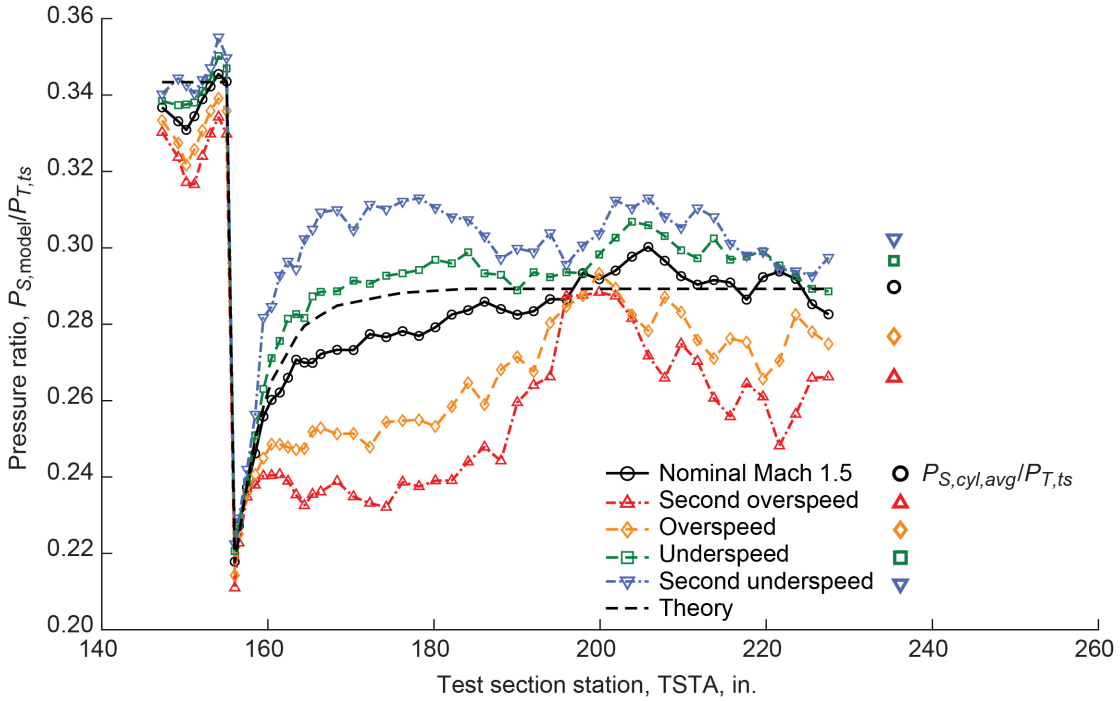

Figure 19.—Axial static pressure distributions along 4-inch-diameter cone cylinder with cone tip at test section station 144.375 in 8- by 6-ft test section. Data acquired during 2019 test section characterization entry at flexwall setting of Mach 1.5.

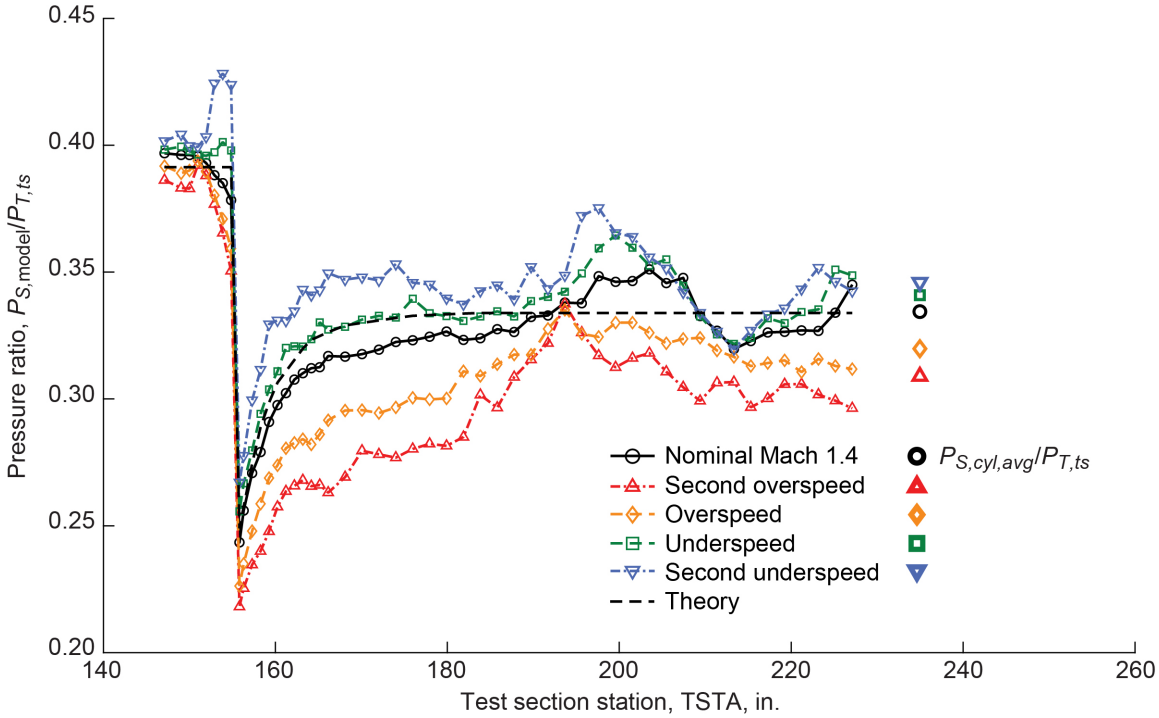

Figure 20.—Axial static pressure distributions along 4-inch-diameter cone cylinder with cone tip at test section station 144.375 in 8- by 6-ft test section. Data acquired during 2019 test section characterization entry at flexwall setting of Mach 1.4.

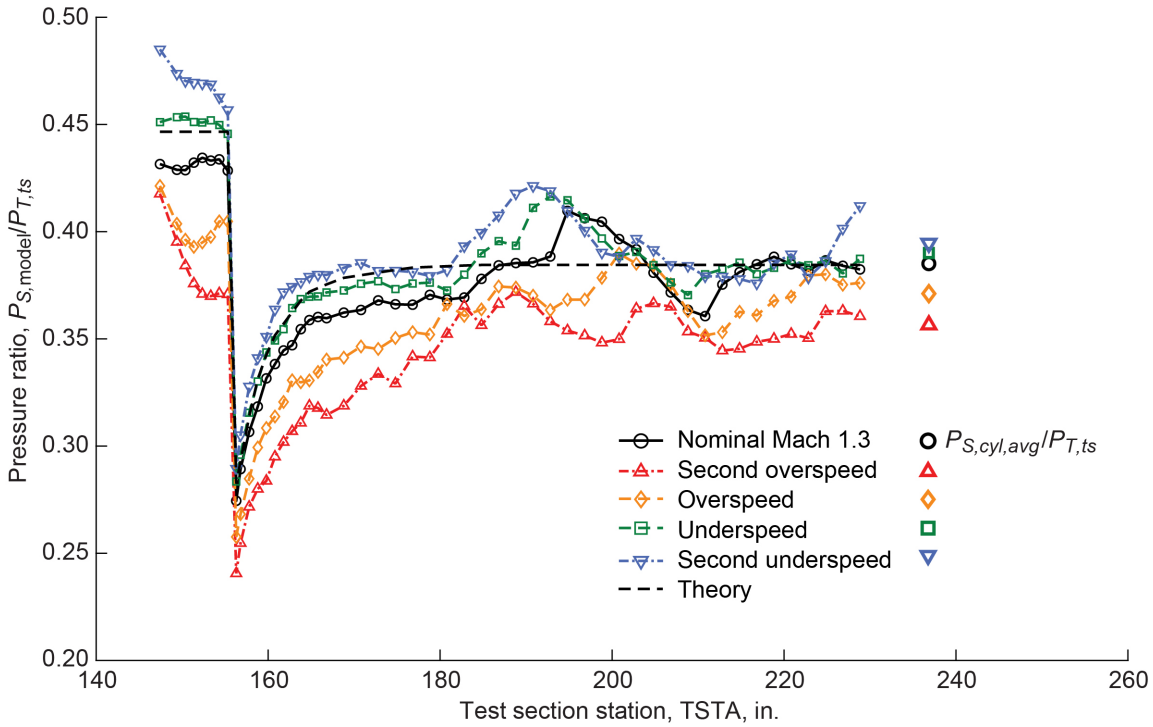

Figure 21.—Axial static pressure distributions along 4-inch-diameter cone cylinder with cone tip at test section station 144.375 in 8- by 6-ft test section. Data acquired during 2019 test section characterization entry at flexwall setting of Mach 1.3.

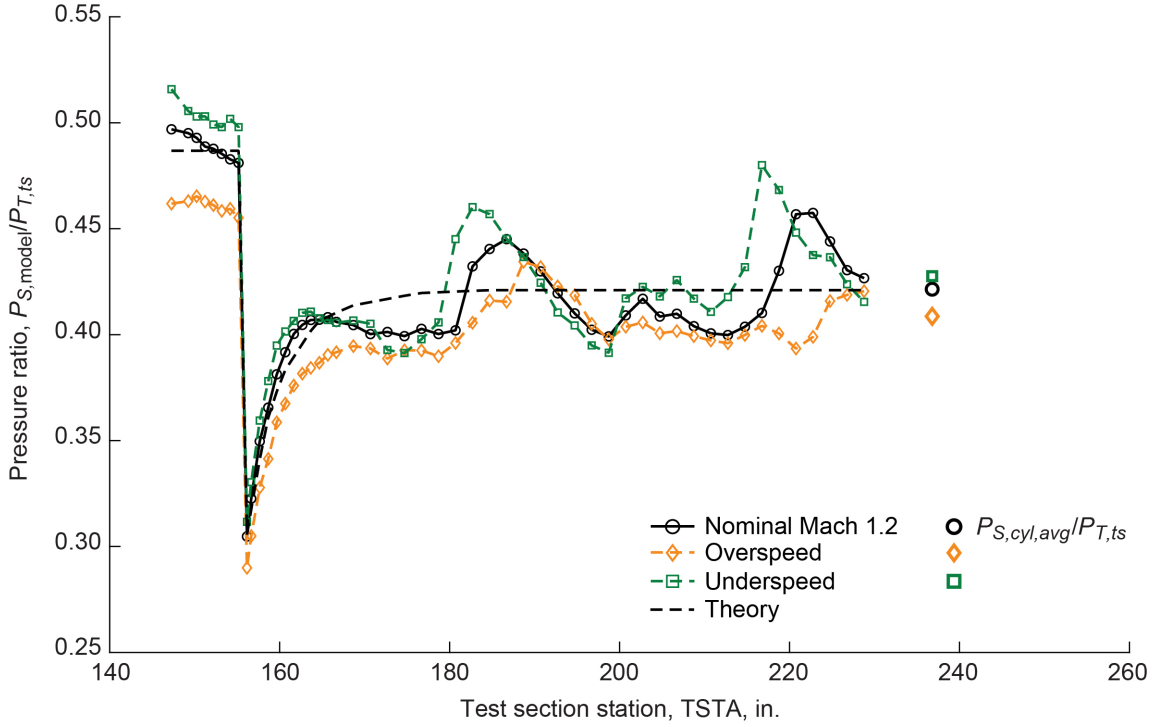

Figure 22.—Axial static pressure distributions along 4-inch-diameter cone cylinder with cone tip at test section station 144.375 in 8- by 6-ft test section. Data acquired during 2019 test section characterization entry at flexwall setting of Mach 1.2.

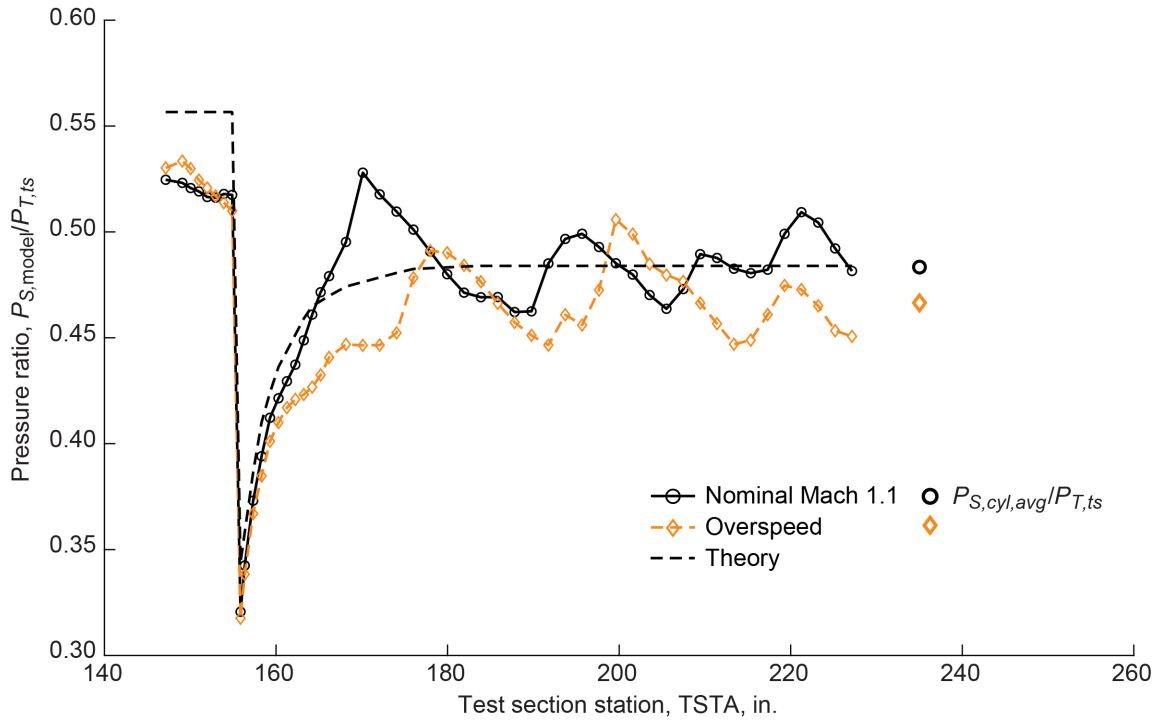

Figure 23.—Axial static pressure distributions along 4-inch-diameter cone cylinder with cone tip at test section station 144.375 in 8- by 6-ft test section. Data acquired during 2019 test section characterization entry at flexwall setting of Mach 1.1.

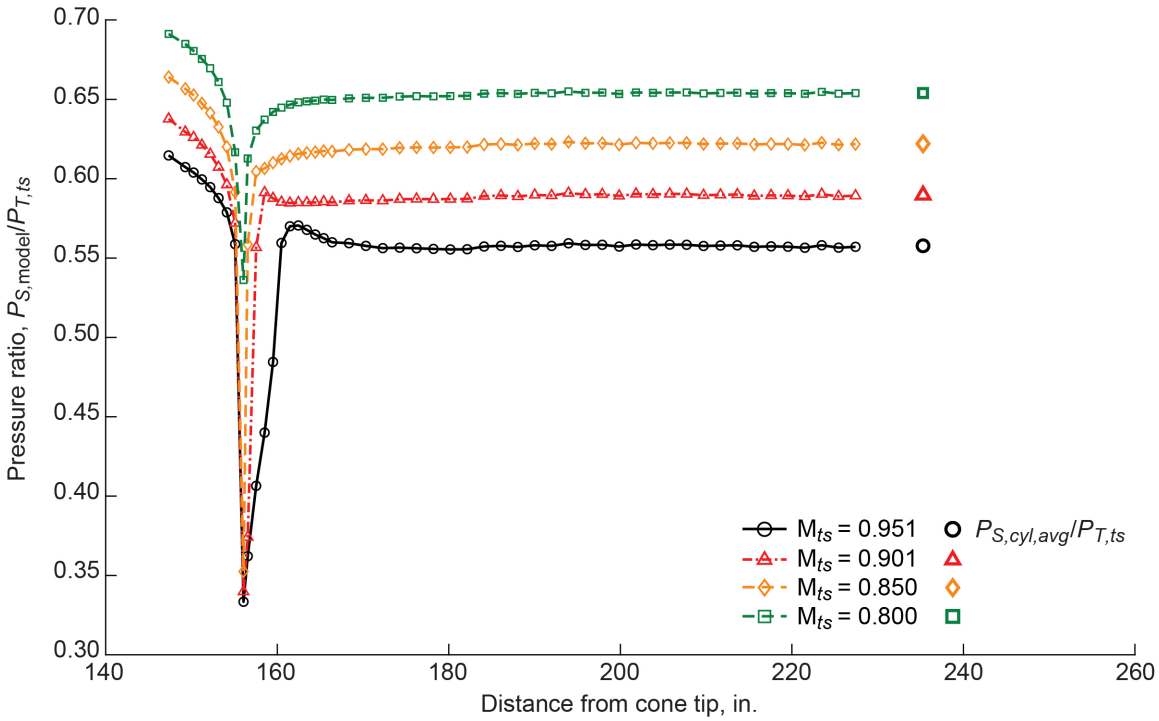

Figure 24.—Axial static pressure distributions along 4-inch-diameter cone cylinder with cone tip at test section station 144.375 in 8- by 6-ft test section. Data acquired during 2019 test section characterization entry at subsonic conditions between Mach 0.951 and 0.800.

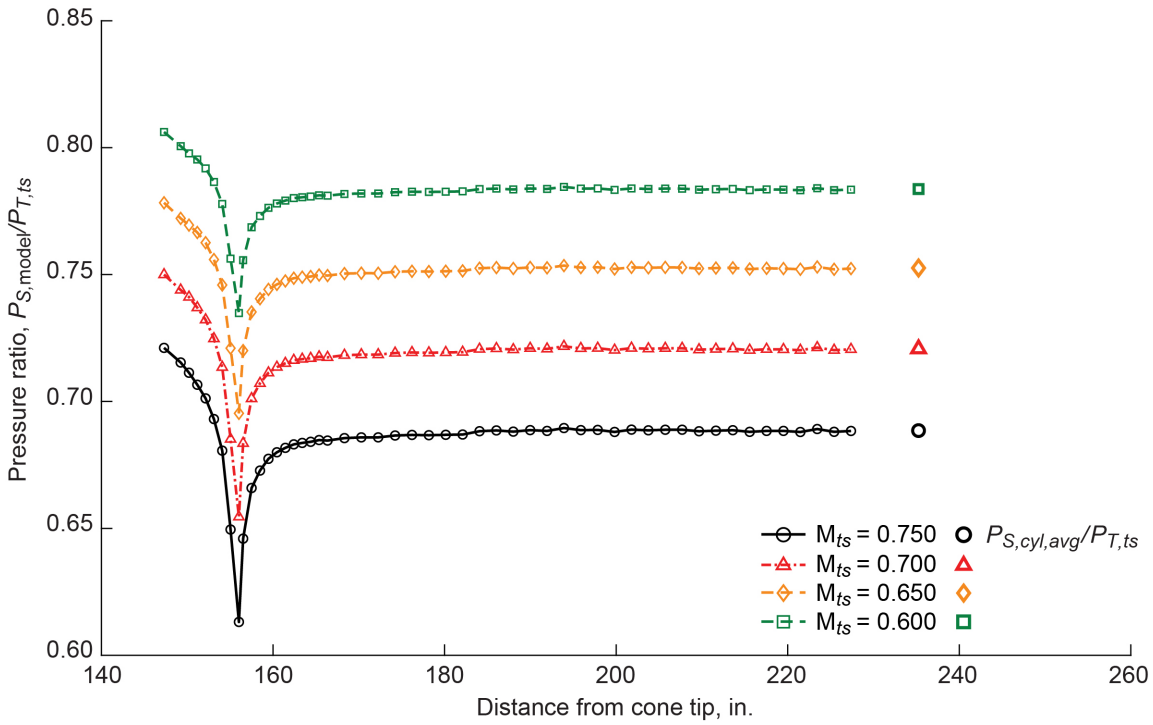

Figure 25.—Axial static pressure distributions along 4-inch-diameter cone cylinder with cone tip at test section station 144.375 in 8- by 6-ft test section. Data acquired during 2019 test section characterization entry at subsonic conditions between Mach 0.750 and 0.600.

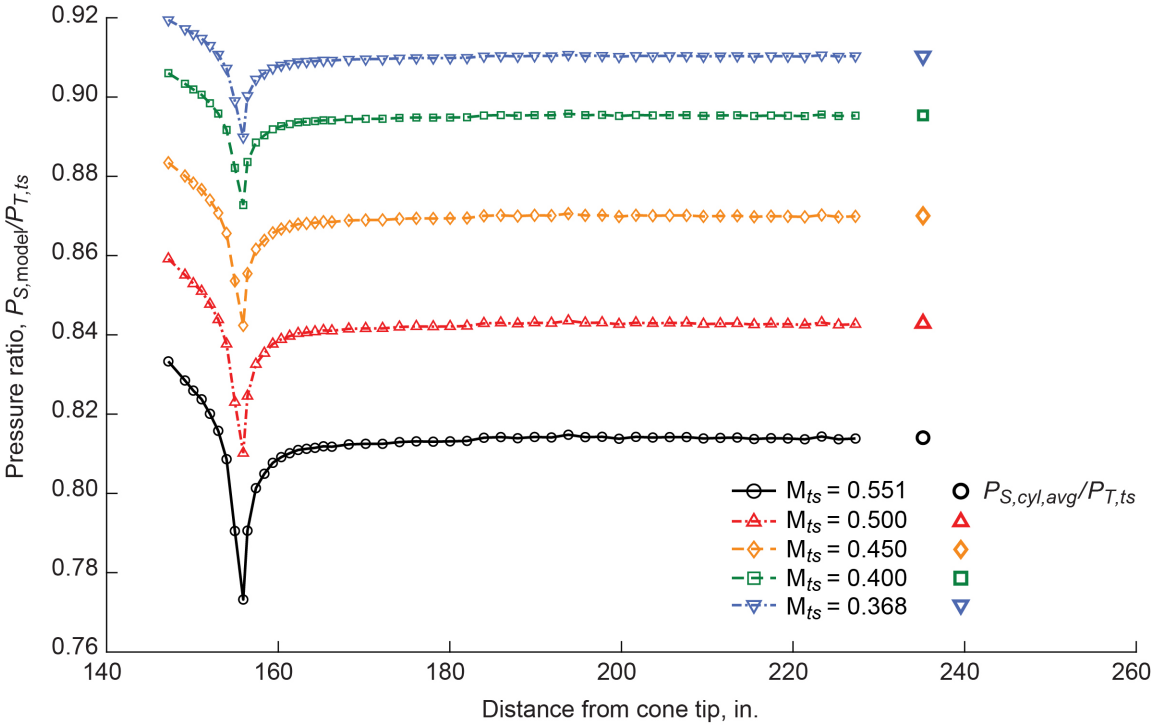

Figure 26.—Axial static pressure distributions along 4-inch-diameter cone cylinder with cone tip at test section station 144.375 in 8- by 6-ft test section. Data acquired during 2019 test section characterization entry at subsonic conditions between Mach 0.551 and 0.368 (three-drive-motor operation).

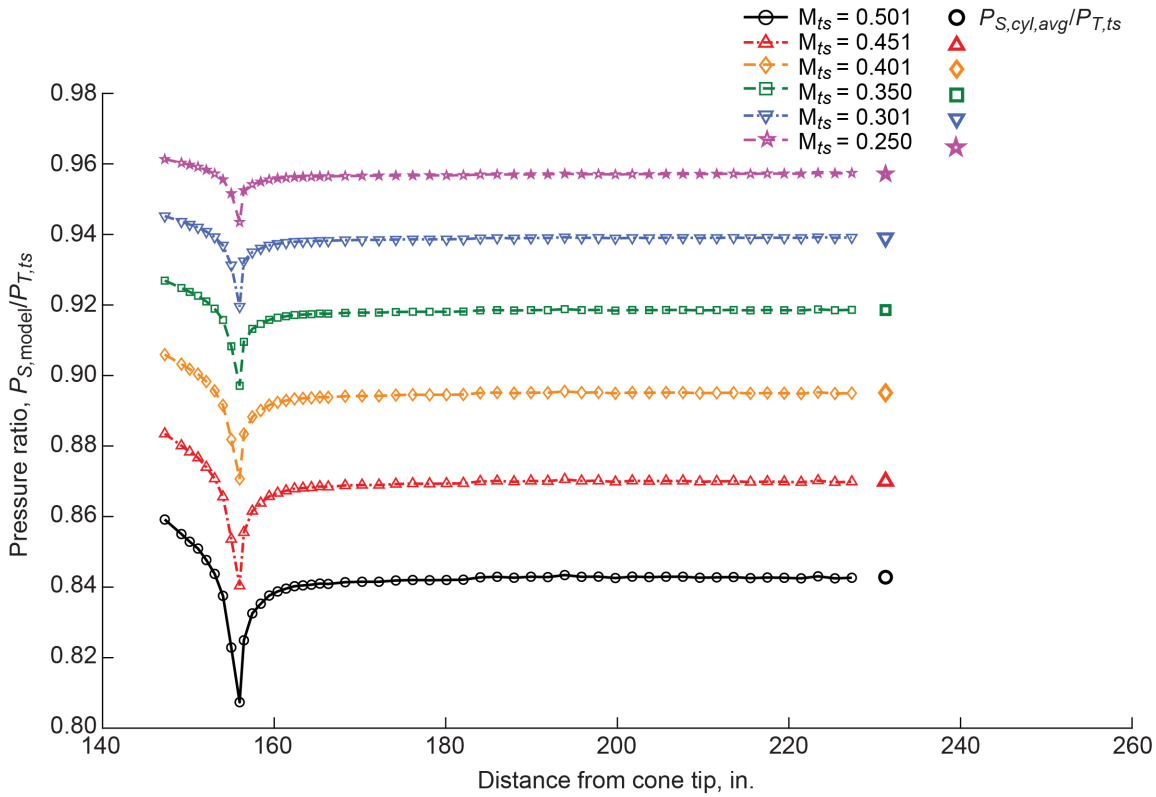

Figure 27.—Axial static pressure distributions along 4-inch-diameter cone cylinder with cone tip at test section station 144.375 in 8- by 6-ft test section. Data acquired during 2019 test section characterization entry at subsonic conditions between Mach 0.501 and 0.250 (one-drive-motor operation).

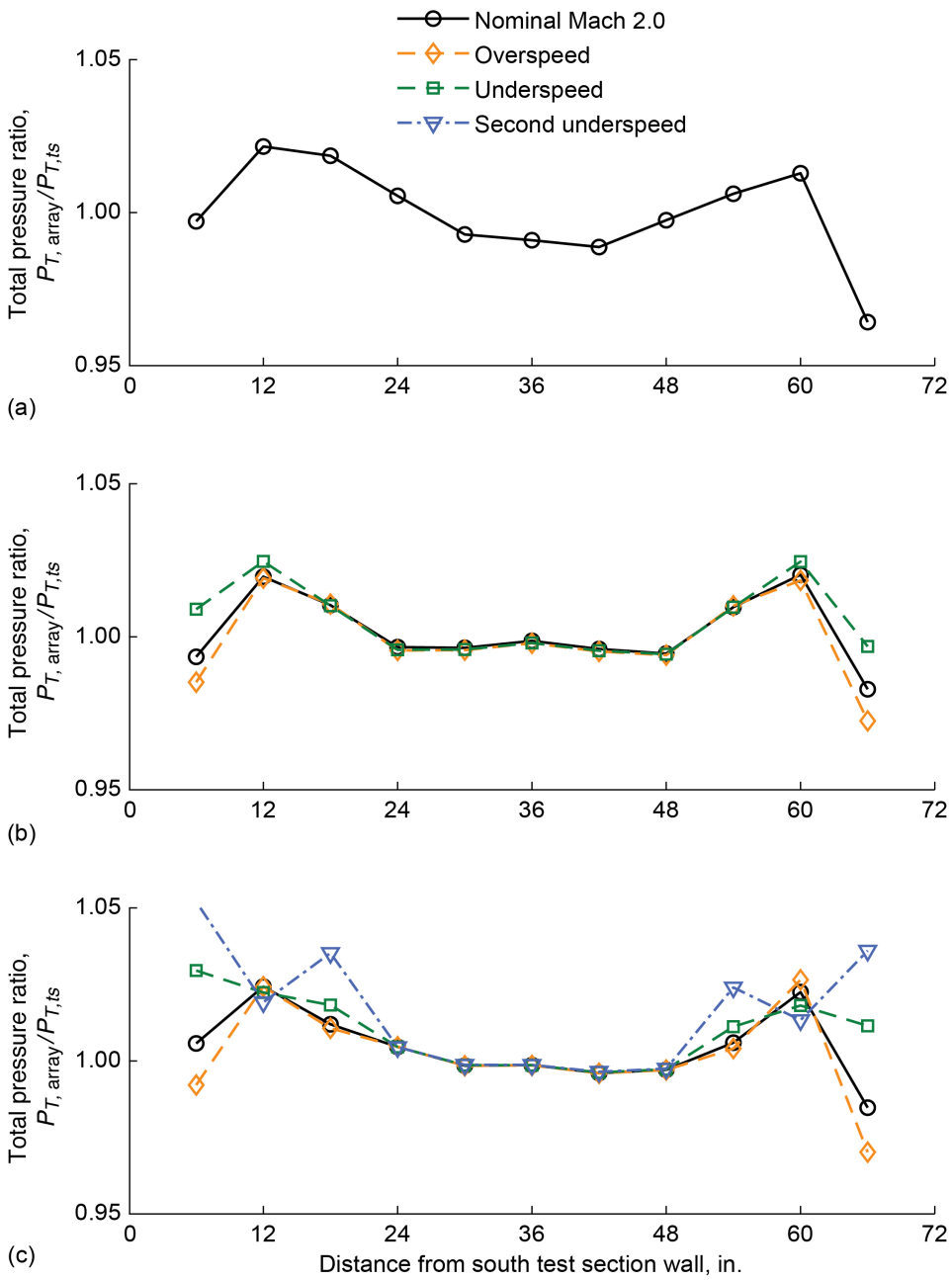

Figure 28.—Total pressure ratio distributions in 8- by 6-ft test section at 14-ft test section measurement plane at centerline (CL) and 1 ft above and below CL. Data acquired during 2019 test section characterization entry at flexwall setting of Mach 2.0. (a) CL + 1 ft; 0.050 = ΔP_T of 1.249 psia. (b) CL; 0.050 = ΔP_T of 1.253 psia. (c) CL – 1 ft; 0.050 = ΔP_T of 1.248 psia.

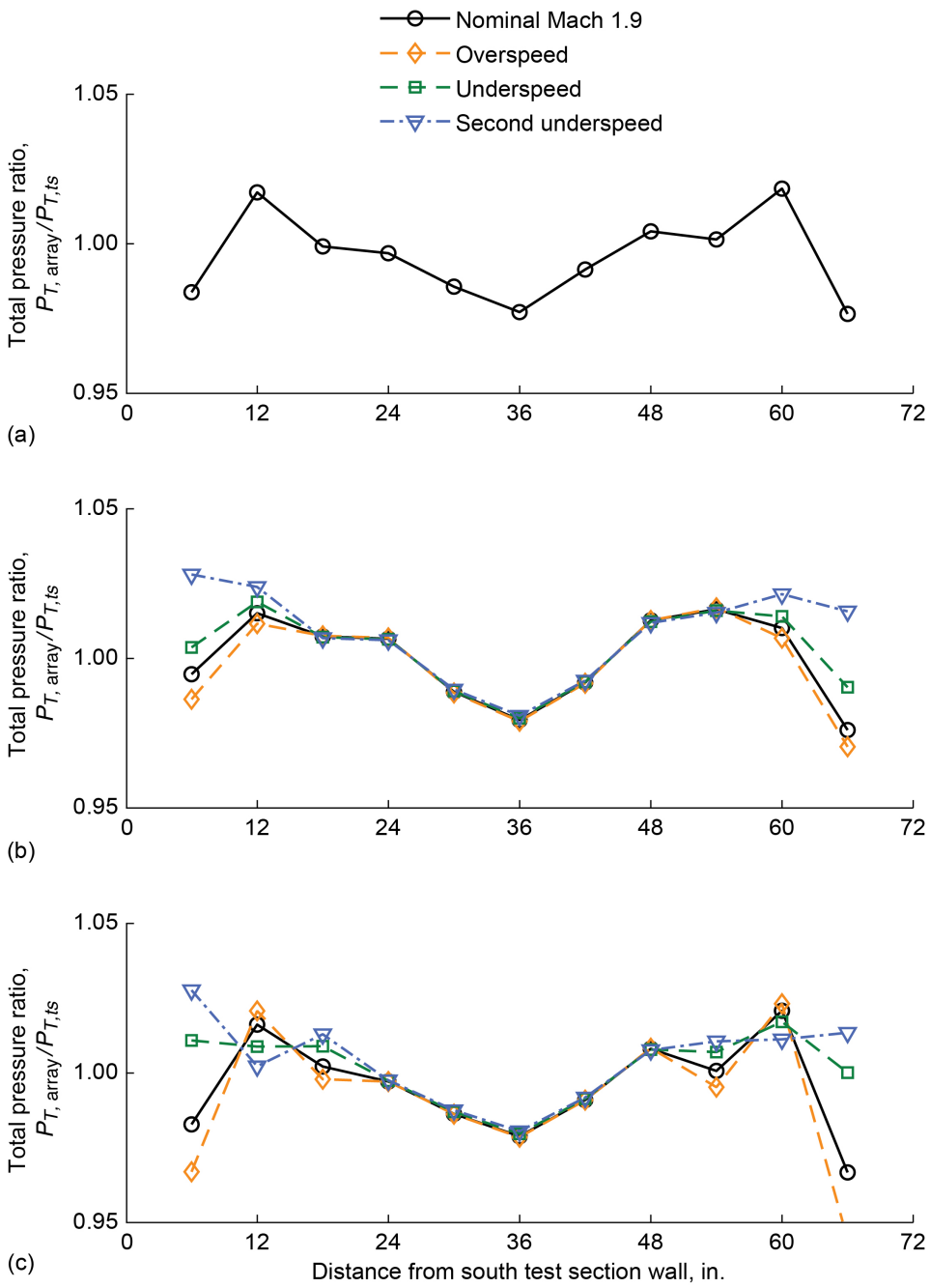

Figure 29.—Total pressure ratio distributions in 8- by 6-ft test section at 14-ft test section measurement plane at centerline (CL) and 1 ft above and below CL. Data acquired during 2019 test section characterization entry at flexwall setting of Mach 1.9. (a) CL + 1 ft; 0.050 = ΔP_T of 1.207 psia. (b) CL; 0.050 = ΔP_T of 1.203 psia. (c) CL – 1 ft; 0.050 = ΔP_T of 1.212 psia.

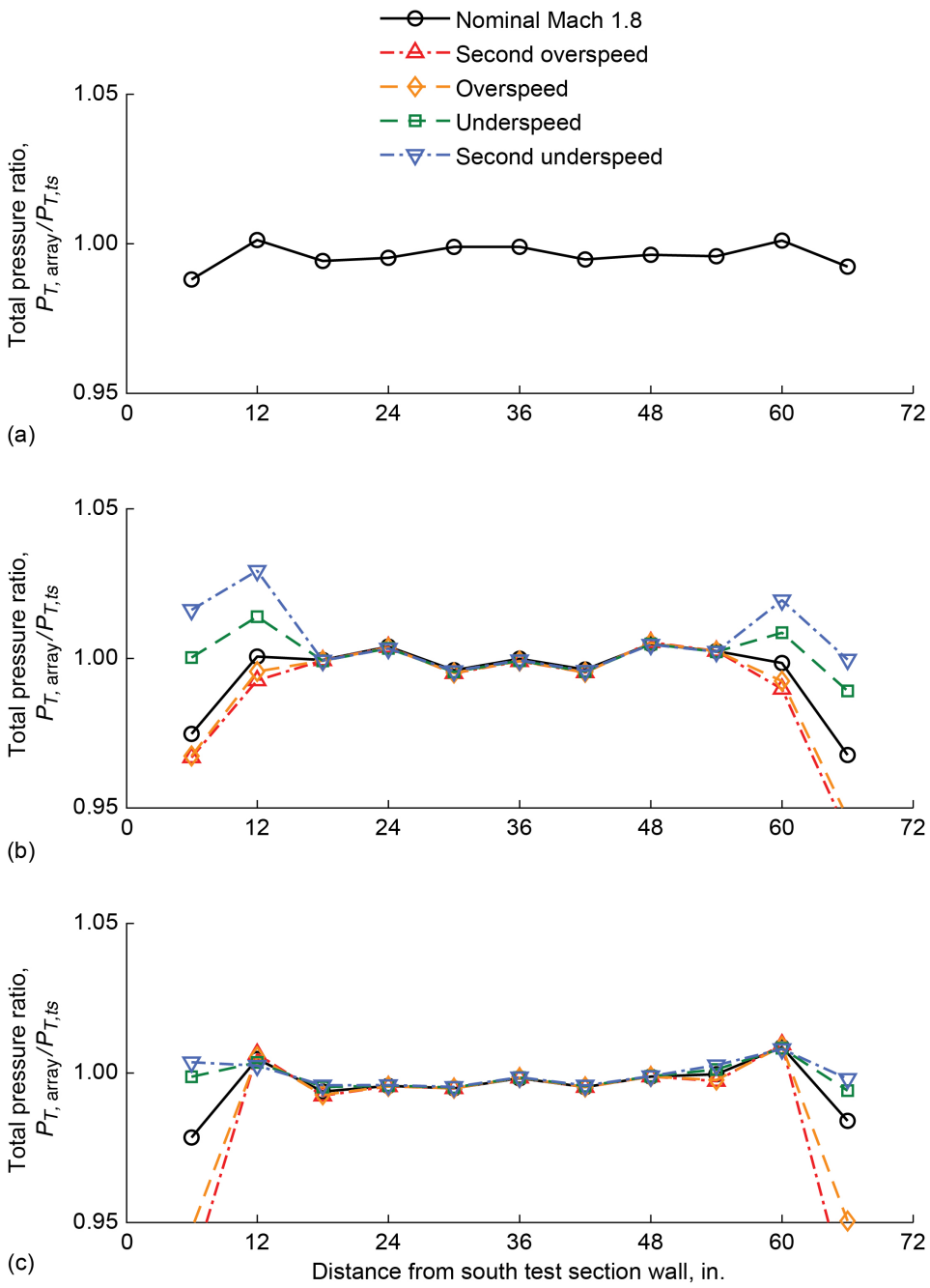

Figure 30.—Total pressure ratio distributions in 8- by 6-ft test section at 14-ft test section measurement plane at centerline (CL) and 1 ft above and below CL. Data acquired during 2019 test section characterization entry at flexwall setting of Mach 1.8. (a) CL + 1 ft; 0.050 = ΔP_T of 1.158 psia. (b) CL; 0.050 = ΔP_T of 1.159 psia. (c) CL – 1 ft; 0.050 = ΔP_T of 1.136 psia.

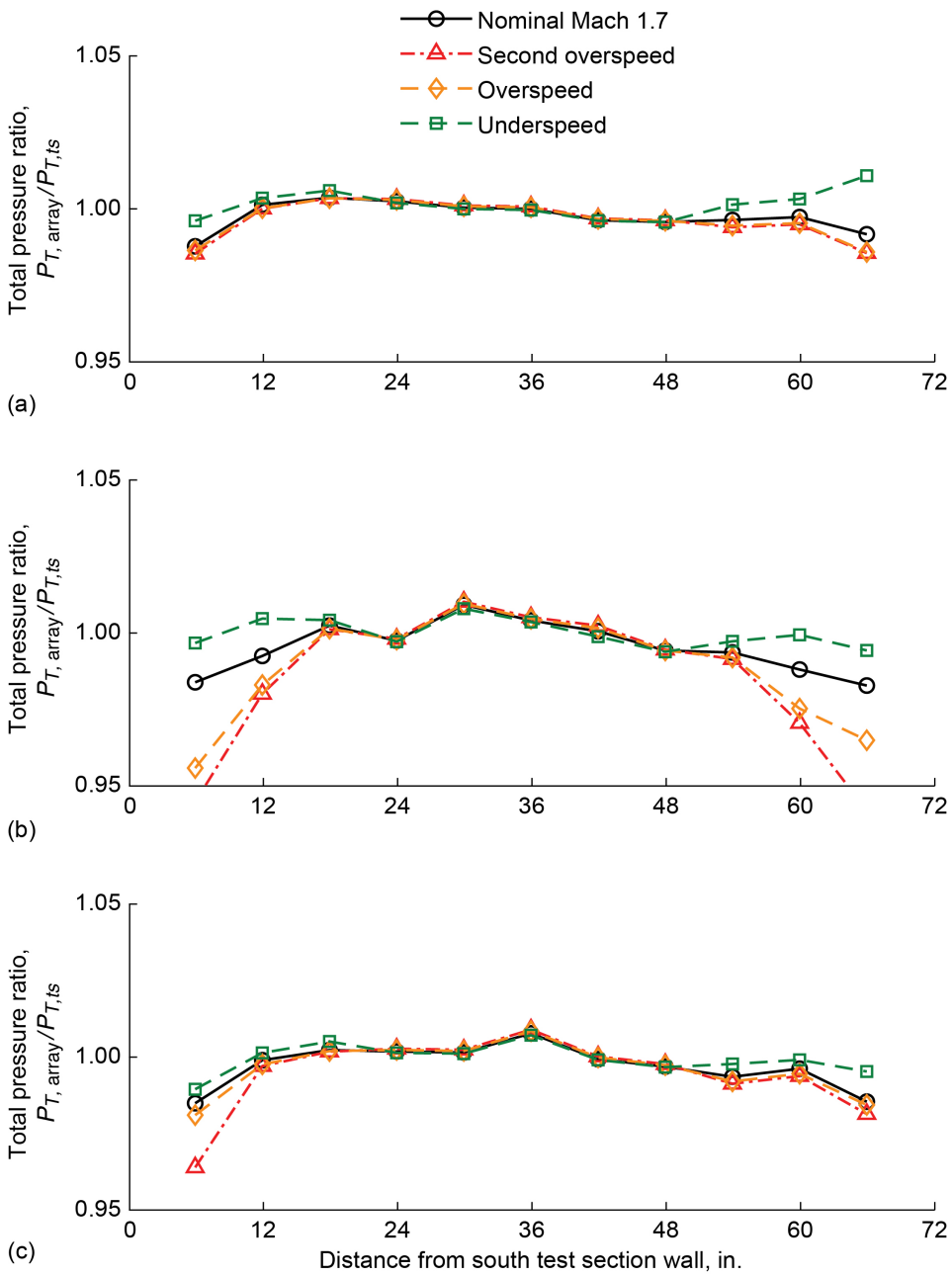

Figure 31.—Total pressure ratio distributions in 8- by 6-ft test section at 14-ft test section measurement plane at centerline (CL) and 1 ft above and below CL. Data acquired during 2019 test section characterization entry at flexwall setting of Mach 1.7. (a) CL + 1 ft; 0.050 = ΔP_T of 1.078 psia. (b) CL; 0.050 = ΔP_T of 1.067 psia. (c) CL – 1 ft; 0.050 = ΔP_T of 1.061 psia.

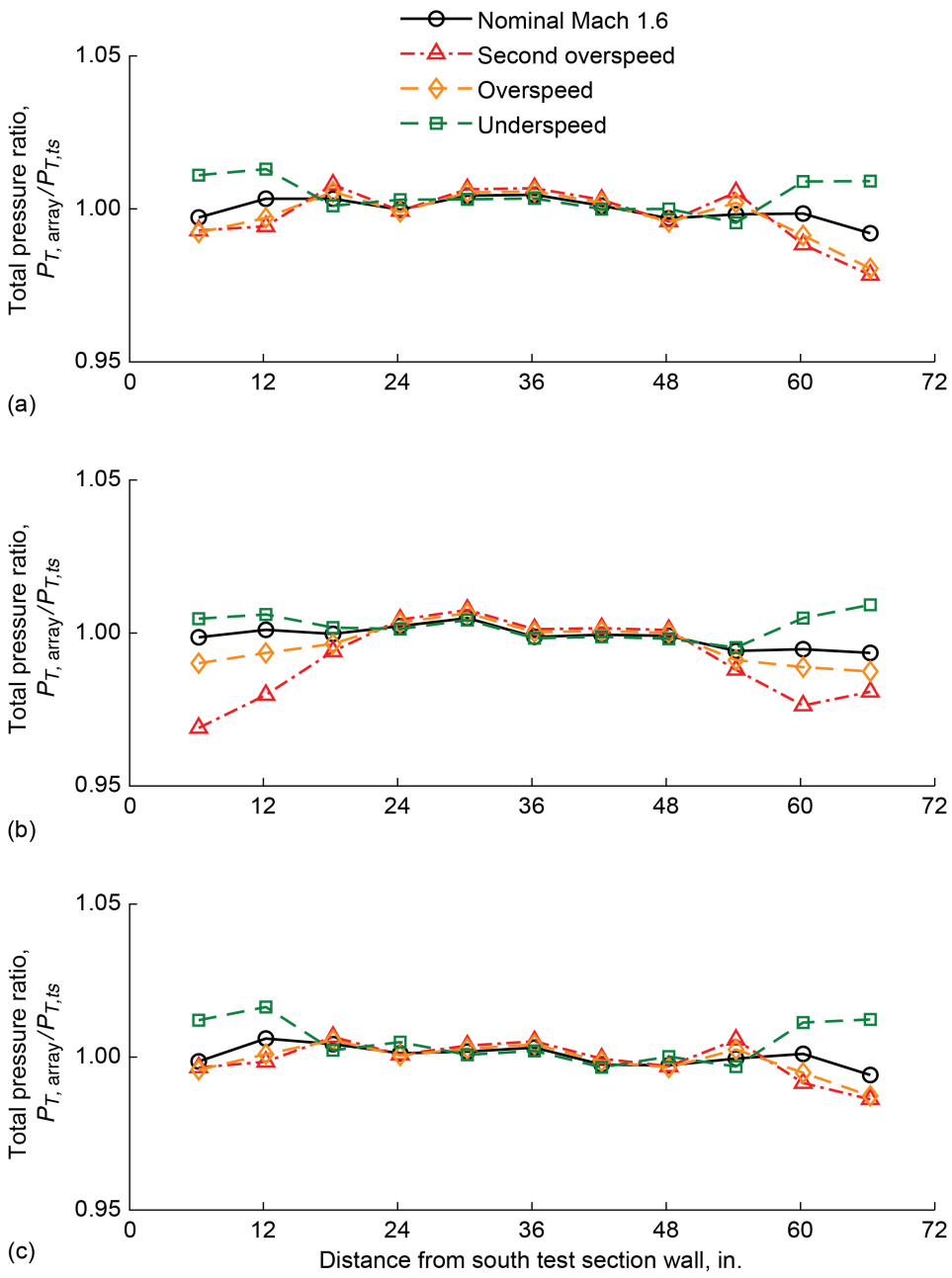

Figure 32.—Total pressure ratio distributions in 8- by 6-ft test section at 14-ft test section measurement plane at centerline (CL) and 1 ft above and below CL. Data acquired during 2019 test section characterization entry at flexwall setting of Mach 1.6. (a) CL + 1 ft; 0.050 = ΔP_T of 1.032 psia. (b) CL; 0.050 = ΔP_T of 1.007 psia. (c) CL – 1 ft; 0.050 = ΔP_T of 1.004 psia.

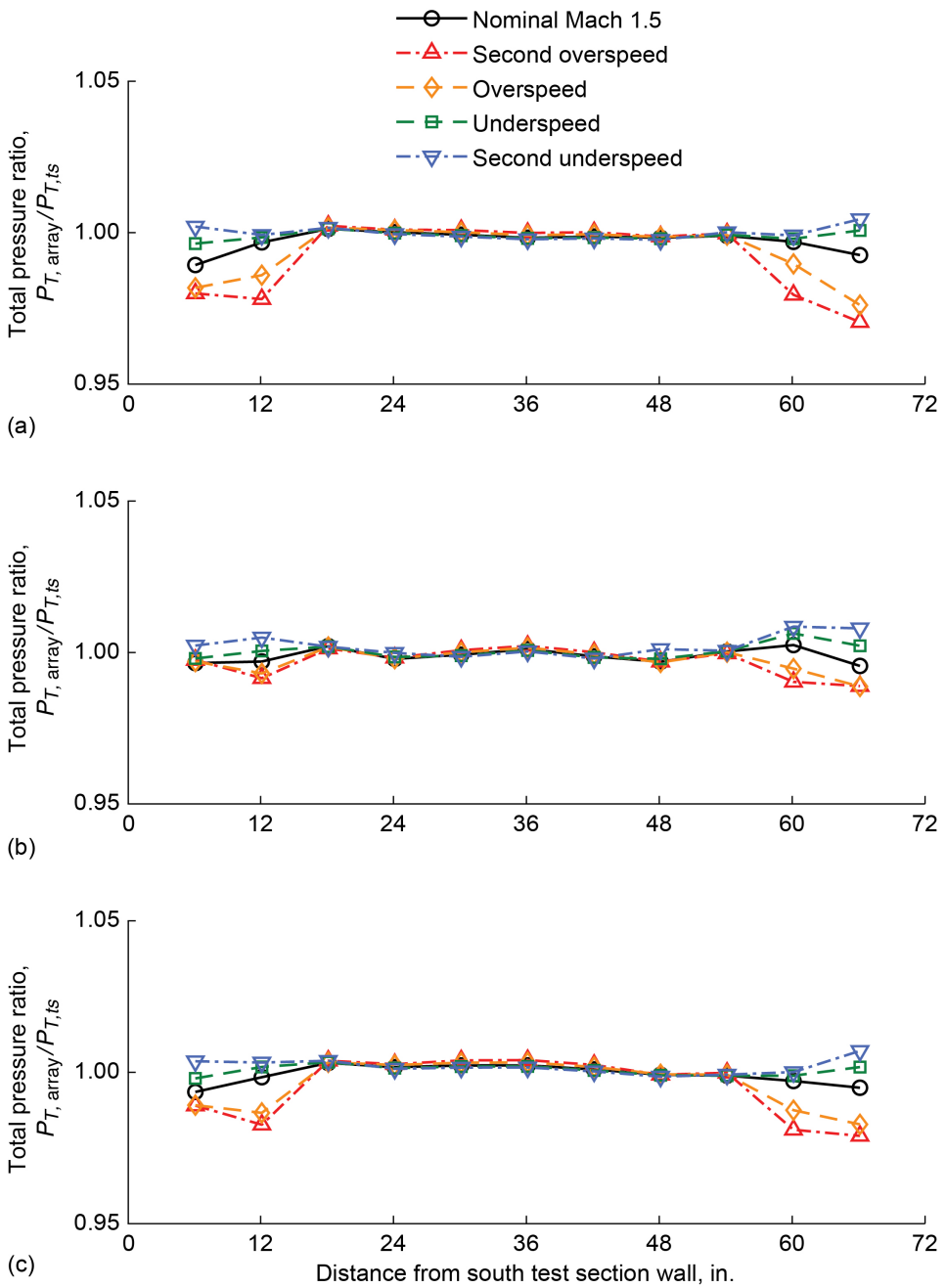

Figure 33.—Total pressure ratio distributions in 8- by 6-ft test section at 14-ft test section measurement plane at centerline (CL) and 1 ft above and below CL. Data acquired during 2019 test section characterization entry at flexwall setting of Mach 1.5. (a) CL + 1 ft; 0.050 = ΔP_T of 0.970 psia. (b) CL; 0.050 = ΔP_T of 0.964 psia. (c) CL – 1 ft; 0.050 = ΔP_T of 0.960 psia.

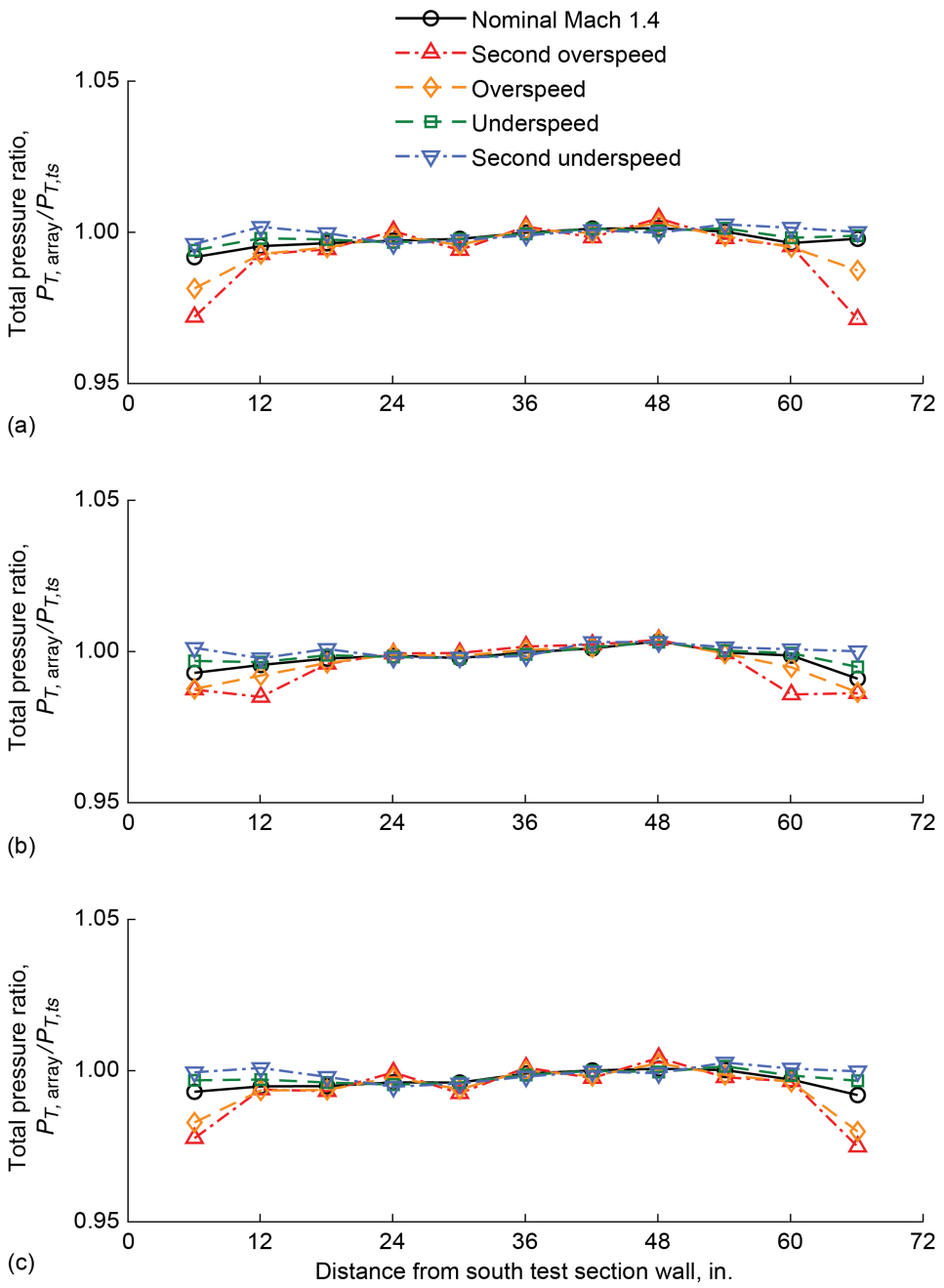

Figure 34.—Total pressure ratio distributions in 8- by 6-ft test section at 14-ft test section measurement plane at centerline (CL) and 1 ft above and below CL. Data acquired during 2019 test section characterization entry at flexwall setting of Mach 1.4. (a) CL + 1 ft; 0.050 = ΔP_T of 0.923 psia. (b) CL; 0.050 = ΔP_T of 0.918 psia. (c) CL – 1 ft; 0.050 = ΔP_T of 0.915 psia.

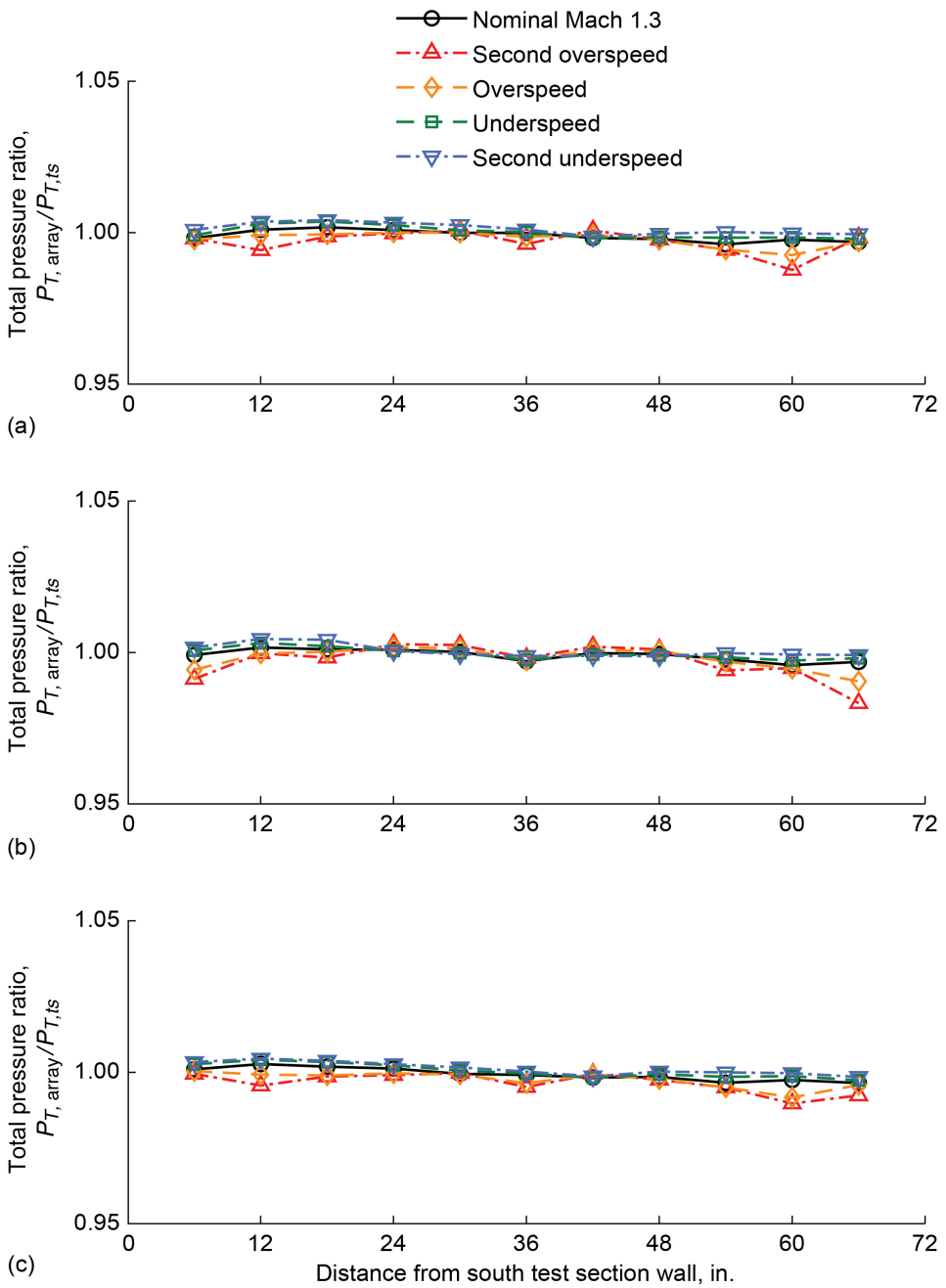

Figure 35.—Total pressure ratio distributions in 8- by 6-ft test section at 14-ft test section measurement plane at centerline (CL) and 1 ft above and below CL. Data acquired during 2019 test section characterization entry at flexwall setting of Mach 1.3. (a) CL + 1 ft; 0.050 = ΔP_T of 0.897 psia. (b) CL; 0.050 = ΔP_T of 0.895 psia. (c) CL – 1 ft; 0.050 = ΔP_T of 0.890 psia.

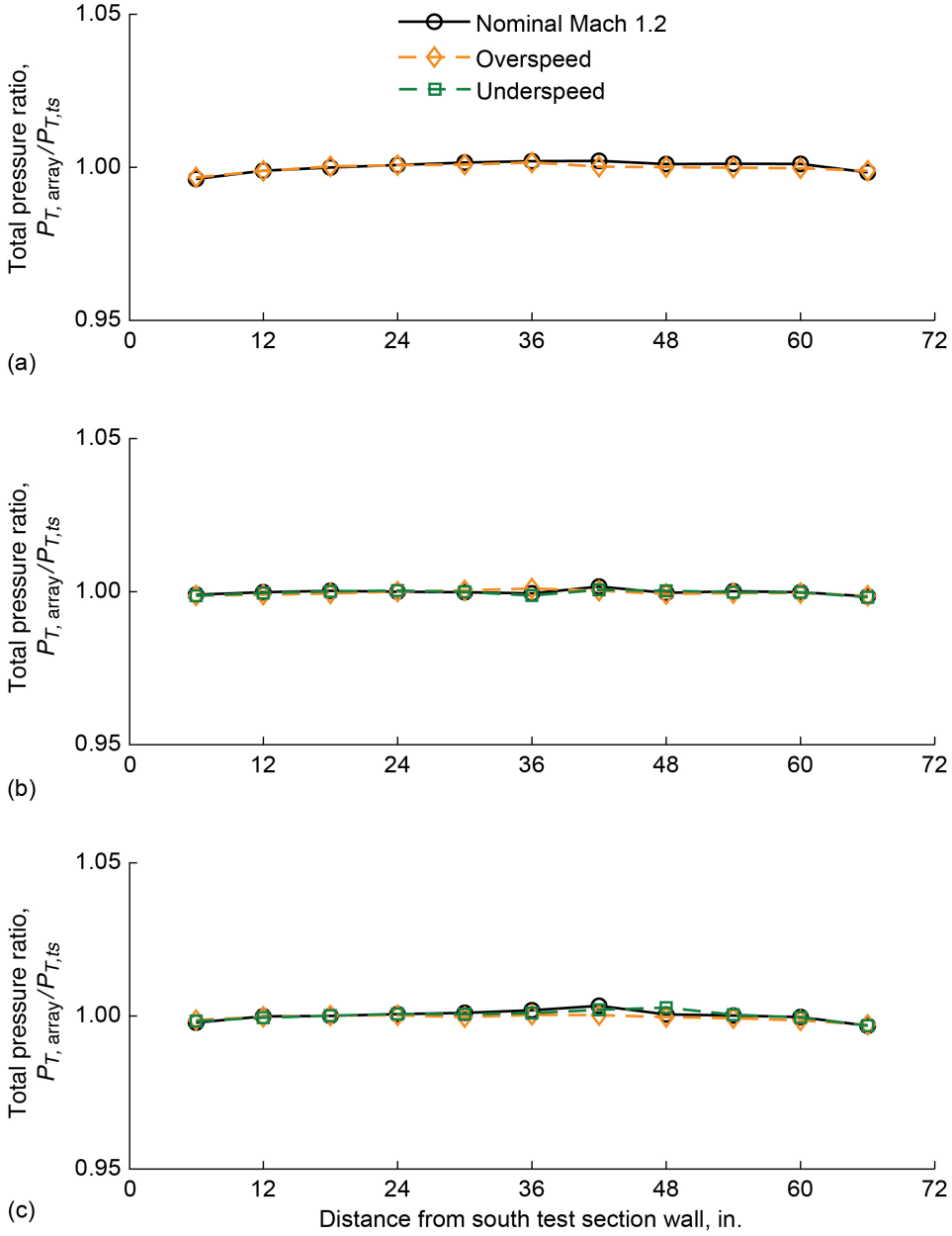

Figure 36.—Total pressure ratio distributions in 8- by 6-ft test section at 14-ft test section measurement plane at centerline (CL) and 1 ft above and below CL. Data acquired during 2019 test section characterization entry at flexwall setting of Mach 1.2. (a) CL + 1 ft; 0.050 = ΔP_T of 0.891 psia. (b) CL; 0.050 = ΔP_T of 0.888 psia. (c) CL – 1 ft; 0.050 = ΔP_T of 0.883 psia.

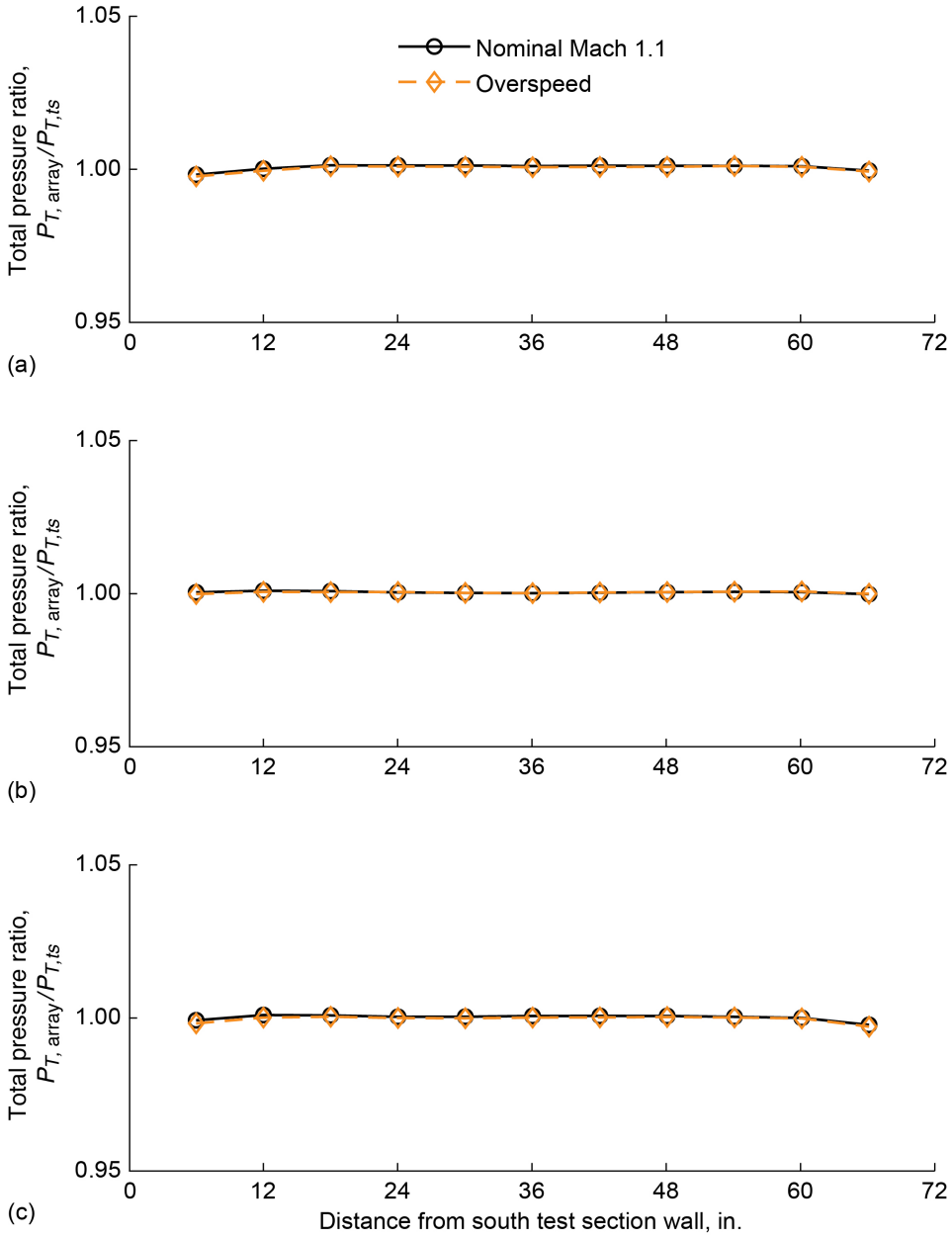

Figure 37.—Total pressure ratio distributions in 8- by 6-ft test section at 14-ft test section measurement plane at centerline (CL) and 1 ft above and below CL. Data acquired during 2019 test section characterization entry at flexwall setting of Mach 1.1. (a) CL + 1 ft; 0.050 = ΔP_T of 0.878 psia. (b) CL; 0.050 = ΔP_T of 0.871 psia. (c) CL – 1 ft; 0.050 = ΔP_T of 0.870 psia.

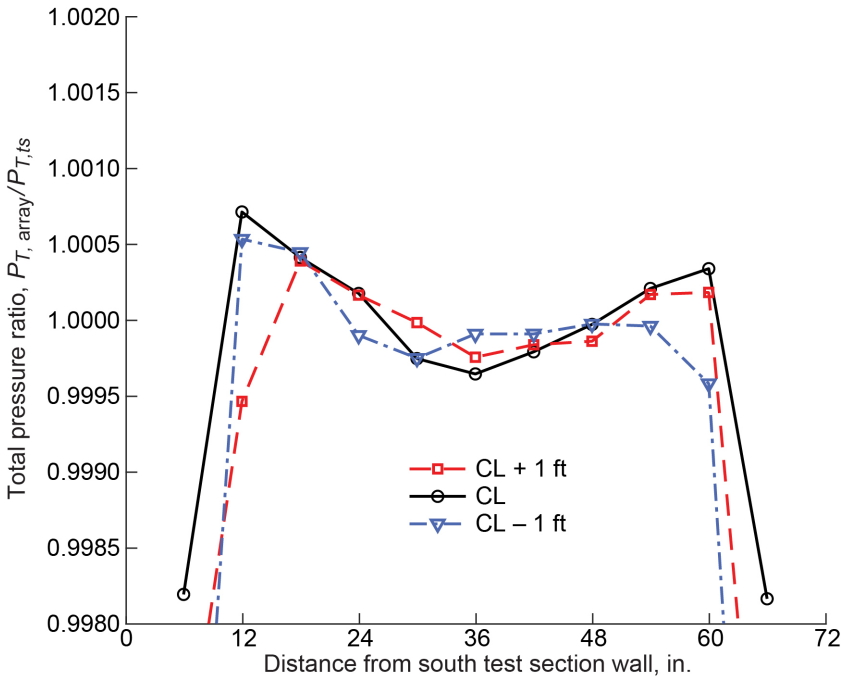

Figure 38.—Total pressure ratio distributions in 8- by 6-ft test section at 14-ft test section measurement plane at centerline (CL) and 1 ft above and below CL. Data acquired during 2019 test section characterization entry at transonic array Mach number of 0.951 (three-drive-motor operation). 0.0005 = ΔP_T of 0.0084 psia.

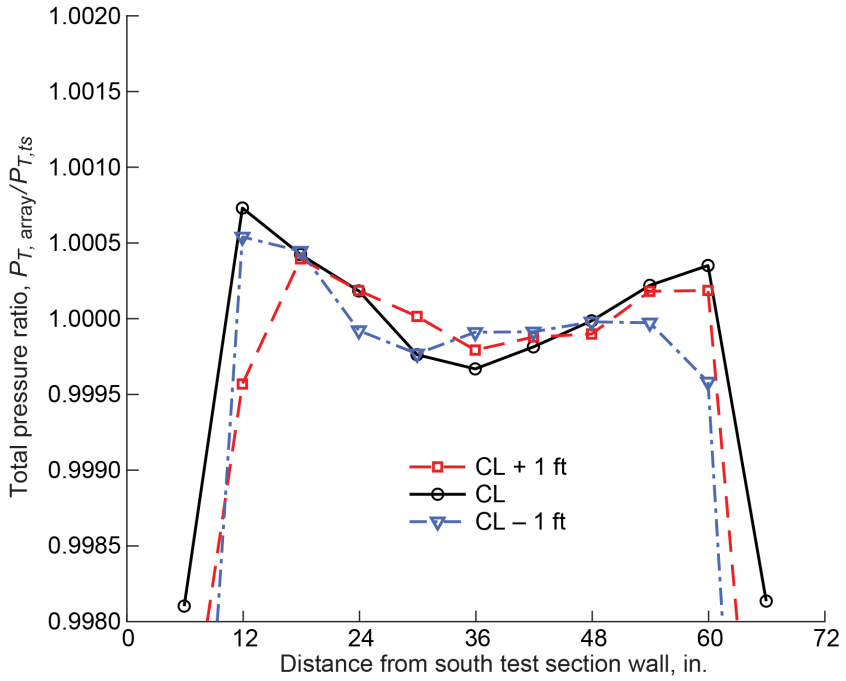

Figure 39.—Total pressure ratio distributions in 8- by 6-ft test section at 14-ft test section measurement plane at centerline (CL) and 1 ft above and below CL. Data acquired during 2019 test section characterization entry at transonic array Mach number of 0.900 (three-drive-motor operation). 0.0005 = ΔP_T of 0.0084 psia.

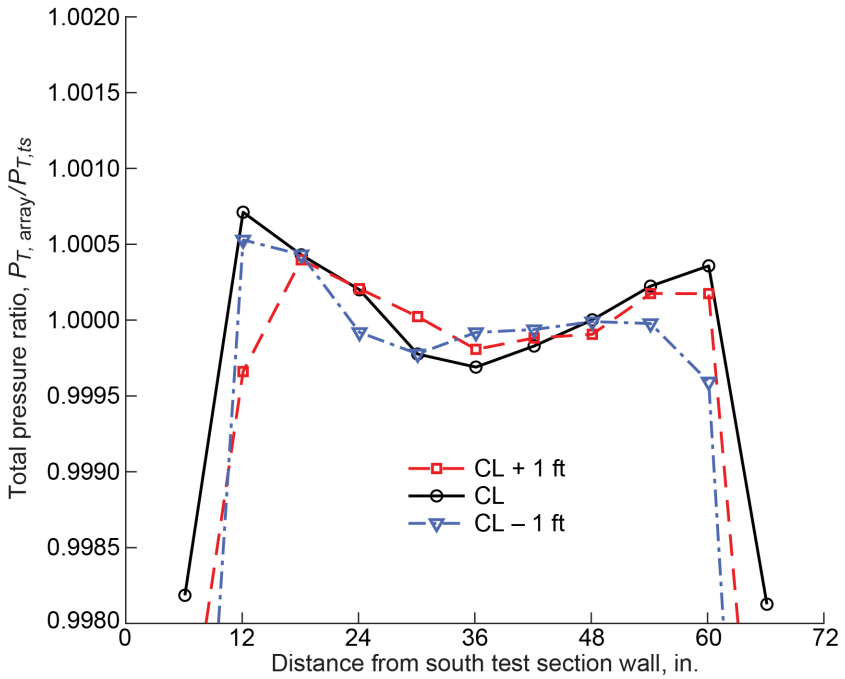

Figure 40.—Total pressure ratio distributions in 8- by 6-ft test section at 14-ft test section measurement plane at centerline (CL) and 1 ft above and below CL. Data acquired during 2019 test section characterization entry at transonic array Mach number of 0.849 (three-drive-motor operation). 0.0005 = ΔP_T of 0.0084 psia.

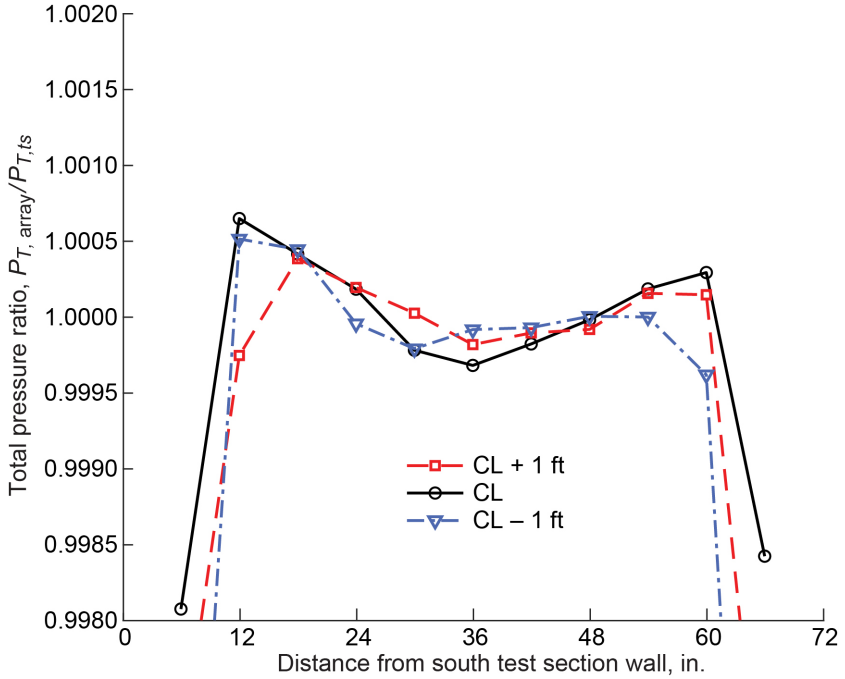

Figure 41.—Total pressure ratio distributions in 8- by 6-ft test section at 14-ft test section measurement plane at centerline (CL) and 1 ft above and below CL. Data acquired during 2019 test section characterization entry at transonic array Mach number of 0.800 (three-drive-motor operation). 0.0005 = ΔP_T of 0.0086 psia.

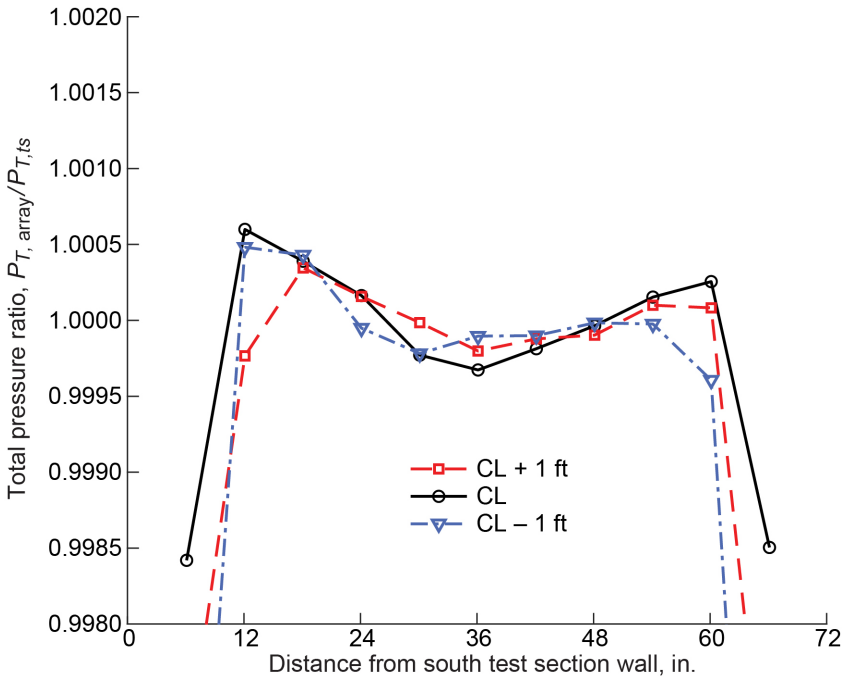

Figure 42.—Total pressure ratio distributions in 8- by 6-ft test section at 14-ft test section measurement plane at centerline (CL) and 1 ft above and below CL. Data acquired during 2019 test section characterization entry at transonic array Mach number of 0.750 (three-drive-motor operation). 0.0005 = ΔP_T of 0.0087 psia.

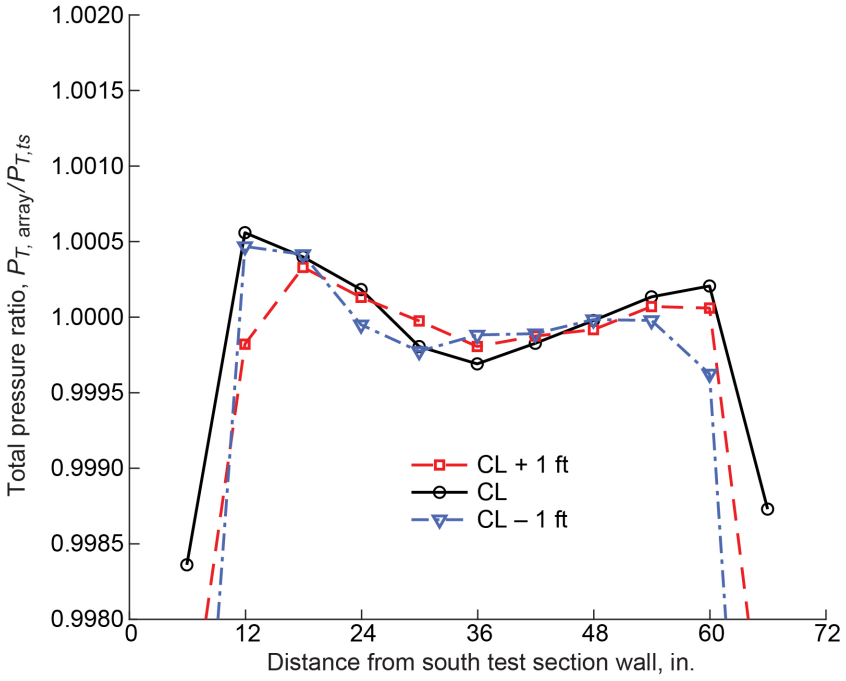

Figure 43.—Total pressure ratio distributions in 8- by 6-ft test section at 14-ft test section measurement plane at centerline (CL) and 1 ft above and below CL. Data acquired during 2019 test section characterization entry at transonic array Mach number of 0.701 (three-drive-motor operation). 0.0005 = ΔP_T of 0.0088 psia.

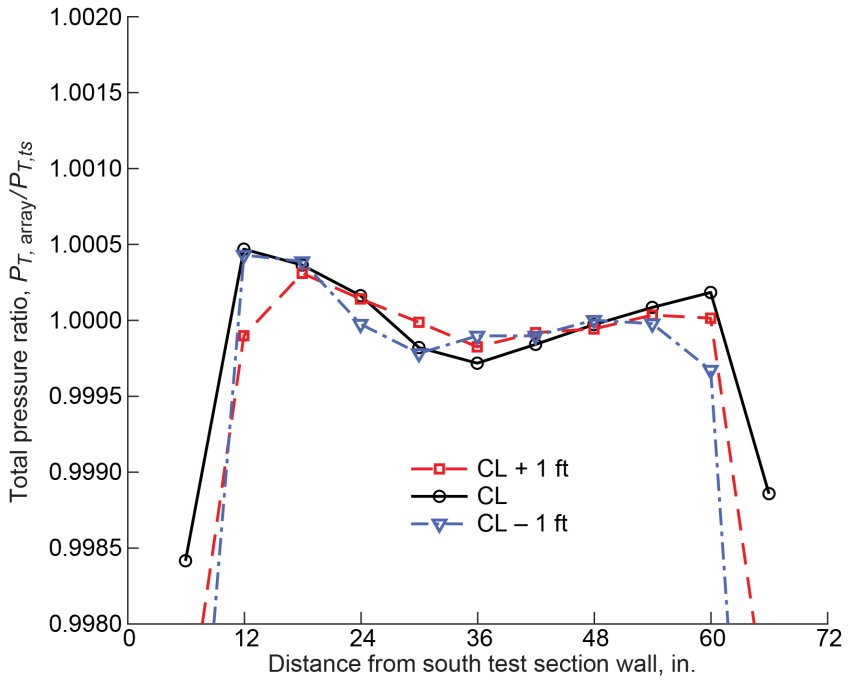

Figure 44.—Total pressure ratio distributions in 8- by 6-ft test section at 14-ft test section measurement plane at centerline (CL) and 1 ft above and below CL. Data acquired during 2019 test section characterization entry at transonic array Mach number of 0.649 (three-drive-motor operation). 0.0005 = ΔP_T of 0.0088 psia.

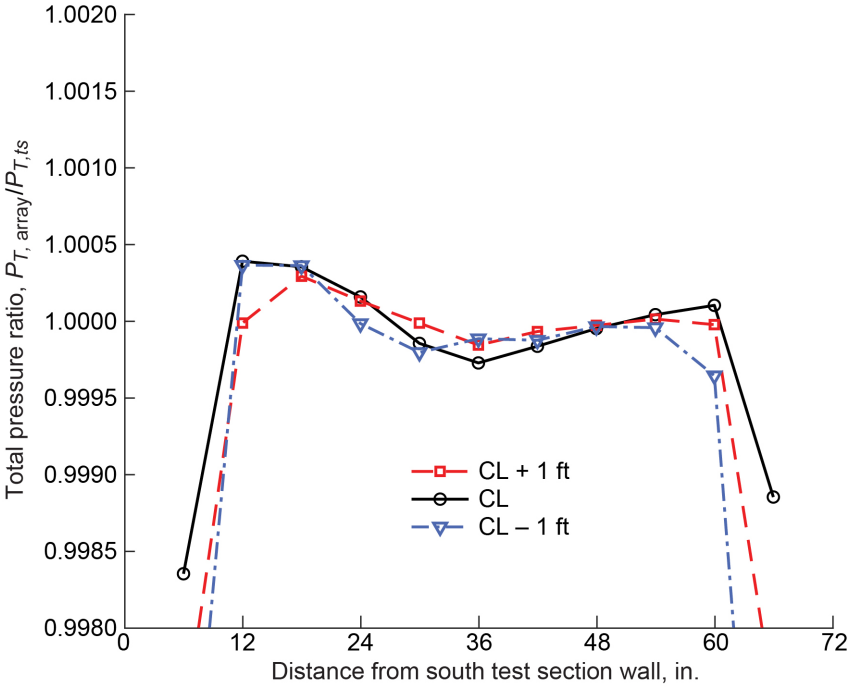

Figure 45.—Total pressure ratio distributions in 8- by 6-ft test section at 14-ft test section measurement plane at centerline (CL) and 1 ft above and below CL. Data acquired during 2019 test section characterization entry at transonic array Mach number of 0.600 (three-drive-motor operation). 0.0005 = ΔP_T of 0.0088 psia.

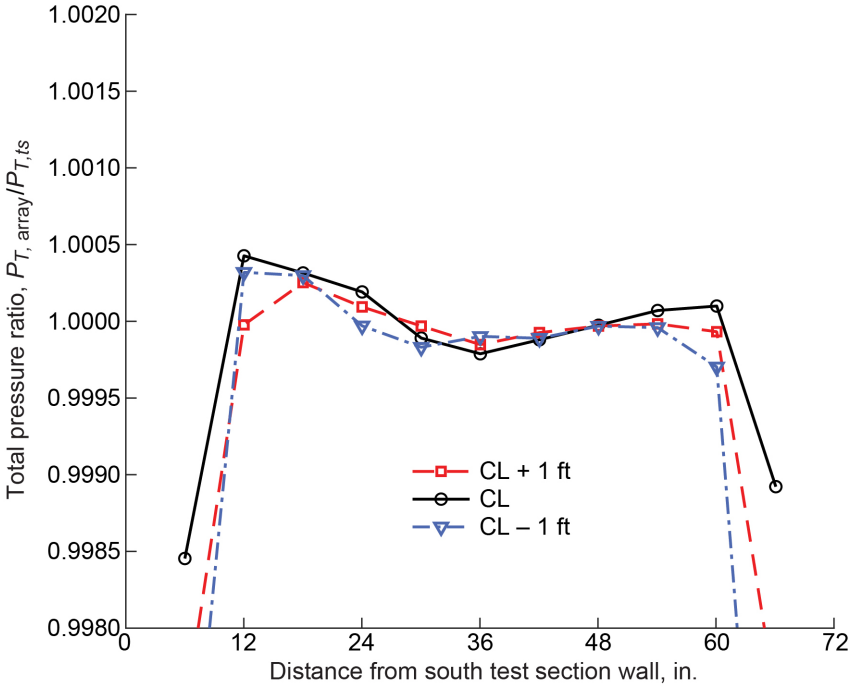

Figure 46.—Total pressure ratio distributions in 8- by 6-ft test section at 14-ft test section measurement plane at centerline (CL) and 1 ft above and below CL. Data acquired during 2019 test section characterization entry at transonic array Mach number of 0.551 (three-drive-motor operation). 0.0005 = ΔP_T of 0.0086 psia.

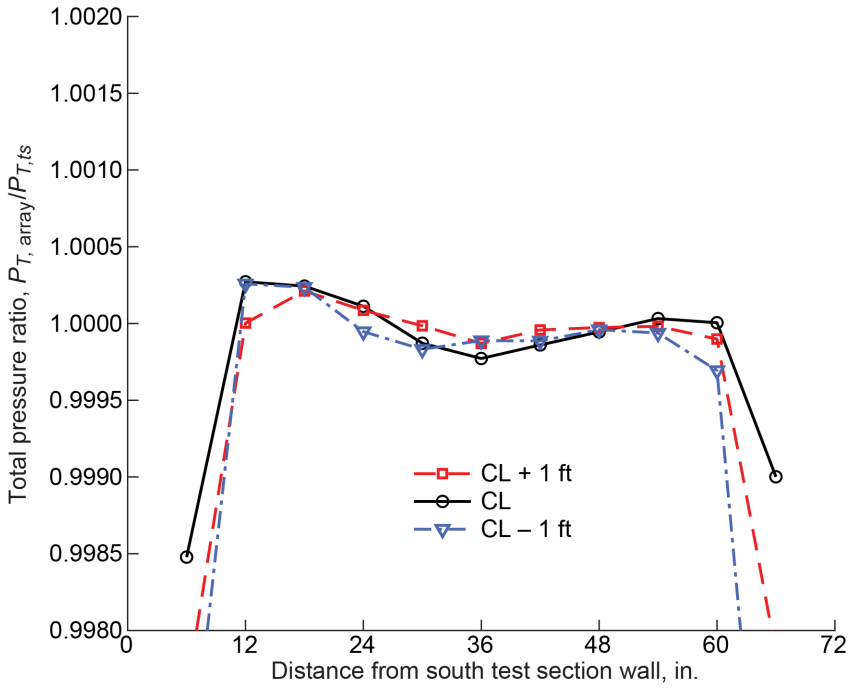

Figure 47.—Total pressure ratio distributions in 8- by 6-ft test section at 14-ft test section measurement plane at centerline (CL) and 1 ft above and below CL. Data acquired during 2019 test section characterization entry at transonic array Mach number of 0.500 (three-drive-motor operation). 0.0005 = ΔP_T of 0.0085 psia.

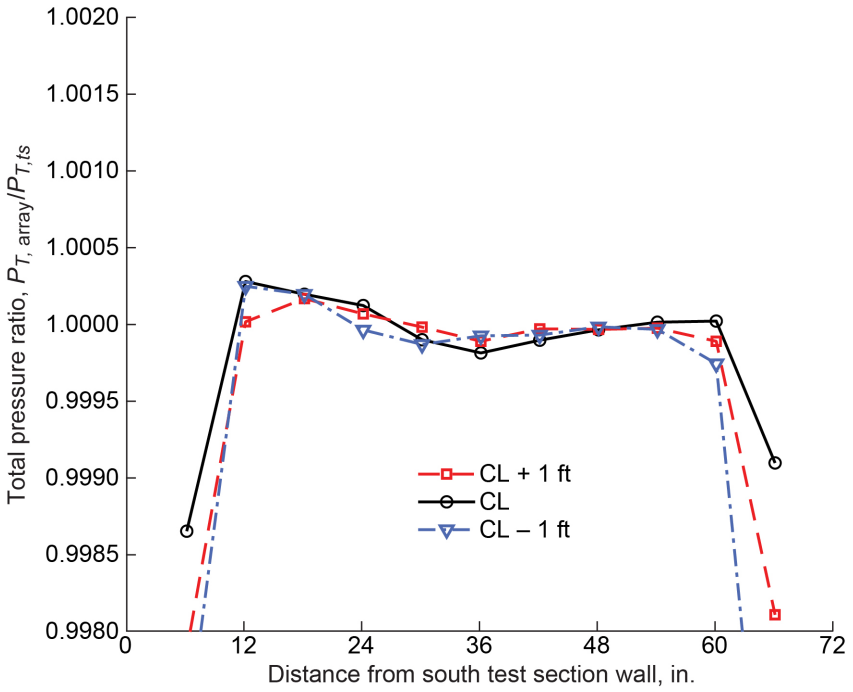

Figure 48.—Total pressure ratio distributions in 8- by 6-ft test section at 14-ft test section measurement plane at centerline (CL) and 1 ft above and below CL. Data acquired during 2019 test section characterization entry at transonic array Mach number of 0.449 (three-drive-motor operation. 0.0005 = ΔP_T of 0.0084 psia.

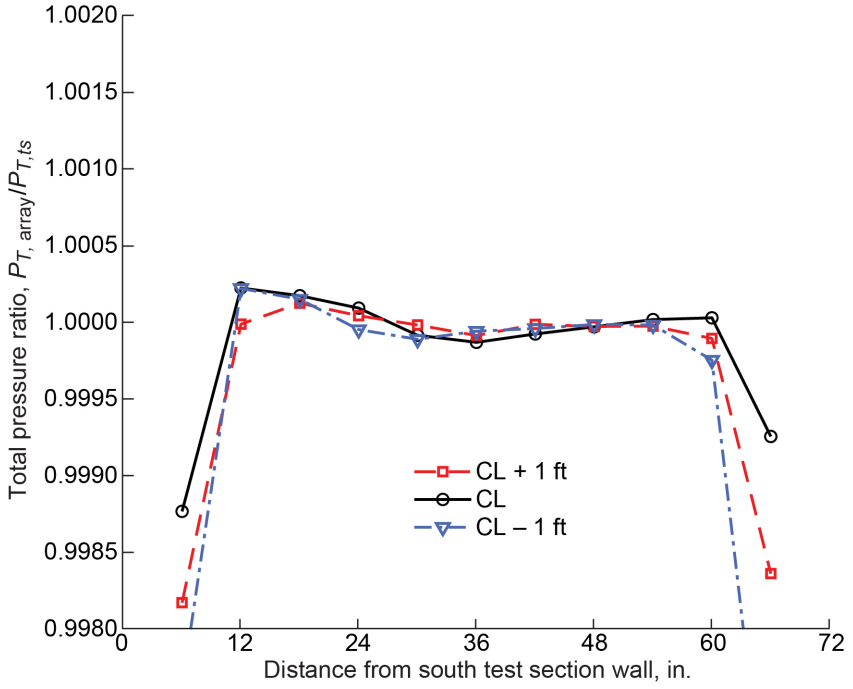

Figure 49.—Total pressure ratio distributions in 8- by 6-ft test section at 14-ft test section measurement plane at centerline (CL) and 1 ft above and below CL. Data acquired during 2019 test section characterization entry at transonic array Mach number of 0.401 (three-drive-motor operation). 0.0005 = ΔP_T of 0.0083 psia.

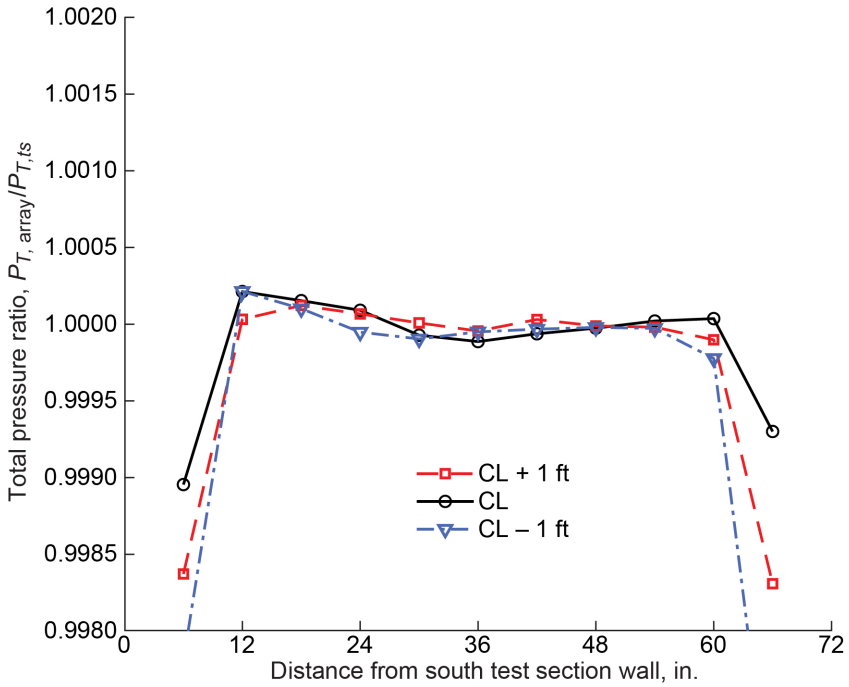

Figure 50.—Total pressure ratio distributions in 8- by 6-ft test section at 14-ft test section measurement plane at centerline (CL) and 1 ft above and below CL. Data acquired during 2019 test section characterization entry at transonic array Mach number of 0.369 (three-drive-motor operation). 0.0005 = ΔP_T of 0.0083 psia.

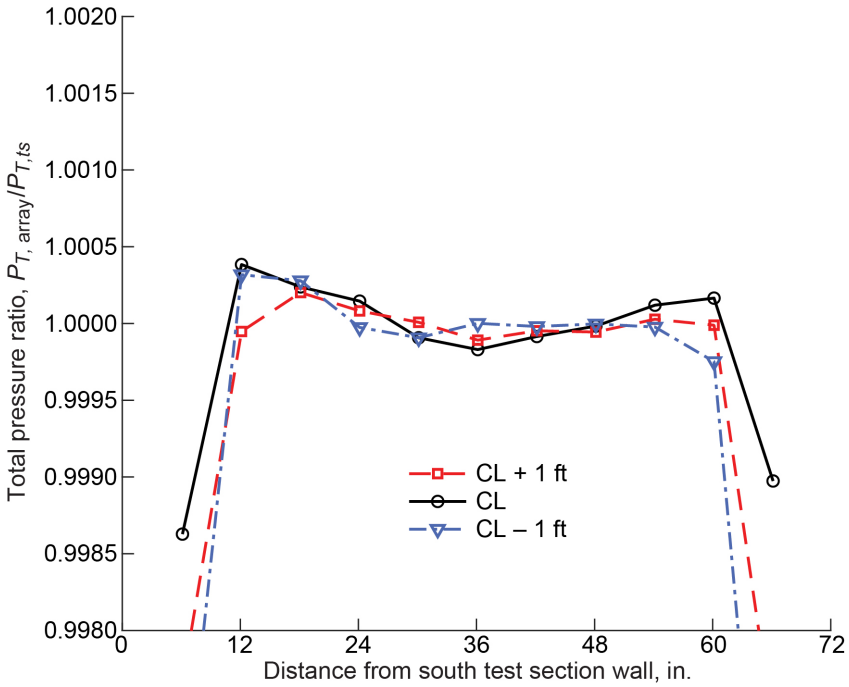

Figure 51.—Total pressure ratio distributions in 8- by 6-ft test section at 14-ft test section measurement plane at centerline (CL) and 1 ft above and below CL. Data acquired during 2019 test section characterization entry at transonic array Mach number of 0.500 (one-drive-motor operation). 0.0005 = ΔP_T of 0.0079 psia.

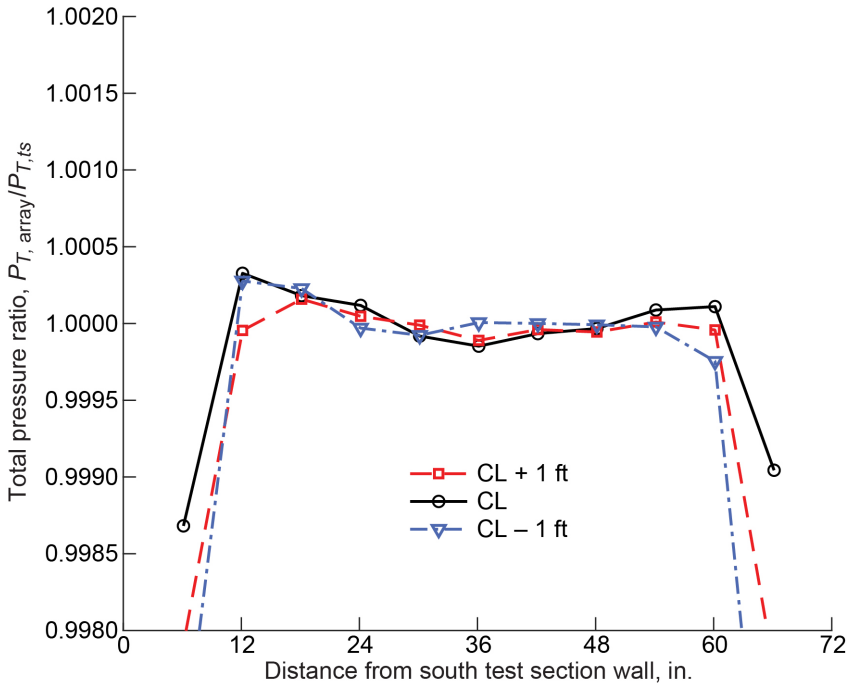

Figure 52.—Total pressure ratio distributions in 8- by 6-ft test section at 14-ft test section measurement plane at centerline (CL) and 1 ft above and below CL. Data acquired during 2019 test section characterization entry at transonic array Mach number of 0.449 (one-drive-motor operation). 0.0005 = ΔP_T of 0.0078 psia.

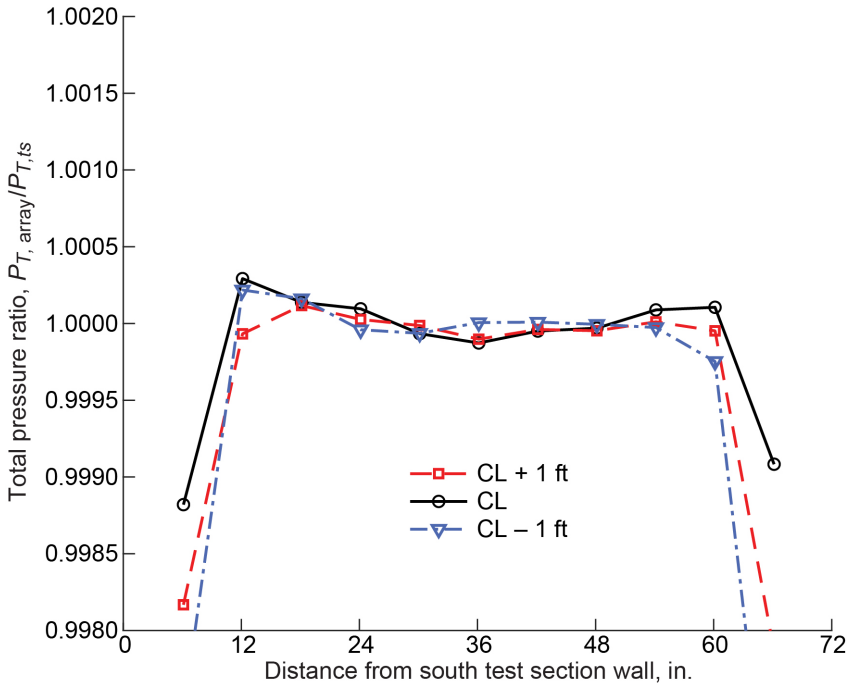

Figure 53.—Total pressure ratio distributions in 8- by 6-ft test section at 14-ft test section measurement plane at centerline (CL) and 1 ft above and below CL. Data acquired during 2019 test section characterization entry at transonic array Mach number of 0.401 (one-drive-motor operation). 0.0005 = ΔP_T of 0.0077 psia.

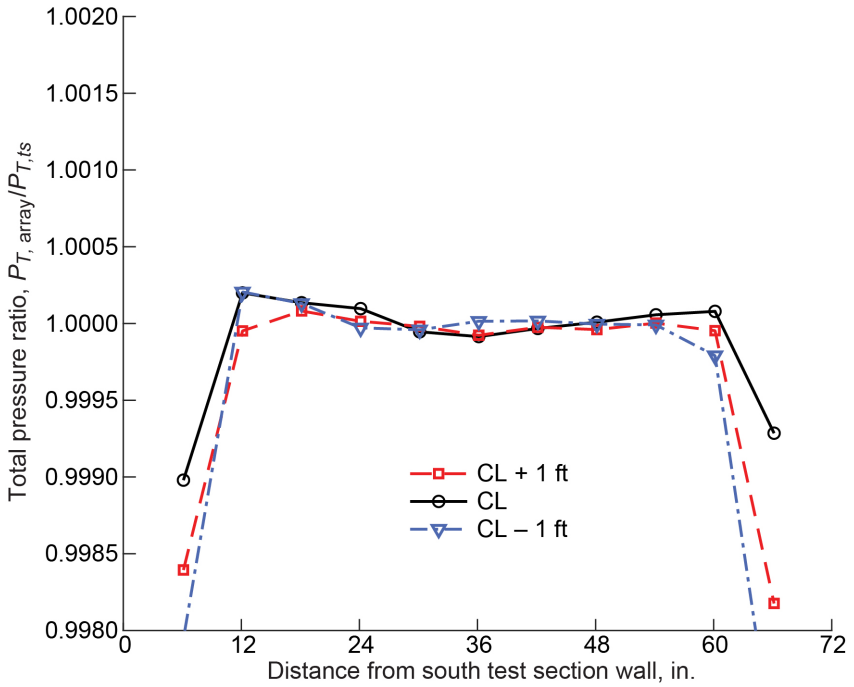

Figure 54.—Total pressure ratio distributions in 8- by 6-ft test section at 14-ft test section measurement plane at centerline (CL) and 1 ft above and below CL. Data acquired during 2019 test section characterization entry at transonic array Mach number of 0.352 (one-drive-motor operation). 0.0005 = ΔP_T of 0.0076 psia.

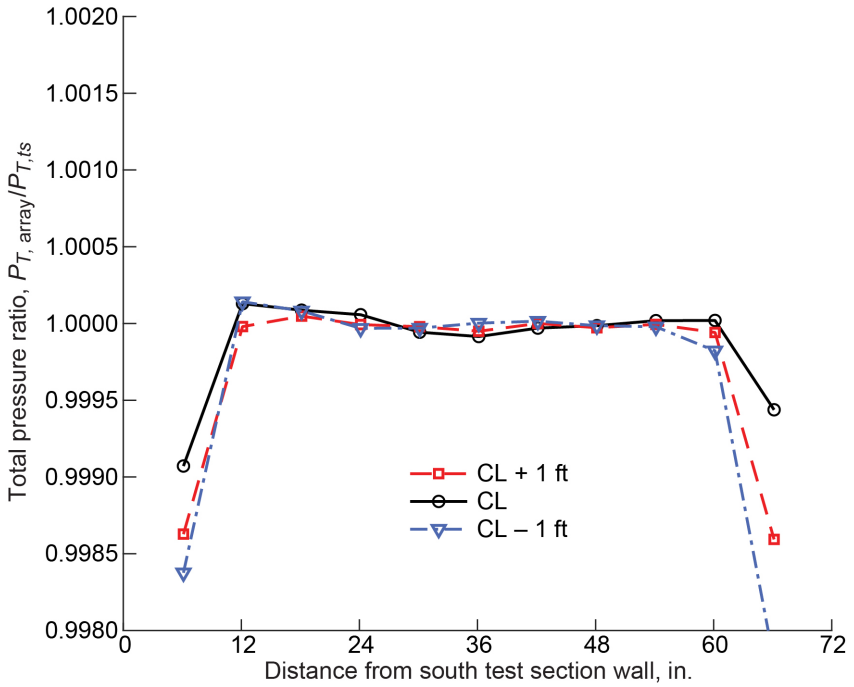

Figure 55.—Total pressure ratio distributions in 8- by 6-ft test section at 14-ft test section measurement plane at centerline (CL) and 1 ft above and below CL. Data acquired during 2019 test section characterization entry at transonic array Mach number of 0.299 (one-drive-motor operation). 0.0005 = ΔP_T of 0.0076 psia.

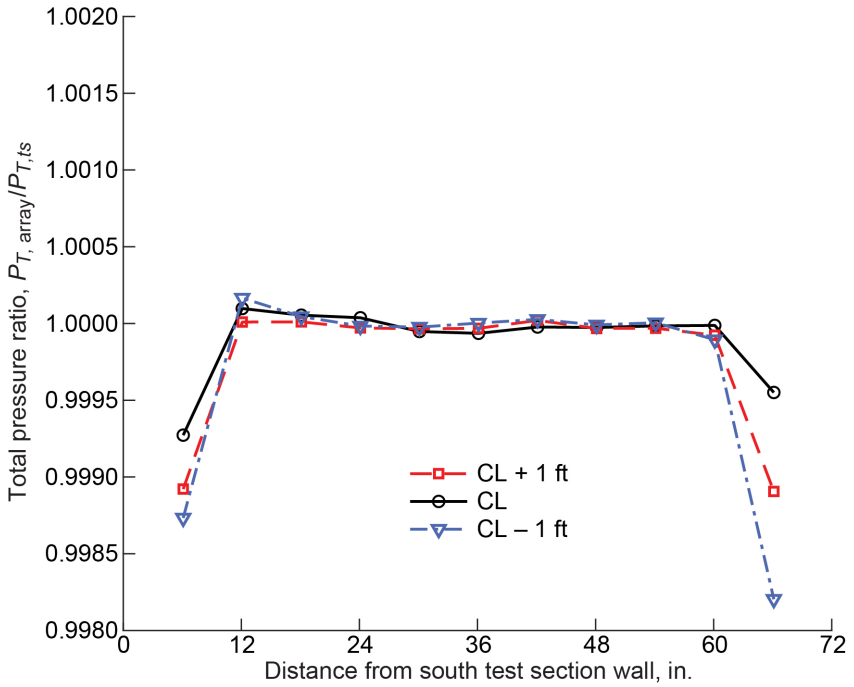

Figure 56.—Total pressure ratio distributions in 8- by 6-ft test section at 14-ft test section measurement plane at centerline (CL) and 1 ft above and below CL. Data acquired during 2019 test section characterization entry at transonic array Mach number of 0.251 (one-drive-motor operation). 0.0005 = ΔP_T of 0.0076 psia.

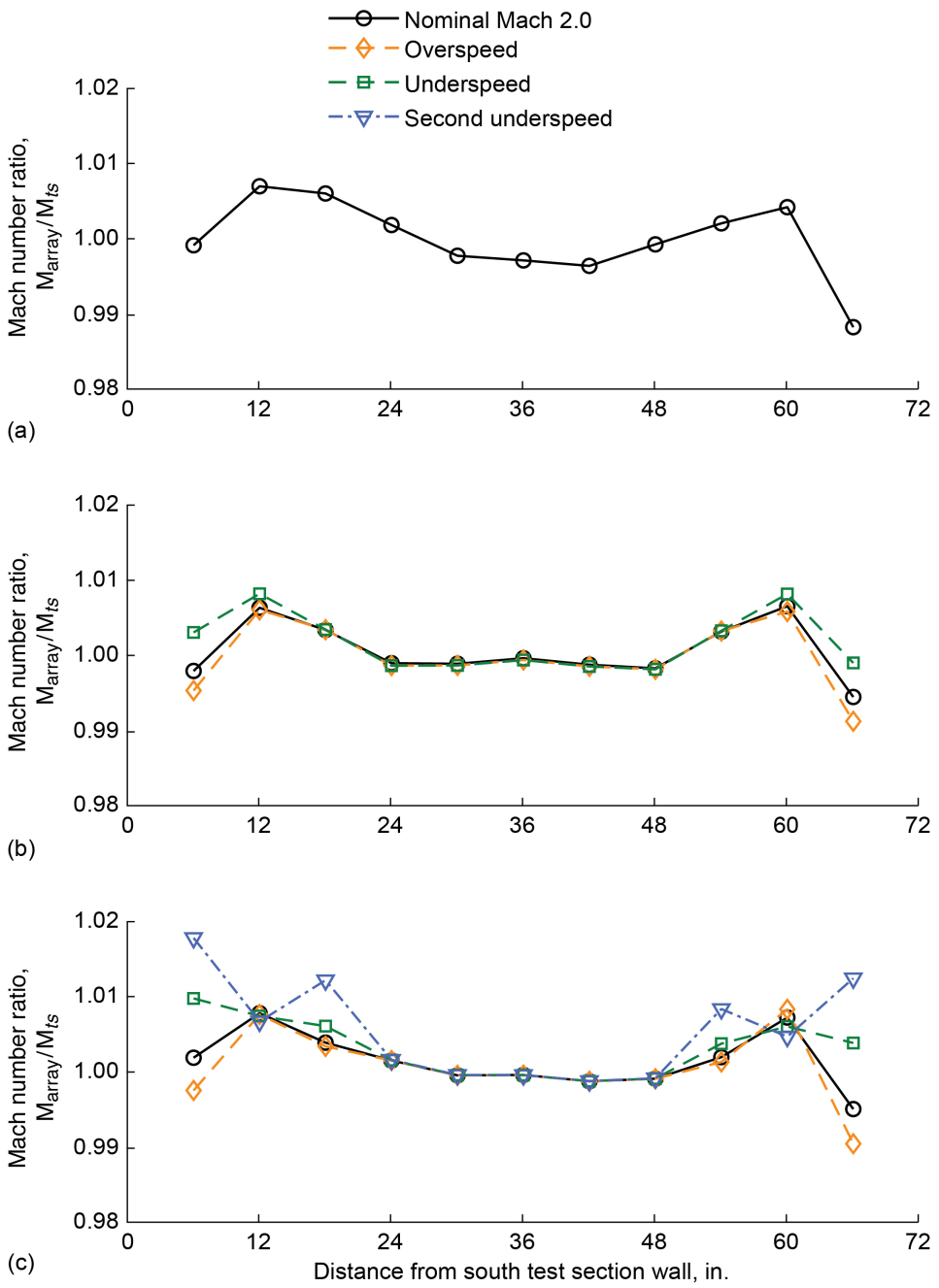

Figure 57.—Mach number ratio distributions in 8- by 6-ft test section at 14-ft test section measurement plane at centerline (CL) and 1 ft above and below CL. Data acquired during 2019 test section characterization entry at flexwall setting of Mach 2.0. (a) CL + 1 ft; 0.010 = ΔM of 0.0198. (b) CL; 0.010 = ΔM of 0.0199. (c) CL – 1 ft; 0.010 = ΔM of 0.0199.

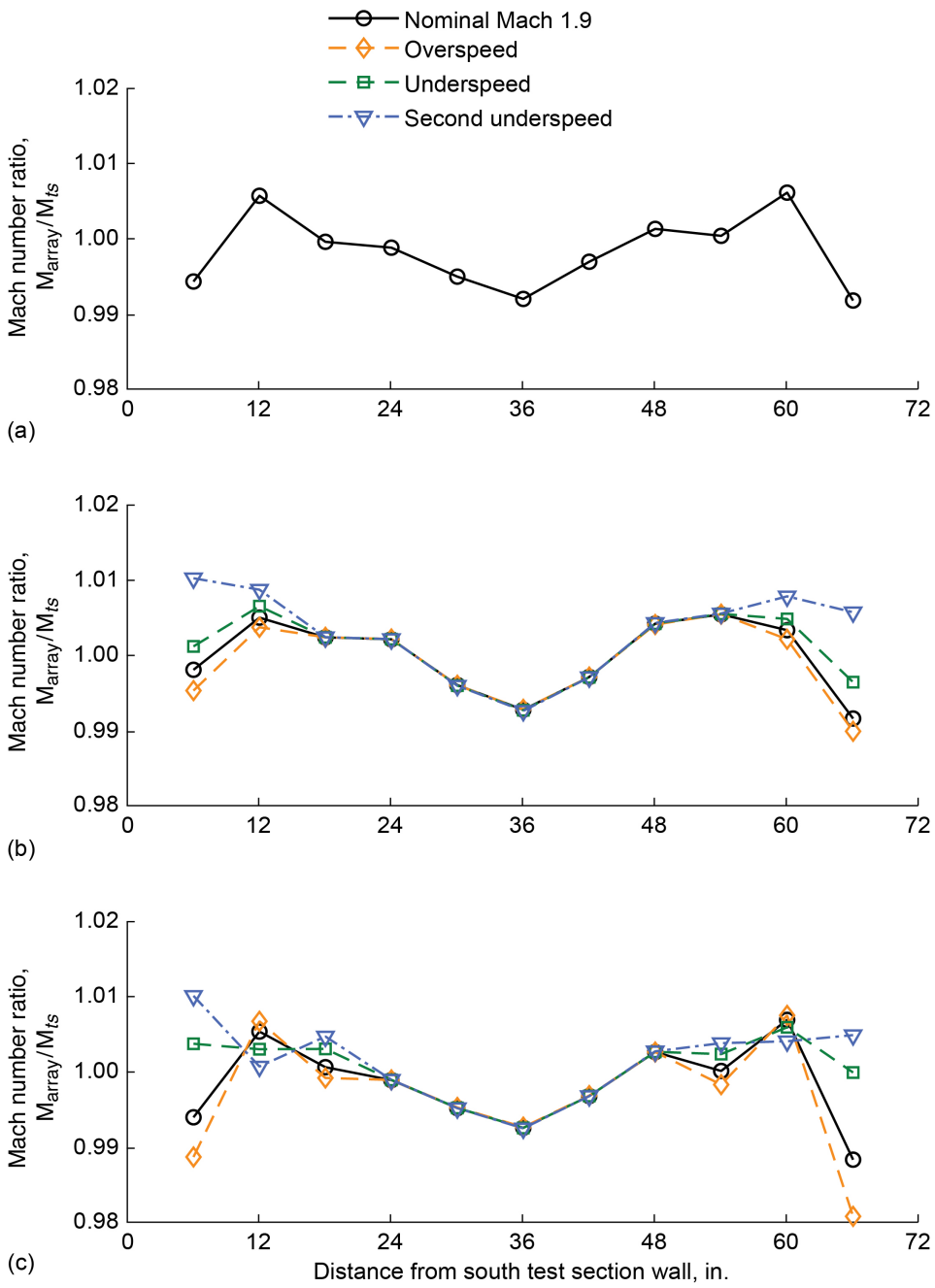

Figure 58.—Mach number ratio distributions in 8- by 6-ft test section at 14-ft test section measurement plane at centerline (CL) and 1 ft above and below CL. Data acquired during 2019 test section characterization entry at flexwall setting of Mach 1.9. (a) CL + 1 ft; 0.010 = ΔM of 0.0190. (b) CL; 0.010 = ΔM of 0.0189. (c) CL – 1 ft; 0.010 = ΔM of 0.0190.

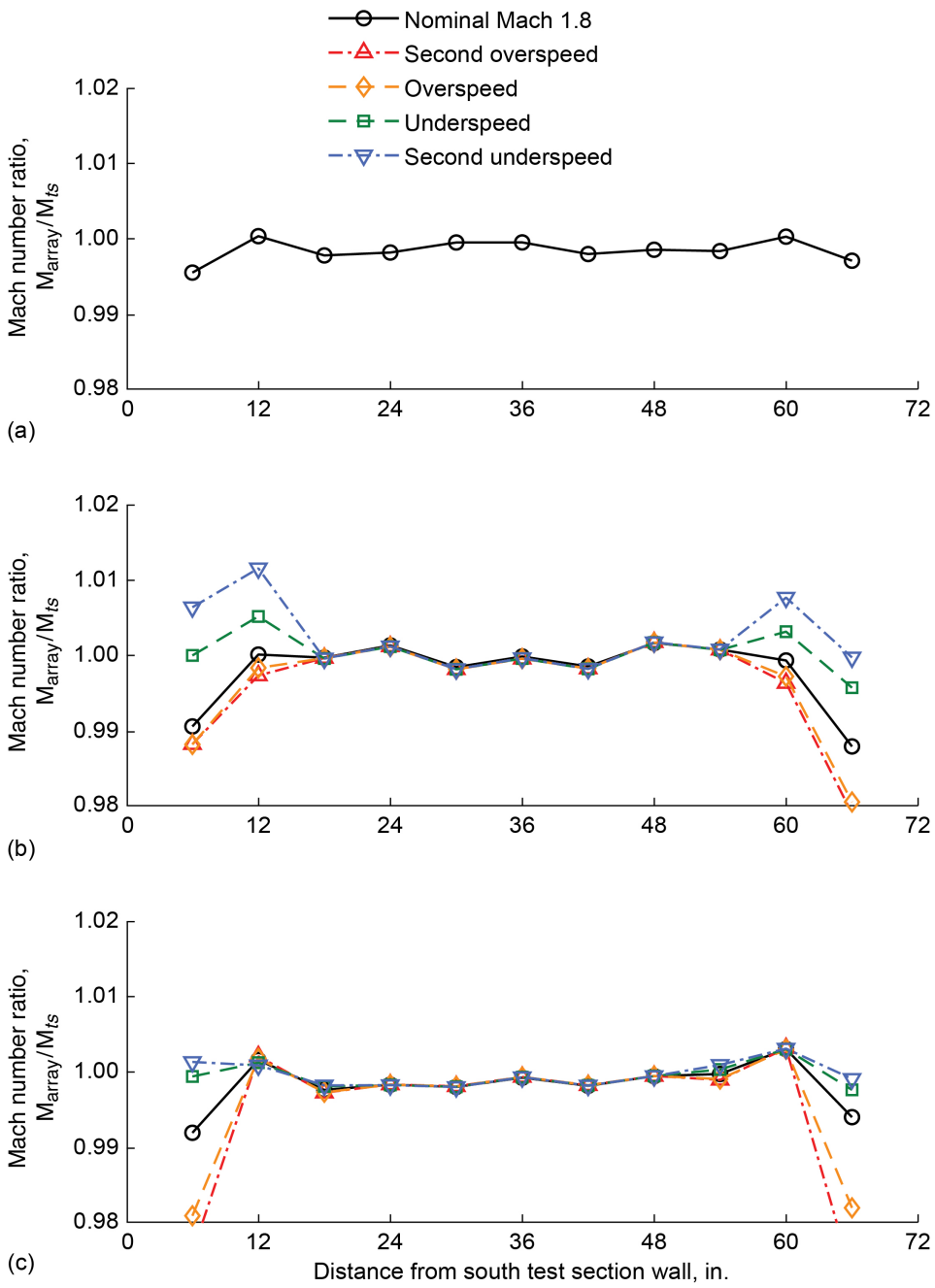

Figure 59.—Mach number ratio distributions in 8- by 6-ft test section at 14-ft test section measurement plane at centerline (CL) and 1 ft above and below CL. Data acquired during 2019 test section characterization entry at flexwall setting of Mach 1.8. (a) CL + 1 ft; 0.010 = ΔM of 0.0179. (b) CL; 0.010 = ΔM of 0.0179. (c) CL – 1 ft; 0.010 = ΔM of 0.0179.

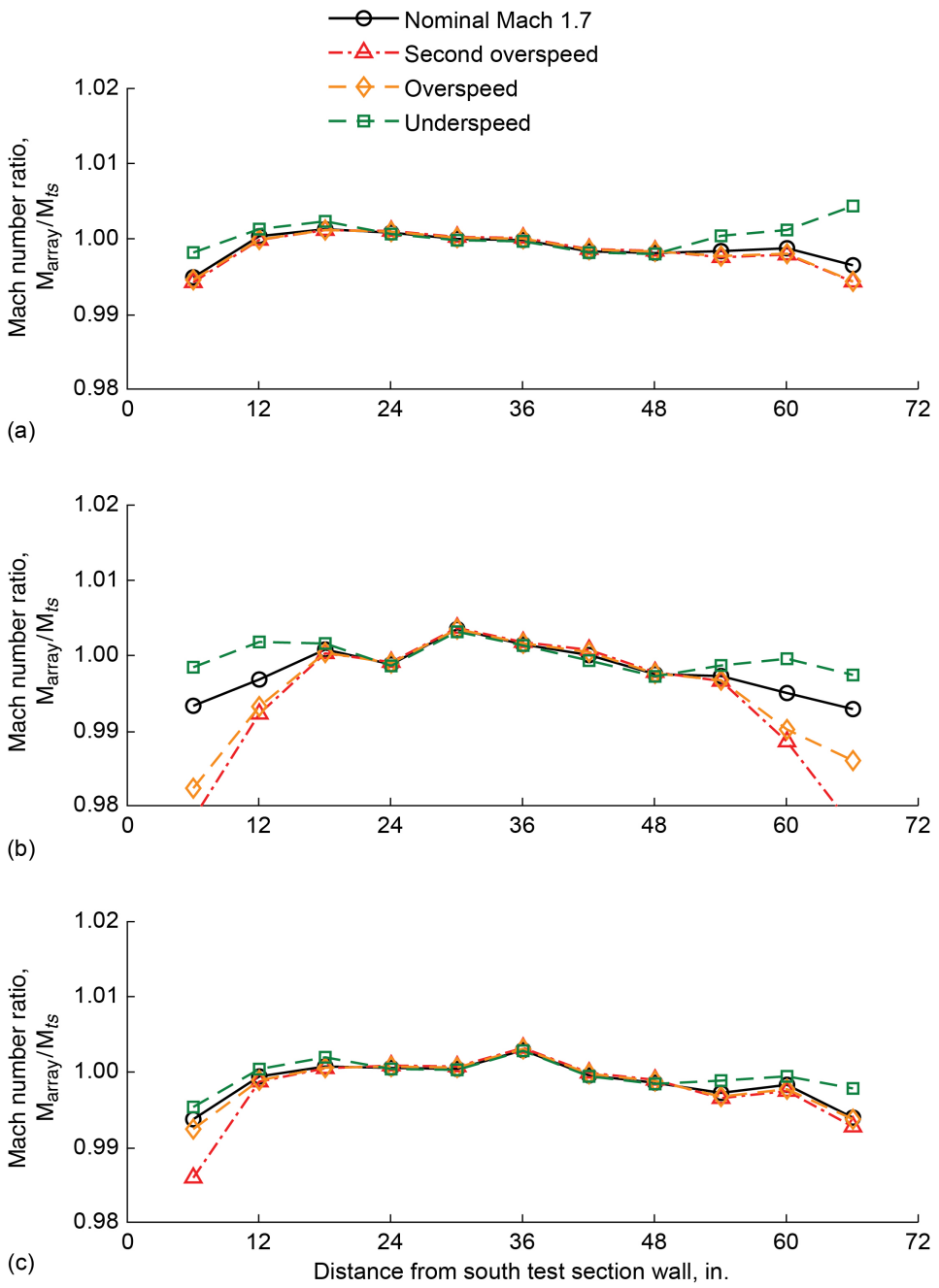

Figure 60.—Mach number ratio distributions in 8- by 6-ft test section at 14-ft test section measurement plane at centerline (CL) and 1 ft above and below CL. Data acquired during 2019 test section characterization entry at flexwall setting of Mach 1.7. (a) CL + 1 ft; 0.010 = ΔM of 0.0166. (b) CL; 0.010 = ΔM of 0.0166. (c) CL – 1 ft; 0.010 = ΔM of 0.0166.

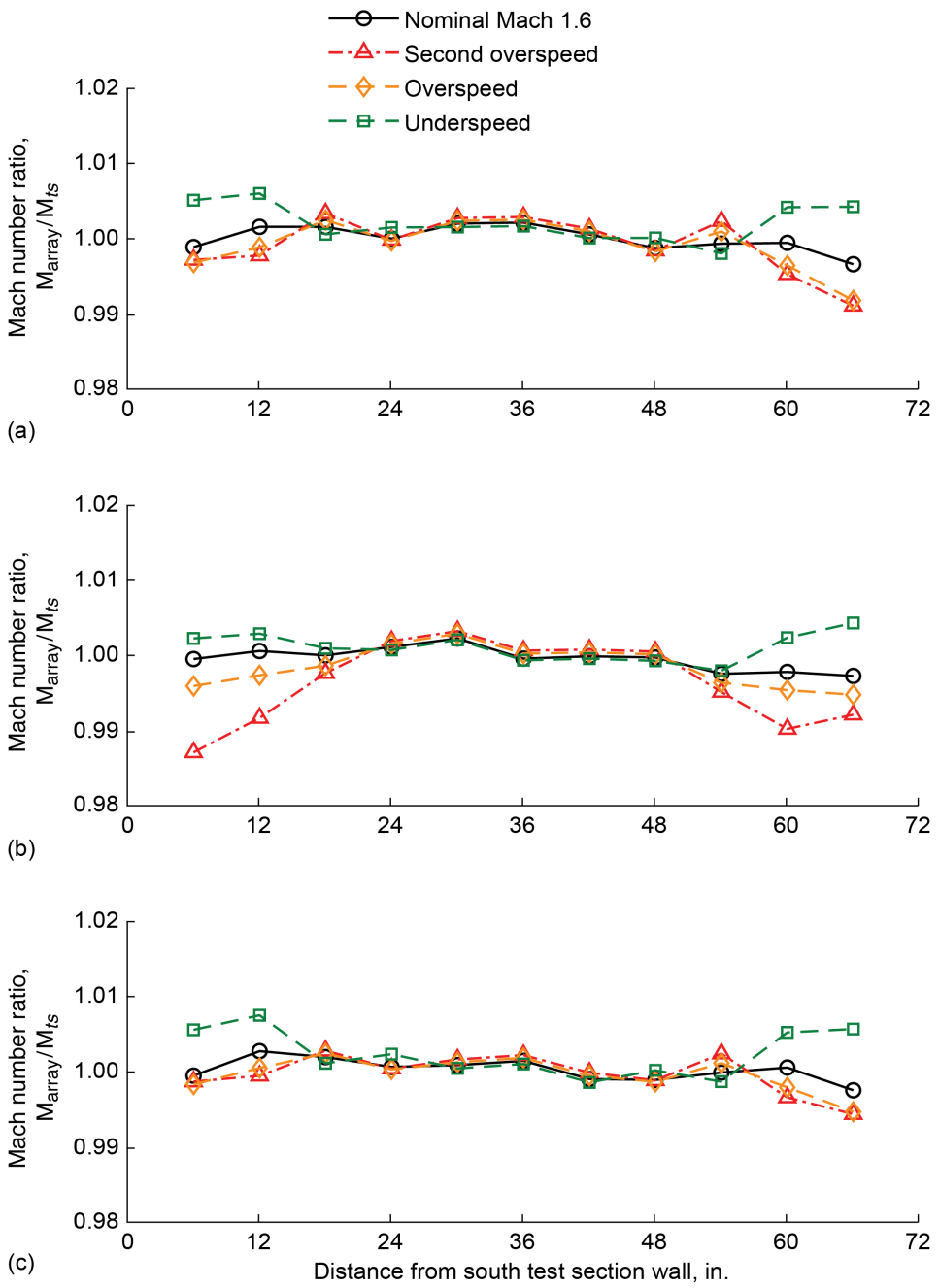

Figure 61.—Mach number ratio distributions in 8- by 6-ft test section at 14-ft test section measurement plane at centerline (CL) and 1 ft above and below CL. Data acquired during 2019 test section characterization entry at flexwall setting of Mach 1.6. (a) CL + 1 ft; 0.010 = ΔM of 0.0155. (b) CL; 0.010 = ΔM of 0.0155. (c) CL – 1 ft; 0.010 = ΔM of 0.0155.

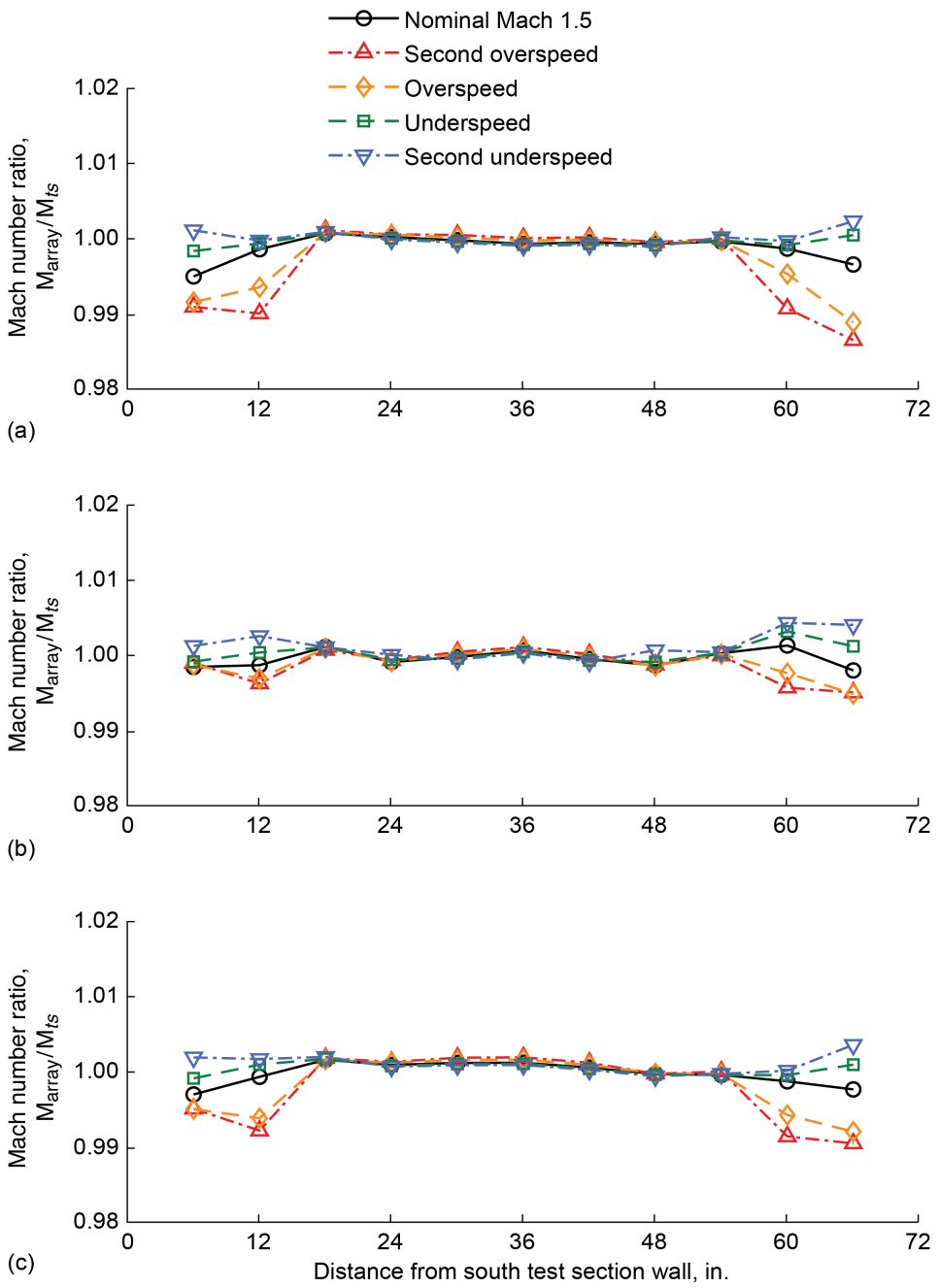

Figure 62.—Mach number ratio distributions in 8- by 6-ft test section at 14-ft test section measurement plane at centerline (CL) and 1 ft above and below CL. Data acquired during 2019 test section characterization entry at flexwall setting of Mach 1.5. (a) CL + 1 ft; 0.010 = ΔM of 0.0146. (b) CL; 0.010 = ΔM of 0.0146. (c) CL – 1 ft; 0.010 = ΔM of 0.0146.

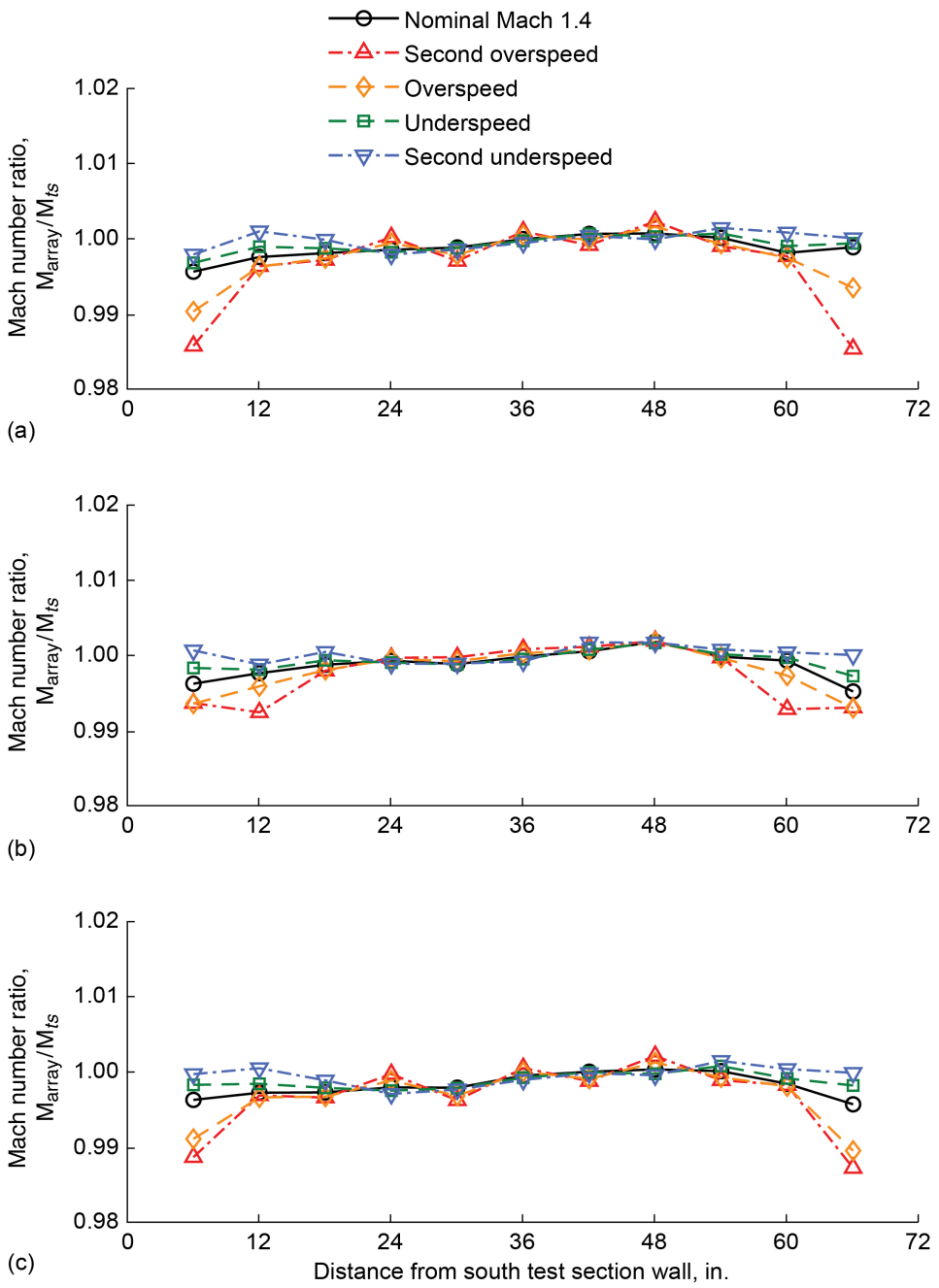

Figure 63.—Mach number ratio distributions in 8- by 6-ft test section at 14-ft test section measurement plane at centerline (CL) and 1 ft above and below CL. Data acquired during 2019 test section characterization entry at flexwall setting of Mach 1.4. (a) CL + 1 ft; 0.010 = ΔM of 0.0136. (b) CL; 0.010 = ΔM of 0.0136. (c) CL – 1 ft; 0.010 = ΔM of 0.0136.

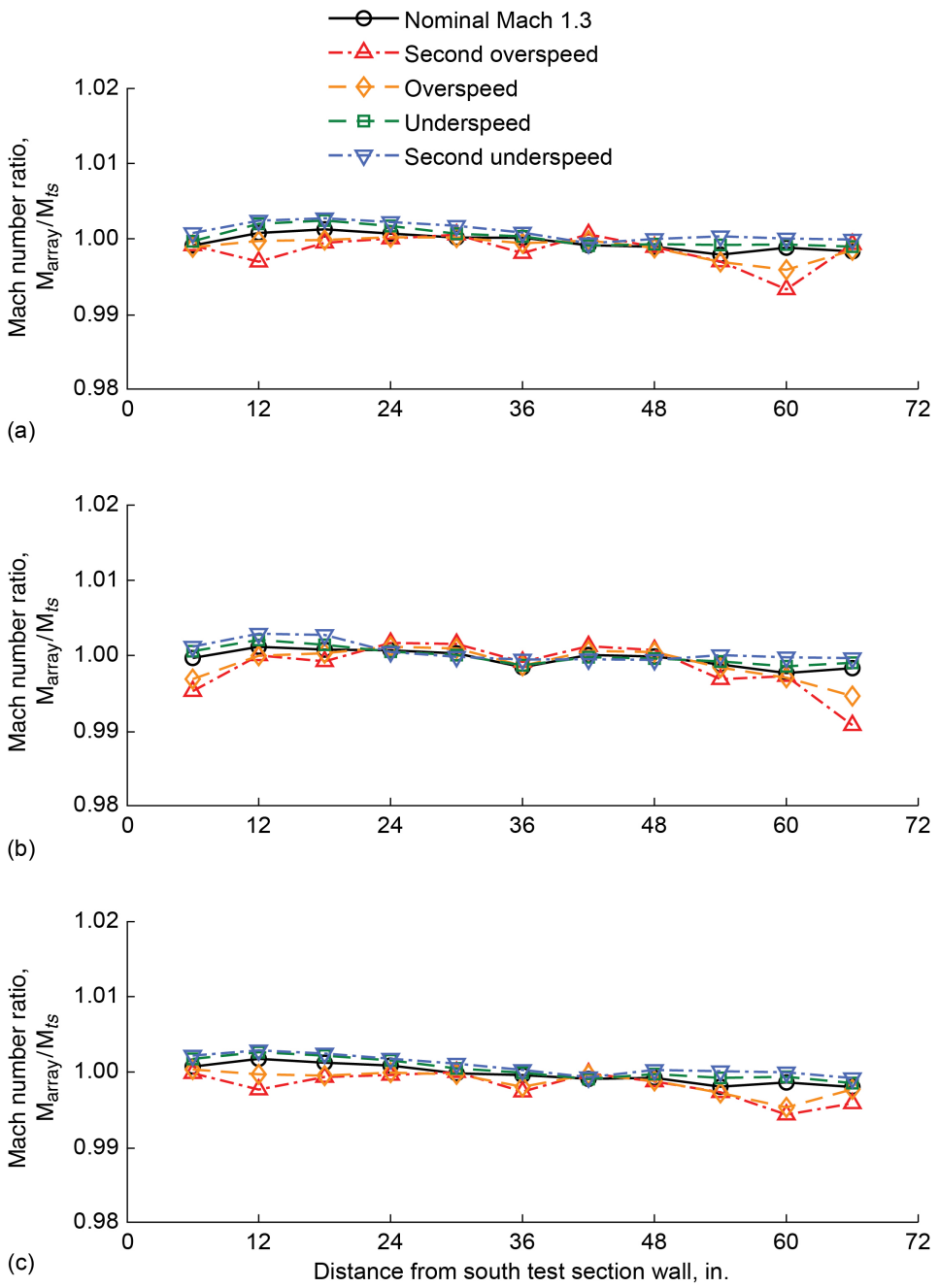

Figure 64.—Mach number ratio distributions in 8- by 6-ft test section at 14-ft test section measurement plane at centerline (CL) and 1 ft above and below CL. Data acquired during 2019 test section characterization entry at flexwall setting of Mach 1.3. (a) CL + 1 ft; 0.010 = ΔM of 0.0125. (b) CL; 0.010 = ΔM of 0.0125. (c) CL – 1 ft; 0.010 = ΔM of 0.0125.

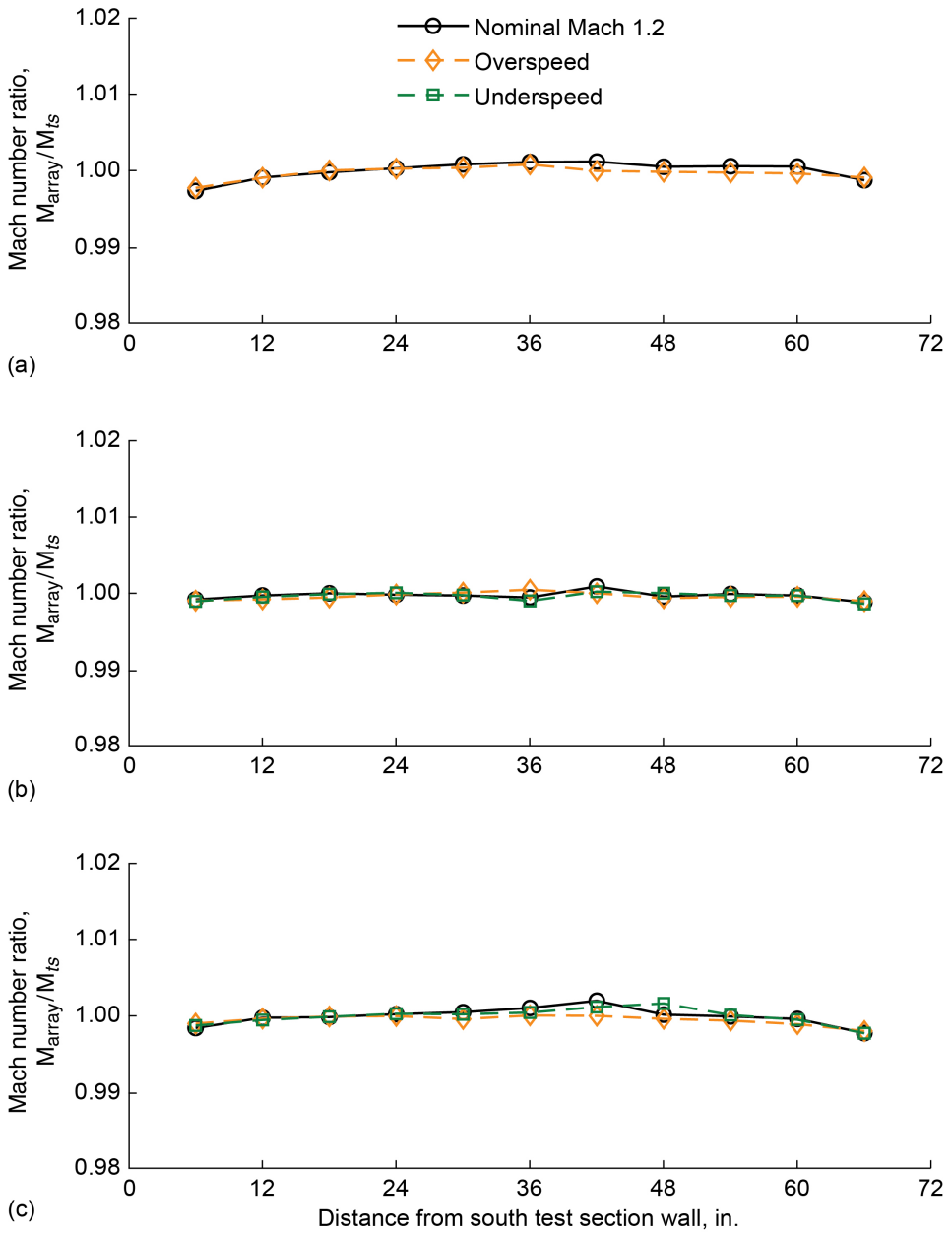

Figure 65.—Mach number ratio distributions in 8- by 6-ft test section at 14-ft test section measurement plane at centerline (CL) and 1 ft above and below CL. Data acquired during 2019 test section characterization entry at flexwall setting of Mach 1.2. (a) CL + 1 ft; 0.010 = ΔM of 0.0118. (b) CL; 0.010 = ΔM of 0.0118. (c) CL – 1 ft; 0.010 = ΔM of 0.0118.

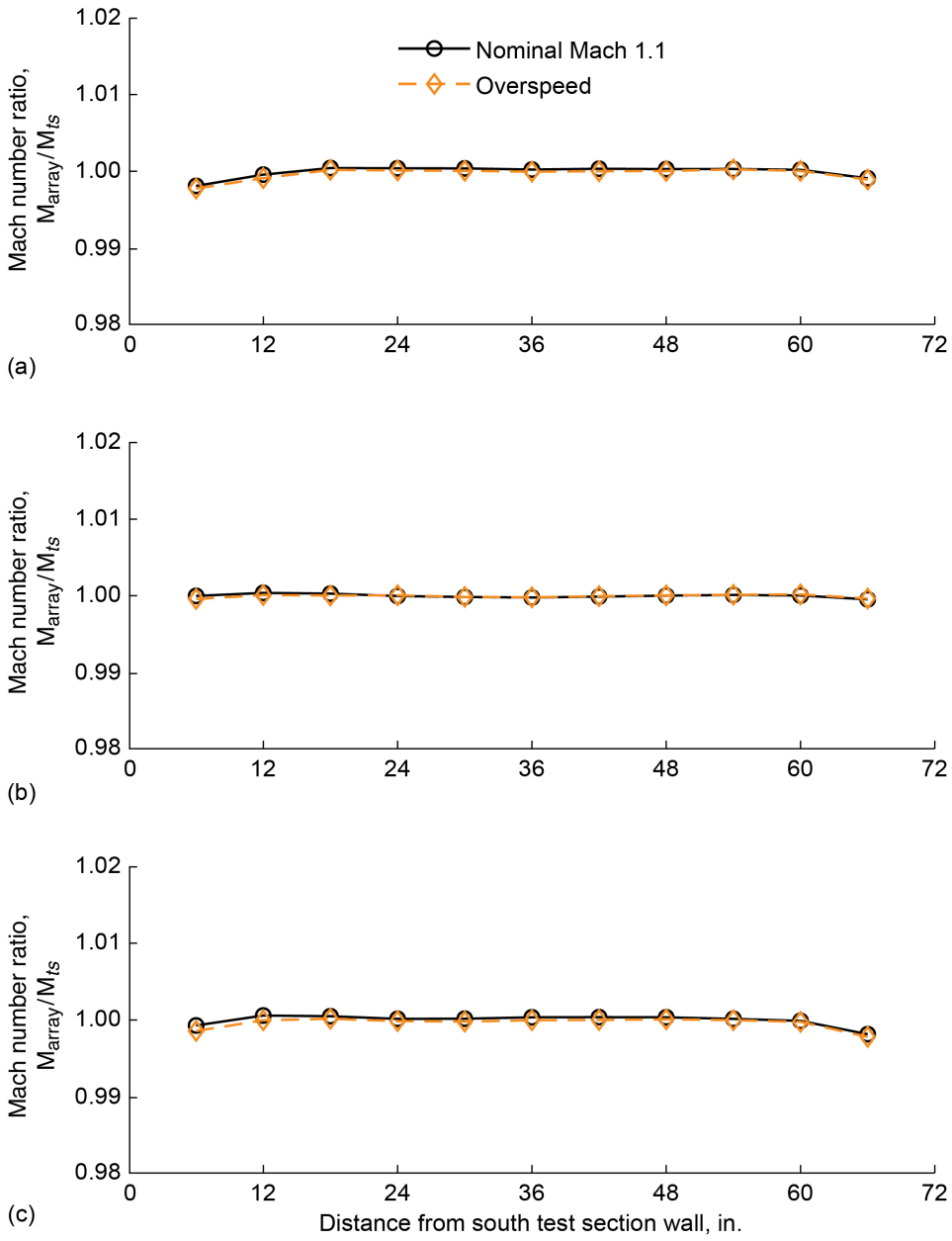

Figure 66.—Mach number ratio distributions in 8- by 6-ft test section at 14-ft test section measurement plane at centerline (CL) and 1 ft above and below CL. Data acquired during 2019 test section characterization entry at flexwall setting of Mach 1.1. (a) CL + 1 ft; 0.010 = ΔM of 0.0108. (b) CL; 0.010 = ΔM of 0.0108. (c) CL – 1 ft; 0.010 = ΔM of 0.0108.

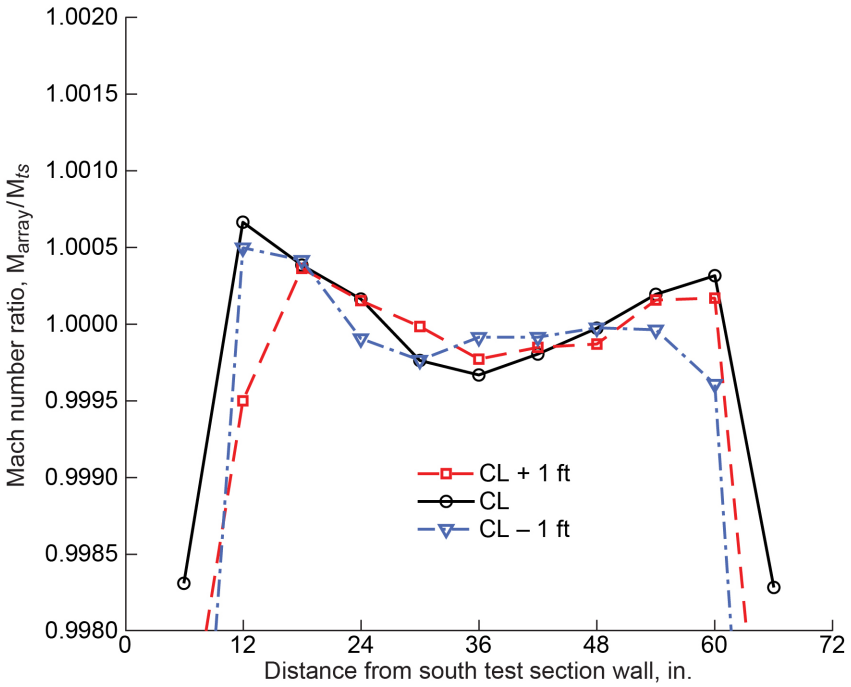

Figure 67.—Mach number ratio distributions in 8- by 6-ft test section at 14-ft test section measurement plane at centerline (CL) and 1 ft above and below CL. Data acquired during 2019 test section characterization entry at transonic array Mach number of 0.951 (three-drive-motor operation). 0.0005 = ΔM of 0.0005.

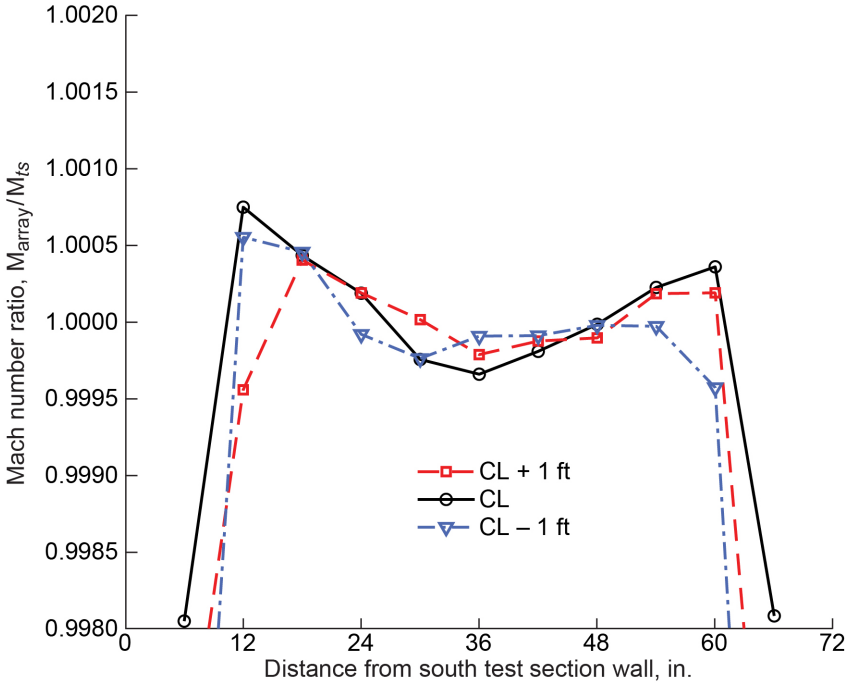

Figure 68.—Mach number ratio distributions in 8- by 6-ft test section at 14-ft test section measurement plane at centerline (CL) and 1 ft above and below CL. Data acquired during 2019 test section characterization entry at transonic array Mach number of 0.900 (three-drive-motor operation). 0.0005 = ΔM of 0.0004.

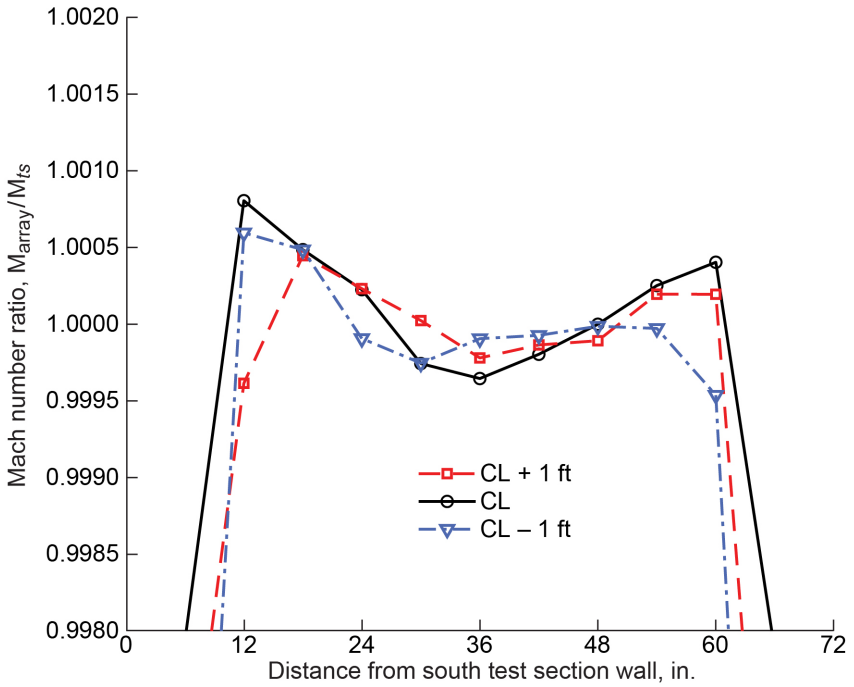

Figure 69.—Mach number ratio distributions in 8- by 6-ft test section at 14-ft test section measurement plane at centerline (CL) and 1 ft above and below CL. Data acquired during 2019 test section characterization entry at transonic array Mach number of 0.849 (three-drive-motor operation). 0.0005 = ΔM of 0.0004.

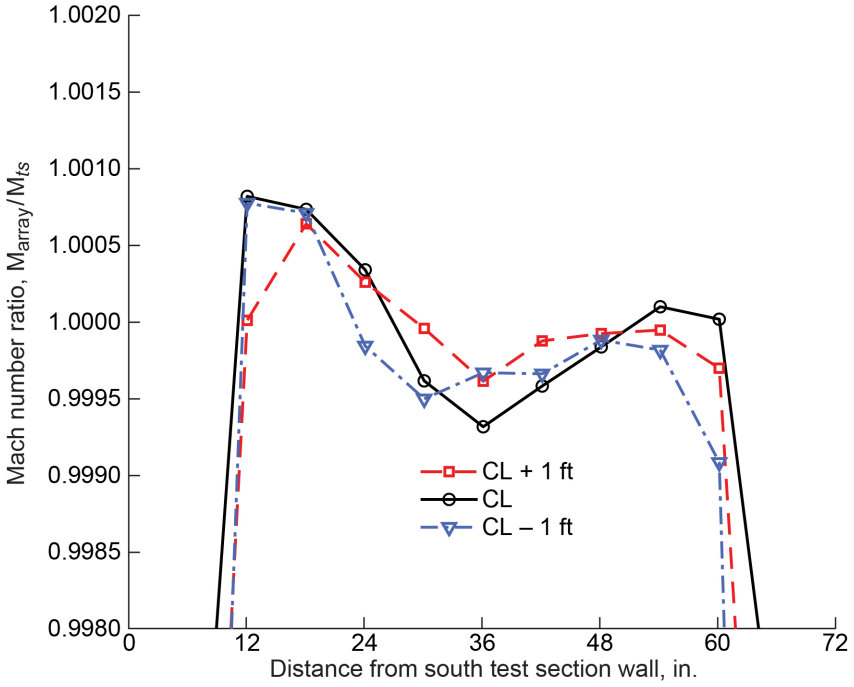

Figure 70.—Mach number ratio distributions in 8- by 6-ft test section at 14-ft test section measurement plane at centerline (CL) and 1 ft above and below CL. Data acquired during 2019 test section characterization entry at transonic array Mach number of 0.800 (three-drive-motor operation). 0.0005 = ΔM of 0.0004.

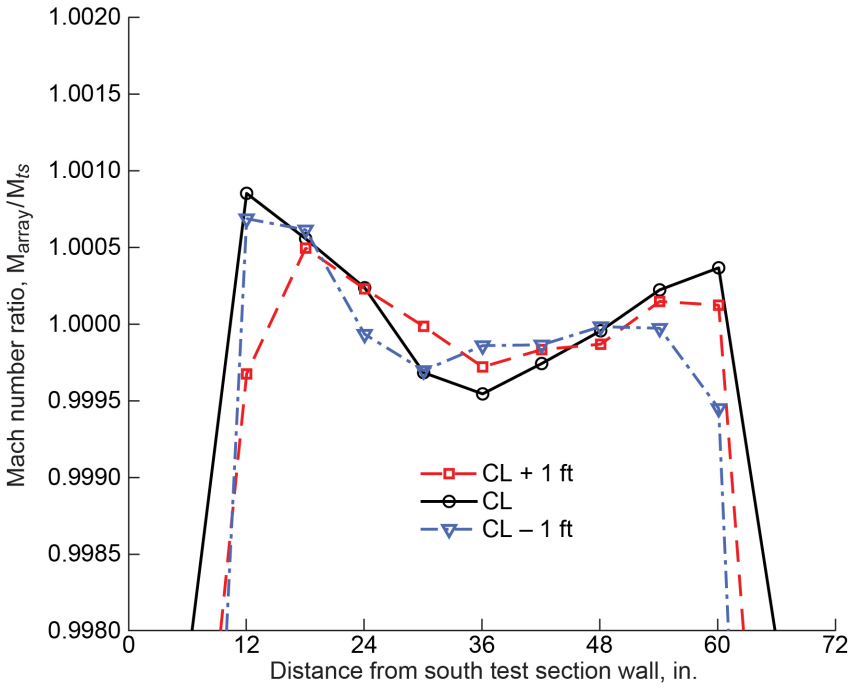

Figure 71.—Mach number ratio distributions in 8- by 6-ft test section at 14-ft test section measurement plane at centerline (CL) and 1 ft above and below CL. Data acquired during 2019 test section characterization entry at transonic array Mach number of 0.750 (three-drive-motor operation). 0.0005 = ΔM of 0.0004.

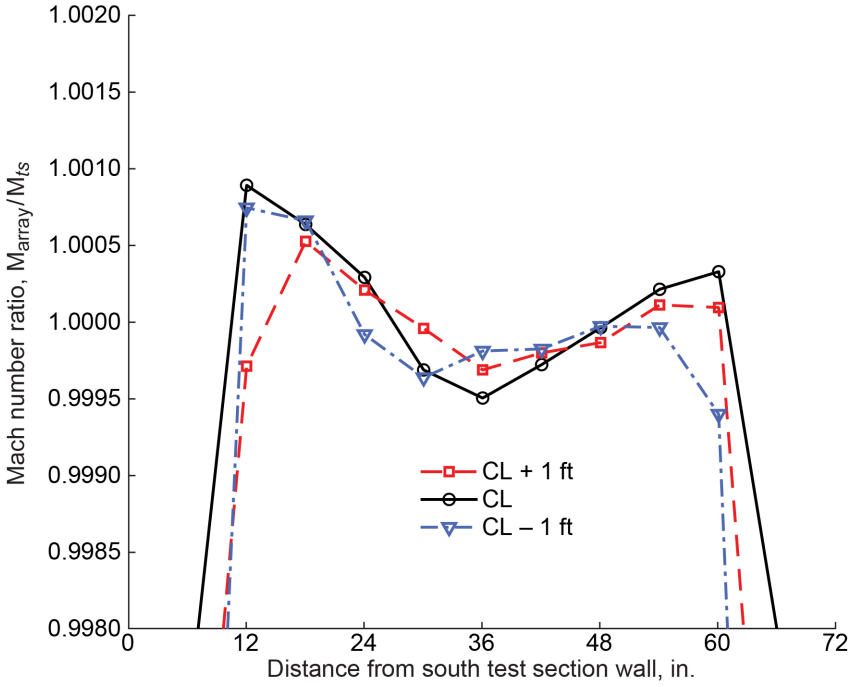

Figure 72.—Mach number ratio distributions in 8- by 6-ft test section at 14-ft test section measurement plane at centerline (CL) and 1 ft above and below CL. Data acquired during 2019 test section characterization entry at transonic array Mach number of 0.701 (three-drive-motor operation). 0.0005 = ΔM of 0.0004.

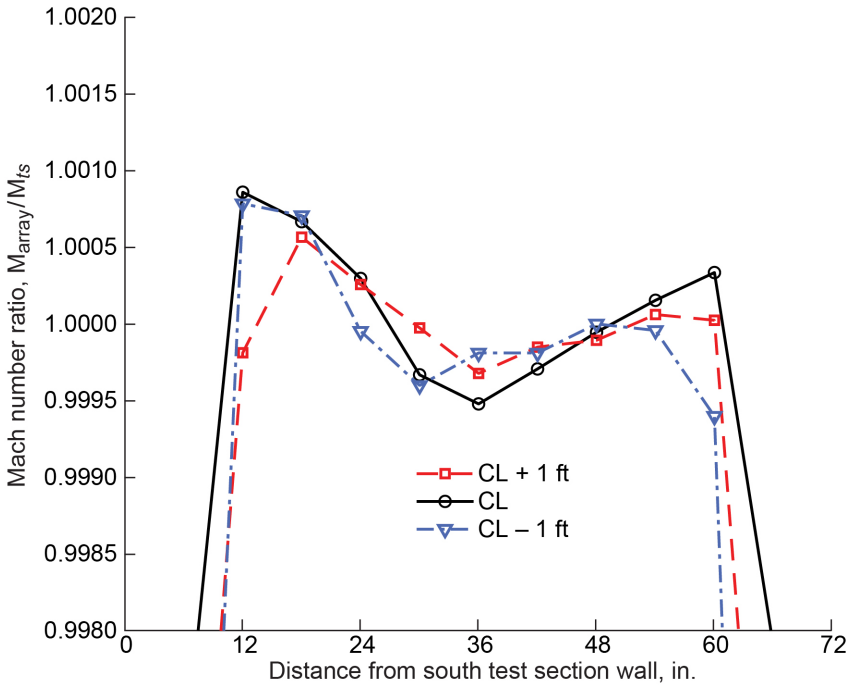

Figure 73.—Mach number ratio distributions in 8- by 6-ft test section at 14-ft test section measurement plane at centerline (CL) and 1 ft above and below CL. Data acquired during 2019 test section characterization entry at transonic array Mach number of 0.649 (three-drive-motor operation). 0.0005 = ΔM of 0.0003.

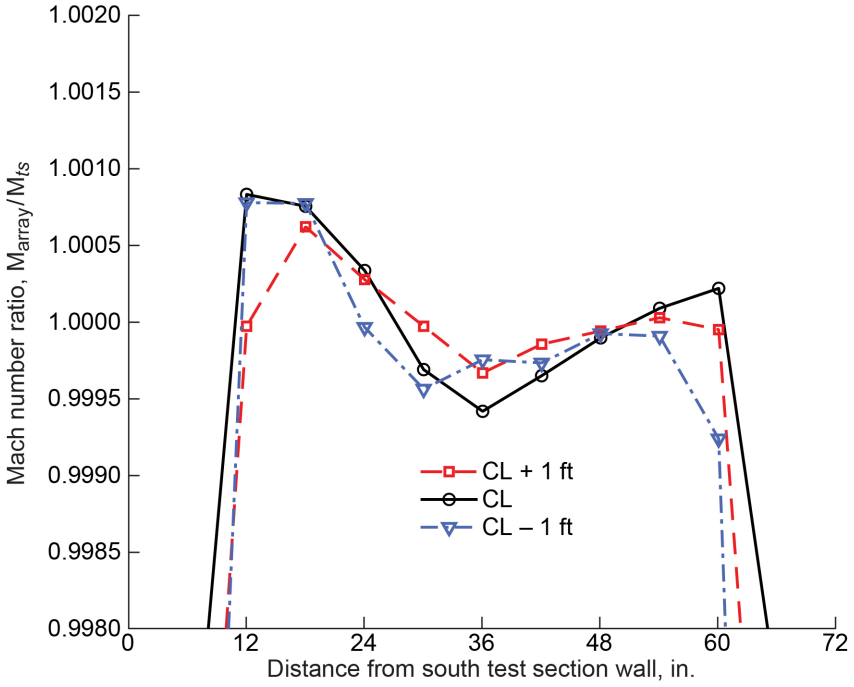

Figure 74.—Mach number ratio distributions in 8- by 6-ft test section at 14-ft test section measurement plane at centerline (CL) and 1 ft above and below CL. Data acquired during 2019 test section characterization entry at transonic array Mach number of 0.600 (three-drive-motor operation). 0.0005 = ΔM of 0.0003.

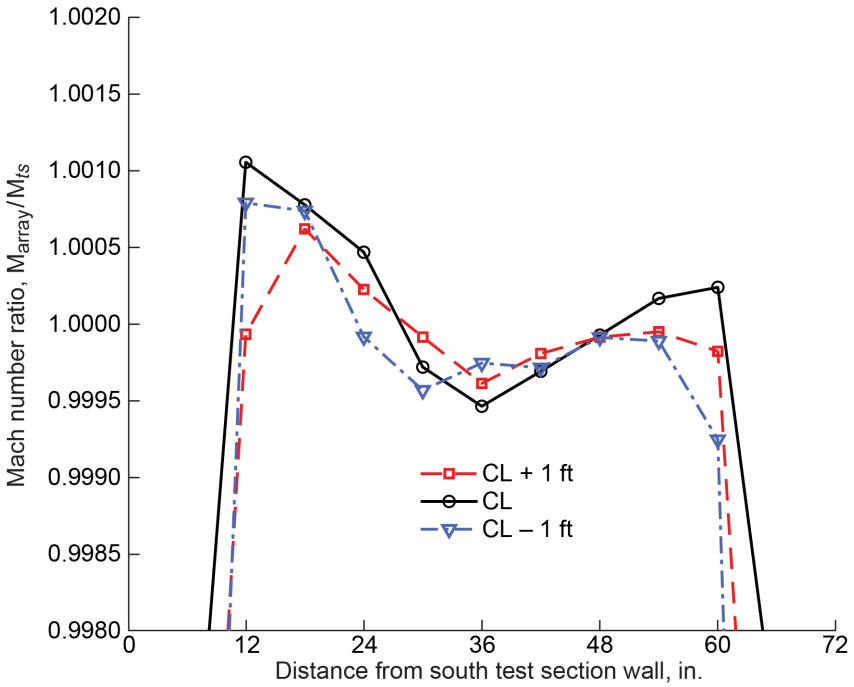

Figure 75.—Mach number ratio distributions in 8- by 6-ft test section at 14-ft test section measurement plane at centerline (CL) and 1 ft above and below CL. Data acquired during 2019 test section characterization entry at transonic array Mach number of 0.551 (three-drive-motor operation). 0.0005 = ΔM of 0.0003.

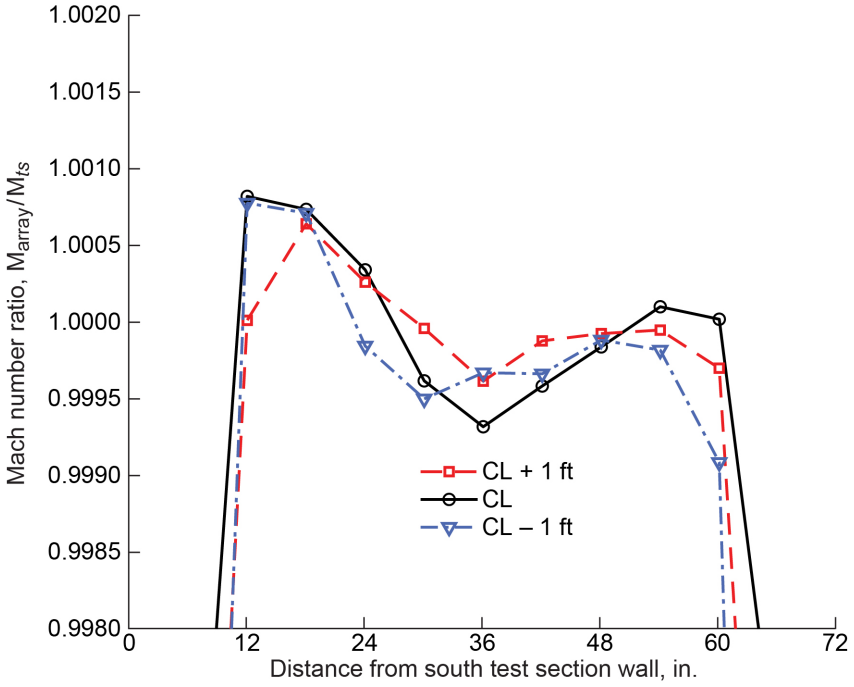

Figure 76.—Mach number ratio distributions in 8- by 6-ft test section at 14-ft test section measurement plane at centerline (CL) and 1 ft above and below CL. Data acquired during 2019 test section characterization entry at transonic array Mach number of 0.500 (three-drive-motor operation). 0.0005 = ΔM of 0.0002.

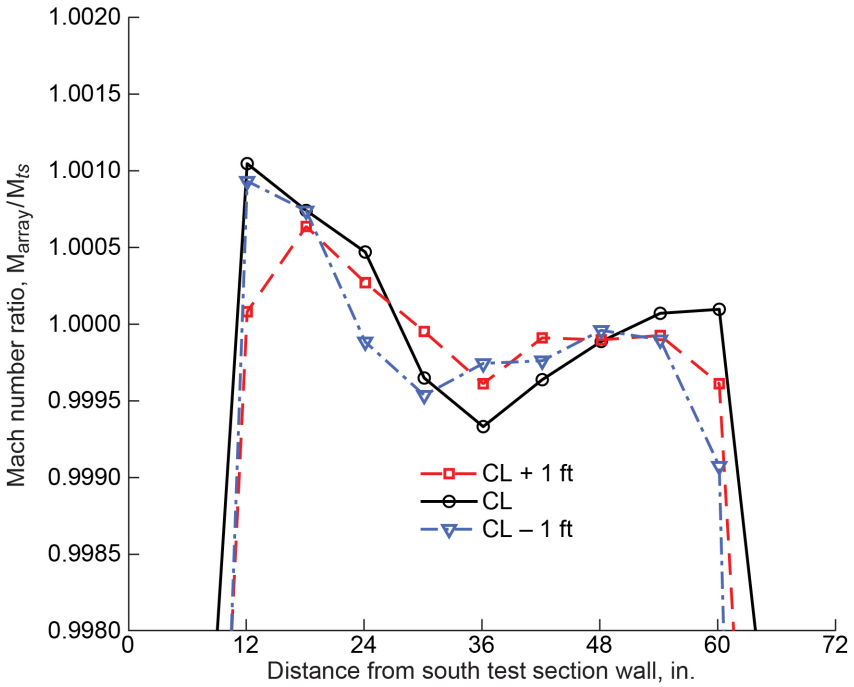

Figure 77.—Mach number ratio distributions in 8- by 6-ft test section at 14-ft test section measurement plane at centerline (CL) and 1 ft above and below CL. Data acquired during 2019 test section characterization entry at transonic array Mach number of 0.449 (three-drive-motor operation). 0.0005 = ΔM of 0.0002.

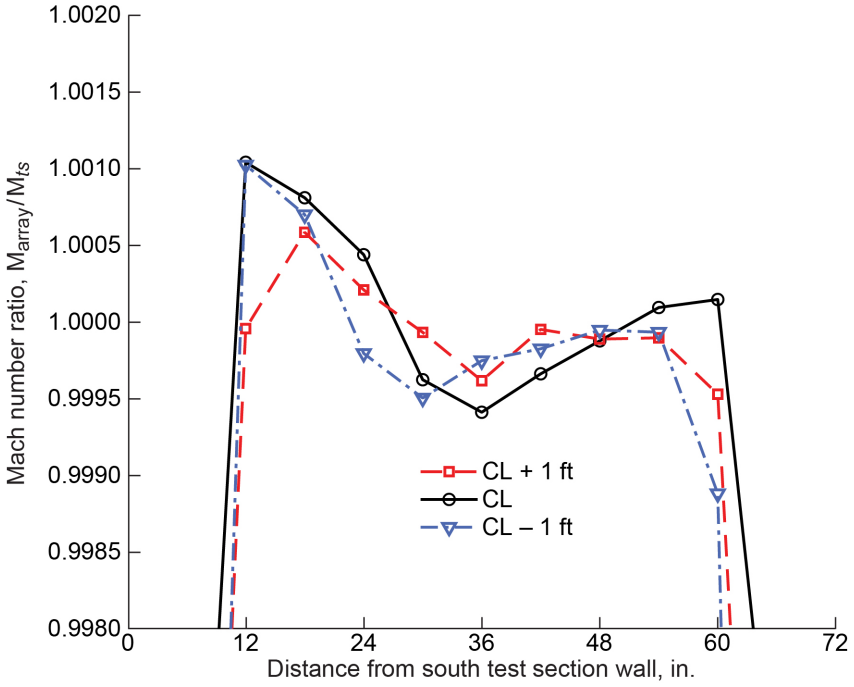

Figure 78.—Mach number ratio distributions in 8- by 6-ft test section at 14-ft test section measurement plane at centerline (CL) and 1 ft above and below CL. Data acquired during 2019 test section characterization entry at transonic array Mach number of 0.401 (three-drive-motor operation). 0.0005 = ΔM of 0.0002.

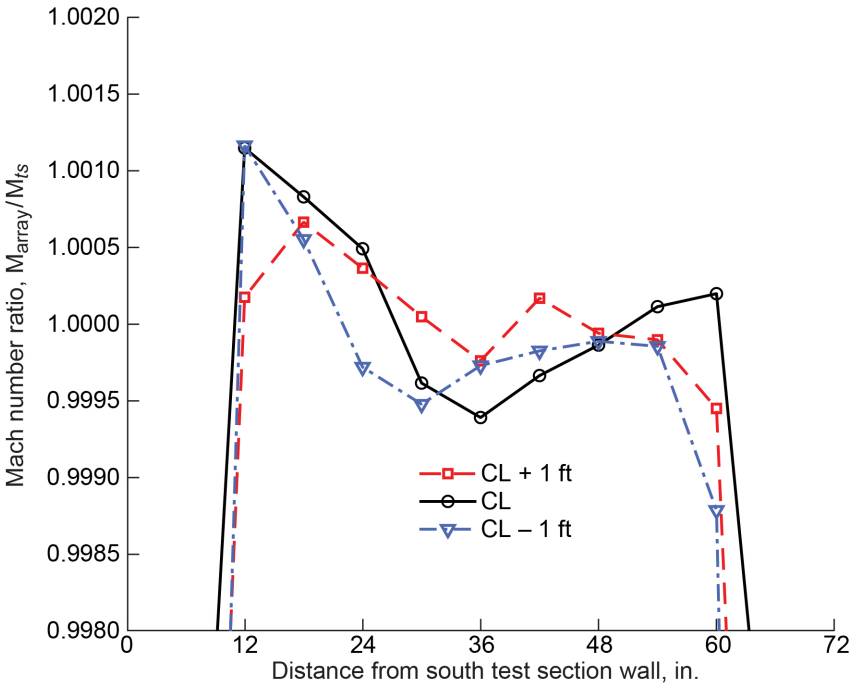

Figure 79.—Mach number ratio distributions in 8- by 6-ft test section at 14-ft test section measurement plane at centerline (CL) and 1 ft above and below CL. Data acquired during 2019 test section characterization entry at transonic array Mach number of 0.369 (three-drive-motor operation). 0.0005 = ΔM of 0.0002.

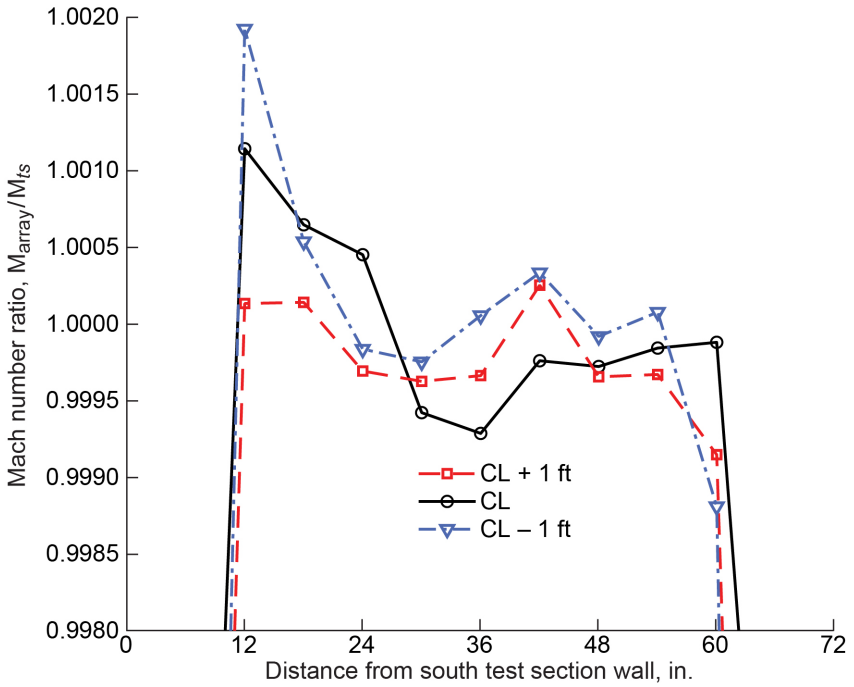

Figure 80.—Mach number ratio distributions in 8- by 6-ft test section at 14-ft test section measurement plane at centerline (CL) and 1 ft above and below CL. Data acquired during 2019 test section characterization entry at transonic array Mach number of 0.500 (one-drive-motor operation). 0.0005 = ΔM of 0.0003.

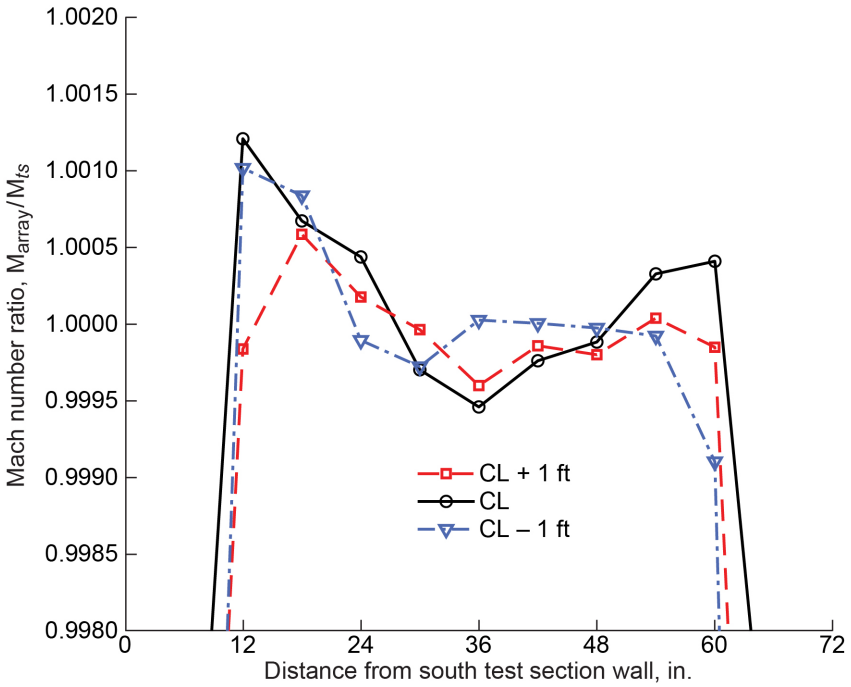

Figure 81.—Mach number ratio distributions in 8- by 6-ft test section at 14-ft test section measurement plane at centerline (CL) and 1 ft above and below CL. Data acquired during 2019 test section characterization entry at transonic array Mach number of 0.449 (one-drive-motor operation). 0.0005 = ΔM of 0.0002.

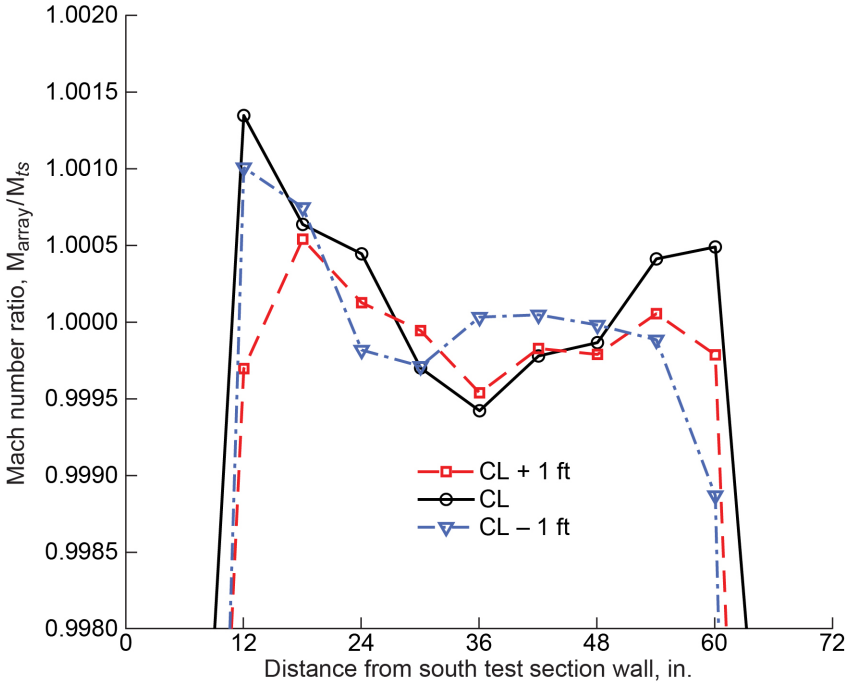

Figure 82.—Mach number ratio distributions in 8- by 6-ft test section at 14-ft test section measurement plane at centerline (CL) and 1 ft above and below CL. Data acquired during 2019 test section characterization entry at transonic array Mach number of 0.401 (one-drive-motor operation). 0.0005 = ΔM of 0.0002.

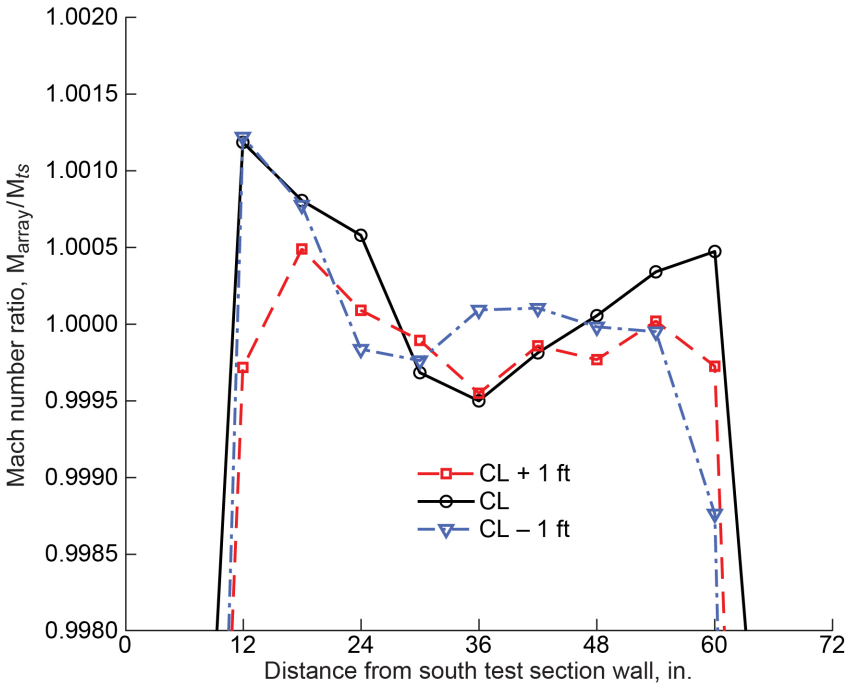

Figure 83.—Mach number ratio distributions in 8- by 6-ft test section at 14-ft test section measurement plane at centerline (CL) and 1 ft above and below CL. Data acquired during 2019 test section characterization entry at transonic array Mach number of 0.352 (one-drive-motor operation). 0.0005 = ΔM of 0.0002.

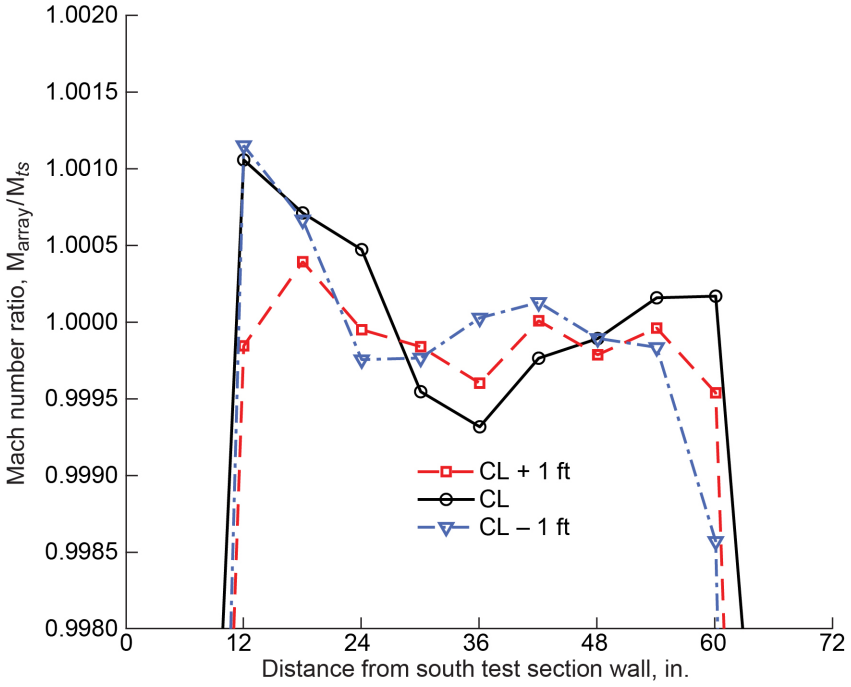

Figure 84.—Mach number ratio distributions in 8- by 6-ft test section at 14-ft test section measurement plane at centerline (CL) and 1 ft above and below CL. Data acquired during 2019 test section characterization entry at transonic array Mach number of 0.299 (one-drive-motor operation). 0.0005 = ΔM of 0.0001.

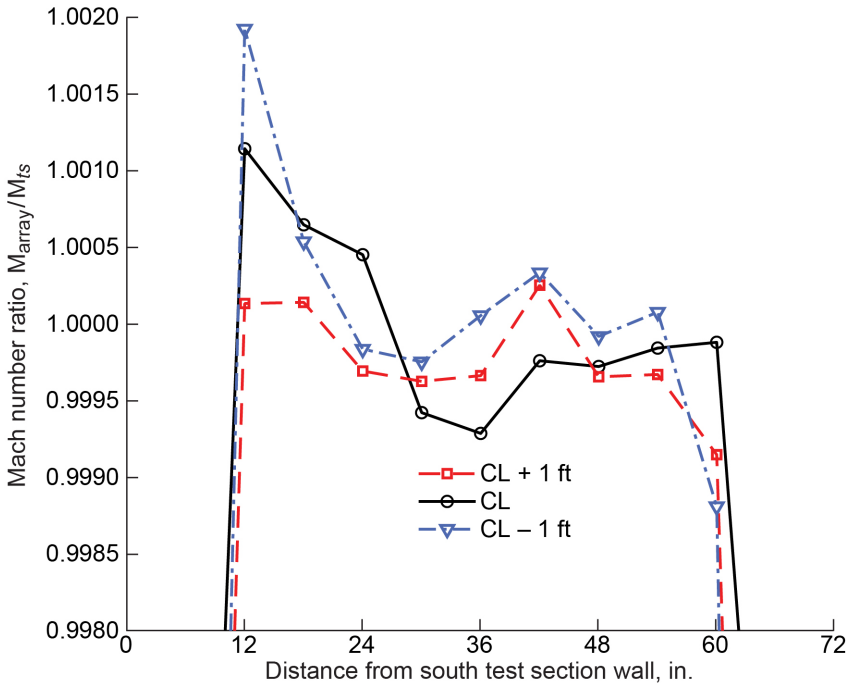

Figure 85.—Mach number ratio distributions in 8- by 6-ft test section at 14-ft test section measurement plane at centerline (CL) and 1 ft above and below CL. Data acquired during 2019 test section characterization entry at transonic array Mach number of 0.251 (one-drive-motor operation). 0.0005 = ΔM of 0.0001.

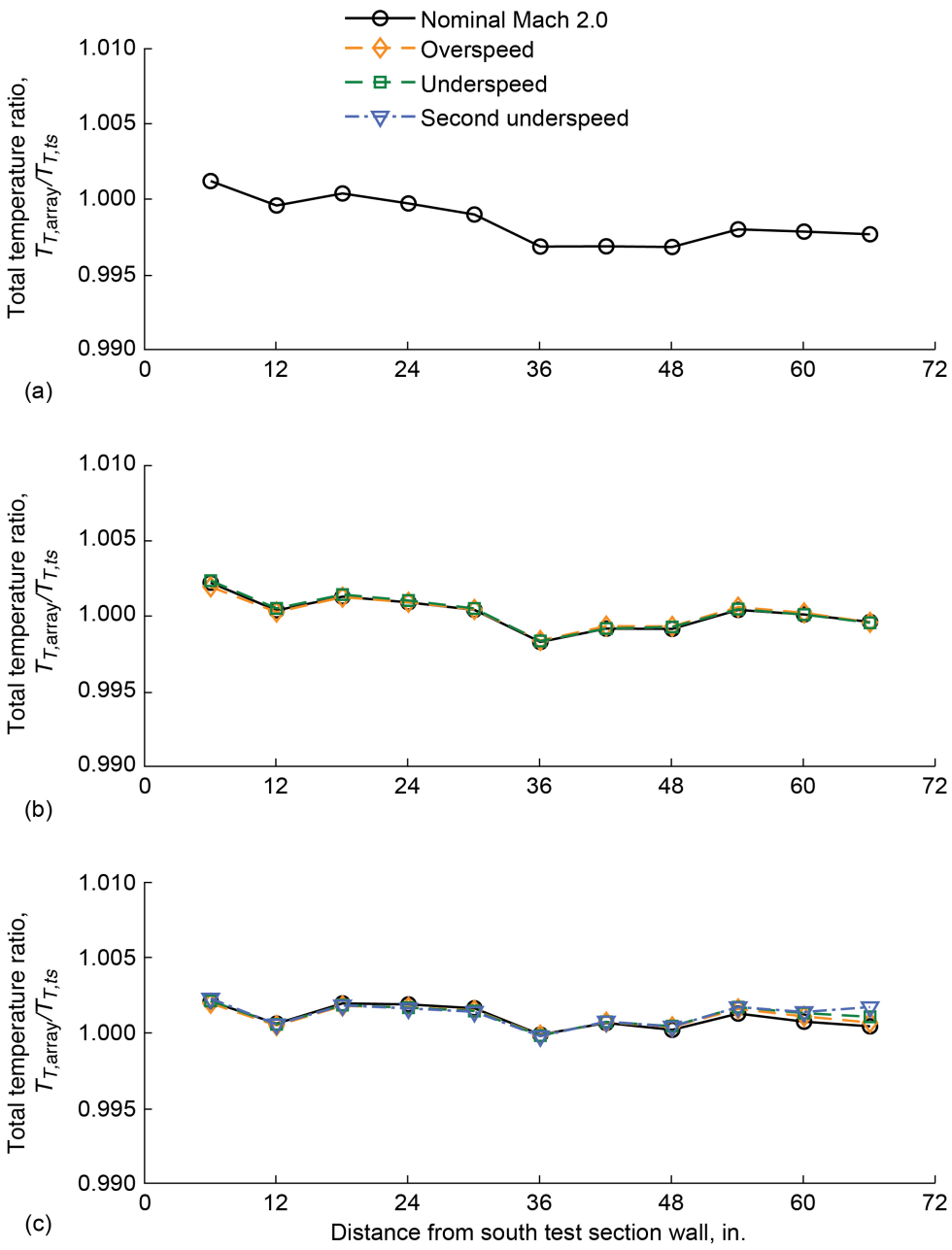

Figure 86.—Total temperature ratio distributions in 8- by 6-ft test section at 14-ft test section measurement plane at centerline (CL) and 1 ft above and below CL. Data acquired during 2019 test section characterization entry at flexwall setting of Mach 2.0. (a) CL + 1 ft; 0.005 = ΔT_T of 3.20 R. (b) CL; 0.005 = ΔT_T of 3.25 R. (c) CL – 1 ft; 0.005 = ΔT_T of 3.21 R.

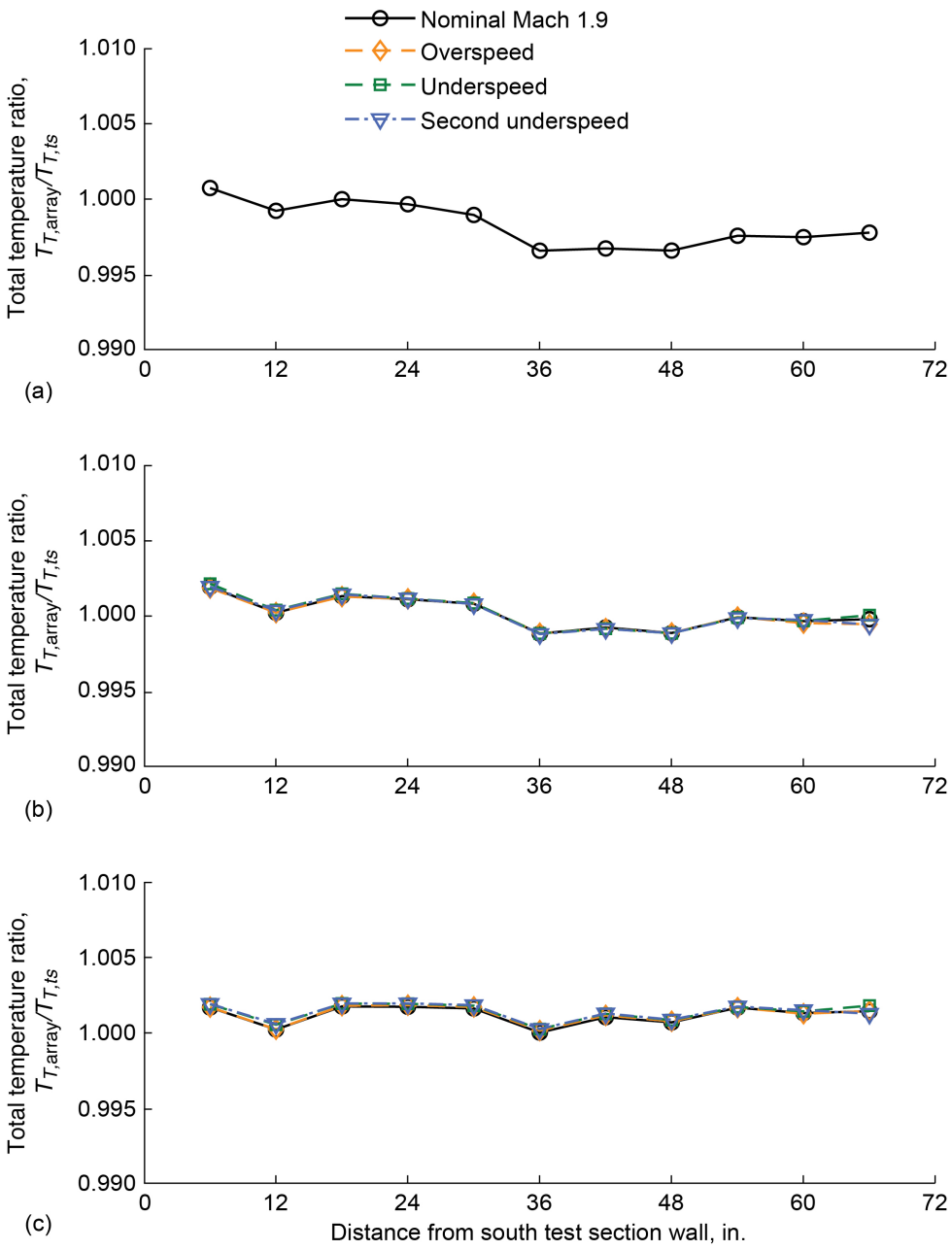

Figure 87.—Total temperature ratio distributions in 8- by 6-ft test section at 14-ft test section measurement plane at centerline (CL) and 1 ft above and below CL. Data acquired during 2019 test section characterization entry at flexwall setting of Mach 1.9. (a) CL + 1 ft; 0.005 = ΔT_T of 3.18 R. (b) CL; 0.005 = ΔT_T of 3.23 R. (c) CL – 1 ft; 0.005 = ΔT_T of 3.23 R.

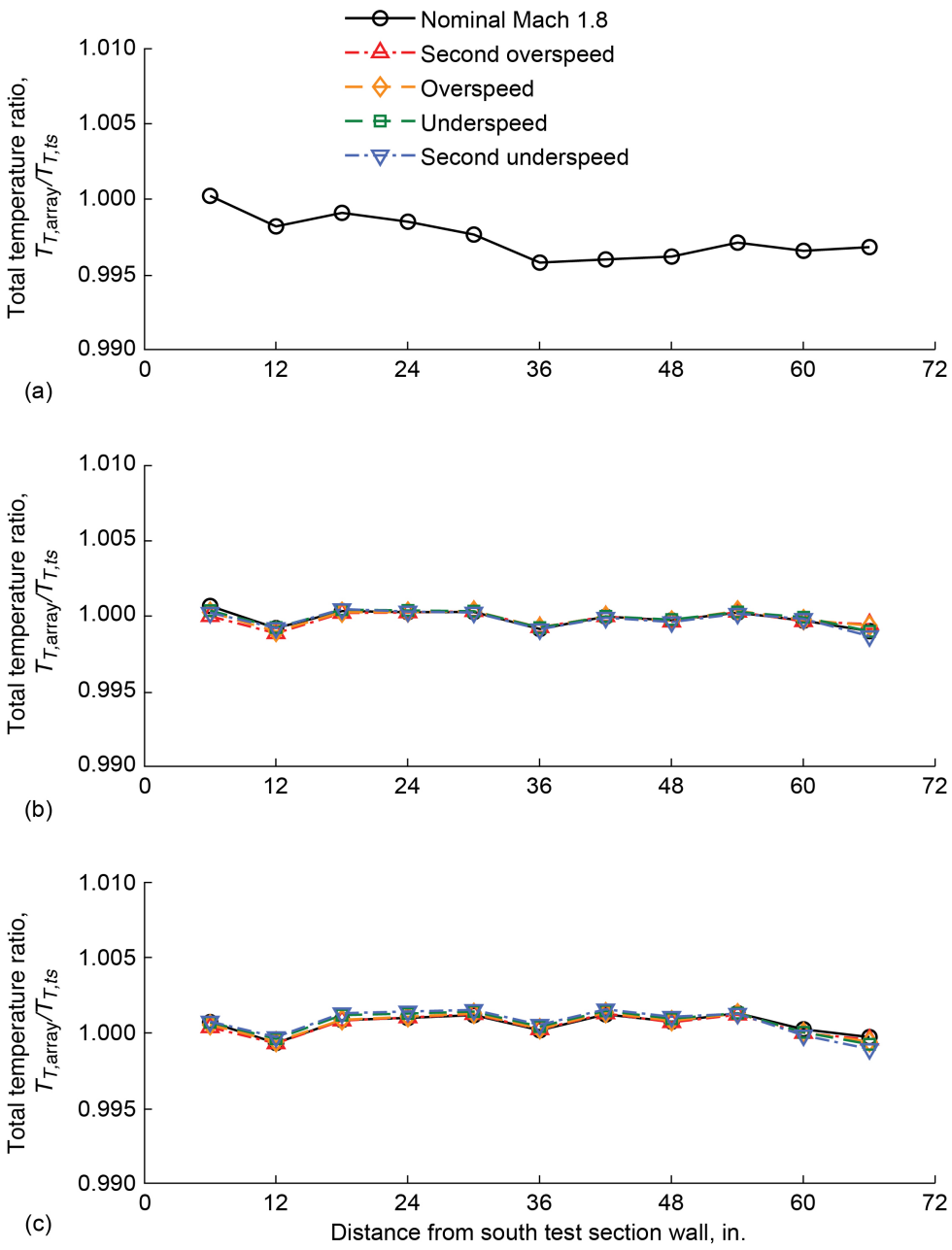

Figure 88.—Total temperature ratio distributions in 8- by 6-ft test section at 14-ft test section measurement plane at centerline (CL) and 1 ft above and below CL. Data acquired during 2019 test section characterization entry at flexwall setting of Mach 1.8. (a) CL + 1 ft; 0.005 = ΔT_T of 3.16 R. (b) CL; 0.005 = ΔT_T of 3.13 R. (c) CL – 1 ft; 0.005 = ΔT_T of 3.21 R.

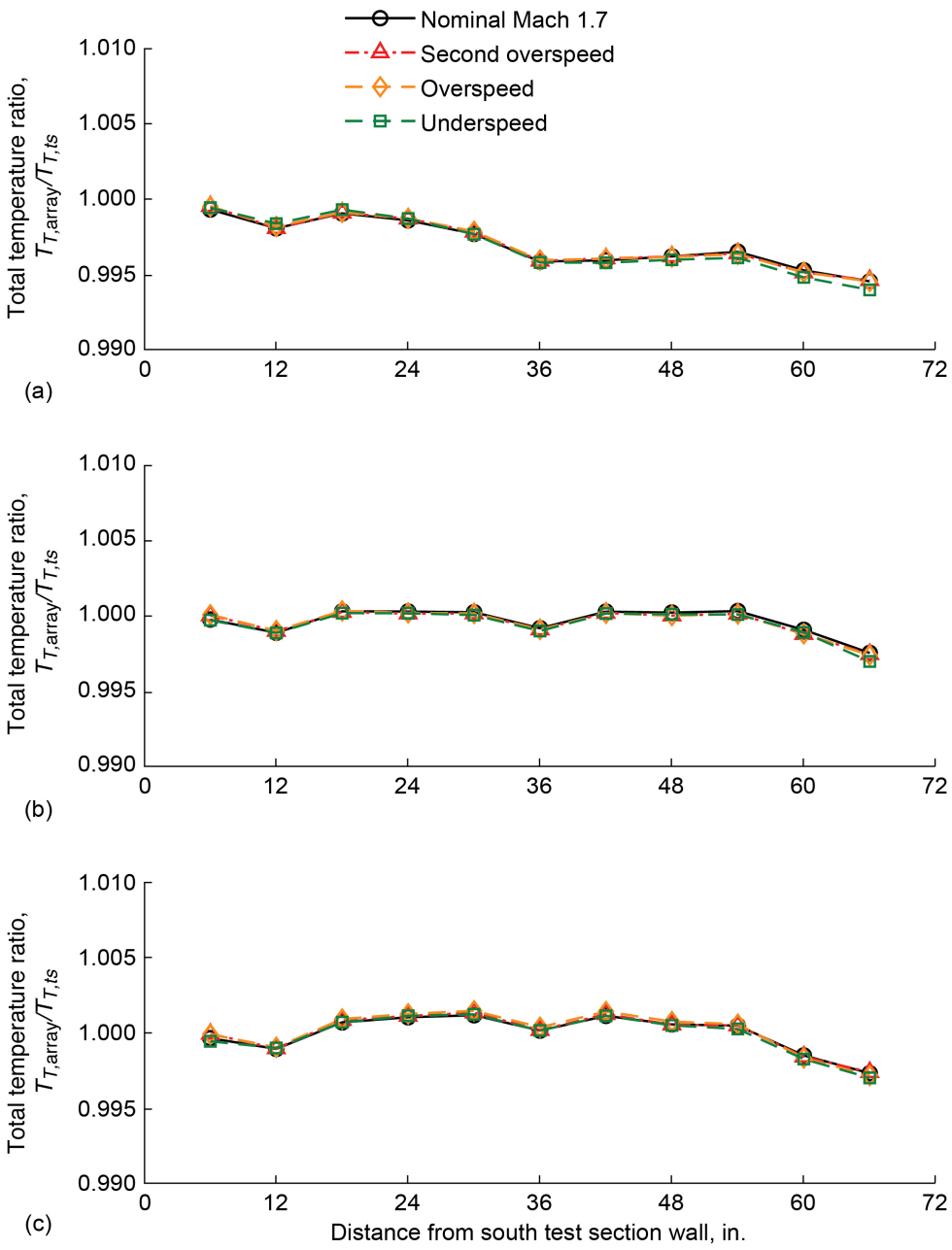

Figure 89.—Total temperature ratio distributions in 8- by 6-ft test section at 14-ft test section measurement plane at centerline (CL) and 1 ft above and below CL. Data acquired during 2019 test section characterization entry at flexwall setting of Mach 1.7. (a) CL + 1 ft; 0.005 = ΔT_T of 3.13 R. (b) CL; 0.005 = ΔT_T of 3.16 R. (c) CL – 1 ft; 0.005 = ΔT_T of 3.17 R.

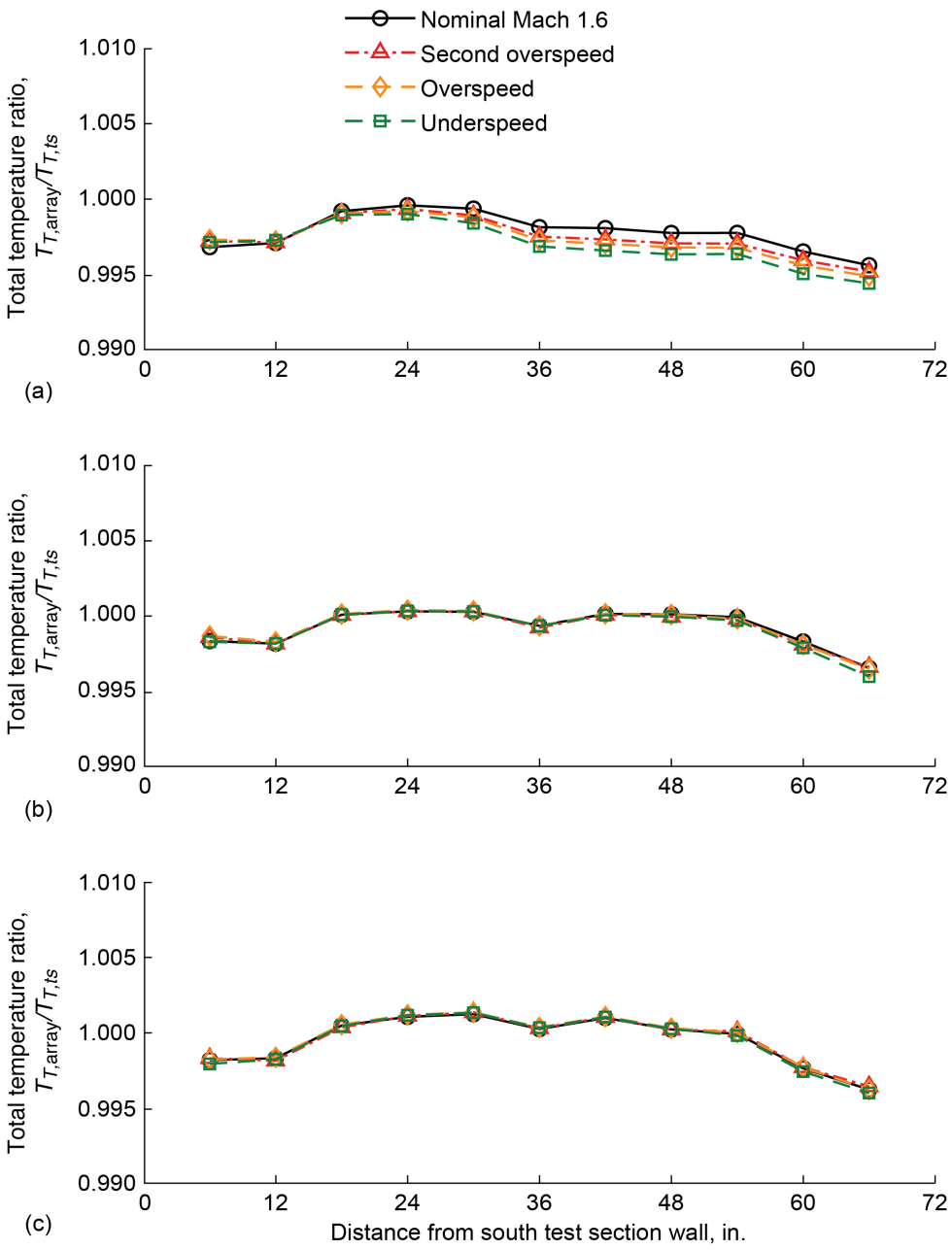

Figure 90.—Total temperature ratio distributions in 8- by 6-ft test section at 14-ft test section measurement plane at centerline (CL) and 1 ft above and below CL. Data acquired during 2019 test section characterization entry at flexwall setting of Mach 1.6. (a) CL + 1 ft; 0.005 = ΔT_T of 3.01 R. (b) CL; 0.005 = ΔT_T of 3.12 R. (c) CL – 1 ft; 0.005 = ΔT_T of 3.12 R.

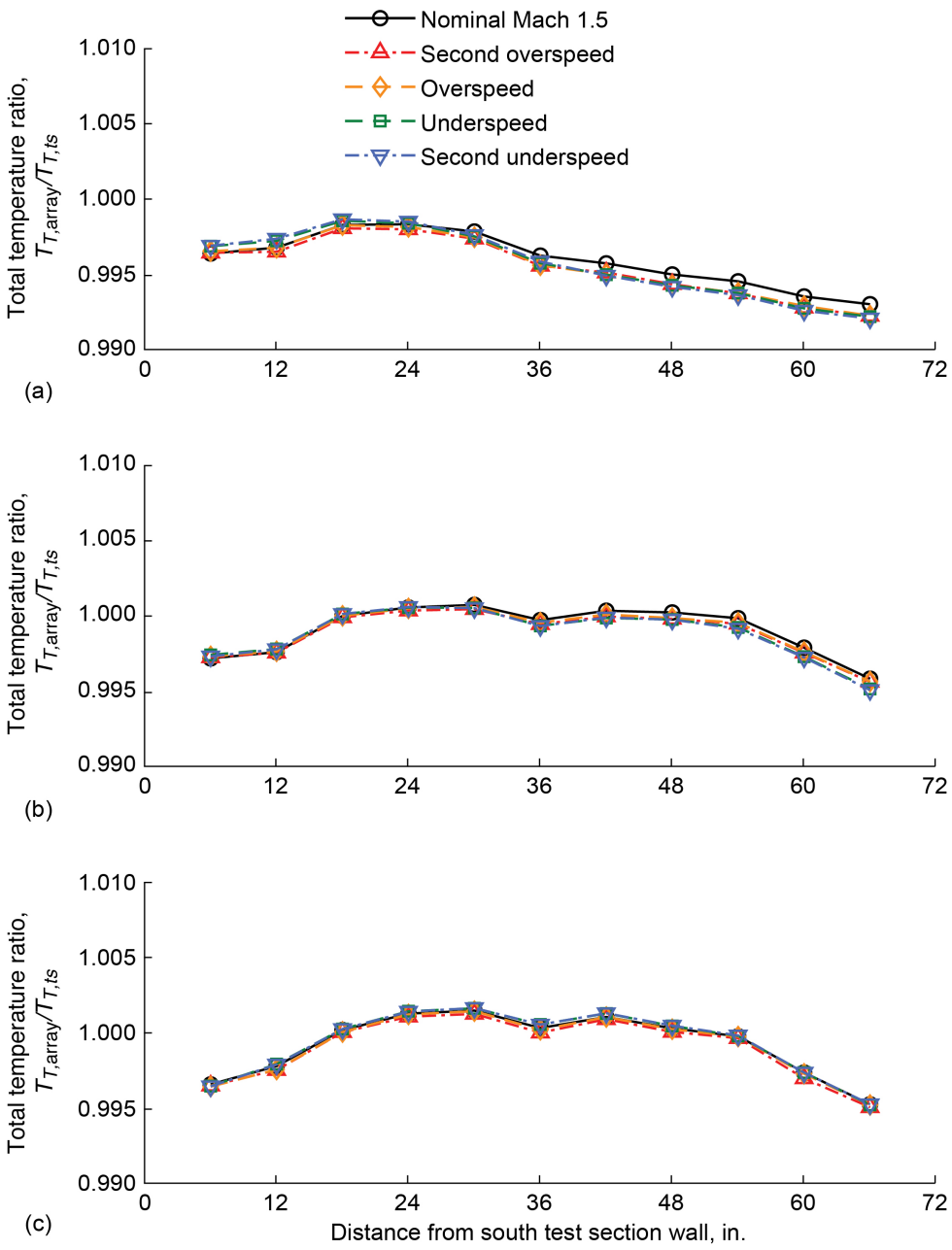

Figure 91.—Total temperature ratio distributions in 8- by 6-ft test section at 14-ft test section measurement plane at centerline (CL) and 1 ft above and below CL. Data acquired during 2019 test section characterization entry at flexwall setting of Mach 1.5. (a) CL + 1 ft; 0.005 = ΔT_T of 3.07 R. (b) CL; 0.005 = ΔT_T of 3.08 R. (c) CL – 1 ft; 0.005 = ΔT_T of 3.08 R.

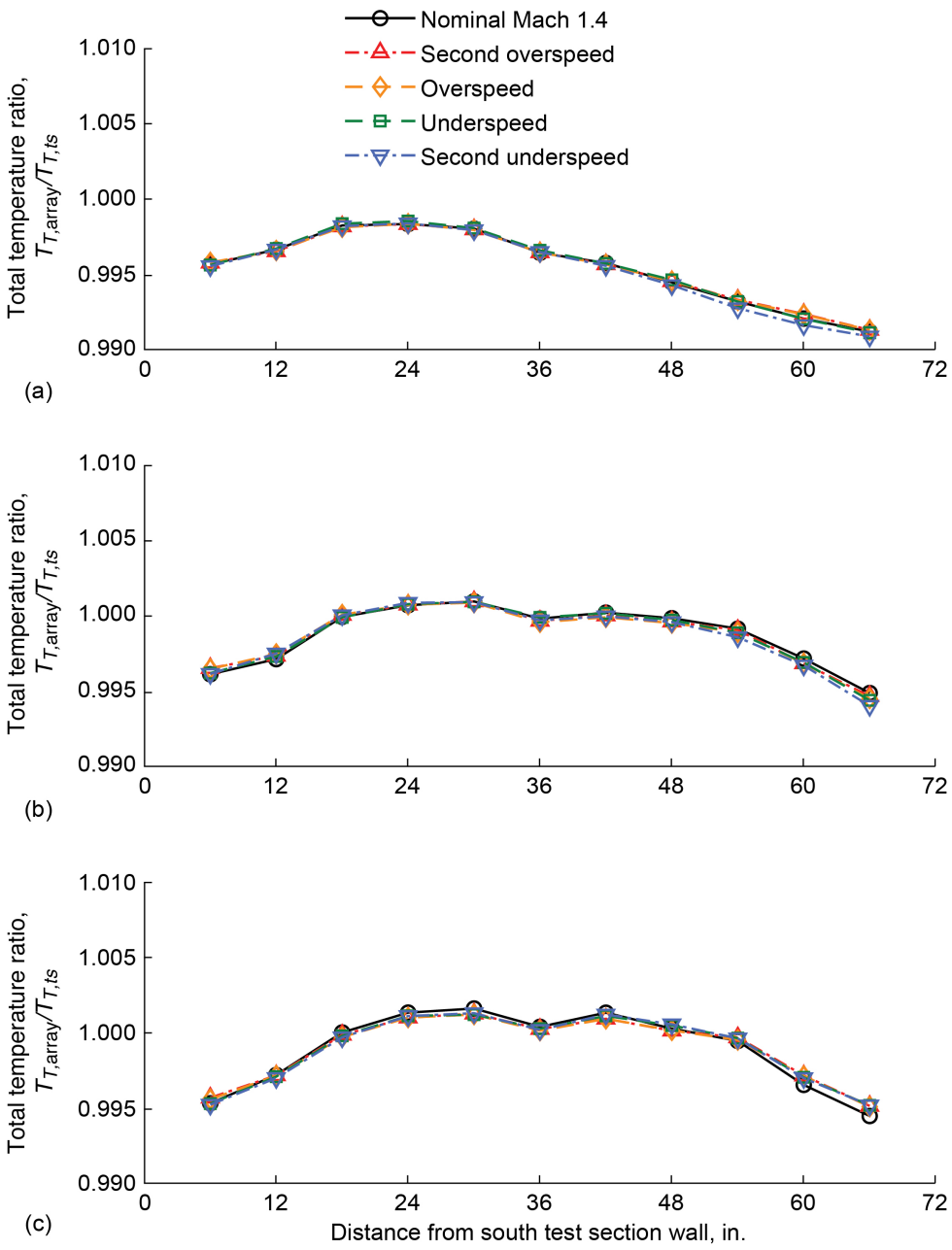

Figure 92.—Total temperature ratio distributions in 8- by 6-ft test section at 14-ft test section measurement plane at centerline (CL) and 1 ft above and below CL. Data acquired during 2019 test section characterization entry at flexwall setting of Mach 1.4. (a) CL + 1 ft; 0.005 = ΔT_T of 3.02 R. (b) CL; 0.005 = ΔT_T of 3.04 R. (c) CL – 1 ft; 0.005 = ΔT_T of 3.03 R.

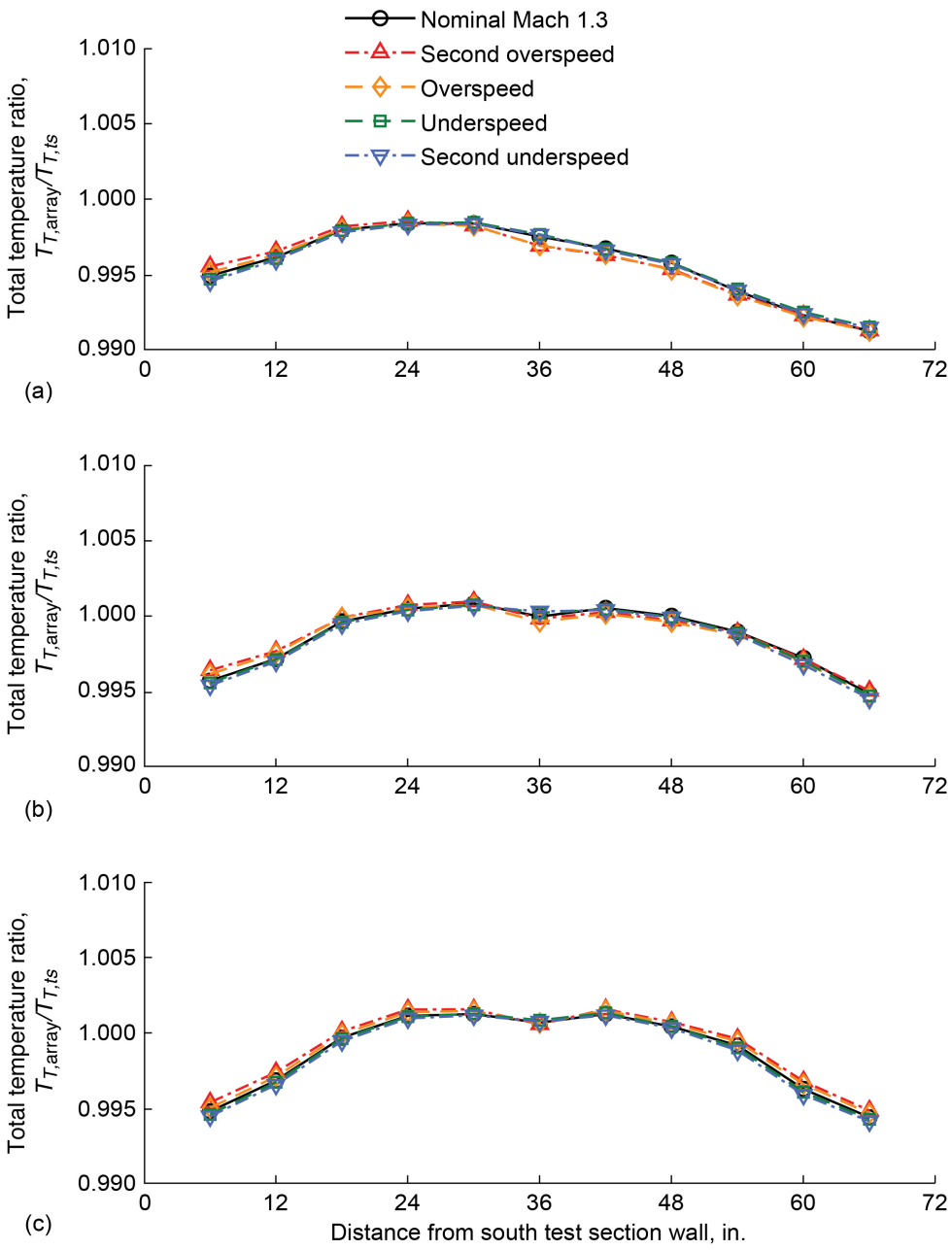

Figure 93.—Total temperature ratio distributions in 8- by 6-ft test section at 14-ft test section measurement plane at centerline (CL) and 1 ft above and below CL. Data acquired during 2019 test section characterization entry at flexwall setting of Mach 1.3. (a) CL + 1 ft; 0.005 = ΔT_T of 3.00 R. (b) CL; 0.005 = ΔT_T of 3.00 R. (c) CL – 1 ft; 0.005 = ΔT_T of 3.00 R.

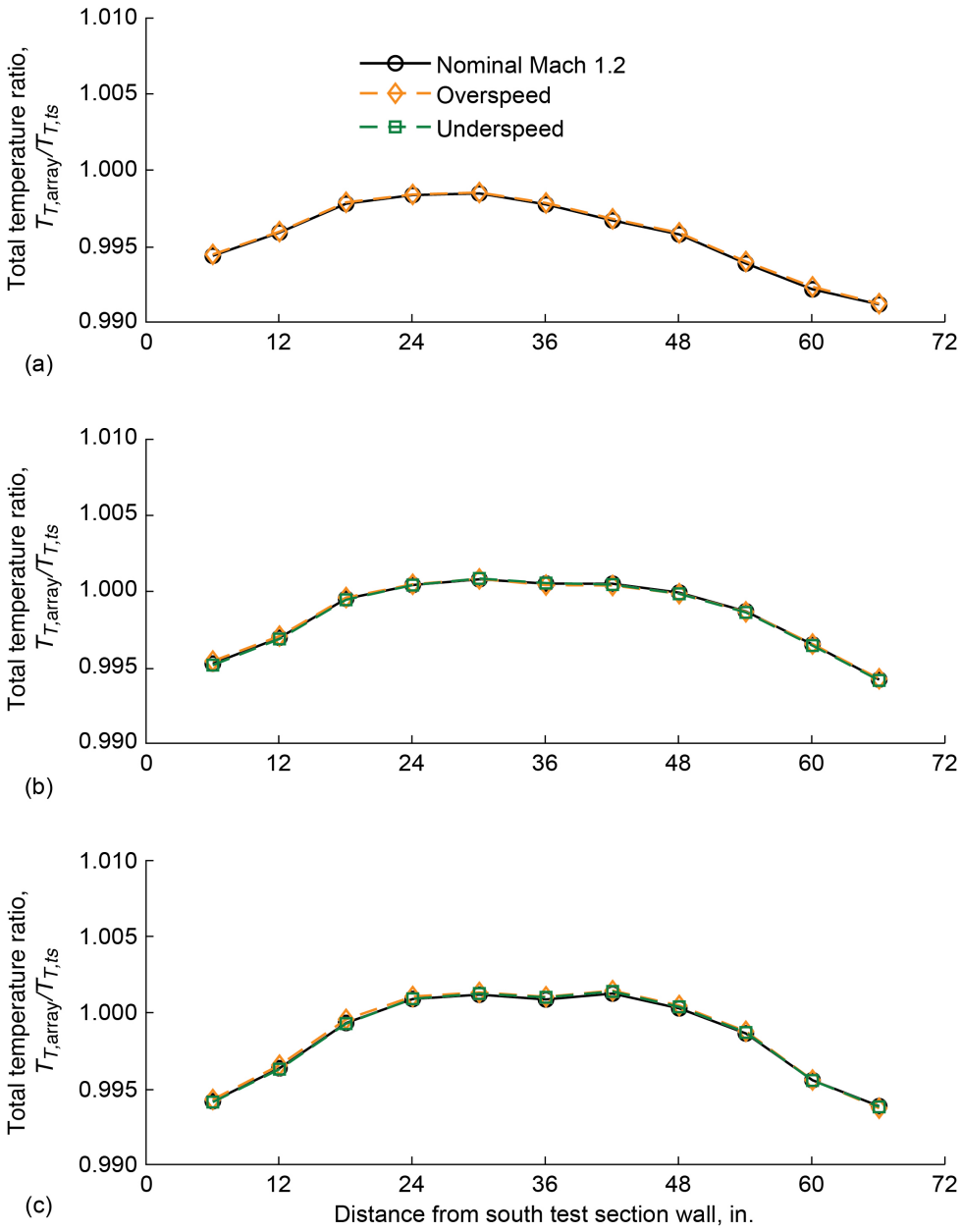

Figure 94.—Total temperature ratio distributions in 8- by 6-ft test section at 14-ft test section measurement plane at centerline (CL) and 1 ft above and below CL. Data acquired during 2019 test section characterization entry at flexwall setting of Mach 1.2. (a) CL + 1 ft; 0.005 = ΔT_T of 2.99 R. (b) CL; 0.005 = ΔT_T of 3.00 R. (c) CL – 1 ft; 0.005 = ΔT_T of 3.00 R.

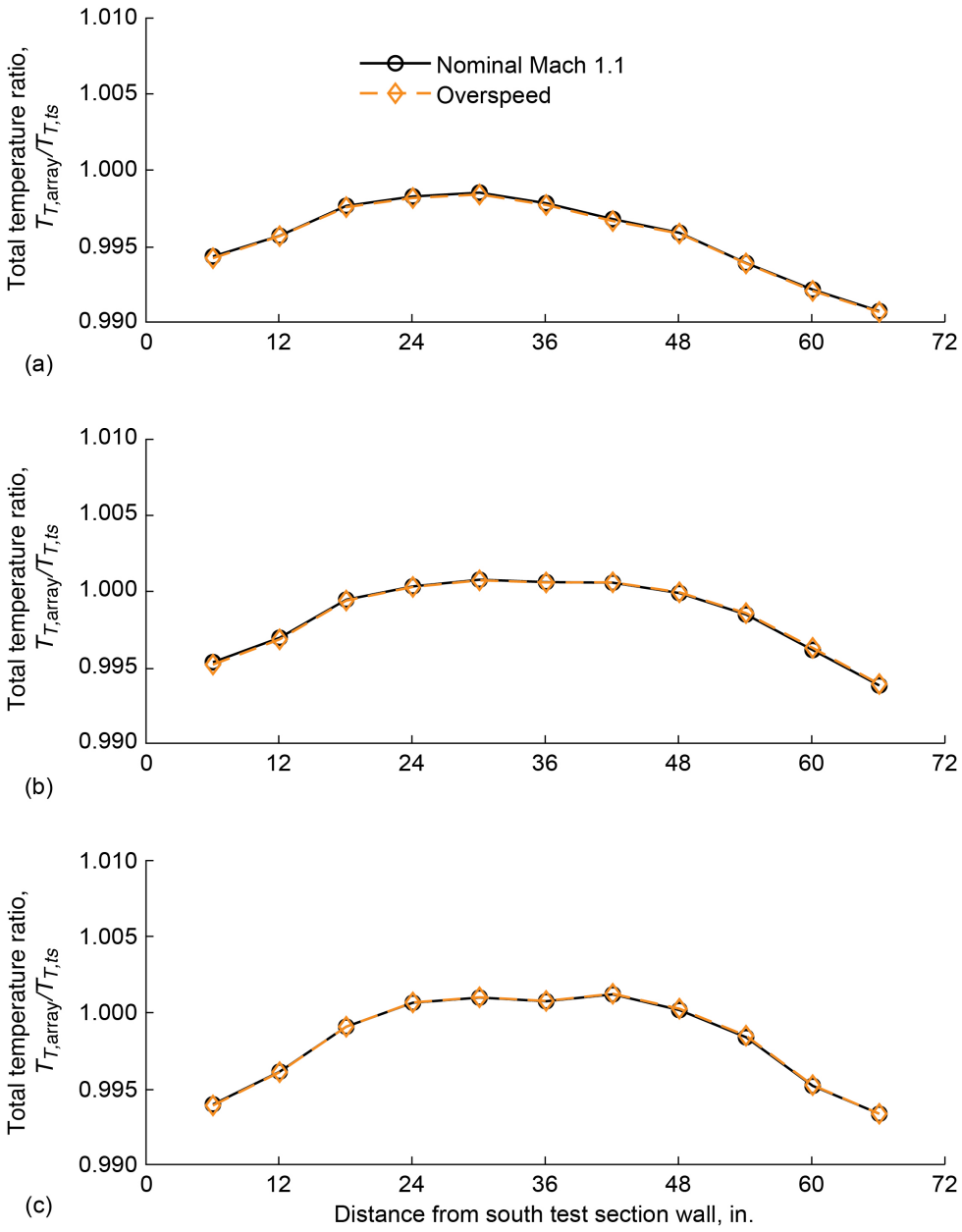

Figure 95.—Total temperature ratio distributions in 8- by 6-ft test section at 14-ft test section measurement plane at centerline (CL) and 1 ft above and below CL. Data acquired during 2019 test section characterization entry at flexwall setting of Mach 1.1. (a) CL + 1 ft; 0.005 = ΔT_T of 2.99 R. (b) CL; 0.005 = ΔT_T of 2.99 R. (c) CL – 1 ft; 0.005 = ΔT_T of 3.00 R.

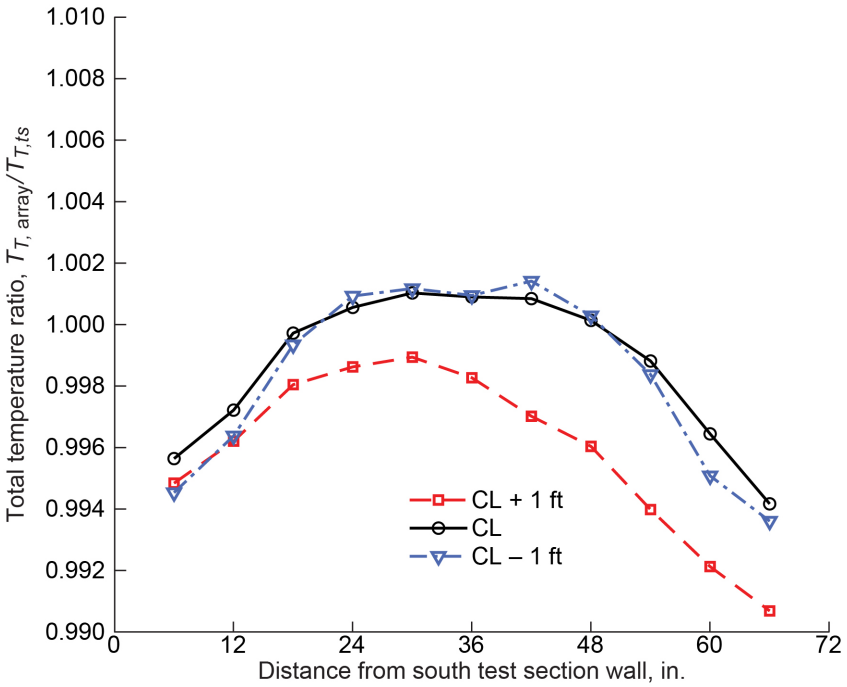

Figure 96.—Total temperature ratio distributions in 8- by 6-ft test section at 14-ft test section measurement plane at centerline (CL) and 1 ft above and below CL. Data acquired during 2019 test section characterization entry at transonic array Mach number of 0.951 (three-drive-motor operation). 0.0020 = ΔT_T of 1.18 R.

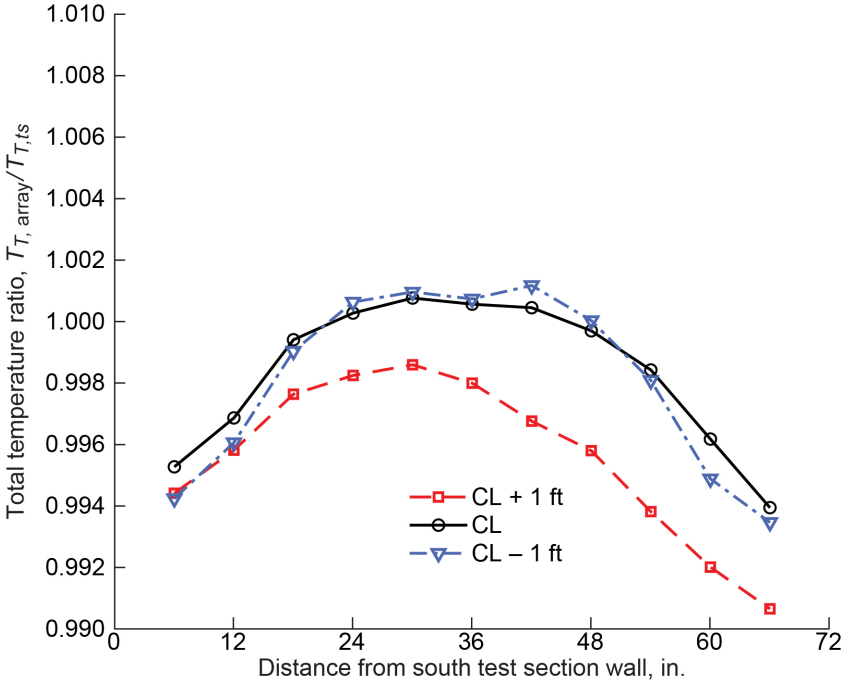

Figure 97.—Total temperature ratio distributions in 8- by 6-ft test section at 14-ft test section measurement plane at centerline (CL) and 1 ft above and below CL. Data acquired during 2019 test section characterization entry at transonic array Mach number of 0.900 (three-drive-motor operation). 0.0020 = ΔT_T of 1.18 R.

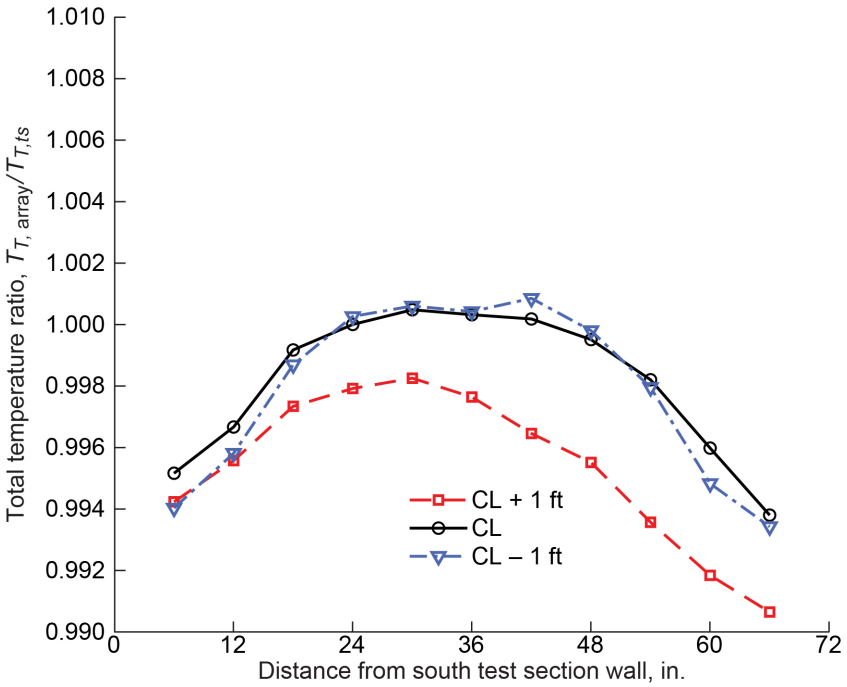

Figure 98.—Total temperature ratio distributions in 8- by 6-ft test section at 14-ft test section measurement plane at centerline (CL) and 1 ft above and below CL. Data acquired during 2019 test section characterization entry at transonic array Mach number of 0.849 (three-drive-motor operation). 0.0020 = ΔT_T of 1.18 R.

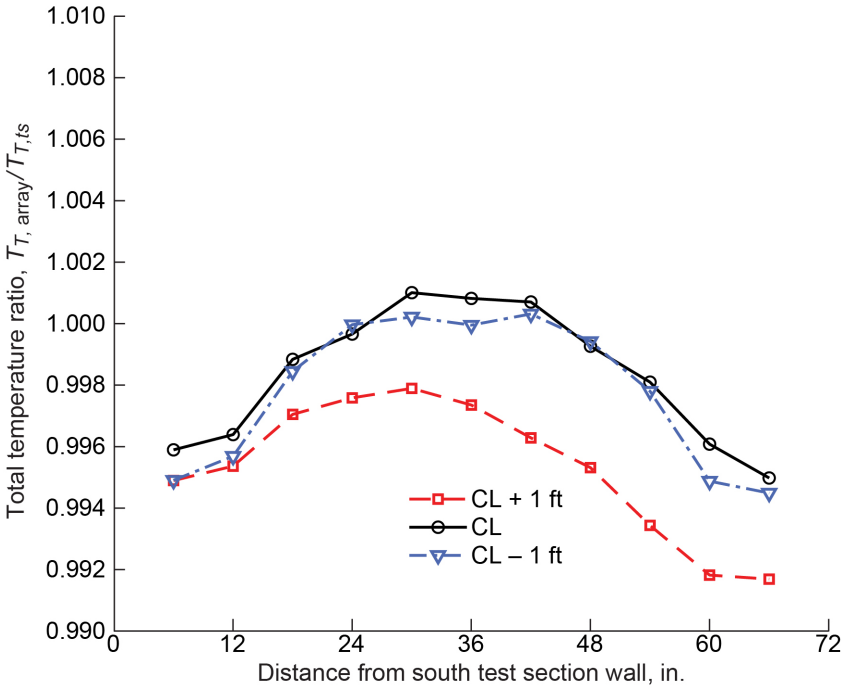

Figure 99.—Total temperature ratio distributions in 8- by 6-ft test section at 14-ft test section measurement plane at centerline (CL) and 1 ft above and below CL. Data acquired during 2019 test section characterization entry at transonic array Mach number of 0.800 (three-drive-motor operation). 0.0020 = ΔT_T of 1.19 R.

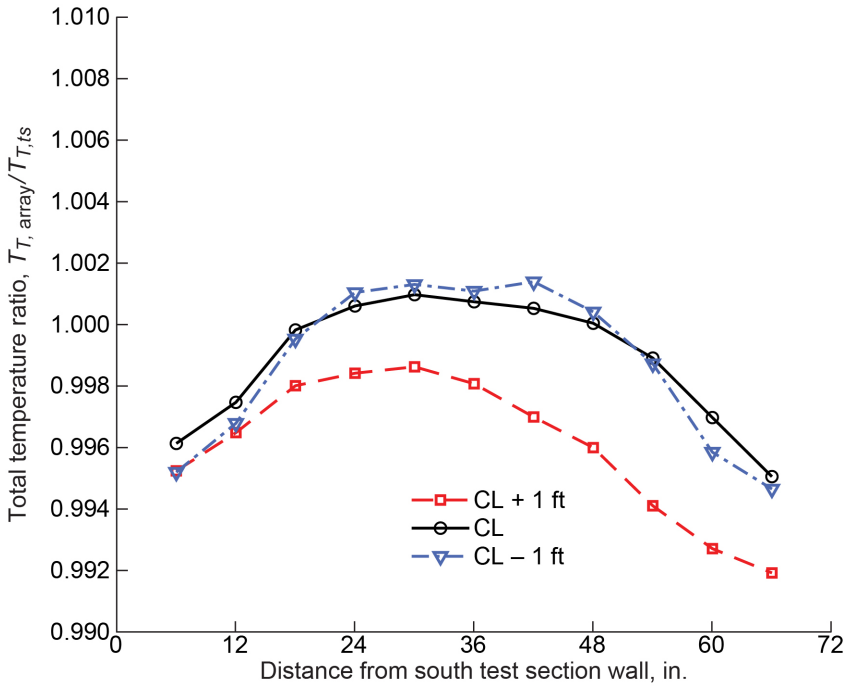

Figure 100.—Total temperature ratio distributions in 8- by 6-ft test section at 14-ft test section measurement plane at centerline (CL) and 1 ft above and below CL. Data acquired during 2019 test section characterization entry at transonic array Mach number of 0.750 (three-drive-motor operation). 0.0020 = ΔT_T of 1.19 R.

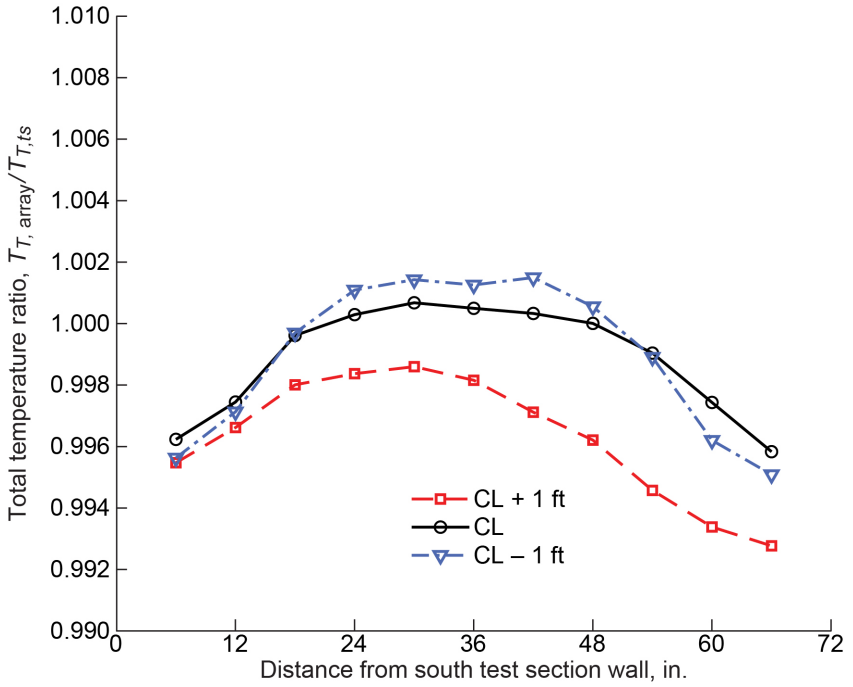

Figure 101.—Total temperature ratio distributions in 8- by 6-ft test section at 14-ft test section measurement plane at centerline (CL) and 1 ft above and below CL. Data acquired during 2019 test section characterization entry at transonic array Mach number of 0.701 (three-drive-motor operation). 0.0020 = ΔT_T of 1.19 R.

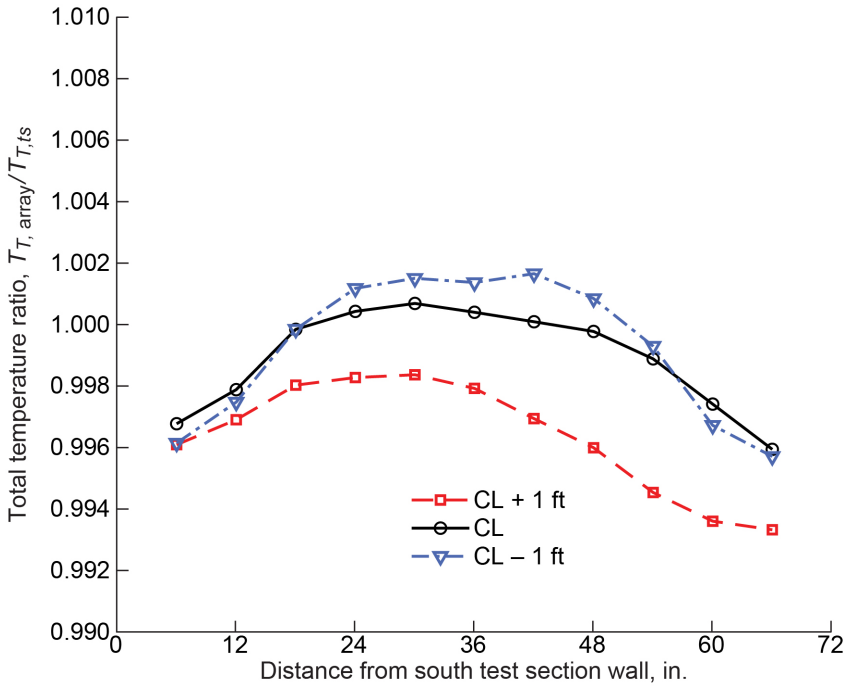

Figure 102.—Total temperature ratio distributions in 8- by 6-ft test section at 14-ft test section measurement plane at centerline (CL) and 1 ft above and below CL. Data acquired during 2019 test section characterization entry at transonic array Mach number of 0.649 (three-drive-motor operation). 0.0020 = ΔT_T of 1.19 R.

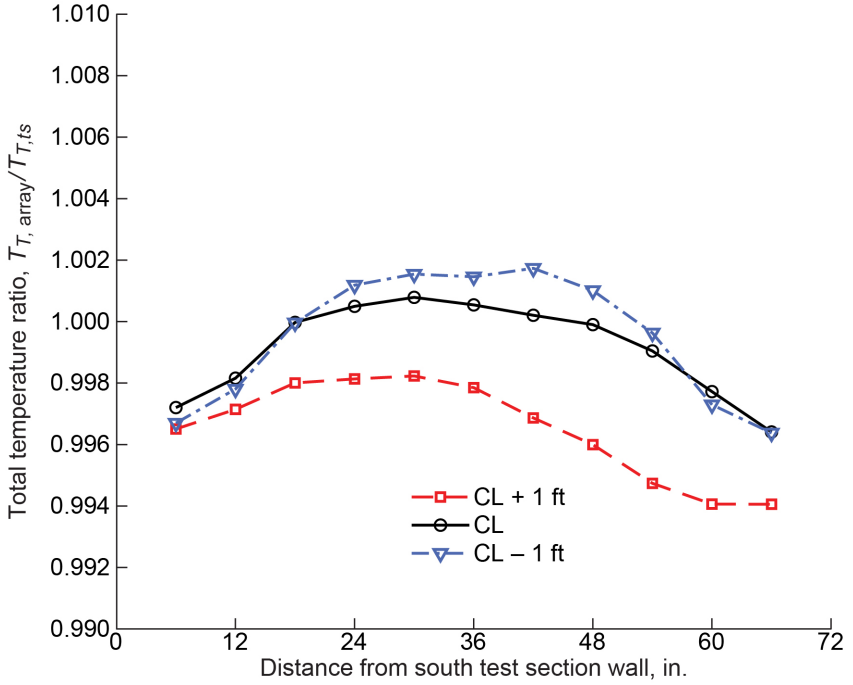

Figure 103.—Total temperature ratio distributions in 8- by 6-ft test section at 14-ft test section measurement plane at centerline (CL) and 1 ft above and below CL. Data acquired during 2019 test section characterization entry at transonic array Mach number of 0.600 (three-drive-motor operation). 0.0020 = ΔT_T of 1.18 R.

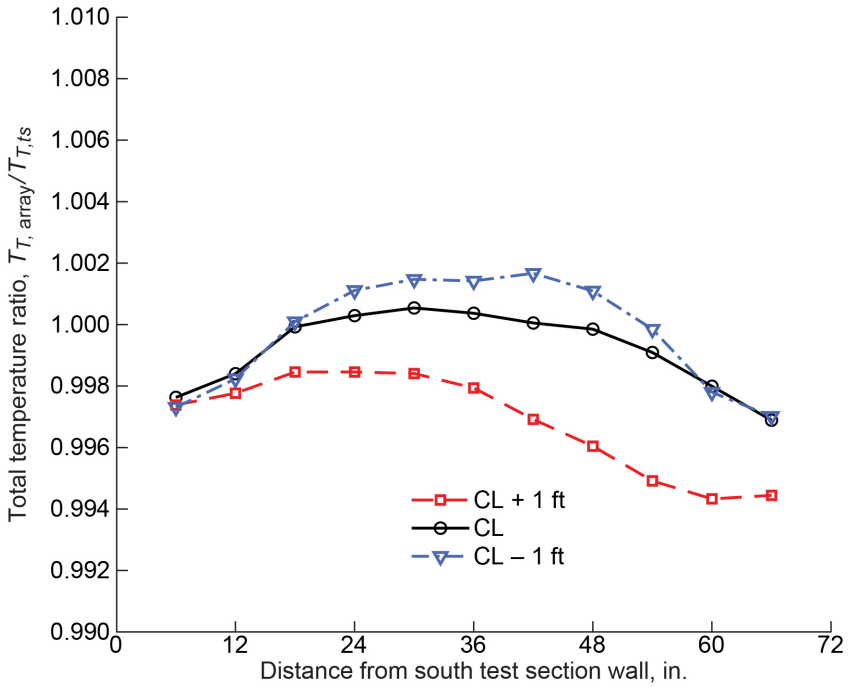

Figure 104.—Total temperature ratio distributions in 8- by 6-ft test section at 14-ft test section measurement plane at centerline (CL) and 1 ft above and below CL. Data acquired during 2019 test section characterization entry at transonic array Mach number of 0.551 (three-drive-motor operation). 0.0020 = ΔT_T of 1.17 R.

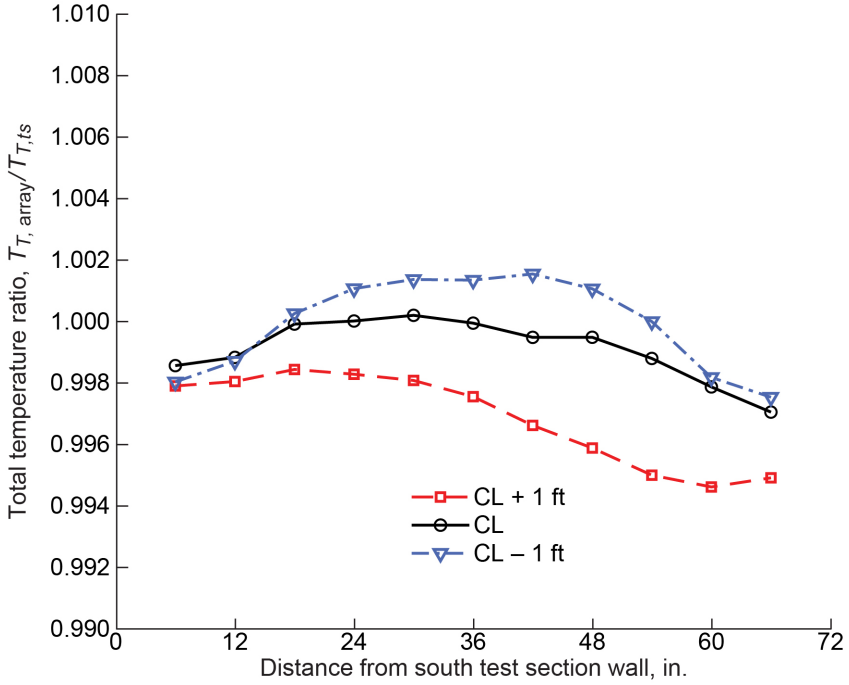

Figure 105.—Total temperature ratio distributions in 8- by 6-ft test section at 14-ft test section measurement plane at centerline (CL) and 1 ft above and below CL. Data acquired during 2019 test section characterization entry at transonic array Mach number of 0.500 (three-drive-motor operation). 0.0020 = ΔT_T of 1.16 R.

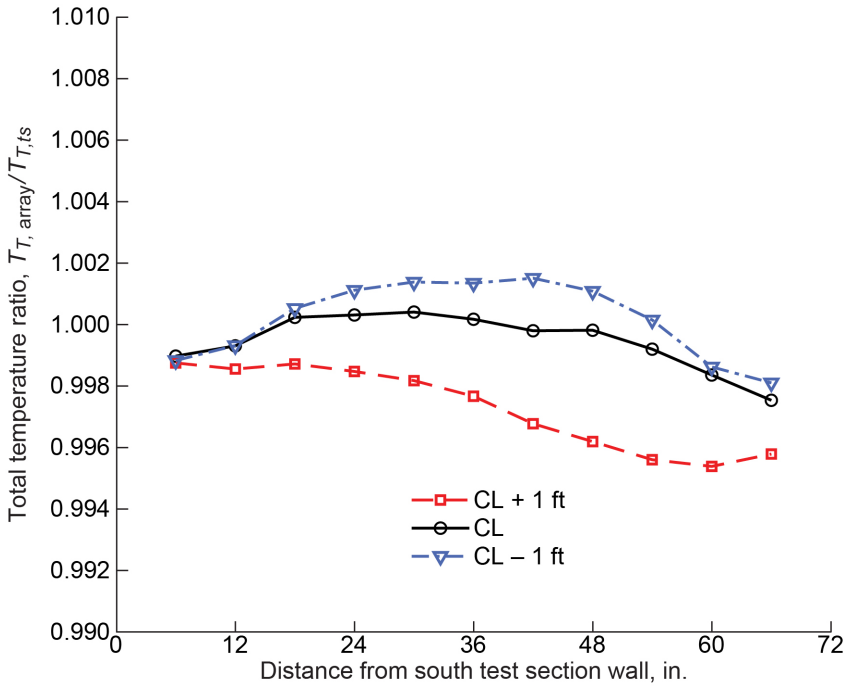

Figure 106.—Total temperature ratio distributions in 8- by 6-ft test section at 14-ft test section measurement plane at centerline (CL) and 1 ft above and below CL. Data acquired during 2019 test section characterization entry at transonic array Mach number of 0.449 (three-drive-motor operation). 0.0020 = ΔT_T of 1.15 R.

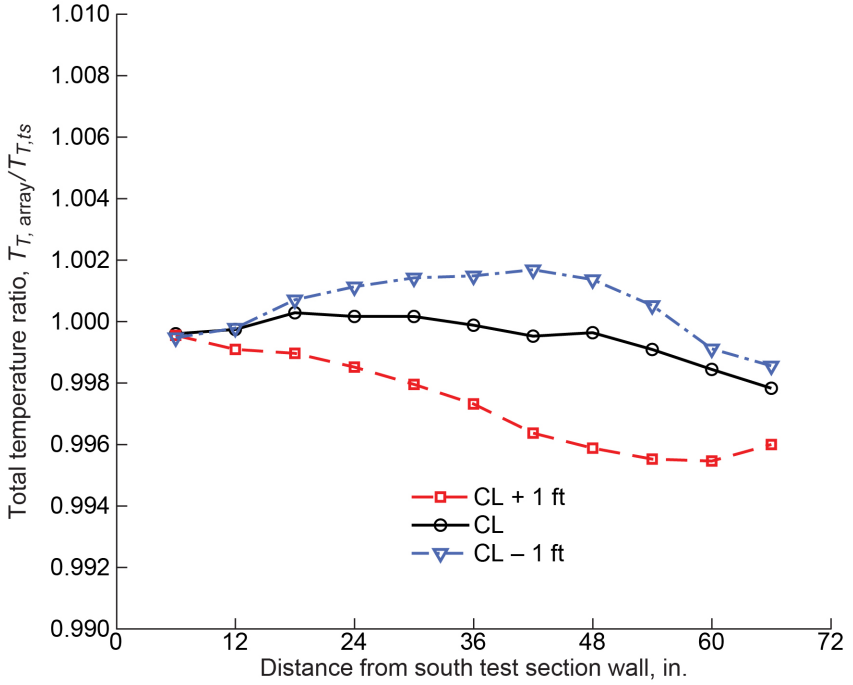

Figure 107.—Total temperature ratio distributions in 8- by 6-ft test section at 14-ft test section measurement plane at centerline (CL) and 1 ft above and below CL. Data acquired during 2019 test section characterization entry at transonic array Mach number of 0.401 (three-drive-motor operation). 0.0020 = ΔT_T of 1.14 R.

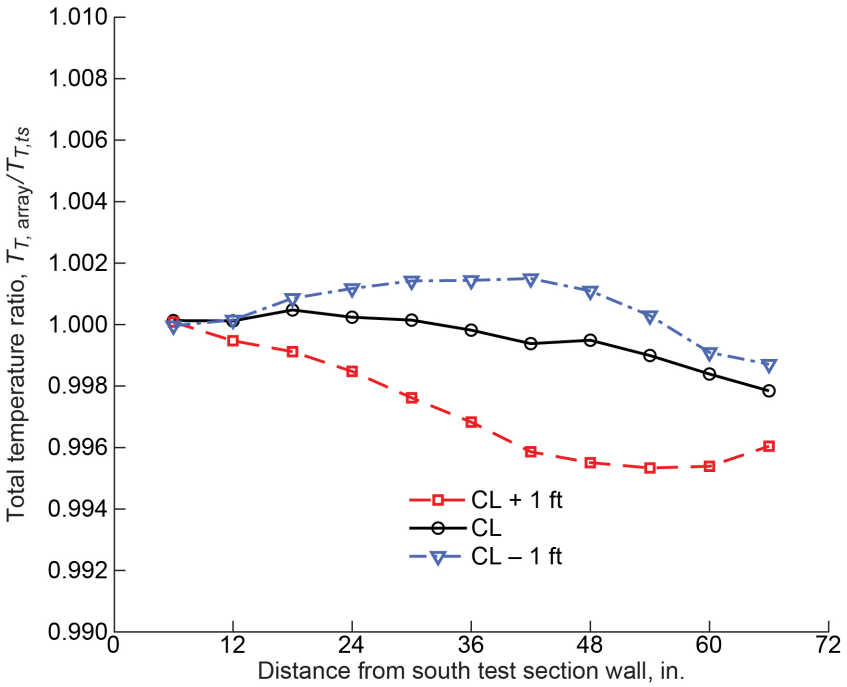

Figure 108.—Total temperature ratio distributions in 8- by 6-ft test section at 14-ft test section measurement plane at centerline (CL) and 1 ft above and below CL. Data acquired during 2019 test section characterization entry at transonic array Mach number of 0.369 (three-drive-motor operation). 0.0020 = ΔT_T of 1.13 R.

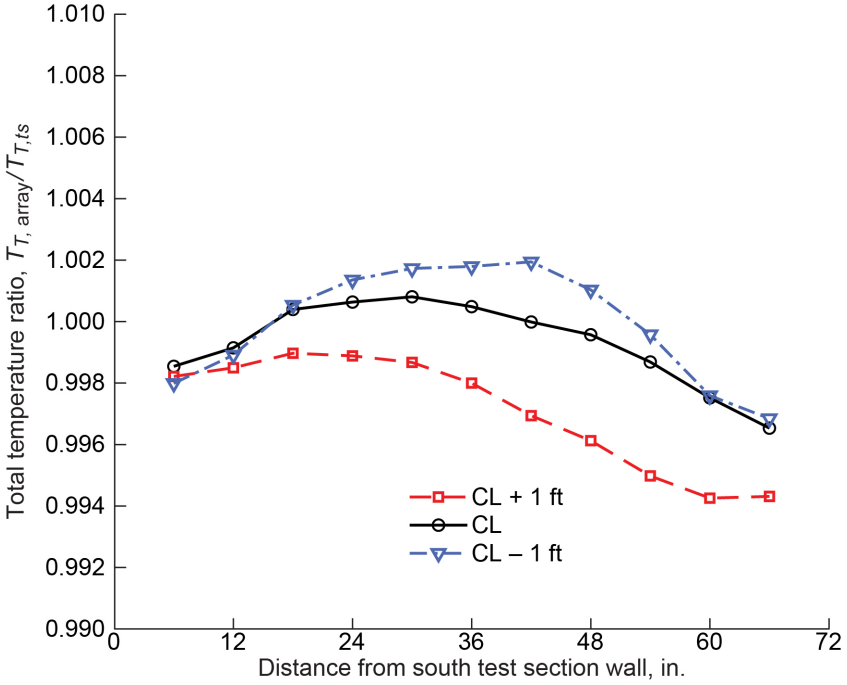

Figure 109.—Total temperature ratio distributions in 8- by 6-ft test section at 14-ft test section measurement plane at centerline (CL) and 1 ft above and below CL. Data acquired during 2019 test section characterization entry at transonic array Mach number of 0.500 (one-drive-motor operation). 0.0020 = ΔT_T of 1.13 R.

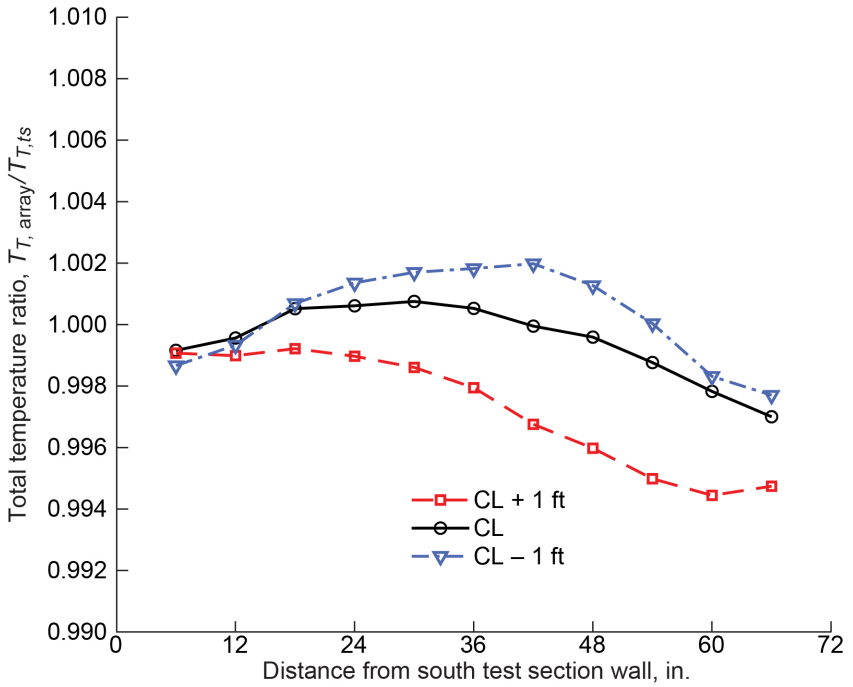

Figure 110.—Total temperature ratio distributions in 8- by 6-ft test section at 14-ft test section measurement plane at centerline (CL) and 1 ft above and below CL. Data acquired during 2019 test section characterization entry at transonic array Mach number of 0.449 (one-drive-motor operation). 0.0020 = ΔT_T of 1.12 R.

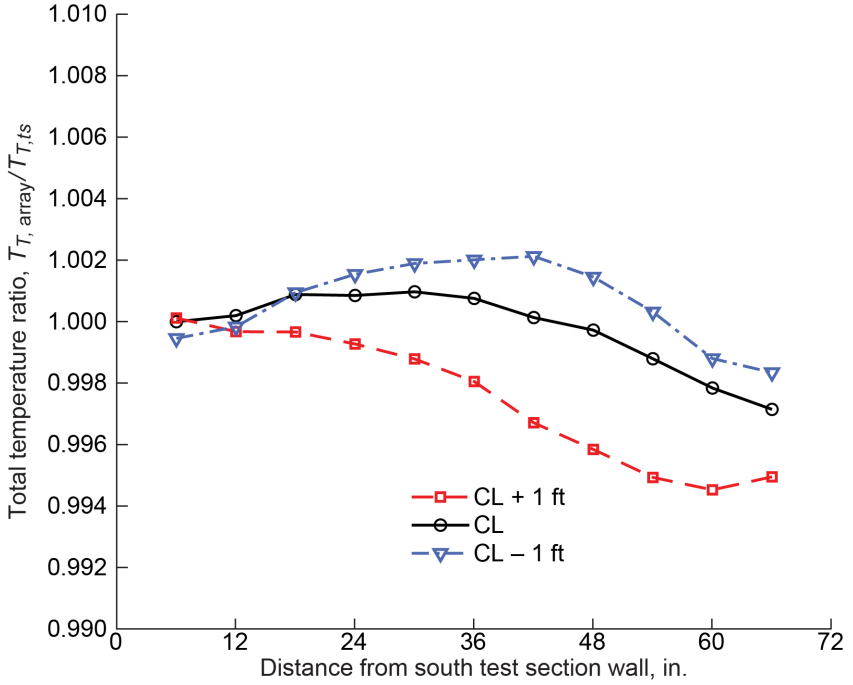

Figure 111.—Total temperature ratio distributions in 8- by 6-ft test section at 14-ft test section measurement plane at centerline (CL) and 1 ft above and below CL. Data acquired during 2019 test section characterization entry at transonic array Mach number of 0.401 (one-drive-motor operation). 0.0020 = ΔT_T of 1.11 R.

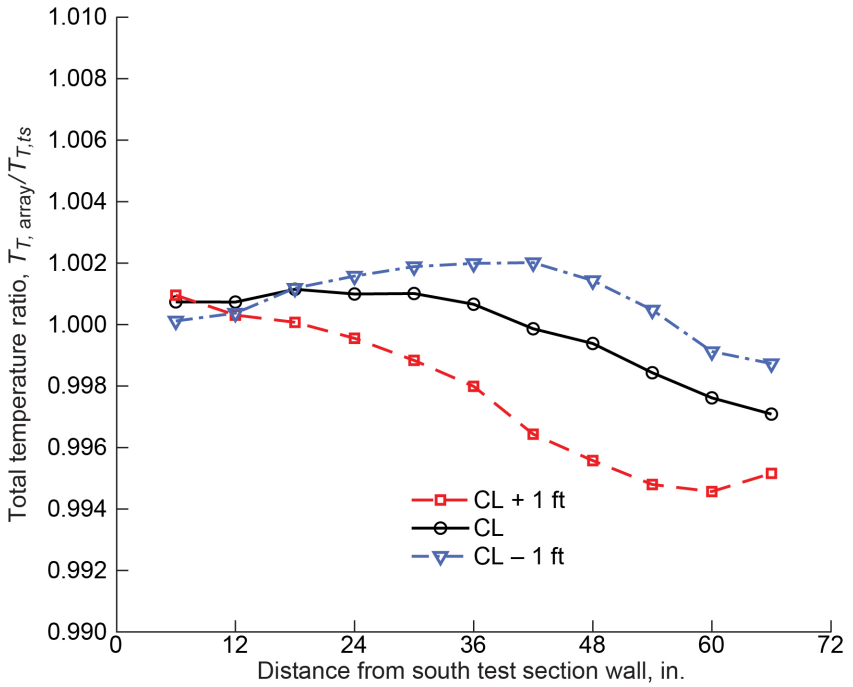

Figure 112.—Total temperature ratio distributions in 8- by 6-ft test section at 14-ft test section measurement plane at centerline (CL) and 1 ft above and below CL. Data acquired during 2019 test section characterization entry at transonic array Mach number of 0.352 (one-drive-motor operation). 0.0020 = ΔT_T of 1.10 R.

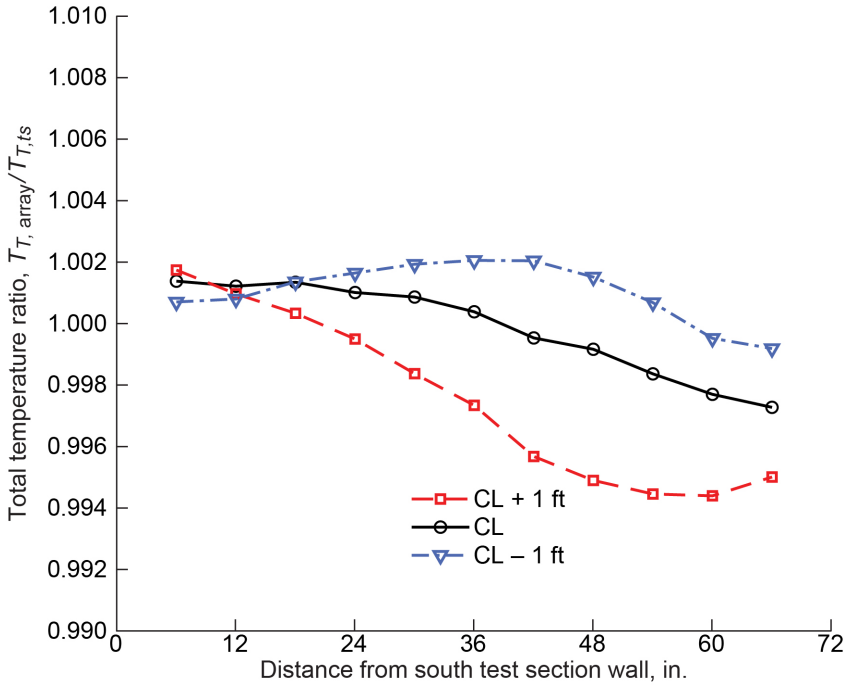

Figure 113.—Total temperature ratio distributions in 8- by 6-ft test section at 14-ft test section measurement plane at centerline (CL) and 1 ft above and below CL. Data acquired during 2019 test section characterization entry at transonic array Mach number of 0.299 (one-drive-motor operation). 0.0020 = ΔT_T of 1.10 R.

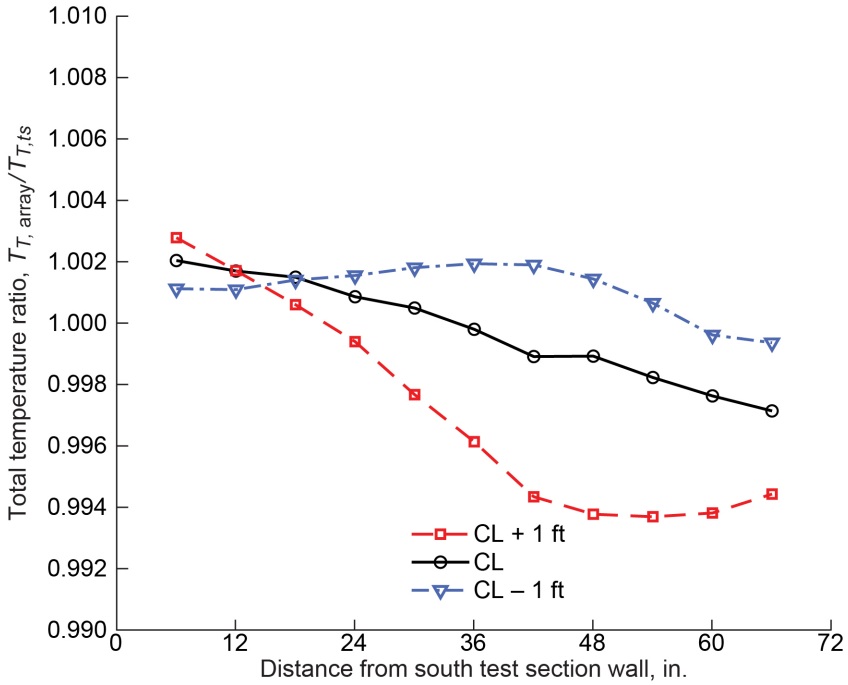

Figure 114.—Total temperature ratio distributions in 8- by 6-ft test section at 14-ft test section measurement plane at centerline (CL) and 1 ft above and below CL. Data acquired during 2019 test section characterization entry at transonic array Mach number of 0.251 (one-drive-motor operation). 0.0020 = ΔT_T of 1.09 R.

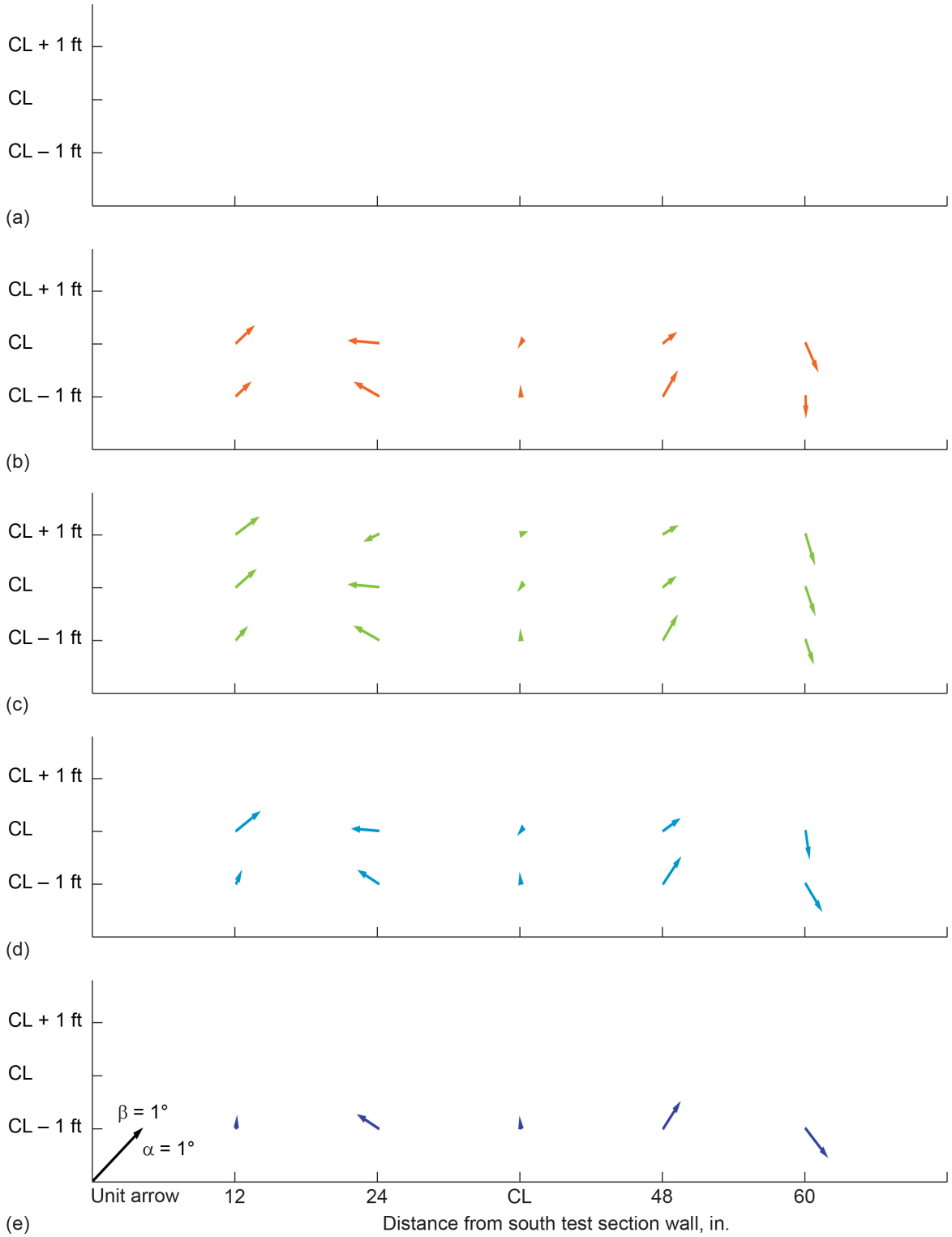

Figure 115.—Pitch and yaw flow angles in 8- by 6-ft test section at 14-ft test section measurement plane at centerline (CL) and 1 ft above and below CL. Positive pitch flow angle, α, is from floor to ceiling and positive yaw flow angle, β, is from left to right when upstream looking aft. Data acquired during 2019 test section characterization entry at flexwall setting of Mach 2.0. (a) Second overspeed. (b) First overspeed. (c) Nominal. (d) First underspeed. (e) Second underspeed.

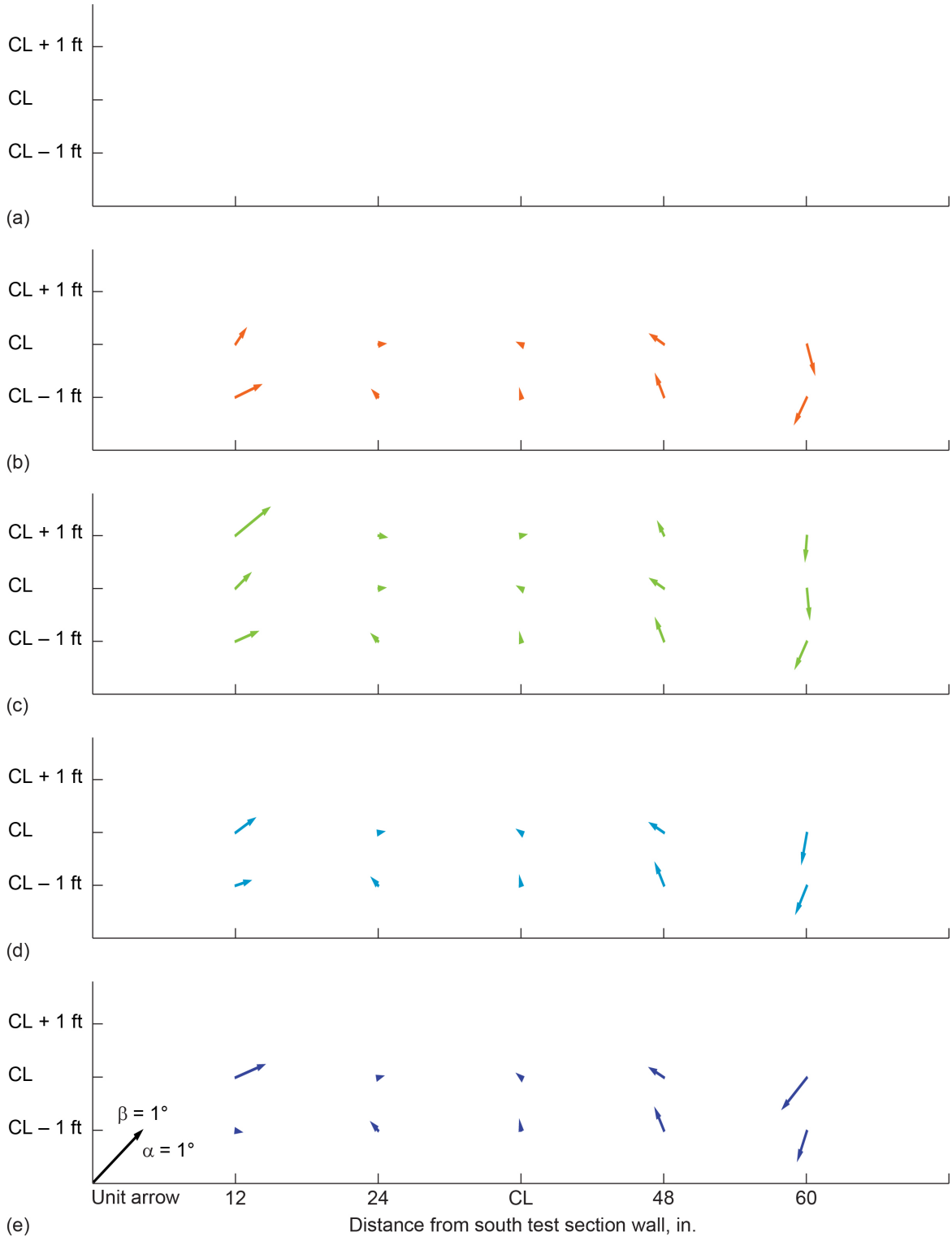

Figure 116.—Pitch and yaw flow angles in 8- by 6-ft test section at 14-ft test section measurement plane at centerline (CL) and 1 ft above and below CL. Positive pitch flow angle, α, is from floor to ceiling and positive yaw flow angle, β, is from left to right when upstream looking aft. Data acquired during 2019 test section characterization entry at flexwall setting of Mach 1.9. (a) Second overspeed. (b) First overspeed. (c) Nominal. (d) First underspeed. (e) Second underspeed.

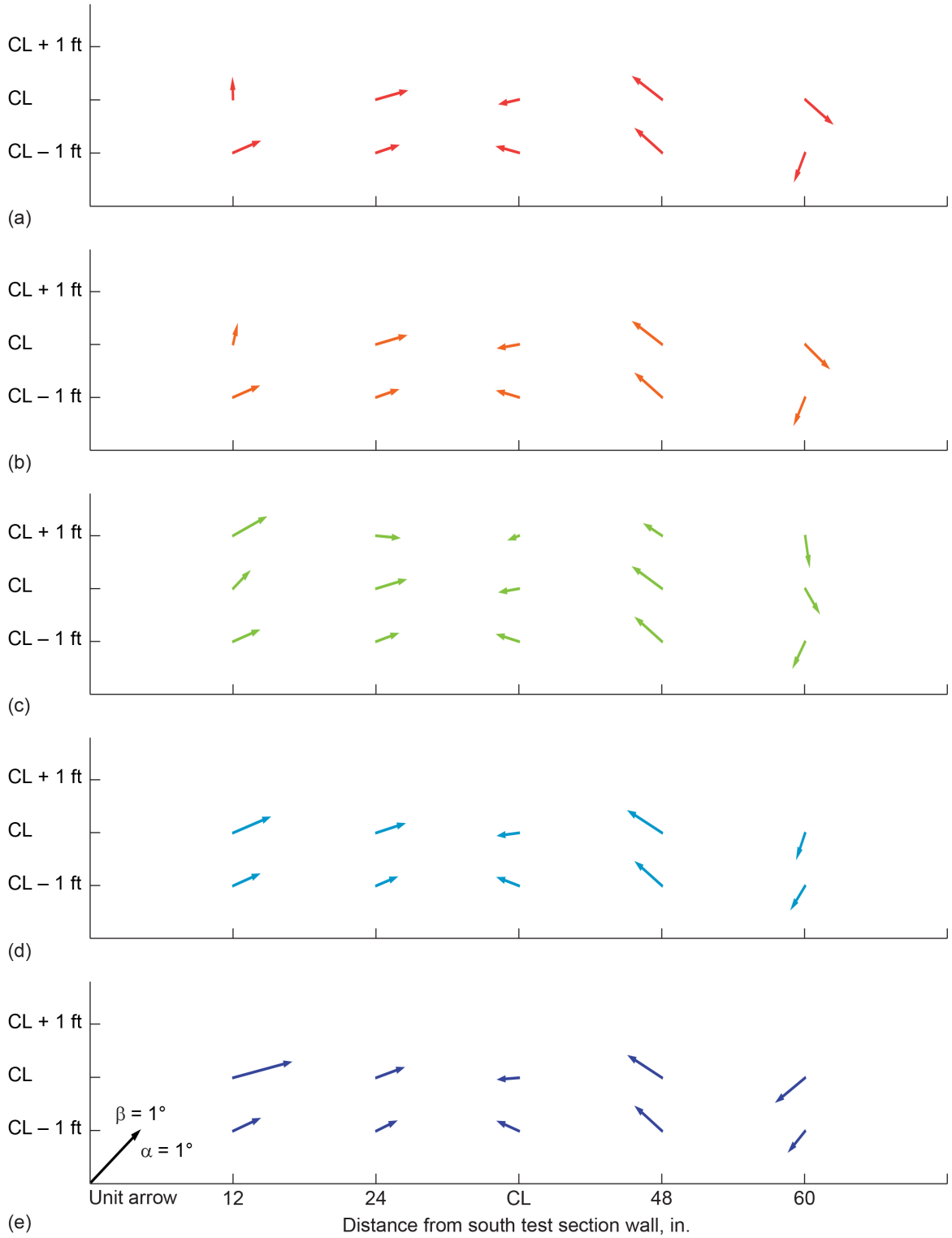

Figure 117.—Pitch and yaw flow angles in 8- by 6-ft test section at 14-ft test section measurement plane at centerline (CL) and 1 ft above and below CL. Positive pitch flow angle, α, is from floor to ceiling and positive yaw flow angle, β, is from left to right when upstream looking aft. Data acquired during 2019 test section characterization entry at flexwall setting of Mach 1.8. (a) Second overspeed. (b) First overspeed. (c) Nominal. (d) First underspeed. (e) Second underspeed.

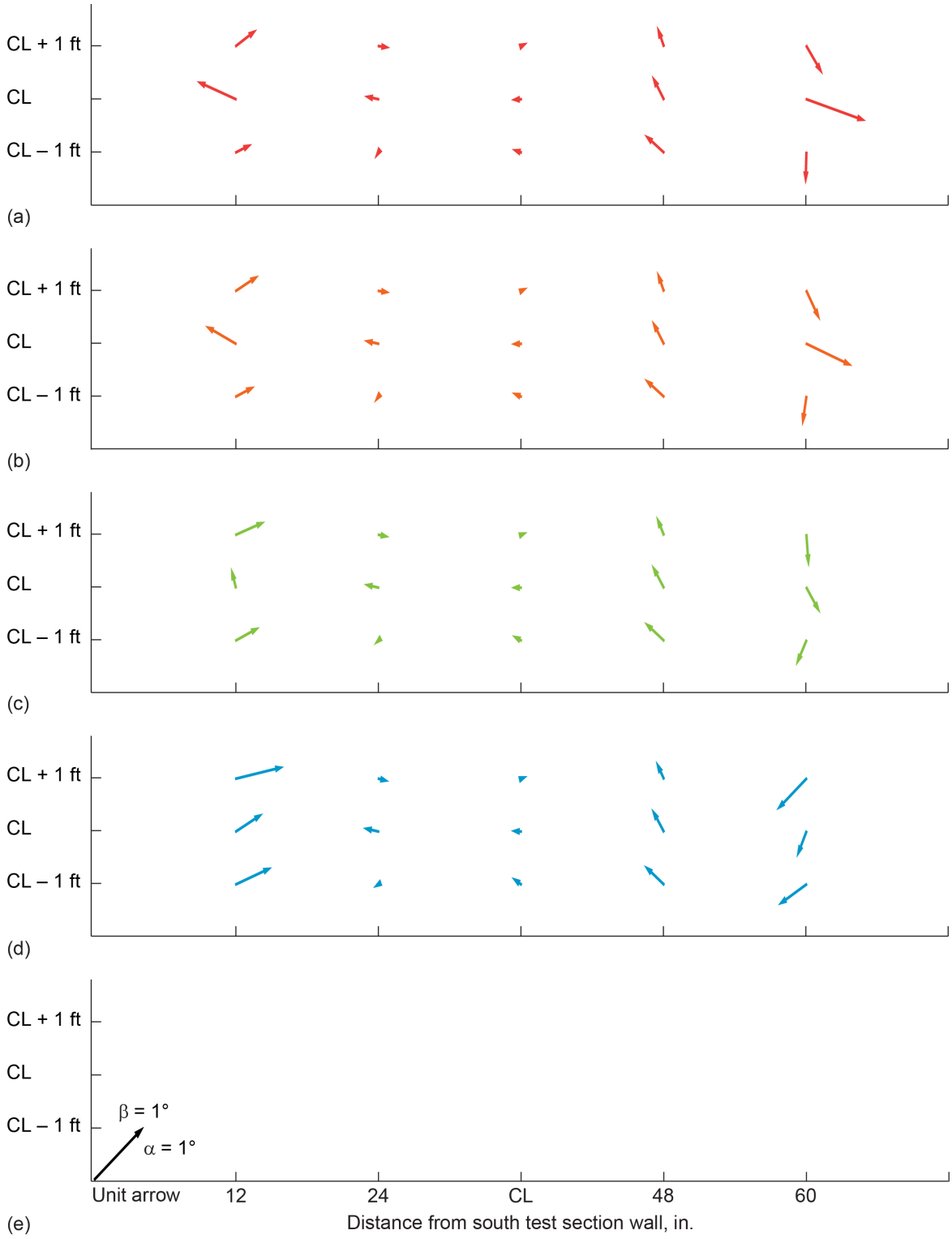

Figure 118.—Pitch and yaw flow angles in 8- by 6-ft test section at 14-ft test section measurement plane at centerline (CL) and 1 ft above and below CL. Positive pitch flow angle, α, is from floor to ceiling and positive yaw flow angle, β, is from left to right when upstream looking aft. Data acquired during 2019 test section characterization entry at flexwall setting of Mach 1.7. (a) Second overspeed. (b) First overspeed. (c) Nominal. (d) First underspeed. (e) Second underspeed.

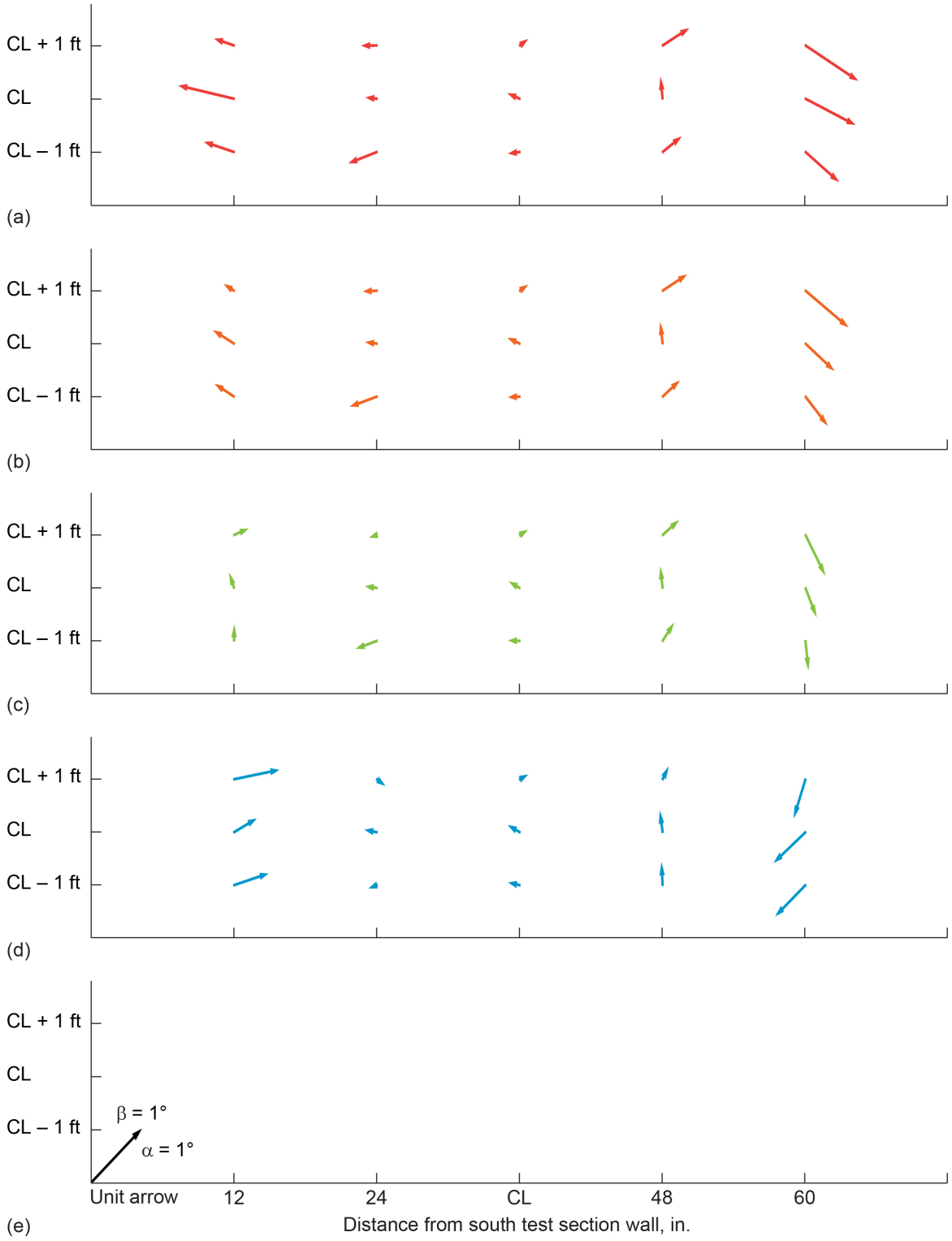

Figure 119.—Pitch and yaw flow angles in 8- by 6-ft test section at 14-ft test section measurement plane at centerline (CL) and 1 ft above and below CL. Positive pitch flow angle, α, is from floor to ceiling and positive yaw flow angle, β, is from left to right when upstream looking aft. Data acquired during 2019 test section characterization entry at flexwall setting of Mach 1.6. (a) Second overspeed. (b) First overspeed. (c) Nominal. (d) First underspeed. (e) Second underspeed.

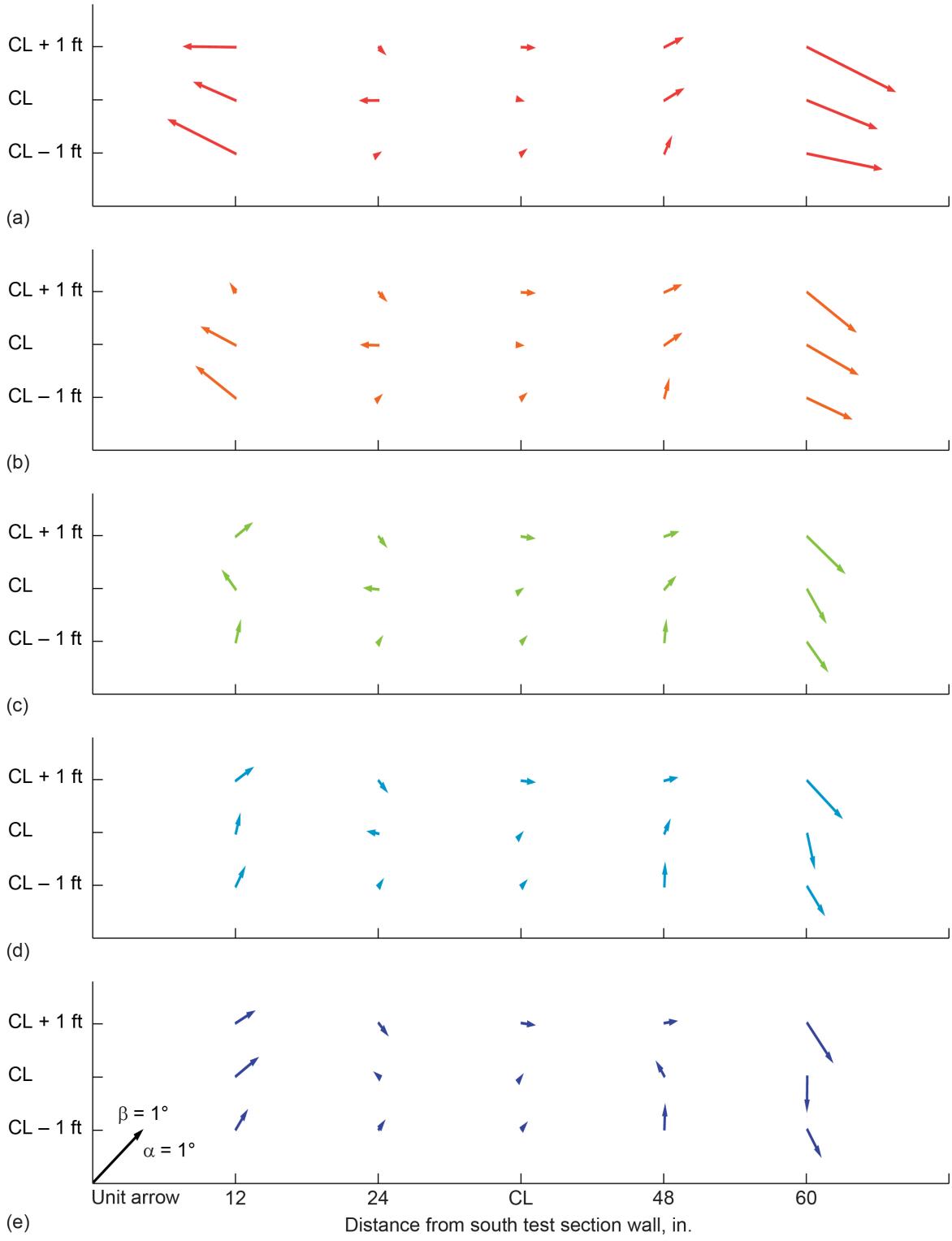

Figure 120.—Pitch and yaw flow angles in 8- by 6-ft test section at 14-ft test section measurement plane at centerline (CL) and 1 ft above and below CL. Positive pitch flow angle, α, is from floor to ceiling and positive yaw flow angle, β, is from left to right when upstream looking aft. Data acquired during 2019 test section characterization entry at flexwall setting of Mach 1.5. (a) Second overspeed. (b) First overspeed. (c) Nominal. (d) First underspeed. (e) Second underspeed.

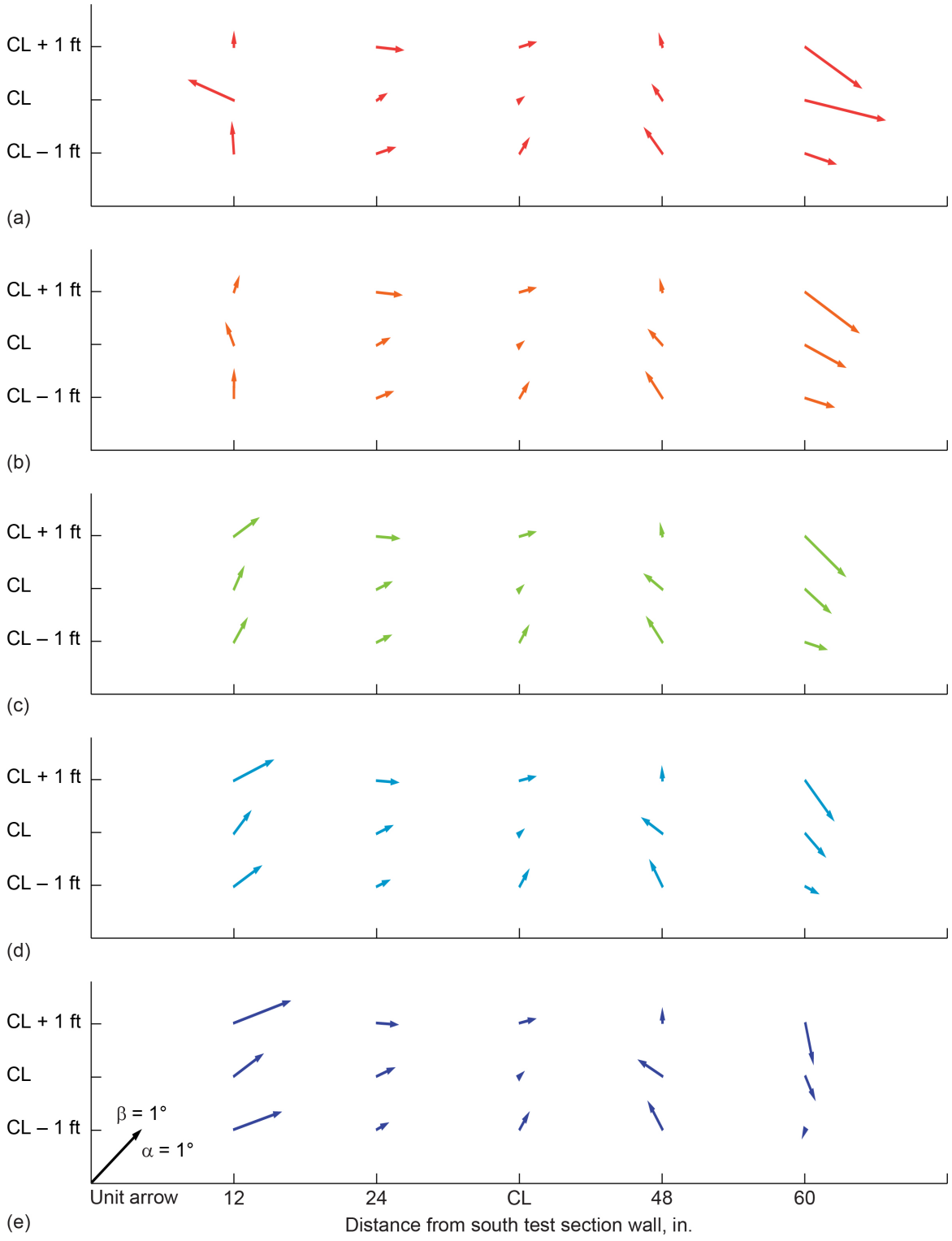

Figure 121.—Pitch and yaw flow angles in 8- by 6-ft test section at 14-ft test section measurement plane at centerline (CL) and 1 ft above and below CL. Positive pitch flow angle, α, is from floor to ceiling and positive yaw flow angle, β, is from left to right when upstream looking aft. Data acquired during 2019 test section characterization entry at flexwall setting of Mach 1.4. (a) Second overspeed. (b) First overspeed. (c) Nominal. (d) First underspeed. (e) Second underspeed.

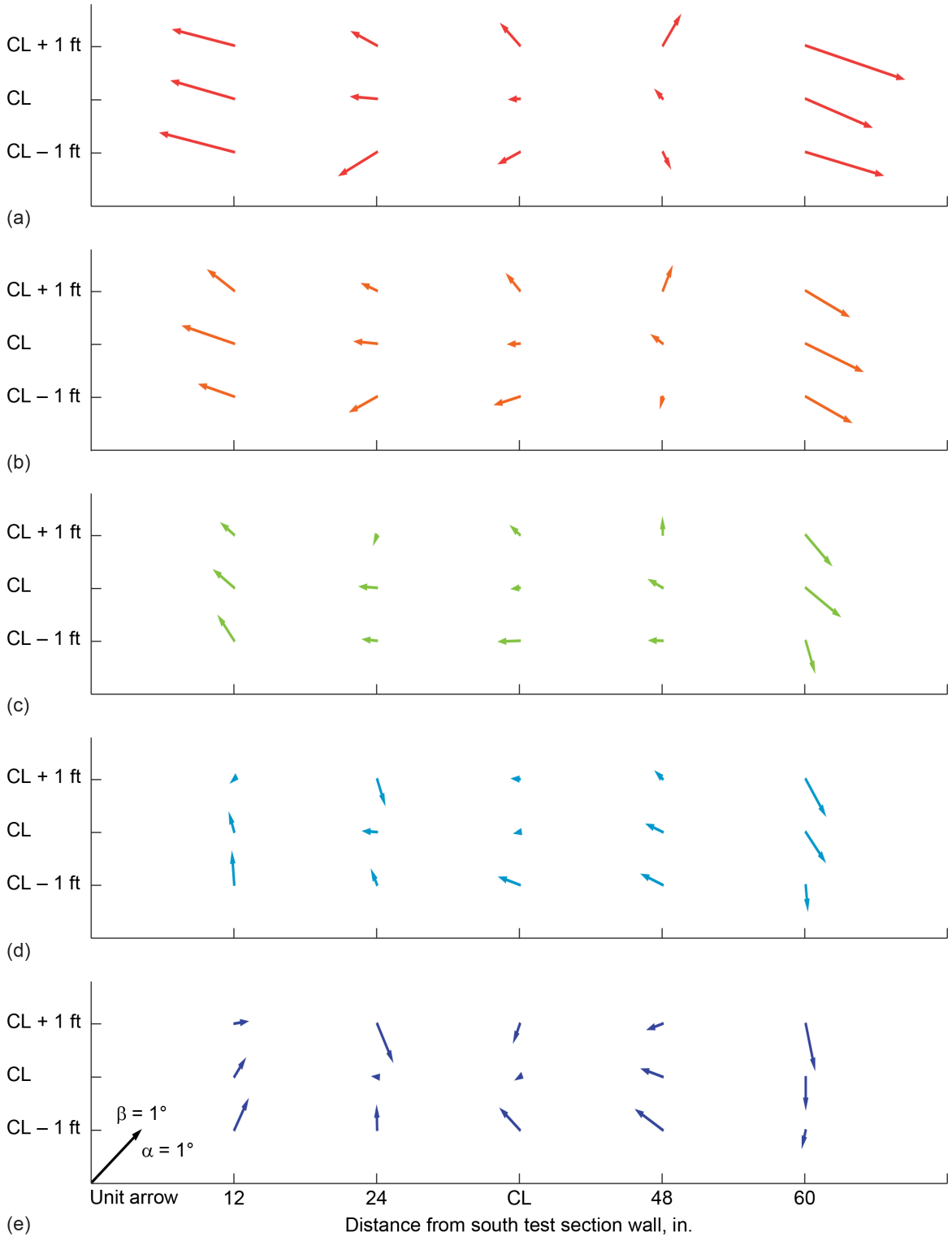

Figure 122.—Pitch and yaw flow angles in 8- by 6-ft test section at 14-ft test section measurement plane at centerline (CL) and 1 ft above and below CL. Positive pitch flow angle, α, is from floor to ceiling and positive yaw flow angle, β, is from left to right when upstream looking aft. Data acquired during 2019 test section characterization entry at flexwall setting of Mach 1.3. (a) Second overspeed. (b) First overspeed. (c) Nominal. (d) First underspeed. (e) Second underspeed.

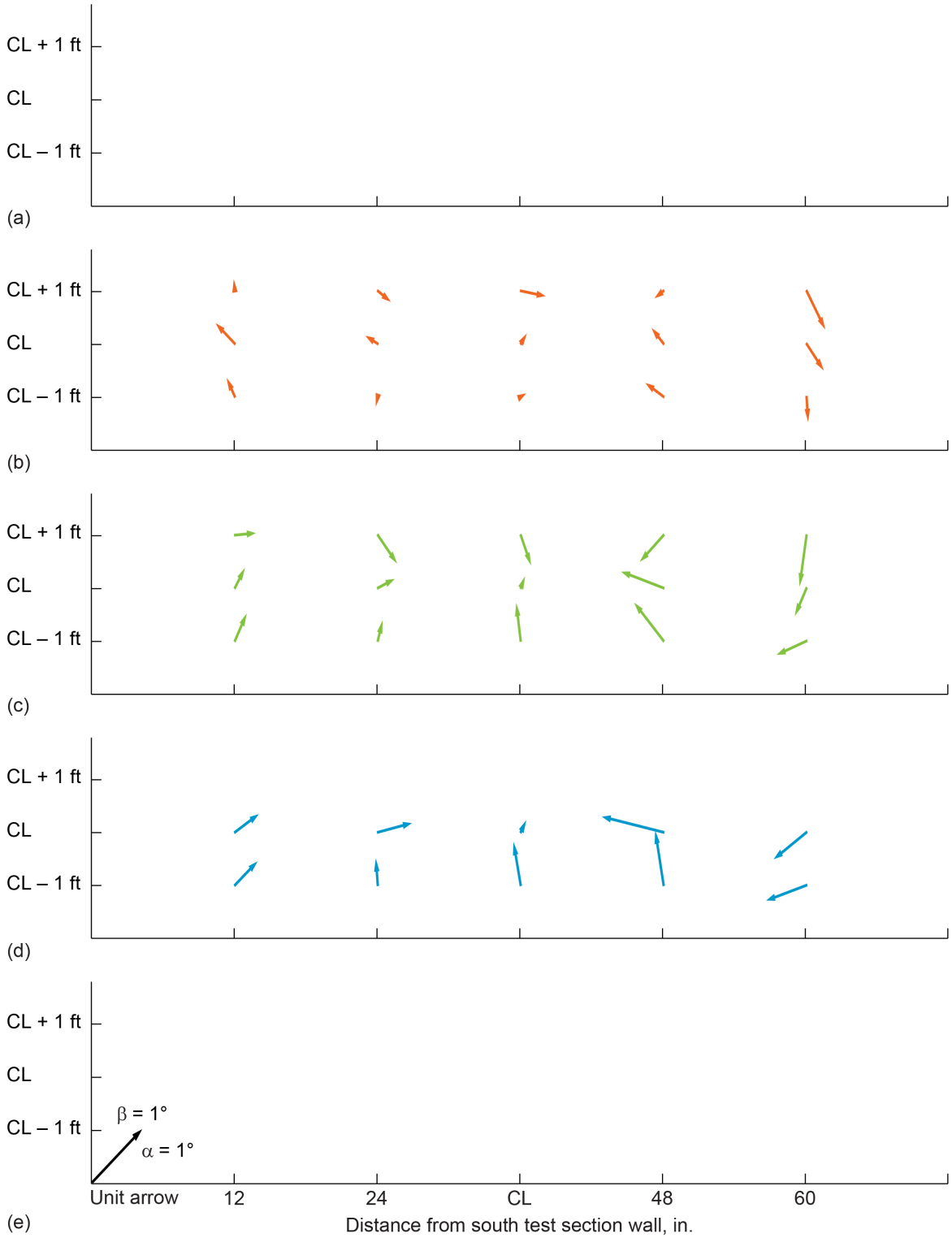

Figure 123.—Pitch and yaw flow angles in 8- by 6-ft test section at 14-ft test section measurement plane at centerline (CL) and 1 ft above and below CL. Positive pitch flow angle, α, is from floor to ceiling and positive yaw flow angle, β, is from left to right when upstream looking aft. Data acquired during 2019 test section characterization entry at flexwall setting of Mach 1.2. (a) Second overspeed. (b) First overspeed. (c) Nominal. (d) First underspeed. (e) Second underspeed.

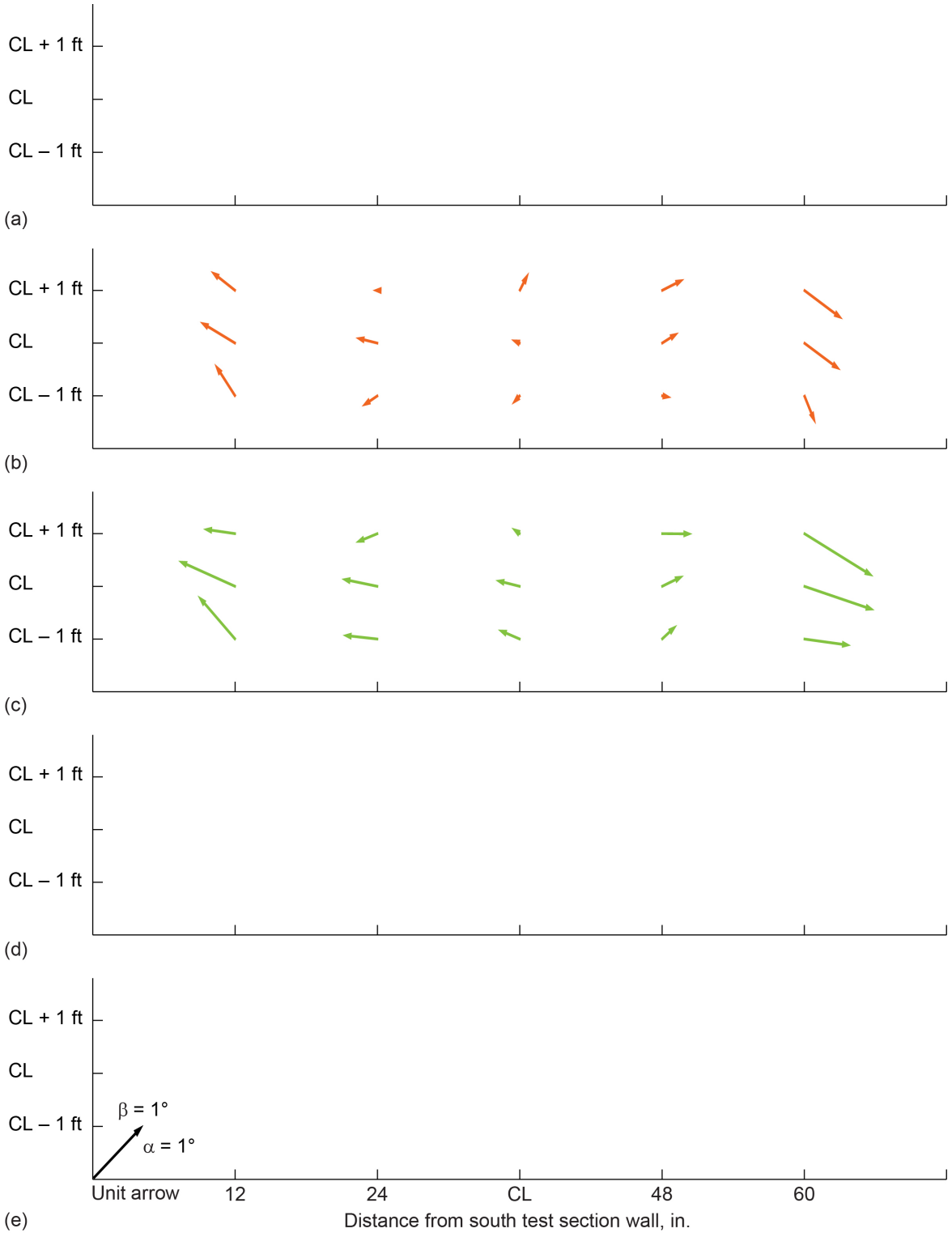

Figure 124.—Pitch and yaw flow angles in 8- by 6-ft test section at 14-ft test section measurement plane at centerline (CL) and 1 ft above and below CL. Positive pitch flow angle, α, is from floor to ceiling and positive yaw flow angle, β, is from left to right when upstream looking aft. Data acquired during 2019 test section characterization entry at flexwall setting of Mach 1.1. (a) Second overspeed. (b) First overspeed. (c) Nominal. (d) First underspeed. (e) Second underspeed.

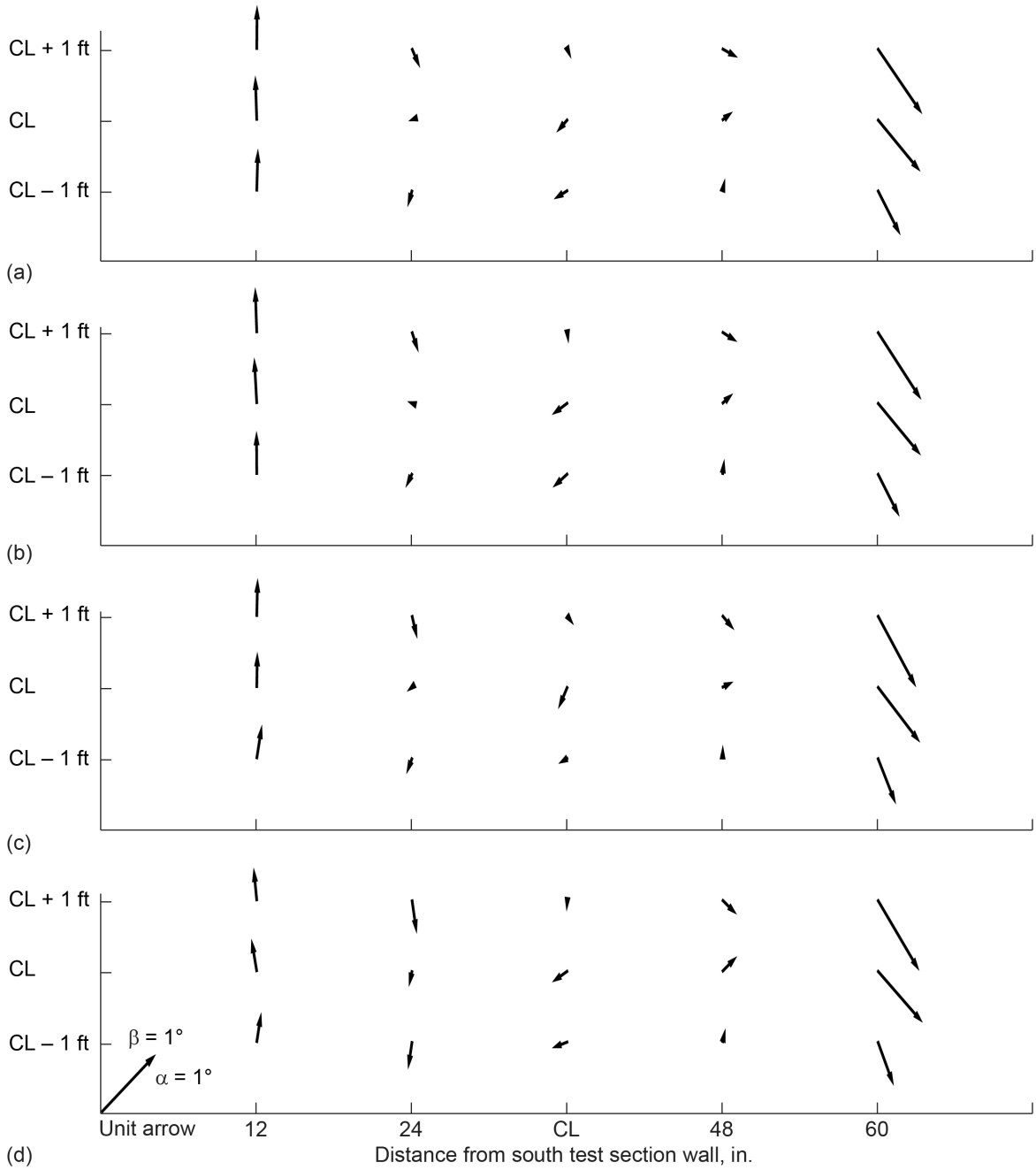

Figure 125.—Pitch and yaw flow angles in 8- by 6-ft test section at 14-ft test section measurement plane at centerline (CL) and 1 ft above and below CL. Positive pitch flow angle, α, is from floor to ceiling and positive yaw flow angle, β, is from left to right when upstream looking aft. Data acquired during 2019 test section characterization entry at subsonic conditions between Mach 0.95 and 0.80 for three-drive-motor operation. (a) M_{ts} = 0.95. (b) M_{ts} = 0.90. (c) M_{ts} = 0.85. (d) M_{ts} = 0.80.

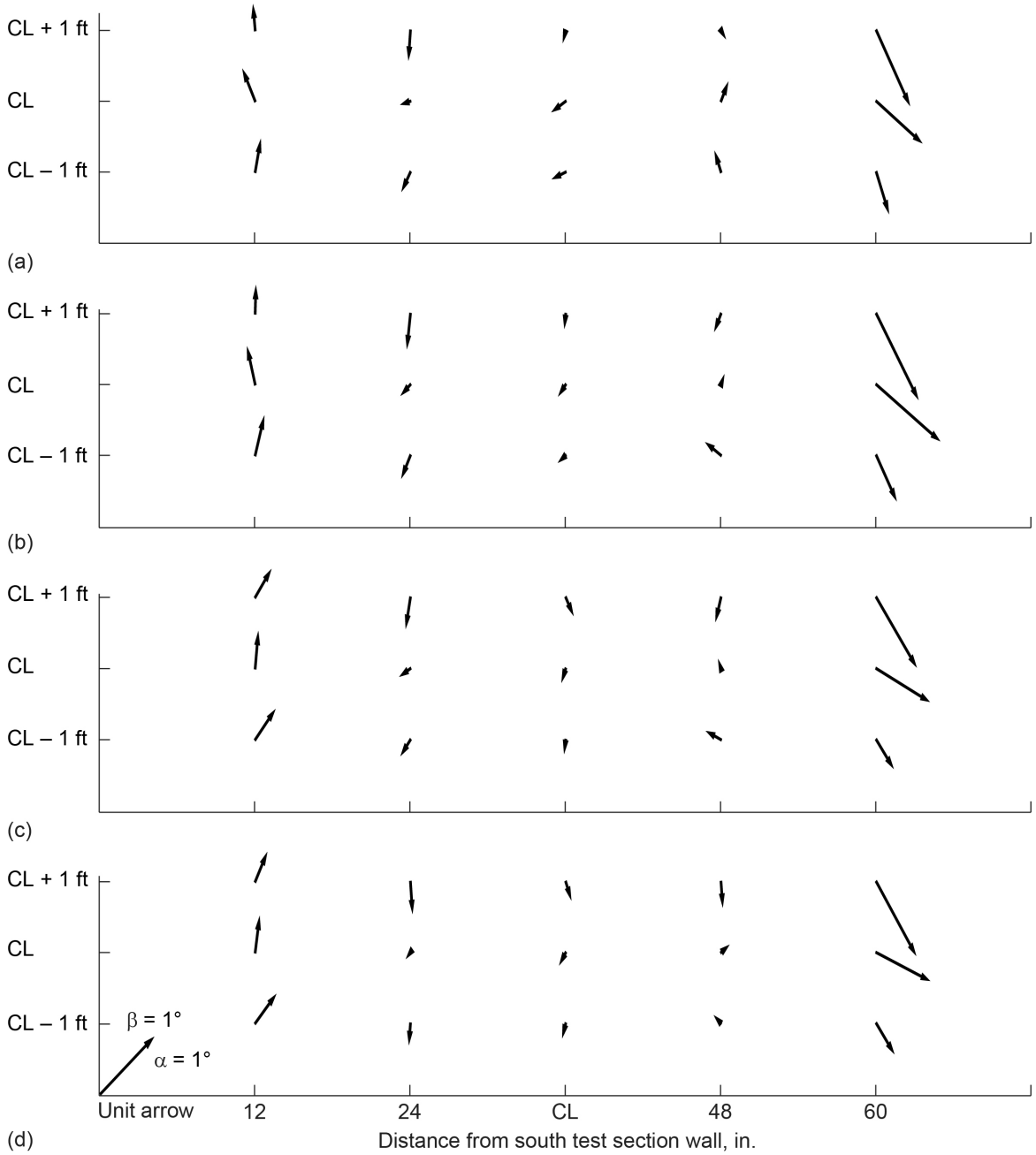

Figure 126.—Pitch and yaw flow angles in 8- by 6-ft test section at 14-ft test section measurement plane at centerline (CL) and 1 ft above and below CL. Positive pitch flow angle, α, is from floor to ceiling and positive yaw flow angle, β, is from left to right when upstream looking aft. Data acquired during 2019 test section characterization entry at subsonic conditions between Mach 0.75 and 0.60 for three-drive-motor operation. (a) M_{ts} = 0.75. (b) M_{ts} = 0.70. (c) M_{ts} = 0.65. (d) M_{ts} = 0.60.

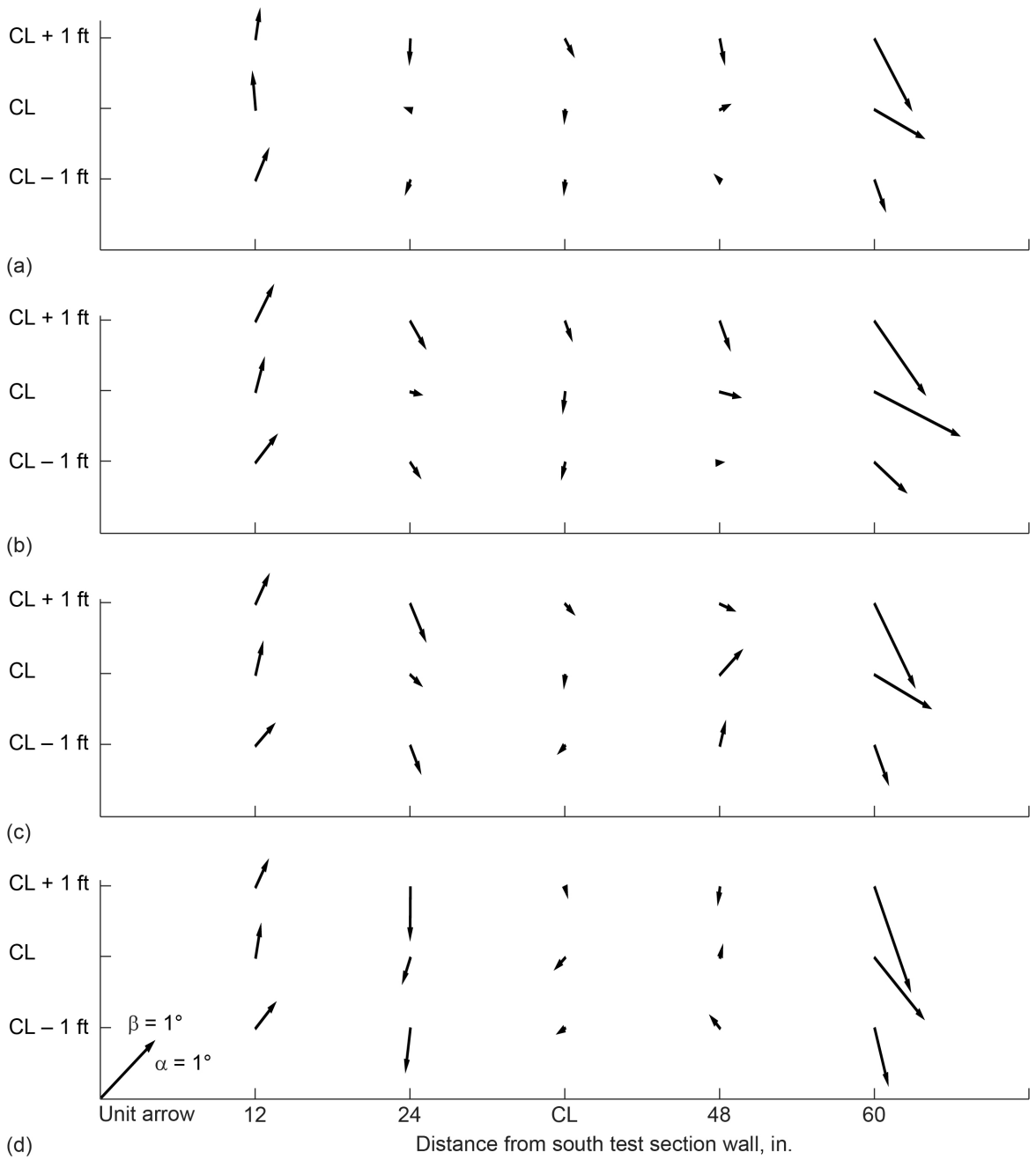

Figure 127.—Pitch and yaw flow angles in 8- by 6-ft test section at 14-ft test section measurement plane at centerline (CL) and 1 ft above and below CL. Positive pitch flow angle, α, is from floor to ceiling and positive yaw flow angle, β, is from left to right when upstream looking aft. Data acquired during 2019 test section characterization entry at subsonic conditions between Mach 0.55 and 0.40 for three-drive-motor operation. (a) M_{ts} = 0.55. (b) M_{ts} = 0.50. (c) M_{ts} = 0.45. (d) M_{ts} = 0.40.

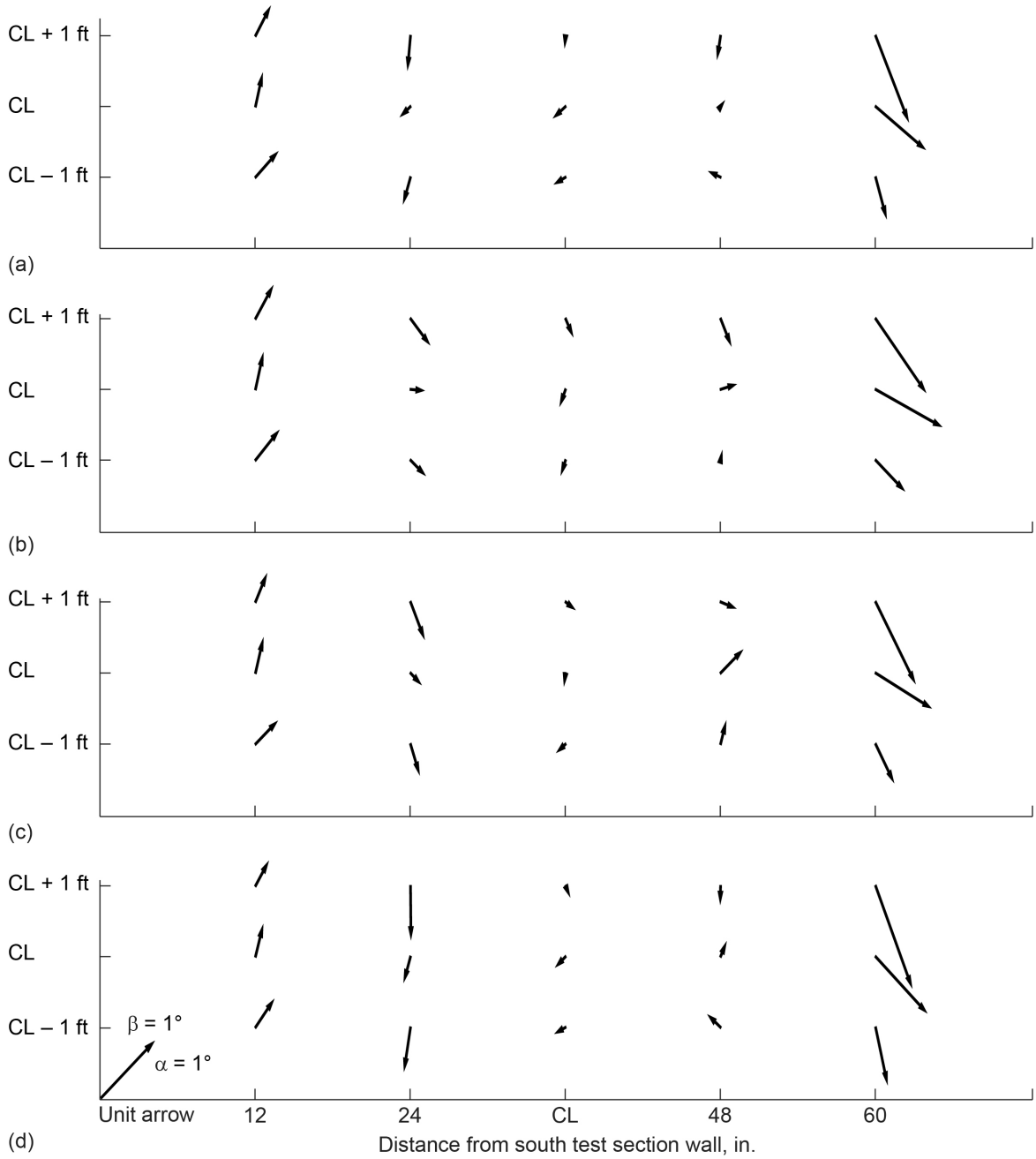

Figure 128.—Pitch and yaw flow angles in 8- by 6-ft test section at 14-ft test section measurement plane at centerline (CL) and 1 ft above and below CL. Positive pitch flow angle, α, is from floor to ceiling and positive yaw flow angle, β, is from left to right when upstream looking aft. Data acquired during 2019 test section characterization entry at subsonic conditions between Mach 0.36 for three-drive-motor operation and Mach 0.50 to 0.40 for one-drive-motor operation. (a) M_{ts} = 0.36. (b) M_{ts} = 0.50. (c) M_{ts} = 0.45. (d) M_{ts} = 0.40.

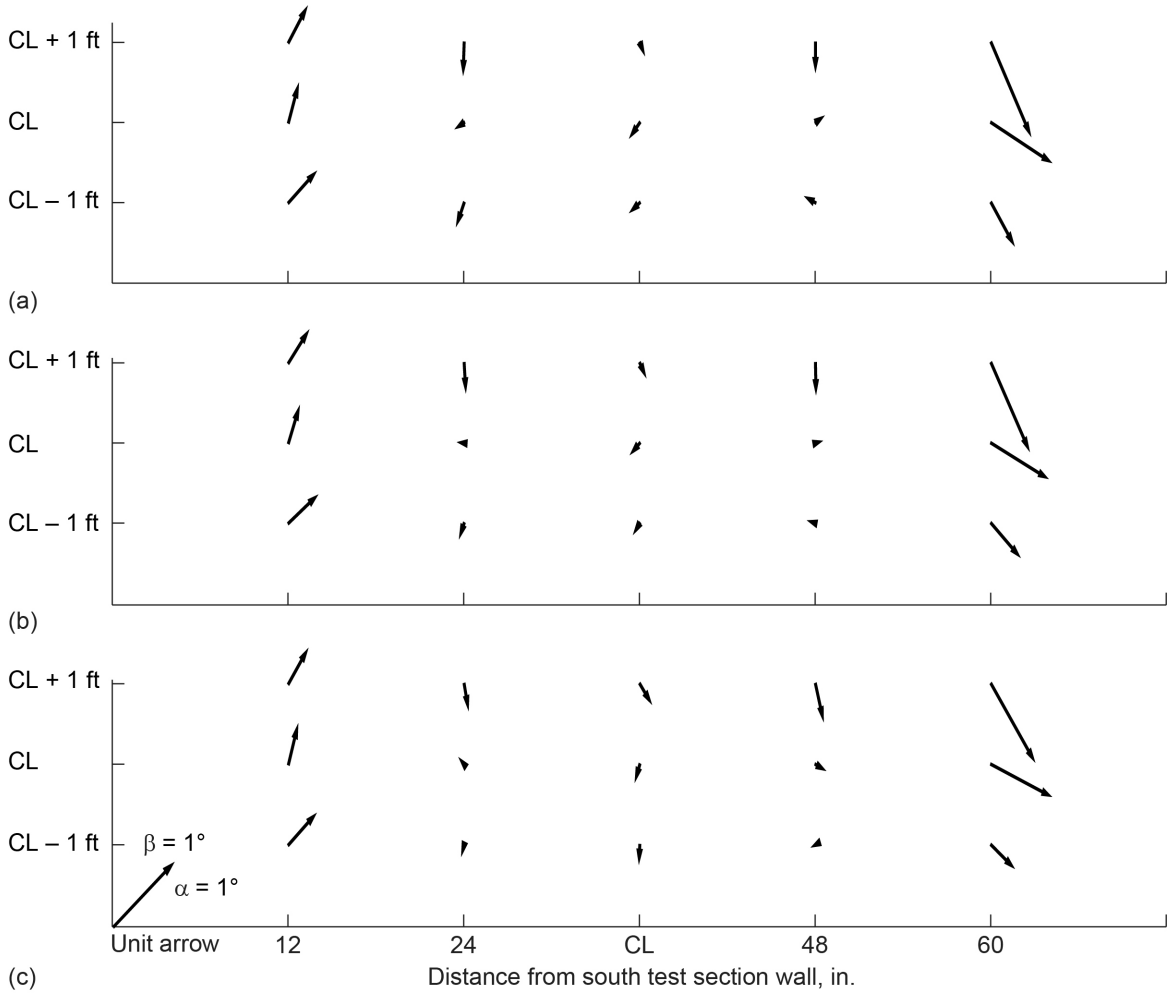

Figure 129.—Pitch and yaw flow angles in 8- by 6-ft test section at 14-ft test section measurement plane at centerline (CL) and 1 ft above and below CL. Positive pitch flow angle, α, is from floor to ceiling and positive yaw flow angle, β, is from left to right when upstream looking aft. Data acquired during 2019 test section characterization entry at subsonic conditions between Mach 0.35 and 0.25 for one-drive-motor operation. (a) M_{ts} = 0.35. (b) M_{ts} = 0.30. (c) M_{ts} = 0.25.

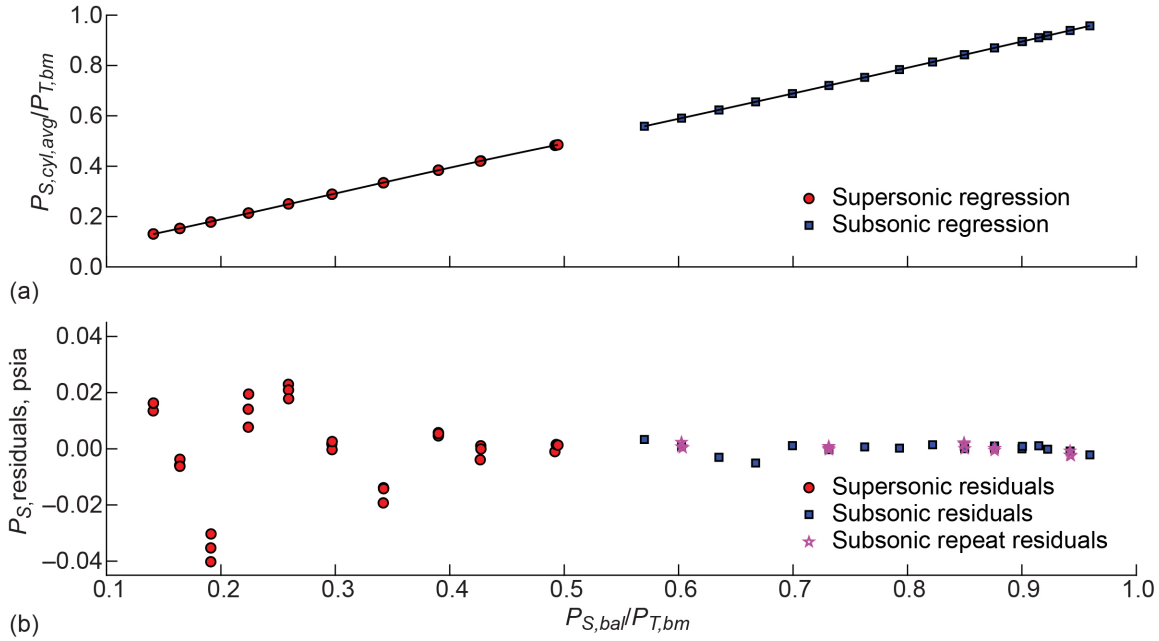

Figure 130.—Static pressure regression models and associated residuals for 8- by 6-ft test section porosity configuration 1 (14-ft test section, 5.8-percent porosity) over entire operating range of the 8- by 6-Foot Supersonic Wind Tunnel. Data collected from aft portion of cylinder on the 4-inch-diameter cone cylinder were used to represent test section static pressure. Regression model residuals were multiplied by measured bellmouth total pressure, $P_{T,bm}$, at each condition to convert residuals to engineering units. (a) Regression models. (b) Residuals.

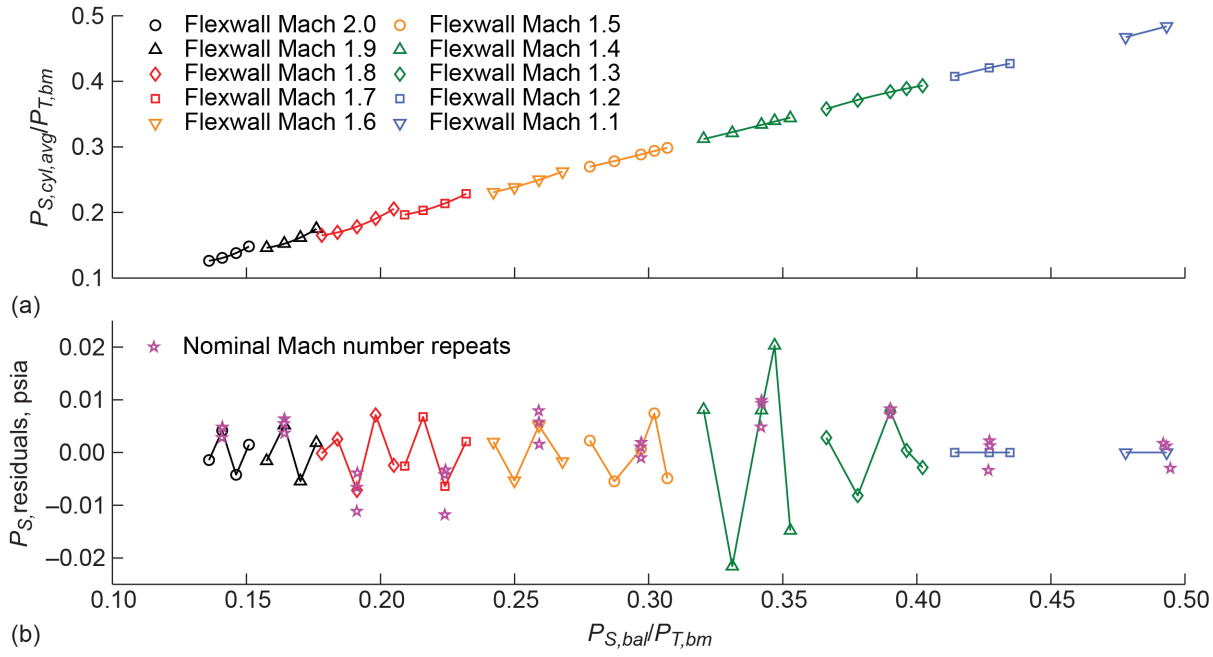

Figure 131.—Local static pressure regression models for each nominal flexwall setting and associated residuals for the 8- by 6-ft test section porosity configuration 1 (14-ft test section, 5.8-percent porosity) over supersonic operating range of the 8- by 6-Foot Supersonic Wind Tunnel. Data collected from aft portion of cylinder on the 4-inch-diameter cone cylinder were used to represent test section static pressure. Regression model residuals were multiplied by the measured bellmouth total pressure, $P_{T,bm}$, at each condition to convert residuals to engineering units. (a) Regression models. (b) Residuals.

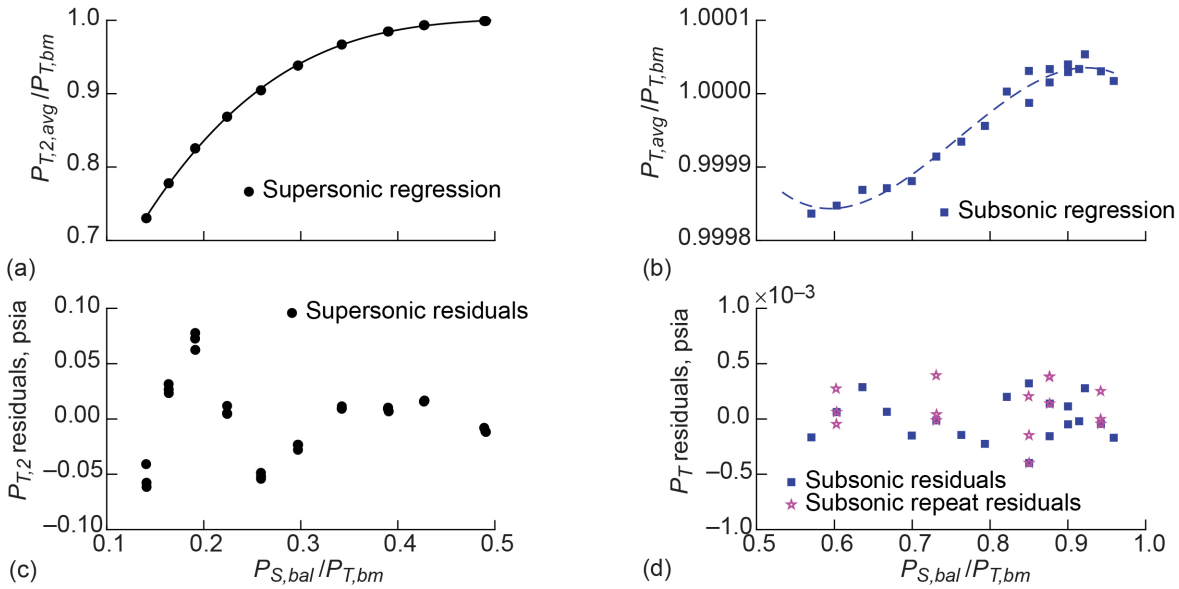

Figure 132.—Total pressure behind normal shock (supersonic) and freestream total pressure (subsonic) regression models and associated residuals for the 8- by 6-ft test section porosity configuration 1 (14-ft test section, 5.8-percent porosity) over entire operating range of the 8- by 6-Foot Supersonic Wind Tunnel. Data collected from center seven pressure probes on the transonic array at test section centerline were used to represent test section total pressure behind a normal shock (supersonic) and freestream total pressure (subsonic). Regression model residuals were multiplied by measured bellmouth total pressure, $P_{T,bm}$, at each condition to convert residuals to engineering units. (a) Supersonic regression models. (b) Subsonic regression models. (c) Supersonic residuals. (d) Subsonic residuals.

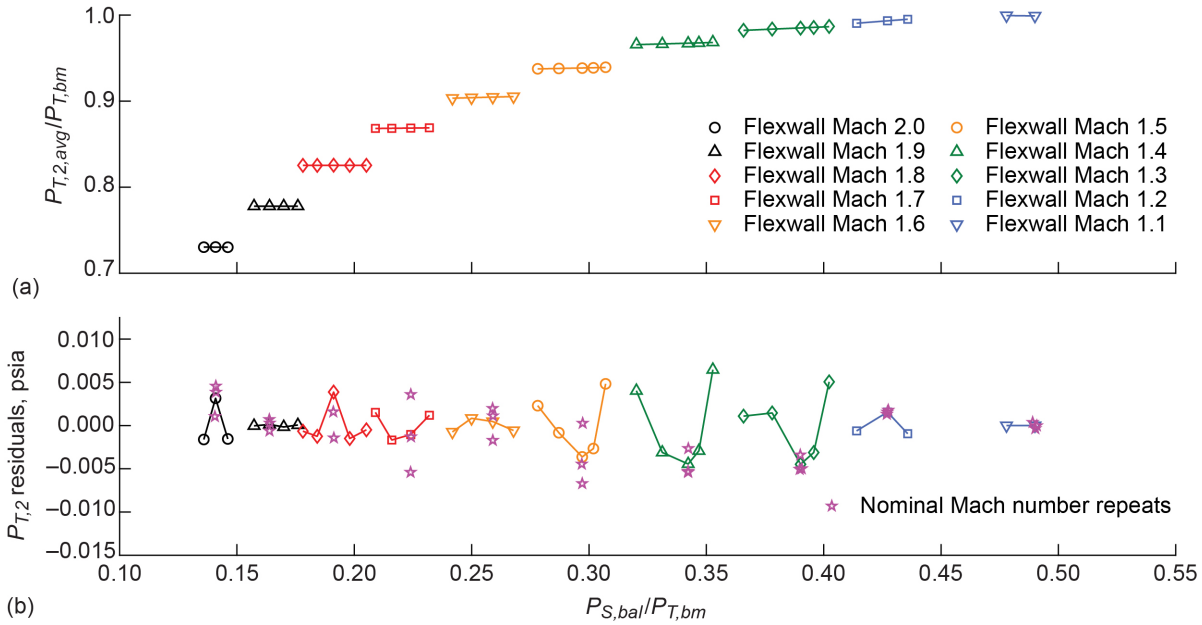

Figure 133.—Local total pressure behind normal shock regression models for each nominal flexwall setting and associated residuals for the 8- by 6-ft test section porosity configuration 1 (14-ft test section, 5.8-percent porosity) over supersonic operating range of the 8- by 6-Foot Supersonic Wind Tunnel. Data collected from center seven pressure probes on the transonic array at test section centerline were used to represent test section total pressure behind a normal shock. Regression model residuals were multiplied by measured bellmouth total pressure, $P_{T,bm}$, at each condition to convert residuals to engineering units. (a) Regression models. (b) Residuals.

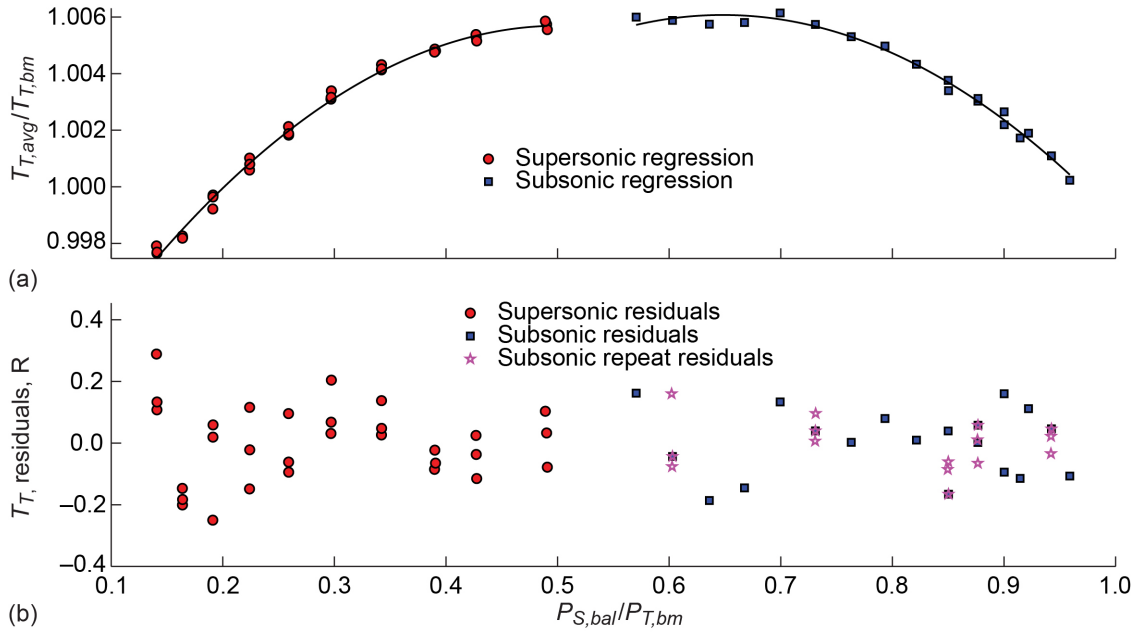

Figure 134.—Total temperature regression models and associated residuals for the 8- by 6-ft test section porosity configuration 1 (14-ft test section, 5.8-percent porosity) over entire operating range of the 8- by 6-Foot Supersonic Wind Tunnel. Data collected from center seven thermocouple probes on the transonic array at test section centerline were used to represent test section total temperature. Regression model residuals were multiplied by measured bellmouth total temperature, $T_{T,bm}$, at each condition to convert residuals to engineering units. (a) Regression models. (b) Residuals.

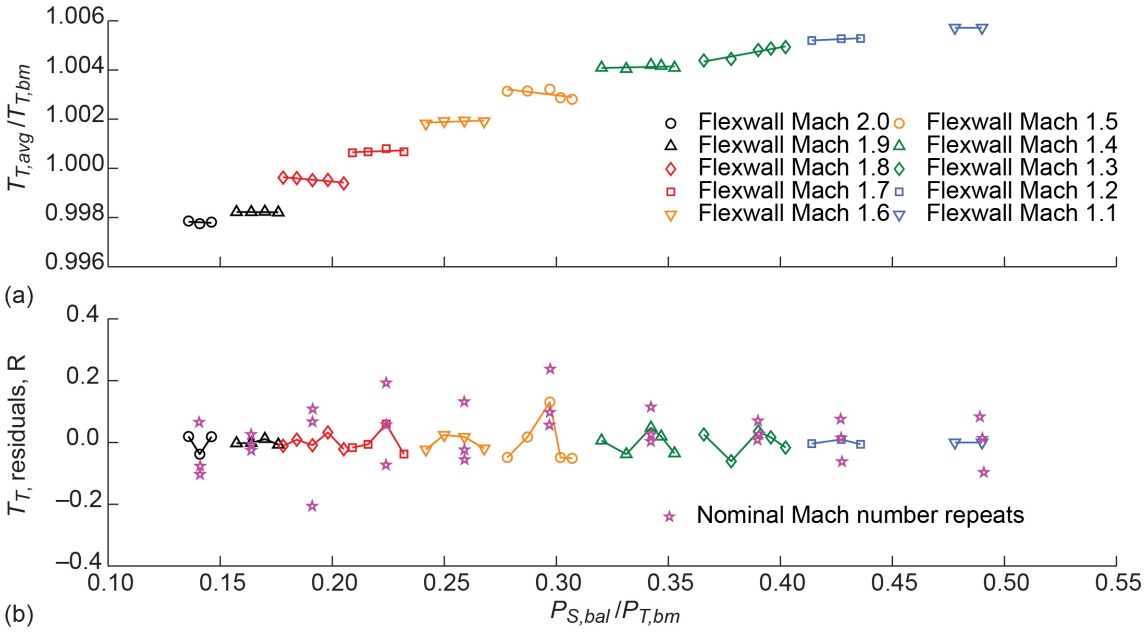

Figure 135.—Local total temperature regression models for each nominal flexwall setting and associated residuals for the 8- by 6-ft test section porosity configuration 1 (14-ft test section, 5.8-percent porosity) over supersonic operating range of the 8- by 6-Foot Supersonic Wind Tunnel. Data collected from center seven thermocouple probes on the transonic array at test section centerline were used to represent test section total temperature. Regression model residuals were multiplied by measured bellmouth total temperature, $T_{T,bm}$, at each condition to convert residuals to engineering units. (a) Regression models. (b) Residuals.

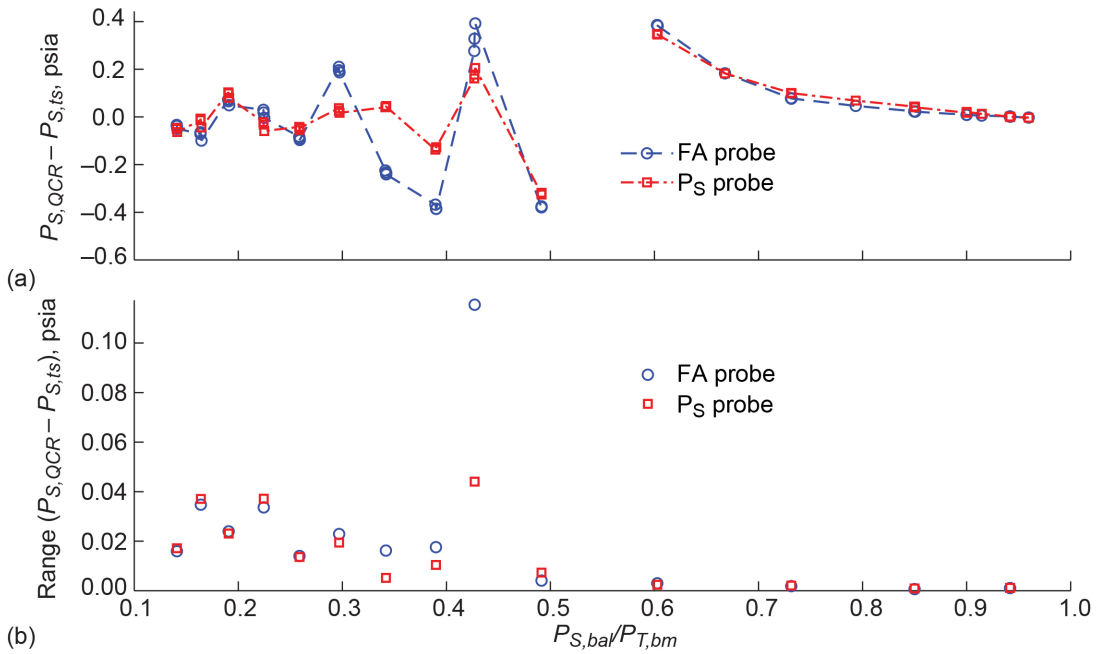

Figure 136.—Static pressure residuals and range of residuals for the 8- by 6-Foot Supersonic Wind Tunnel transonic quick-check rake during 2019 characterization test entry. Test section configured for porosity configuration 1 (14-ft test section, 5.8-percent porosity) and probe tips at test section station 139.875. Flow angle (FA). Static pressure (P_S) (a) Residuals. (b) Range of residuals.

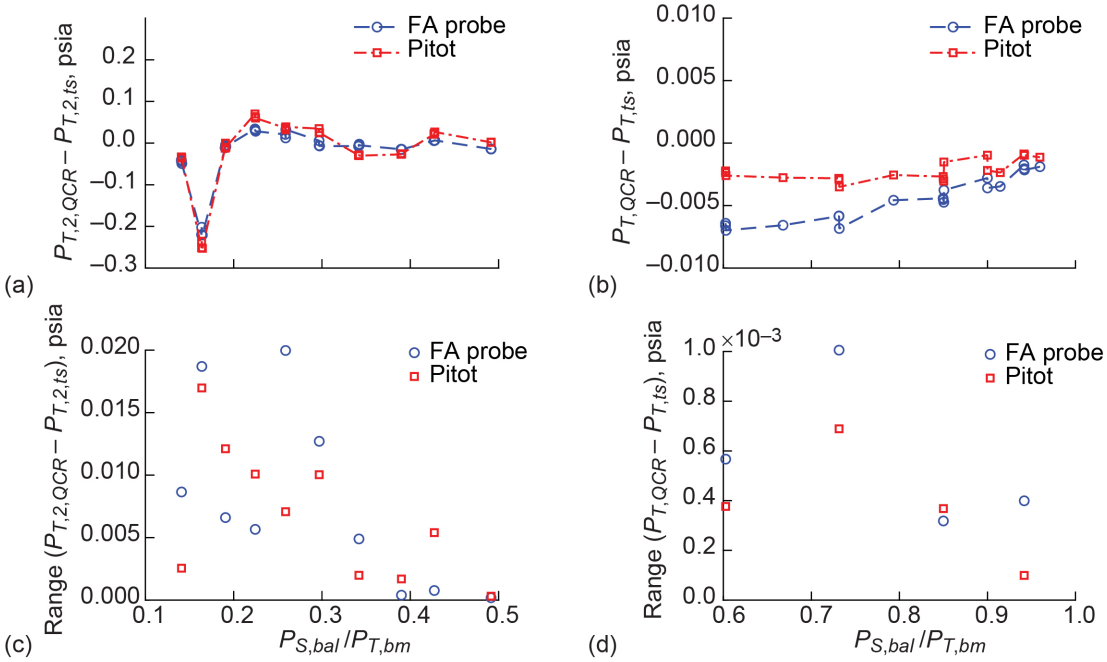

Figure 137.—Total pressure (subsonic) and total pressure aft of normal shock (supersonic) residuals and range of residuals for the 8- by 6-Foot Supersonic Wind Tunnel transonic quick-check rake during 2019 characterization test entry. Test section configured for porosity configuration 1 (14-ft test section, 5.8-percent porosity) and probe tips at test section station 139.875. (a) Subsonic residuals. (b) Supersonic residuals. (c) Subsonic range of residuals. (d) Supersonic range of residuals.

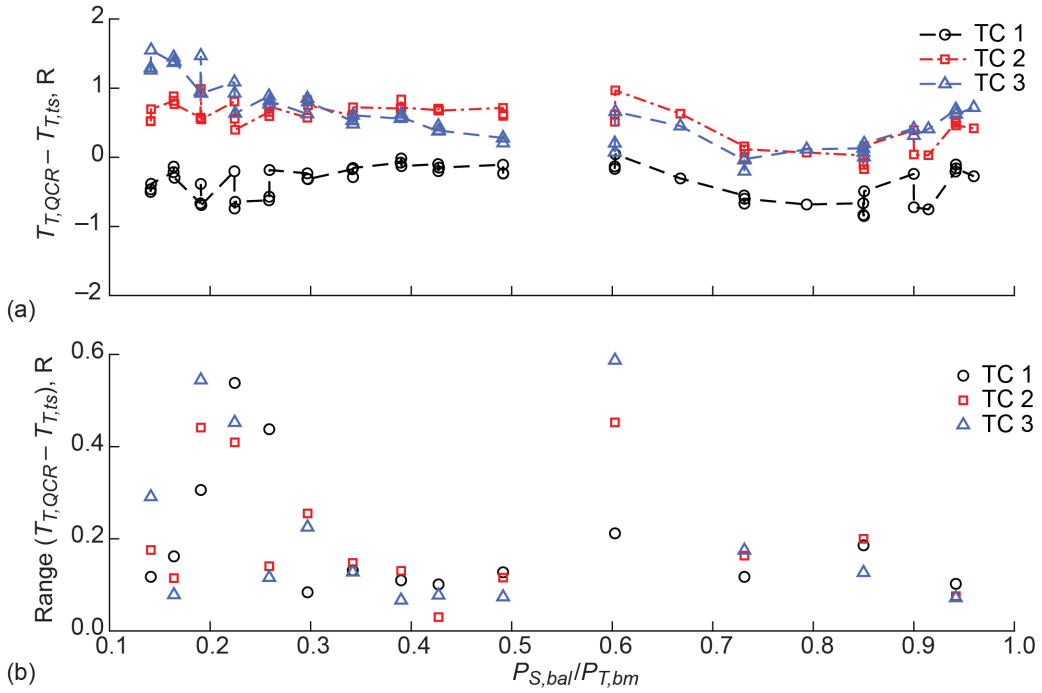

Figure 138.—Total temperature residuals and range of residuals for the 8- by 6-Foot Supersonic Wind Tunnel transonic quick-check rake during 2019 characterization test entry. Test section configured for porosity configuration 1 (14-ft test section, 5.8-percent porosity) and probe tips at test section station 139.875. Thermocouple (TC). (a) Residuals. (b) Range of residuals.

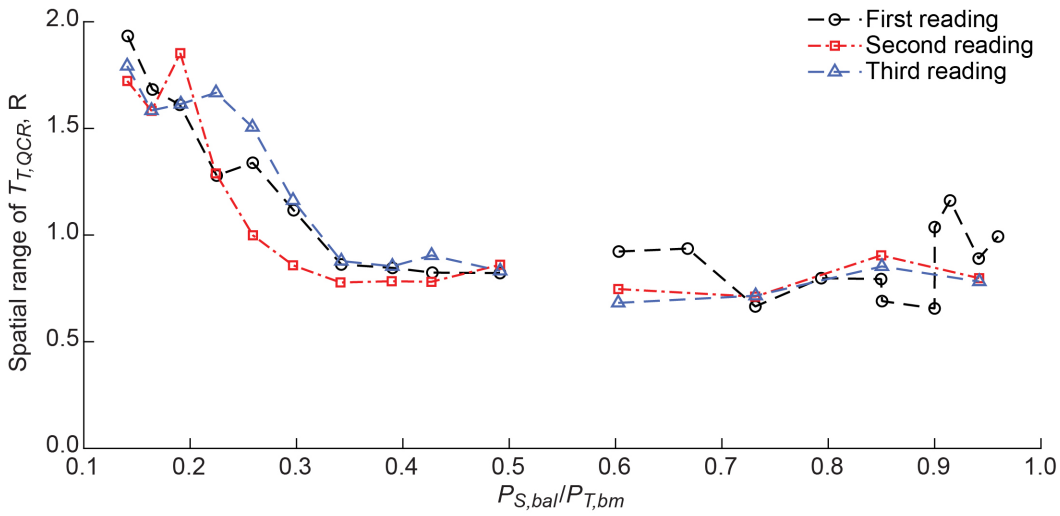

Figure 139.—Spatial variation of total temperature on the 8- by 6-Foot Supersonic Wind Tunnel transonic quick-check rake during 2019 characterization test entry. Test section configured for porosity configuration 1 (14-ft test section, 5.8-percent porosity) and probe tips at test section station 139.875.

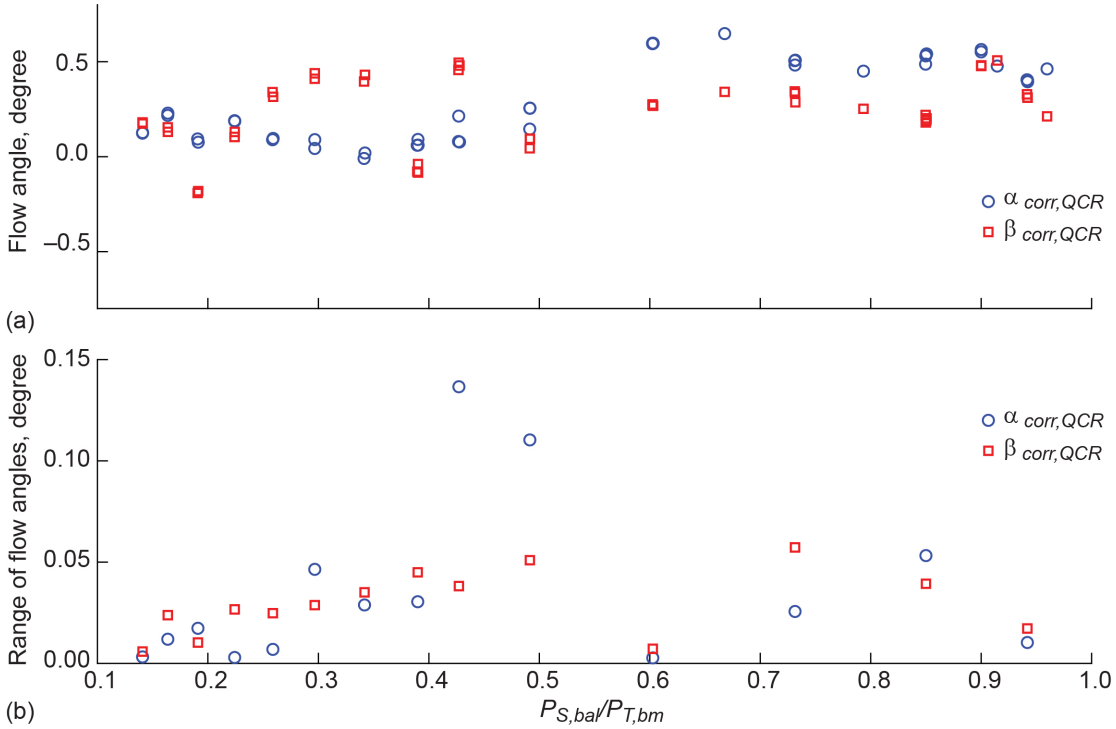

Figure 140.—Flow angles and range of flow angles for the 8- by 6-Foot Supersonic Wind Tunnel transonic quick-check rake during 2019 characterization test entry. Test section configured for porosity configuration 1 (14-ft test section, 5.8-percent porosity) and probe tips at test section station 139.875. (a) Flow angles. (b) Range of flow angles.

Appendix A.—Postconstruction Flow Quality Survey Test Entry (2018 Test)

Following completion of the 9- by 15-Foot Low-Speed Wind Tunnel (9×15 LSWT) acoustic improvement modifications project, a test entry in the 8- by 6-Foot Supersonic Wind Tunnel (8×6 SWT) was conducted to replicate testing conducted in a baseline preconstruction test entry in 2015 (Ref. 1). The postconstruction flow quality survey, commonly referred to as the "validation test entry," was performed immediately before the 8×6 SWT characterization test entry in 2019. This appendix shall summarize the results of the 2018 test entry, specifically related to the following goals defined for 8×6 SWT operation and flow quality, each of which were met after assessment of the data collected during the 2015 (preconstruction) and 2018 (postconstruction) test entries:

1. The 8×6 SWT can reach Mach 2.0, nominally, with the 16-inch-diameter cone cylinder installed in the 8×6 SWT test section.
2. Corner 1 static pressure stays within the allowable structural range over the 8×6 SWT operational range ($\Delta P_{S,\text{Corner1}} \leq 75.5$ psf).
3. The uniformity of the flow through the air dryer beds following the 9×15 LSWT acoustic improvement modifications should be no more than 25 percent worse than the uniformity measured prior to the facility modifications for open- and closed-loop operation:

$$\sigma\left(\frac{V}{\overline{V}}\right)_{post} \leq 125\% \cdot \sigma\left(\frac{V}{\overline{V}}\right)_{pre}$$

where V is the local streamwise velocity at one of the air dryer bed anemometers and $\overline{V}$ is the spatial average of the streamwise velocities measured by the air dryer bed anemometers at a given condition.

For details concerning the facility, hardware and instrumentation, test setup and procedures, and the data reduction for the 16-inch-diameter cone cylinder (Figure A.1) and air dryer bed anemometers (Figure A.2), refer to Reference 1. A few differences exist in the operations of this test entry and the 2015 preconstruction flow quality survey, however, these changes did not impact the ability to make a direct comparison between the results of the two entries. The facility data system was converted to COBRA (Collect, Observe, Broadcast, Record, and Analyze), which ran at a sampling rate of 12.5 Hz; all facility and test section instrumentation data were collected at a rate of 12.5 Hz during the 2018 test entry. Data with the air dryer bed anemometers were acquired with Dewetron (Dewetron Gmbh), the facility's dynamic data system, using 120-s sampling periods at a 1-kHz sampling rate, which encompassed the 100-s 12.5-Hz samples collected by COBRA. Data were acquired, according to the sample sizes discussed for each data system, at each test section condition surveyed during the entry. The air dryer bed anemometer data required additional attention during postprocessing as the health of the anemometers tended to degrade throughout the 2018 test entry. Trimming of erratic spikes in the flow angle and airspeed signals was required through the use of a custom-written MATLAB® (The MathWorks, Inc.) script. Two of the anemometers were unusable for the closed-loop supersonic runs.

The 2018 test entry in the 8×6 SWT covered the full operating envelope of the facility: Mach 0.25 to 2.0 in both open- and closed-loop operating mode. In open-loop (propulsion) operating mode, air is brought into the tunnel circuit through facility doors 4 and 5 and exhausted through facility doors 1 and 2. The test section was set to configuration 6 (14-ft test section with schlieren windows installed in the transonic test section) for the duration of the 2018 test entry.

Figure A.1.—Sixteen-inch-diameter cone cylinder installed in 8- by 6-Foot Supersonic Wind Tunnel during 2018 validation test entry. Cone tip installed at inlet of 8-ft test section with test section configured to porosity configuration 6 (14-ft test section with schlieren windows).

Figure A.2.—Air dryer bed anemometer installed at center of inlet of one of 20 locations in 8- by 6-Foot Supersonic Wind Tunnel air dryer building during 2018 validation test entry.

Table A.1 shows a comparison of the standard deviation of the axial airspeed and the root mean square (RMS) of the yaw flow angle at the air dryer bed inlet plane between the 2015 and 2018 test entries. Overall, the flow uniformity into the air dryer beds for closed-loop operation, as measured by the standard deviation of the axial velocity, is lower than the preconstruction levels. Only in open-loop supersonic operation did the axial velocity distribution in 2018 appear slightly less uniform than the preconstruction values, but within the limits defined in the test objectives. Figure A.3 and Figure A.4 show an example of the data comparison between test entries at a flexwall setting of Mach 1.3 for closed-

and open-loop operation, respectively, with the dryer beds enabled (commonly referred to as “dry air”). Figure A.5 and Figure A.6 show a visualization of the Mach 1.3 air dryer bed inlet flow from the 2018 test entry with air dryer disabled (commonly referred to as “wet air”) for closed- and open-loop operation, respectively. Slightly higher velocities are observed at Mach 1.2 and 1.1, however, data were not available at the four different combinations of facility settings for these Mach numbers to enable comparison.

TABLE A.1.—COMPARISON OF AIR DRYER BED WIND ANEMOMETER AXIAL VELOCITY STANDARD DEVIATIONS AND YAW FLOW ANGLE ROOT-MEAN-SQUARE VALUES DURING 8- BY 6-FOOT SUPERSONIC WIND TUNNEL TEST SECTION CONDITIONS SURVEYED DURING 2015 (PRECONSTRUCTION) AND 2018 (POSTCONSTRUCTION) TEST ENTRIES

No. of drive motors	Nominal Mach no.	σ($V/\bar{V}$)						RMS(β), deg			
		Open loop			Closed loop			Open loop		Closed loop	
		Pre	Post	% Diff.	Pre	Post	% Diff.	Pre	Post	Pre	Post
Three	2.00	-------	0.324	-------	0.476	0.334	–29.9	-------	29.5	32.6	44.6
	1.90	-------	.321	-------	.487	.286	–41.3	-------	29.6	33.2	39.1
	1.80	-------	.318	-------	.485	.284	–41.4	-------	30.1	33.2	39.3
	1.70	-------	.319	-------	.478	.282	–41.0	-------	29.0	32.6	35.9
	1.60	0.300	.320	6.8	.481	.284	–41.0	18.3	29.1	33.2	32.2
	1.50	.300	.324	8.1	.475	.338	–28.9	18.2	34.9	32.6	42.1
	1.40	.302	.318	5.2	.481	.339	–29.5	18.8	29.1	33.0	43.2
	1.30[a]	.302	.316	4.8	.478	.342	–28.4	18.3	29.1	32.7	42.9
	1.20	.306	.315	3.1	-------	.343	-------	20.6	28.9	-------	41.5
	“Dry air” at or above Mach 1.2										
	1.10	0.698	0.657	–5.9	-------	0.696	-------	44.6	50.3	-------	45.4
	.95	-------	.689	-------	-------	.653	-------	-------	42.4	-------	37.3
	.90	.698	.692	–.9	-------	.653	-------	40.4	41.4	-------	37.3
	.85	-------	.693	-------	-------	.653	-------	-------	40.5	-------	37.2
	.80	.696	.695	–.2	-------	.655	-------	44.0	40.7	-------	37.3
	.75	-------	.695	-------	-------	.653	-------	-------	40.5	-------	37.1
	.70	.701	.696	–.7	-------	.654	-------	43.1	40.2	-------	36.9
	.65	-------	.703	-------	-------	.664	-------	-------	40.8	-------	37.6
	.60	.705	.709	.6	-------	.670	-------	47.4	41.7	-------	38.5
	.55	-------	.716	-------	-------	.680	-------	-------	40.6	-------	38.9
	.50	.726	.725	–.2	-------	.686	-------	45.1	40.4	-------	40.3
	.45	-------	.734	-------	-------	.696	-------	-------	40.9	-------	39.8
	.40	.756	.747	–1.2	-------	.706	-------	44.7	41.0	-------	40.9
One	0.50	0.741	0.733	–1.1	-------	0.694	-------	46.8	40.9	-------	38.5
	.40	.767	.757	–1.3	-------	.714	-------	44.4	41.4	-------	41.4
	.30	.814	.796	–2.2	-------	.750	-------	43.0	42.4	-------	44.8
	.25	.840	.807	–3.9	-------	.767	-------	41.9	42.6	-------	39.3

[a]Mach 1.3 closed loop: during preconstruction testing, facility doors 4 and 5 were partially open during test condition (modified closed loop).

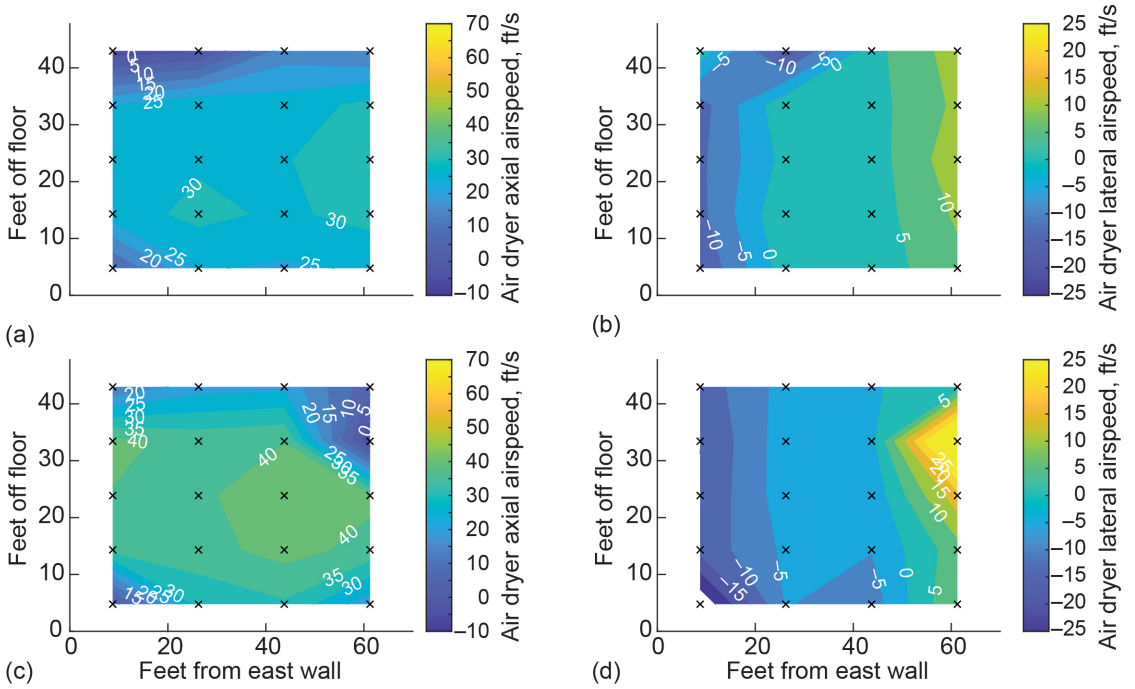

Figure A.3.—Axial and lateral velocity distributions in 8- by 6-Foot Supersonic Wind Tunnel air dryer bed inlet plane during 2018 validation and 2015 preconstruction flow quality survey test entries. Test section Mach number was set to Mach 1.3, nominally, in closed-loop operation with air dryer beds enabled (referred to as “dry air”). View is upstream looking aft at dryer bed inlet. (a) 2018 test entry, axial. (b) 2018 test entry, lateral. (c) 2015 test entry, axial. (d) 2015 test entry, lateral.

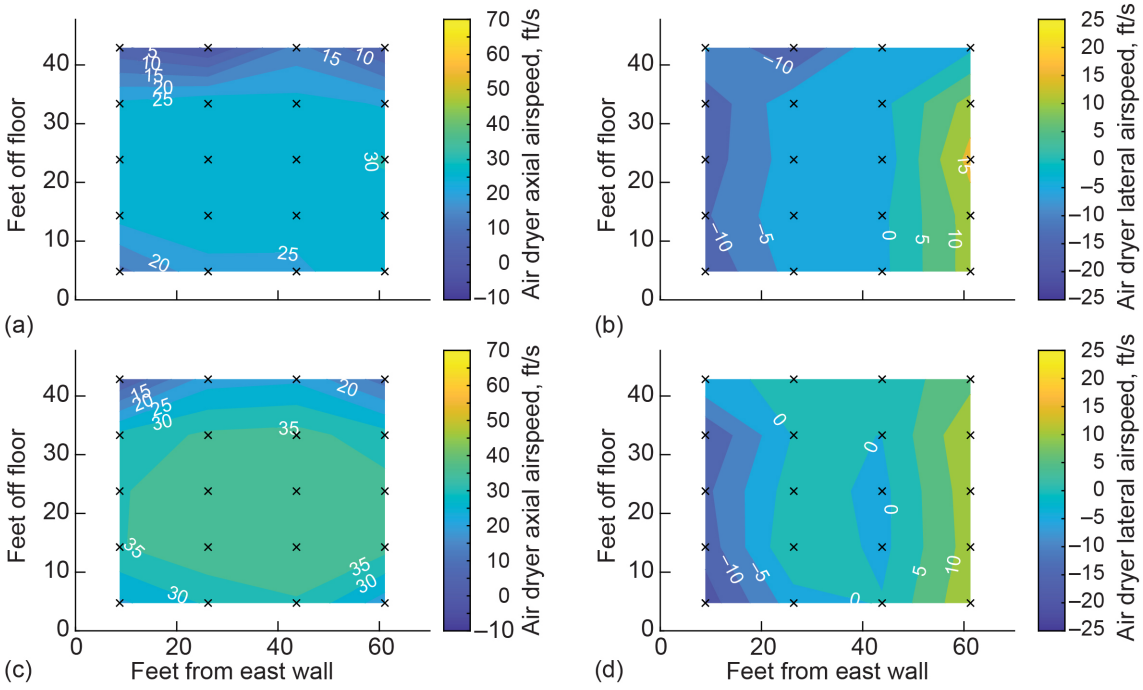

Figure A.4.—Axial and lateral velocity distributions in 8- by 6-Foot Supersonic Wind Tunnel air dryer bed inlet plane during 2018 validation and 2015 preconstruction flow quality survey test entries. Test section Mach number was set to Mach 1.3, nominally, in open-loop operation with air dryer beds enabled (referred to as “dry air”). View is upstream looking aft at dryer bed inlet. (a) 2018 test entry, axial. (b) 2018 test entry, lateral. (c) 2015 test entry, axial. (d) 2015 test entry, lateral.

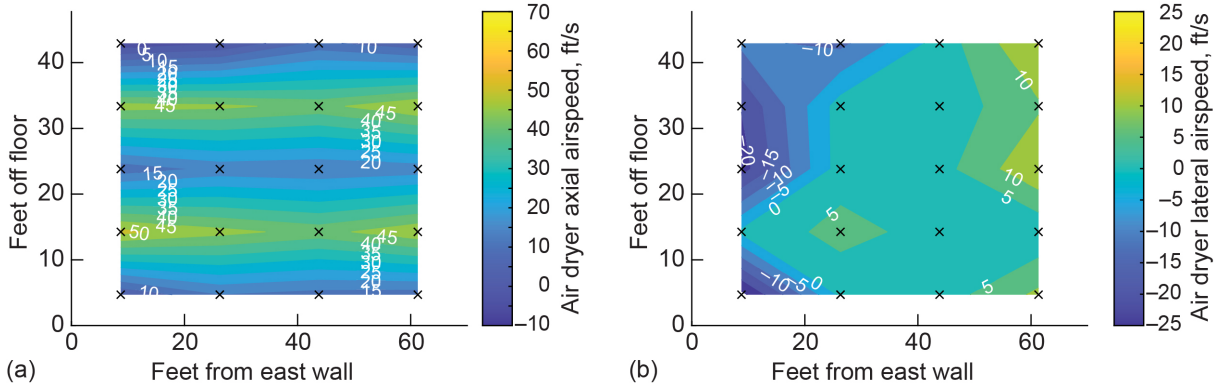

Figure A.5.—Axial and lateral velocity distributions in 8- by 6-Foot Supersonic Wind Tunnel air dryer bed inlet plane during 2018 validation test entry. Test section Mach number was set to Mach 1.3, nominally, in closed-loop operation with air dryer beds disabled (referred to as “wet air”). View is upstream looking aft at dryer bed inlet. (a) Axial. (b) Lateral.

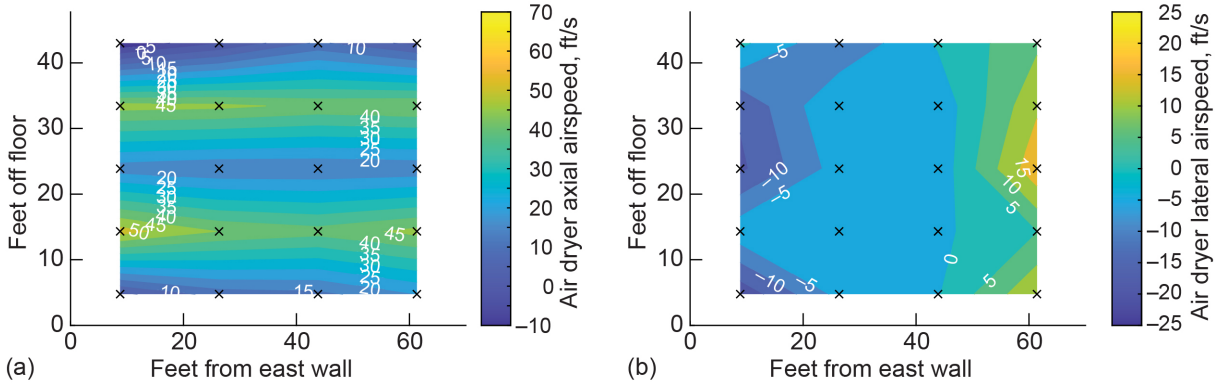

Figure A.6.—Axial and lateral velocity distributions in 8- by 6-Foot Supersonic Wind Tunnel air dryer bed inlet plane during 2018 validation test entry. Test section Mach number was set to Mach 1.3, nominally, in open-loop operation with air dryer beds disabled (referred to as “wet air”). View is upstream looking aft at dryer bed inlet. (a) Axial. (b) Lateral.

Additionally, Table A.2 displays corner 1 delta pressure measurements (relative to atmospheric pressure) from the 2015 and 2018 test entries, including data recorded at Mach 2.0. This indicates that a successful flow survey was conducted with the flexible nozzle walls set to Mach 2.0 with the 16-inch-diameter cone cylinder installed in the 8×6 SWT test section. For additional evidence of Mach 2.0 operation following the acoustic improvement modifications project, Figure A.7 shows Mach number profiles along the 16-inch cone-cylinder model recorded at nominal Mach 2.0 during the 2018 test entry. The test section calibration relationships developed during the 1996 and 1997 test section calibration (Ref. 3) were used to compute the test section total pressure used in the model surface Mach number calculations.

In summary, the three flow quality and operational objectives shown at the beginning of this discussion were met according to the results of the 2018 test entry. Additional contour plots of the flow field at the air dryer bed inlet plane can be produced upon request by the NASA Glenn wind tunnel characterization team.

TABLE A.2.—COMPARISON OF TUNNEL LOOP CORNER 1 DELTA PRESSURE DURING 8- BY 6-FOOT SUPERSONIC WIND TUNNEL TEST SECTION CONDITIONS SURVEYED DURING 2015 (PRECONSTRUCTION) AND 2018 (POSTCONSTRUCTION) TEST ENTRIES

No. of drive motors	Nominal Mach no.	$\Delta P_{S,C1,\,psf}$			
		Open loop		Closed loop	
		Pre	Post	Pre	Post
Three	2.00	-----	16.6	54.6	43.7
	1.90	-----	16.6	57.2	52.0
	1.80	-----	16.6	62.9	52.5
	1.70	-----	16.6	66.0	54.6
	1.60	10.9	17.2	68.6	56.2
	1.50	10.9	17.2	69.1	55.7
	1.40	10.9	17.2	68.6	56.7
	1.30[a]	10.9	17.2	70.2	57.2
	1.20	10.9	17.2	-----	57.2
	Dry air at or above Mach 1.2				
	1.10	10.9	17.7	-----	57.7
	.95	-----	18.2	-----	58.3
	.90	10.9	18.7	-----	58.3
	.85	-----	18.7	-----	57.7
	.80	10.9	18.2	-----	56.7
	.75	-----	18.2	-----	55.1
	.70	10.9	17.2	-----	51.5
	.65	-----	16.6	-----	47.9
	.60	7.8	15.6	-----	42.7
	.55	-----	13.5	-----	40.1
	.50	7.8	10.9	-----	35.9
	.45	-----	9.4	-----	33.3
	.40	5.2	7.8	-----	30.7
One	.50	5.2	8.3	-----	29.1
	.40	5.2	6.8	-----	26.5
	.30	2.6	5.7	-----	15.1
	.25	2.6	4.7	-----	12.0

[a]Mach 1.3 closed loop: during preconstruction testing, facility doors 4 and 5 were partially open during test condition (modified closed loop).

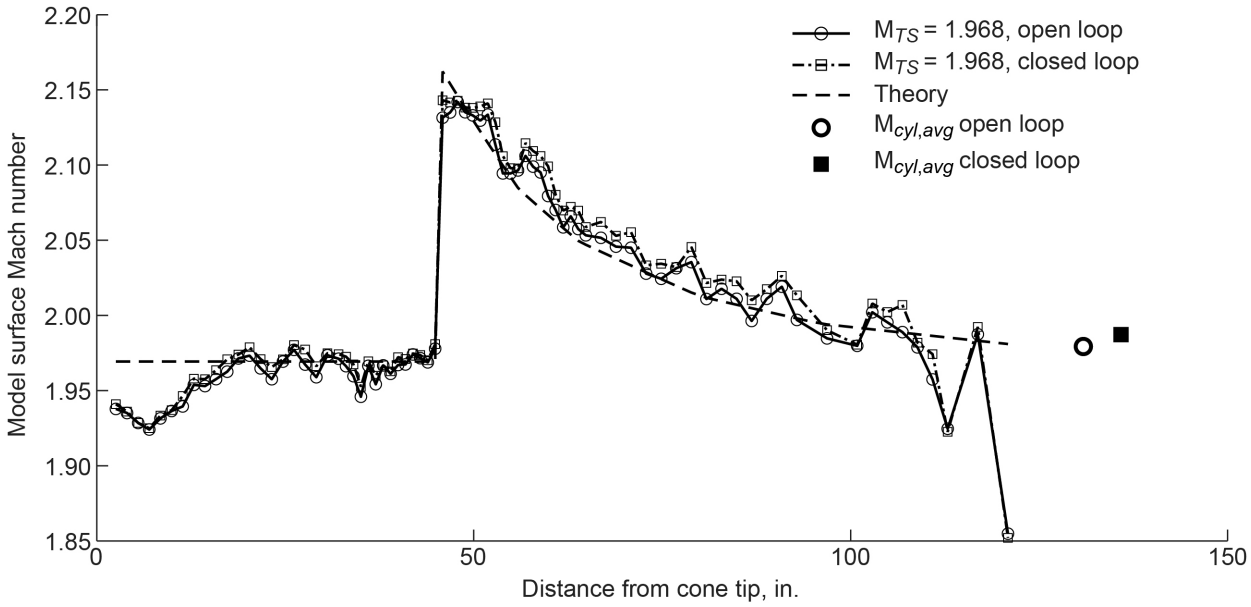

Figure A.7.—Mach number profile on the 16-inch-diameter cone cylinder at nominal Mach 2.0 during 2018 validation test entry in 8- by 6-Foot Supersonic Wind Tunnel. Test section configured to porosity configuration 6 (14-ft test section with schlieren windows).

Appendix B.—9- by 15-Foot Low-Speed Wind Tunnel Acoustic Improvement Modifications Photographs

Several of the large-scale tunnel loop modifications made during the 9- by 15-Foot Low-Speed Wind Tunnel (9×15 LSWT) acoustic improvement modifications project are described in this appendix. The following structural modifications were made as part of this facility improvement effort:

1. Installation of an acoustic fairing on the trailing edge of the central muffler column to limit flow separation exiting the 8- by 6-Foot Supersonic Wind Tunnel muffler. The ladder at the exit of the muffler was removed.
2. Installation of acoustically treated vertical turning vanes in corner 2 (upstream of the 9×15 LSWT; Figure B.1). There are eight vertical turning vanes, an inboard acoustic wall, an outboard acoustic panel, and a mesh screen (0.023-in.-diam. wire and 14 wires per inch) across the inlet plane of the corner 2 turning vanes.
3. Installation of acoustically treated serpentine baffles downstream of the facility cooler and upstream of the 9×15 LSWT honeycomb (14 total baffles; Figure B.2).
4. Installation of fairing plates to smoothly transition the flow into the 9×15 LSWT honeycomb. The fairings extend approximately 1 ft, 2.5 in. from the tunnel walls, floor, and ceiling, and extend approximately 7 ft, 2.375 in. upstream of the face of the 9×15 LSWT honeycomb and have an ogive cross section in the streamwise direction.
5. Modifications to the completely reconstructed 9×15 LSWT test section (Figure B.3):
   a. Transition piece at the test section inlet installed to transition flow from the bellmouth or contraction into the acoustically treated test section. Profile of the transition piece has a radius of 26.292 in. with a streamwise length of 11.25 in. The previous transition had been a flat ramp.
   b. Test section length extended from 28.6 to 33.66 ft.[17] Height, width, and divergence of the test section maintained.[18]
   c. Test section has solid walls (no slots).
   d. A constant thickness of 13 in. of acoustic treatment exists within the 140 acoustic boxes throughout the length of the test section. There are nine streamwise rings of boxes, with five on the floor and ceiling and three on the walls within a ring. There are four boxes used for lighting and cameras for a total of 144 boxes. The face sheets of the acoustic boxes are diffusion bonded panels. Acoustic boxes are typically 48 in. long by 36 in. wide on the tunnel floor and ceiling and typically 48 in. long by 34.66 in. wide on the walls. The first (upstream-most) and ninth (downstream-most) streamwise ring of acoustic boxes are 40 in. and 19.38 in. long, respectively.
6. Modifications to the reconstructed 9×15 LSWT diffuser (Figure B.4):
   a. The diffuser has two stages:
      (1) The “upstream diffuser” has a wall diffusion angle of 2.26° and ceiling and floor diffusion angle of 3.37° over the first 63 ft downstream of the test section. This section’s first 9 ft have a linearly varying thickness of acoustic treatment in the streamwise direction, reaching 8 in.

[17]Test section length defined by test section station (TSTA) 0.0 to end of test section (end of test section defined as the end of the constant height (8 ft, 8 in.) region in the tunnel); TSTA 0.0 is 4 in. upstream of the centerline of I-beam 3 in drawing CD–15763.

[18] Entrance of the test section is still 8 ft, 8 in. by 14 ft, 8 in. and the 0.25° wall divergence of the test section walls was maintained. The point at which the test section is 8 ft, 8 in. by 14 ft, 8 in. is nominally at TSTA 12.0. The outlet of the test section has a width of nominally 14 ft, 10.75 in.

in thickness and then maintaining a constant 8-in. thickness through the remainder of the 63-ft length. Corner fillets in the upstream diffuser begin 10 ft downstream of the end of the test section and end at the hinge station for the acoustically treated double doors (facility doors 6 and 7), which are at the end of the upstream diffuser.

(2) The “downstream diffuser” is a rectangular duct with a constant width of 20 ft, 10 in. and a varying vertical height of 15 ft, 7.5 in. at the upstream end and 18 ft, 11.5 in. at the downstream end. The square duct drops in elevation to meet the corner 3 floor with the duct floor descending at an angle of 3.05° and the duct ceiling descending at a rate of 1.39° over approximately 112 ft.

7. Installation of an acoustically treated turning vane structure in corner 3 (downstream of the 9×15 LSWT diffuser; Figure B.5 and Figure B.6). Because the air dryer bed inlet is approximately 4 times larger than the exit area of the corner 3 turning vane structure, varied turning vane geometries were used to uniformly distribute the flow entering the air dryer inlet. There are seven vertical turning vanes that turn the flow through the corner and have varying exit angles to distribute the flow horizontally from the turning vane exit plane. An additional seven horizontal turning vanes, nominally 10 ft long, are located within the last 15 ft of the vertical turning vanes. The horizontal turning vanes also have varying angles from horizontal to distribute the flow vertically from the turning vane exit plane. All turning vanes have acoustically treated surfaces. An acoustically treated outboard wall, inboard wall, and ceiling form the perimeter surfaces of the flow path of the corner 3 turning vane structure, along with the concrete floor. The width of the corner 3 turning vane structure expands from 20 ft, 10 in. at the inlet to 26 ft, 0.5 in. at the exit. The ceiling panels are level relative to horizontal, and the existing concrete tunnel floor elevation varies only slightly through the turn.

Figure B.1.—Corner 2 turning vanes exit, looking upstream, installed during 9- by 15-Foot Low-Speed Wind Tunnel acoustic improvement modifications project.

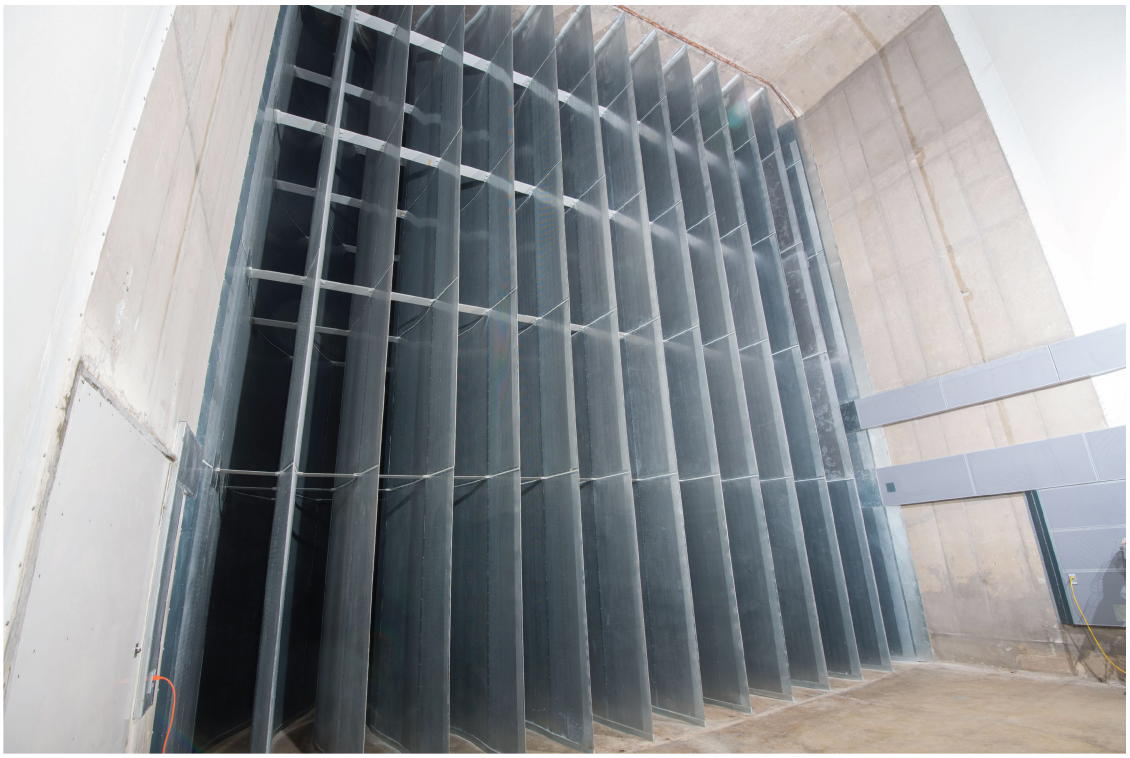

Figure B.2.—Serpentine baffles (downstream of tunnel cooler, upstream of 9- by 15-Foot Low-Speed Wind Tunnel (9×15 LSWT) honeycomb) installed during 9×15 LSWT acoustic improvement modifications project.

Figure B.3.—Test section of 9- by 15-Foot Low-Speed Wind Tunnel (9×15 LSWT), looking upstream, installed during 9×15 LSWT acoustic improvement modifications project.

Figure B.4.—Diffuser section of the 9- by 15-Foot Low-Speed Wind Tunnel (9×15 LSWT), upstream looking aft, installed during 9×15 LSWT acoustic improvement modifications project.

Figure B.5.—Corner 3 turning vanes entrance, upstream looking aft from diffuser, installed during 9- by 15-Foot Low-Speed Wind Tunnel acoustic improvement modifications project.

Figure B.6.—Corner 3 turning vanes exit, looking upstream, installed during 9- by 15-Foot Low-Speed Wind Tunnel acoustic improvement modifications project.

Appendix C.—Flow Angularity in 8- by 6-Foot Supersonic Wind Tunnel Transonic Test Section Configuration 1 (TSCFG 1)

Detailed flow angle plots are included in this appendix for both supersonic and subsonic operation of the 8- by 6-Foot Supersonic Wind Tunnel. The pitch and yaw flow angle distributions in this section are an alternative to the quiver plots presented in this report but contain the same information. See the flow angle subsection of transonic array results for further information. Figure C.1 to Figure C.29 contain the corrected pitch and yaw flow angles measured by the transonic array at the 14-ft test section measurement plane. Note that positive pitch flow angle is air moving from floor to ceiling and positive yaw is air moving from left to right when upstream looking aft in the test section.

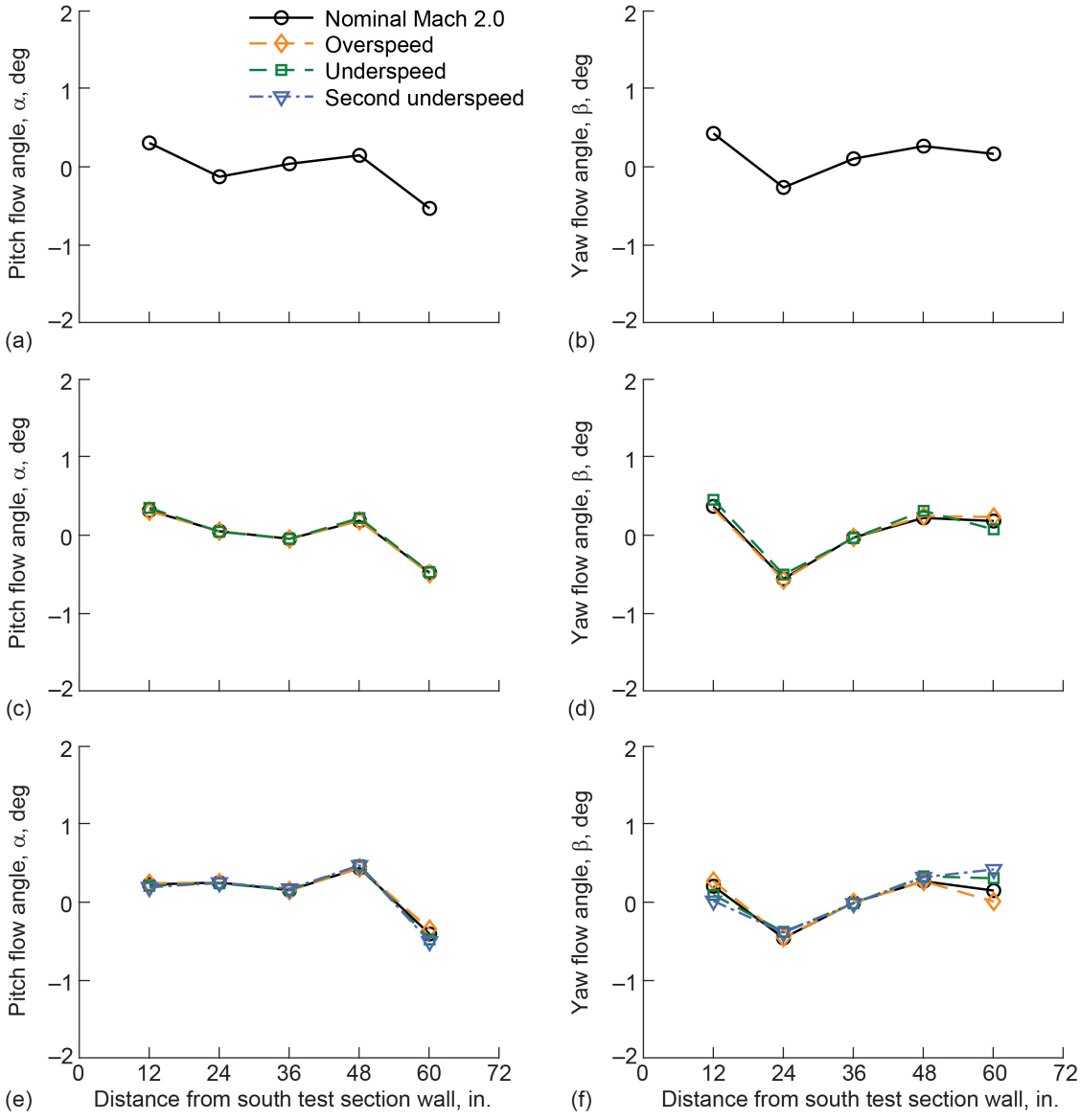

Figure C.1.—Pitch and yaw flow angle profiles in the 8- by 6-ft test section at 14-ft test section measurement plane at centerline (CL) and 1 ft above and below CL. Positive pitch flow angle, α, is from floor to ceiling and positive yaw flow angle, β, is from left to right when upstream looking aft. Data acquired during 2019 test section characterization entry at flexwall setting of Mach 2.0. (a) Pitch at CL + 1 ft. (b) Yaw at CL + 1 ft. (c) Pitch at CL. (d) Yaw at CL. (e) Pitch at CL – 1 ft. (f) Yaw at CL – 1 ft.

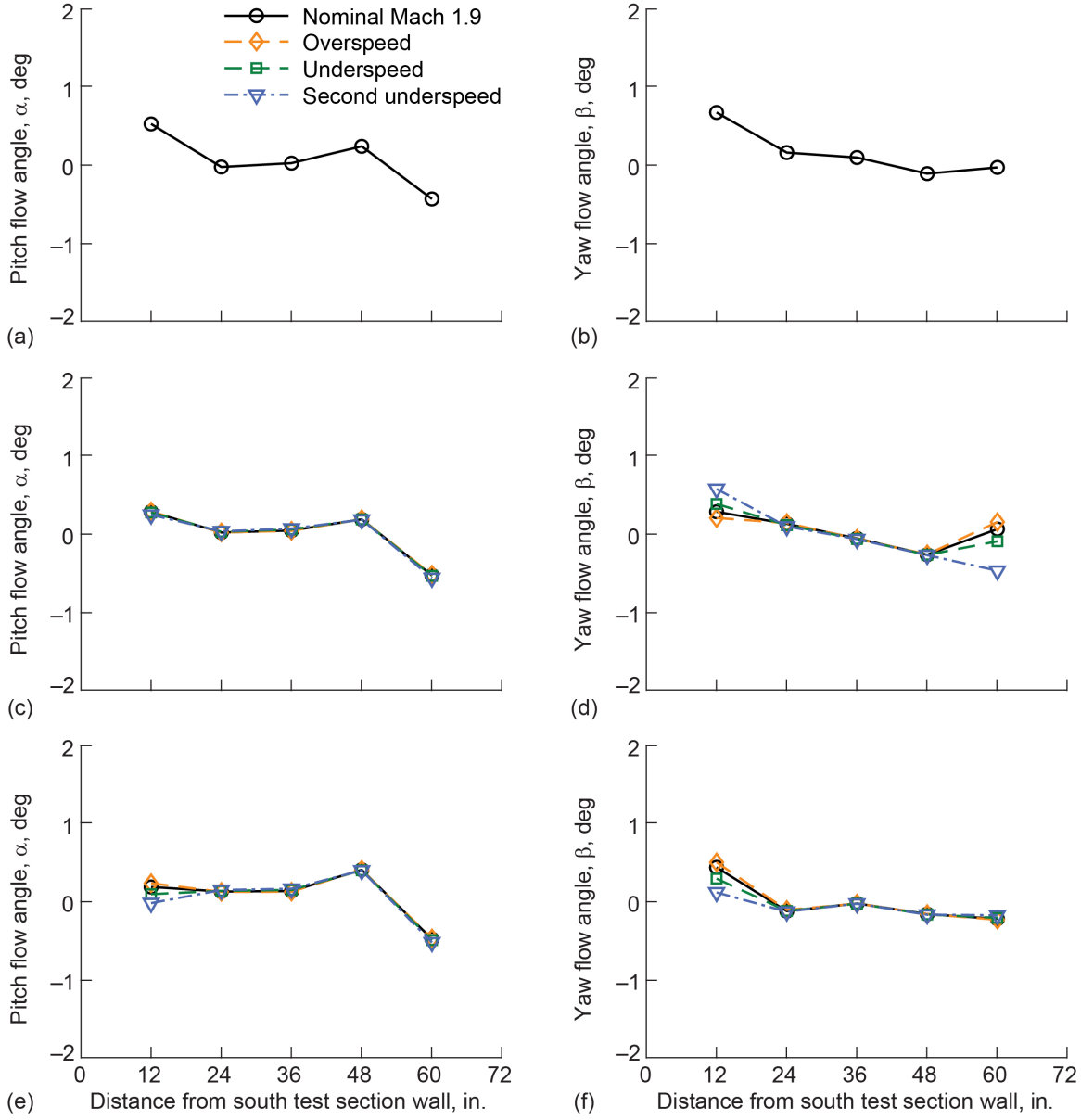

Figure C.2.—Pitch and yaw flow angle profiles in 8- by 6-ft test section at 14-ft test section measurement plane at centerline (CL) and 1 ft above and below CL. Positive pitch flow angle, α, is from floor to ceiling and positive yaw flow angle, β, is from left to right when upstream looking aft. Data acquired during 2019 test section characterization entry at flexwall setting of Mach 1.9. (a) Pitch at CL + 1 ft. (b) Yaw at CL + 1 ft. (c) Pitch at CL. (d) Yaw at CL. (e) Pitch at CL – 1 ft. (f) Yaw at CL – 1 ft.

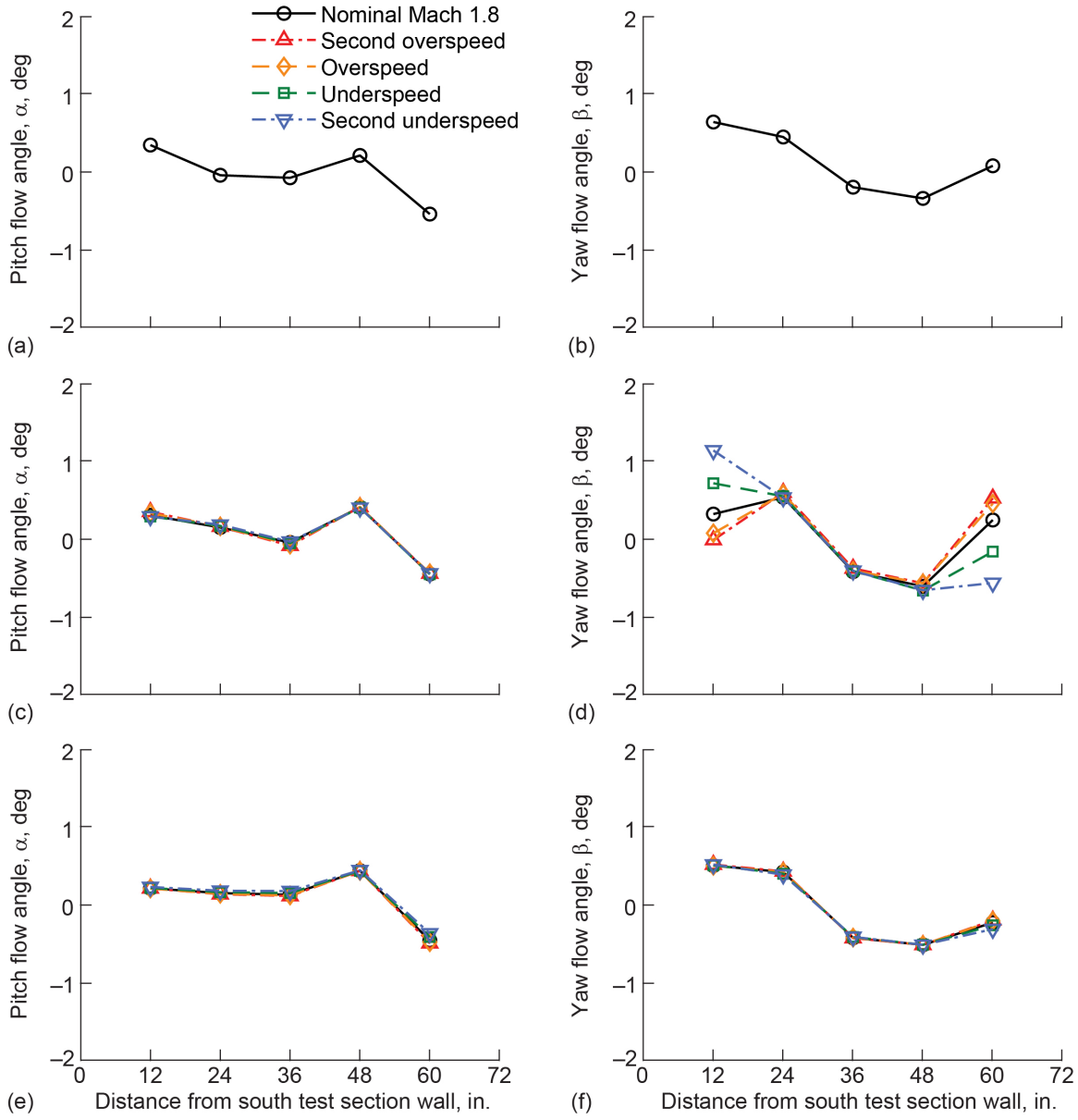

Figure C.3.—Pitch and yaw flow angle profiles in 8- by 6-ft test section at 14-ft test section measurement plane at centerline (CL) and 1 ft above and below CL. Positive pitch flow angle, α, is from floor to ceiling and positive yaw flow angle, β, is from left to right when upstream looking aft. Data acquired during 2019 test section characterization entry at flexwall setting of Mach 1.8. (a) Pitch at CL + 1 ft. (b) Yaw at CL + 1 ft. (c) Pitch at CL. (d) Yaw at CL. (e) Pitch at CL – 1 ft. (f) Yaw at CL – 1 ft.

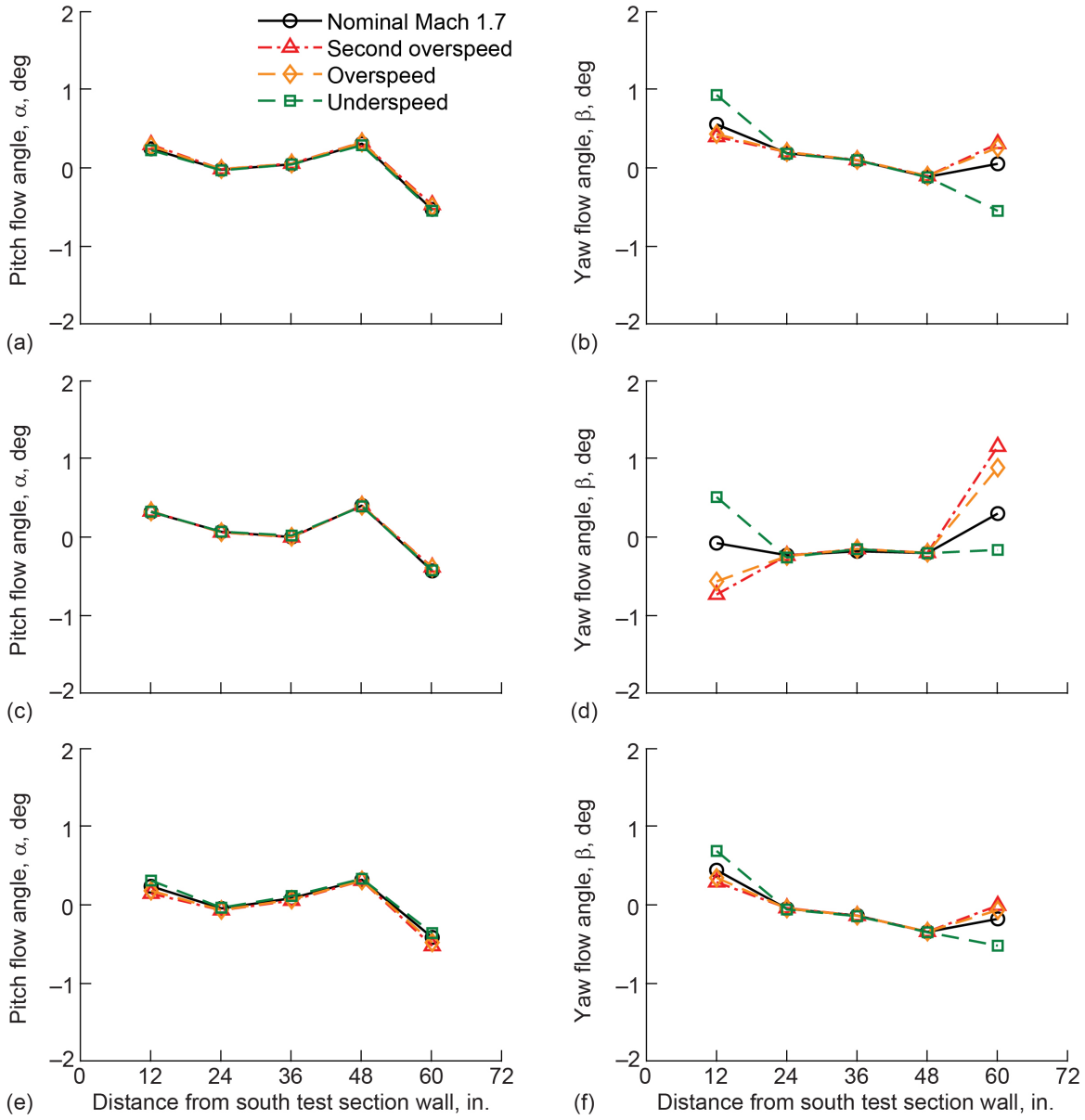

Figure C.4.—Pitch and yaw flow angle profiles in 8- by 6-ft test section at 14-ft test section measurement plane at centerline (CL) and 1 ft above and below CL. Positive pitch flow angle, α, is from floor to ceiling and positive yaw flow angle, β, is from left to right when upstream looking aft. Data acquired during 2019 test section characterization entry at flexwall setting of Mach 1.7. (a) Pitch at CL + 1 ft. (b) Yaw at CL + 1 ft. (c) Pitch at CL. (d) Yaw at CL. (e) Pitch at CL – 1 ft. (f) Yaw at CL – 1 ft.

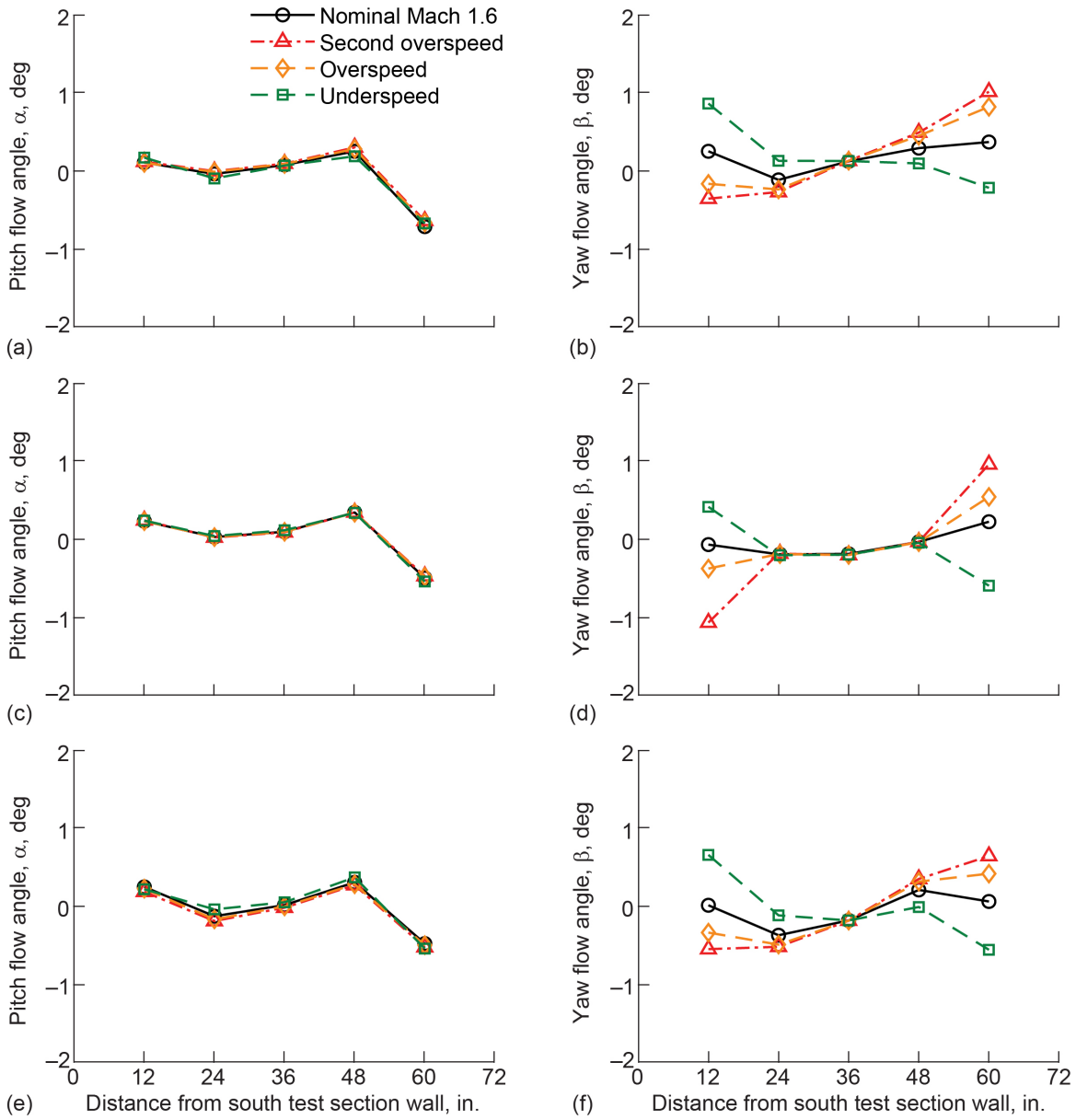

Figure C.5.—Pitch and yaw flow angle profiles in 8- by 6-ft test section at 14-ft test section measurement plane at centerline (CL) and 1 ft above and below CL. Positive pitch flow angle, α, is from floor to ceiling and positive yaw flow angle, β, is from left to right when upstream looking aft. Data acquired during 2019 test section characterization entry at flexwall setting of Mach 1.6. (a) Pitch at CL + 1 ft. (b) Yaw at CL + 1 ft. (c) Pitch at CL. (d) Yaw at CL. (e) Pitch at CL – 1 ft. (f) Yaw at CL – 1 ft.

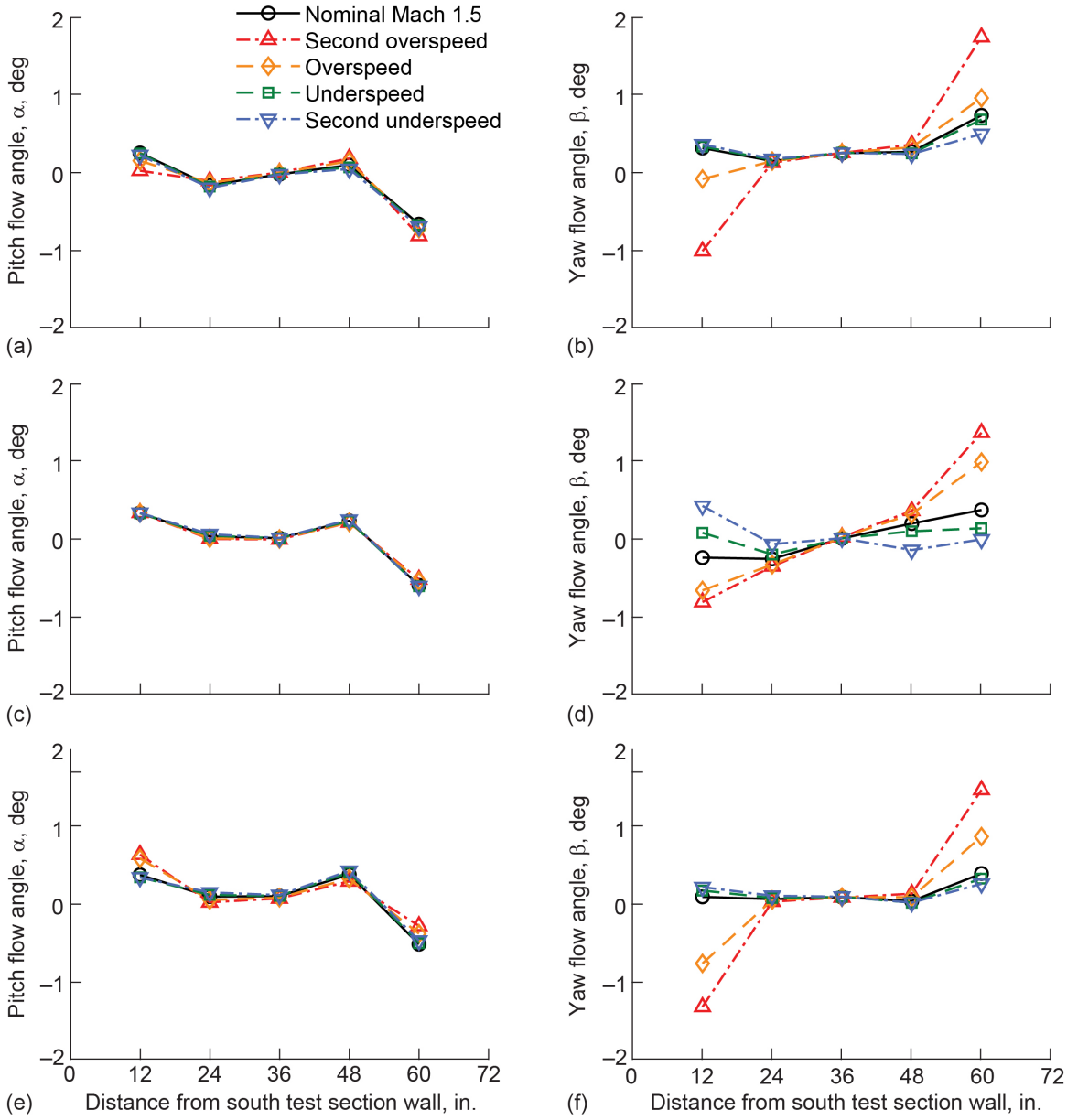

Figure C.6.—Pitch and yaw flow angle profiles in 8- by 6-ft test section at 14-ft test section measurement plane at centerline (CL) and 1 ft above and below CL. Positive pitch flow angle, α, is from floor to ceiling and positive yaw flow angle, β, is from left to right when upstream looking aft. Data acquired during 2019 test section characterization entry at flexwall setting of Mach 1.5. (a) Pitch at CL + 1 ft. (b) Yaw at CL + 1 ft. (c) Pitch at CL. (d) Yaw at CL. (e) Pitch at CL – 1 ft. (f) Yaw at CL – 1 ft.

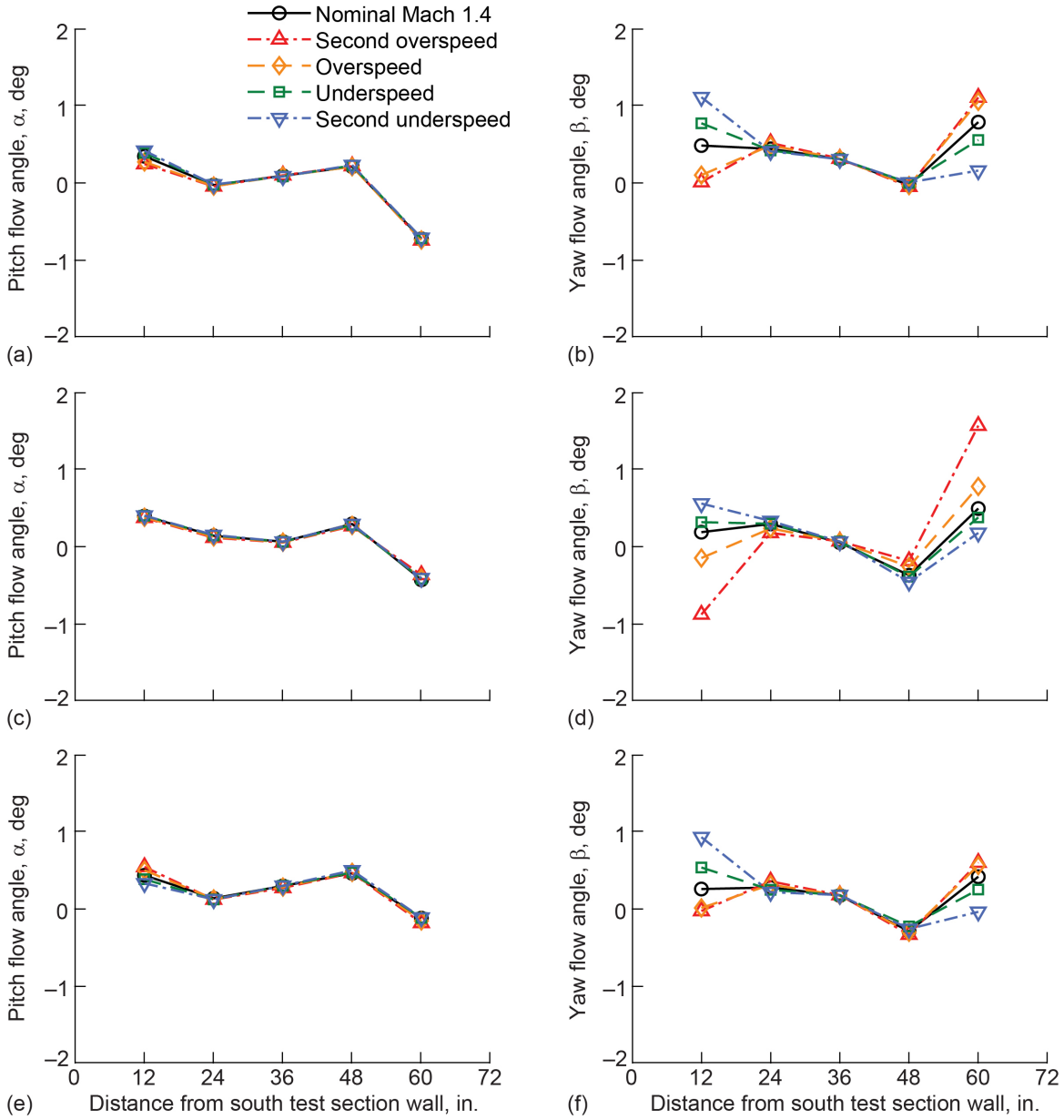

Figure C.7.—Pitch and yaw flow angle profiles in 8- by 6-ft test section at 14-ft test section measurement plane at centerline (CL) and 1 ft above and below CL. Positive pitch flow angle, α, is from floor to ceiling and positive yaw flow angle, β, is from left to right when upstream looking aft. Data acquired during 2019 test section characterization entry at flexwall setting of Mach 1.4. (a) Pitch at CL + 1 ft. (b) Yaw at CL + 1 ft. (c) Pitch at CL. (d) Yaw at CL. (e) Pitch at CL – 1 ft. (f) Yaw at CL – 1 ft.

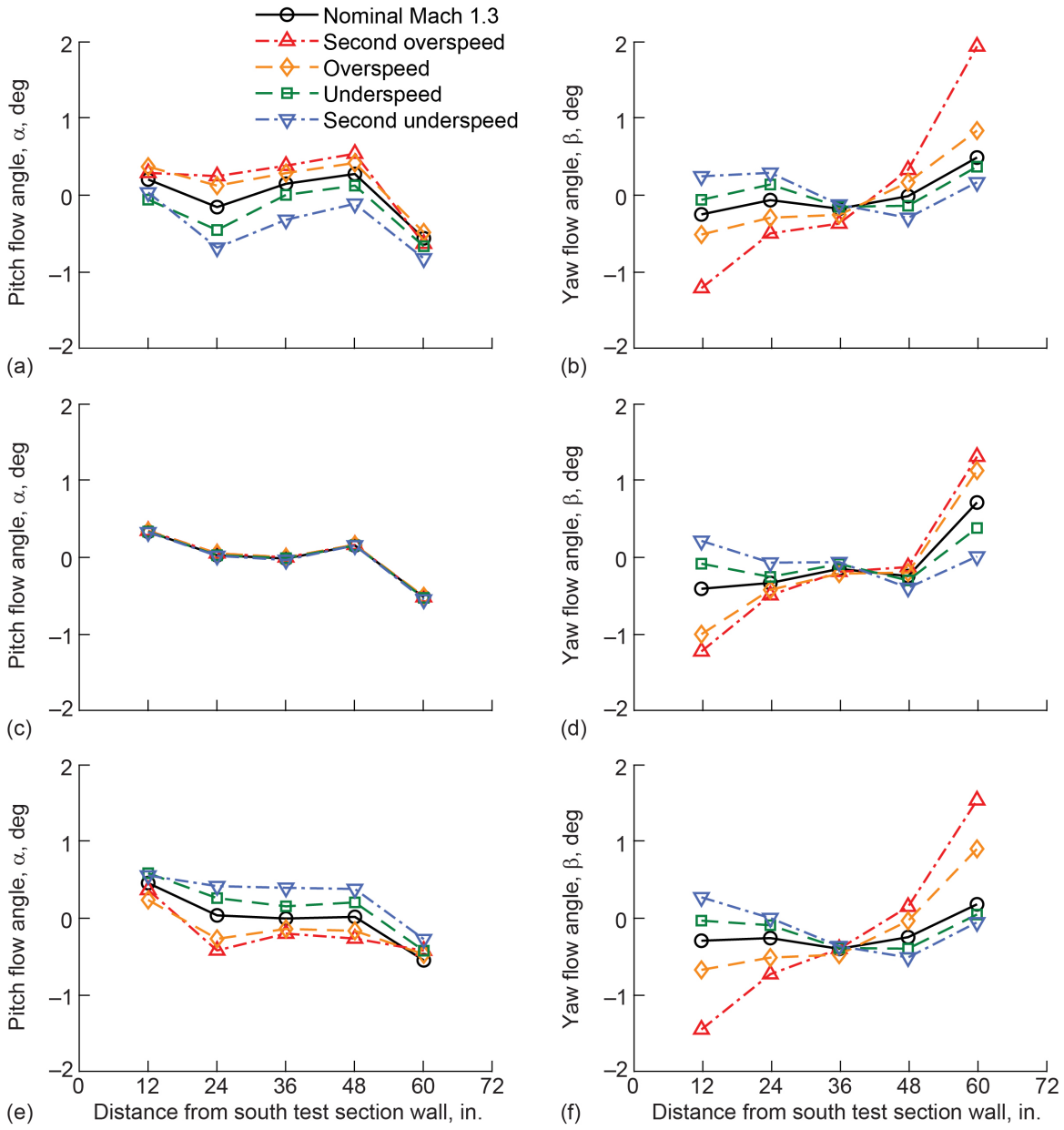

Figure C.8.—Pitch and yaw flow angle profiles in 8- by 6-ft test section at 14-ft test section measurement plane at centerline (CL) and 1 ft above and below CL. Positive pitch flow angle, α, is from floor to ceiling and positive yaw flow angle, β, is from left to right when upstream looking aft. Data acquired during 2019 test section characterization entry at flexwall setting of Mach 1.3. (a) Pich at CL + 1 ft. (b) Yaw at CL + 1 ft. (c) Pitch at CL. (d) Yaw at CL. (e) Pitch at CL – 1 ft. (f) Yaw at CL – 1 ft.

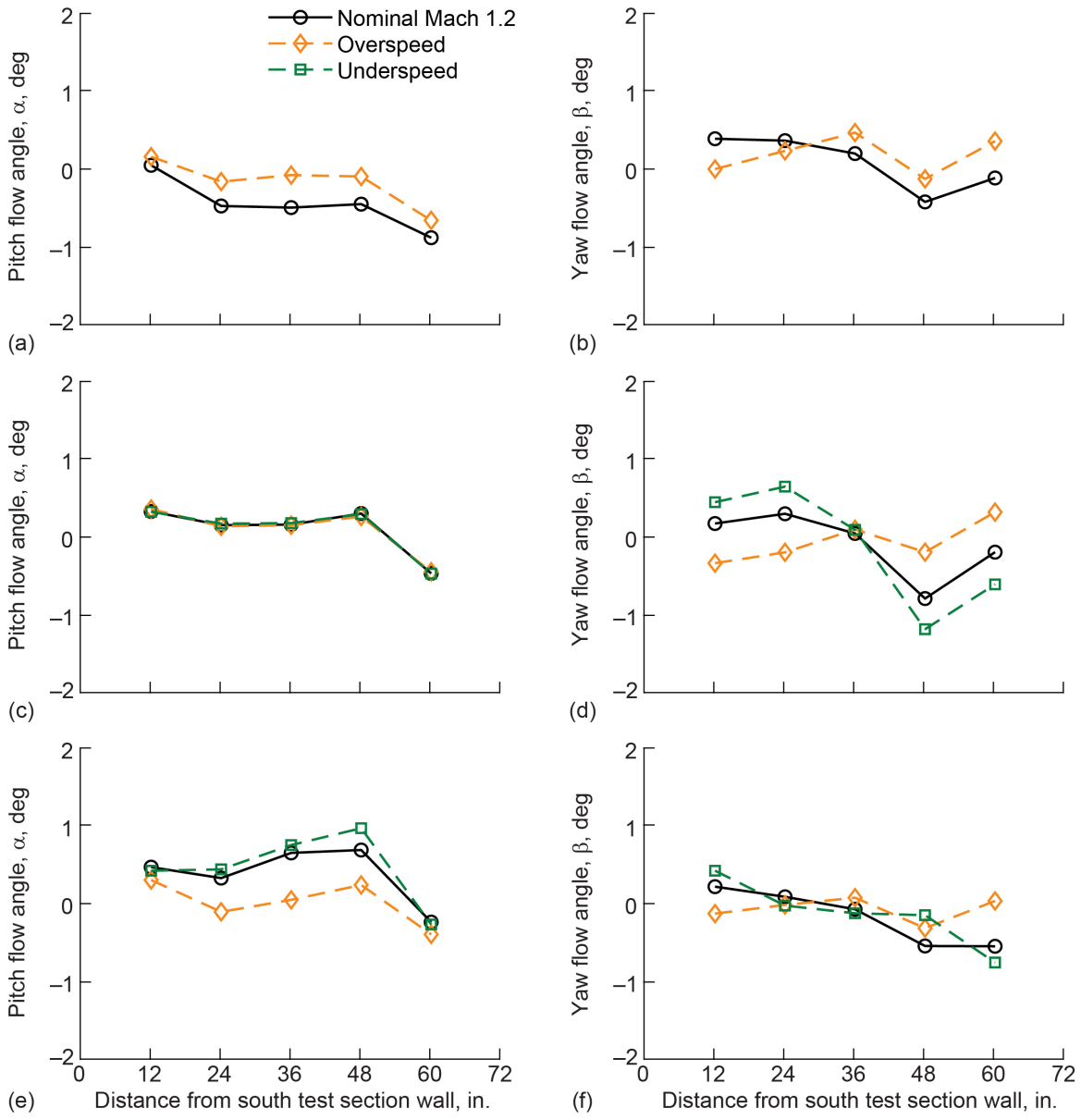

Figure C.9.—Pitch and yaw flow angle profiles in 8- by 6-ft test section at 14-ft test section measurement plane at centerline (CL) and 1 ft above and below CL. Positive pitch flow angle, α, is from floor to ceiling and positive yaw flow angle, β, is from left to right when upstream looking aft. Data acquired during 2019 test section characterization entry at flexwall setting of Mach 1.2. (a) Pitch at CL + 1 ft. (b) Yaw at CL + 1 ft. (c) Pitch at CL. (d) Yaw at CL. (e) Pitch at CL – 1 ft. (f) Yaw at CL – 1 ft.

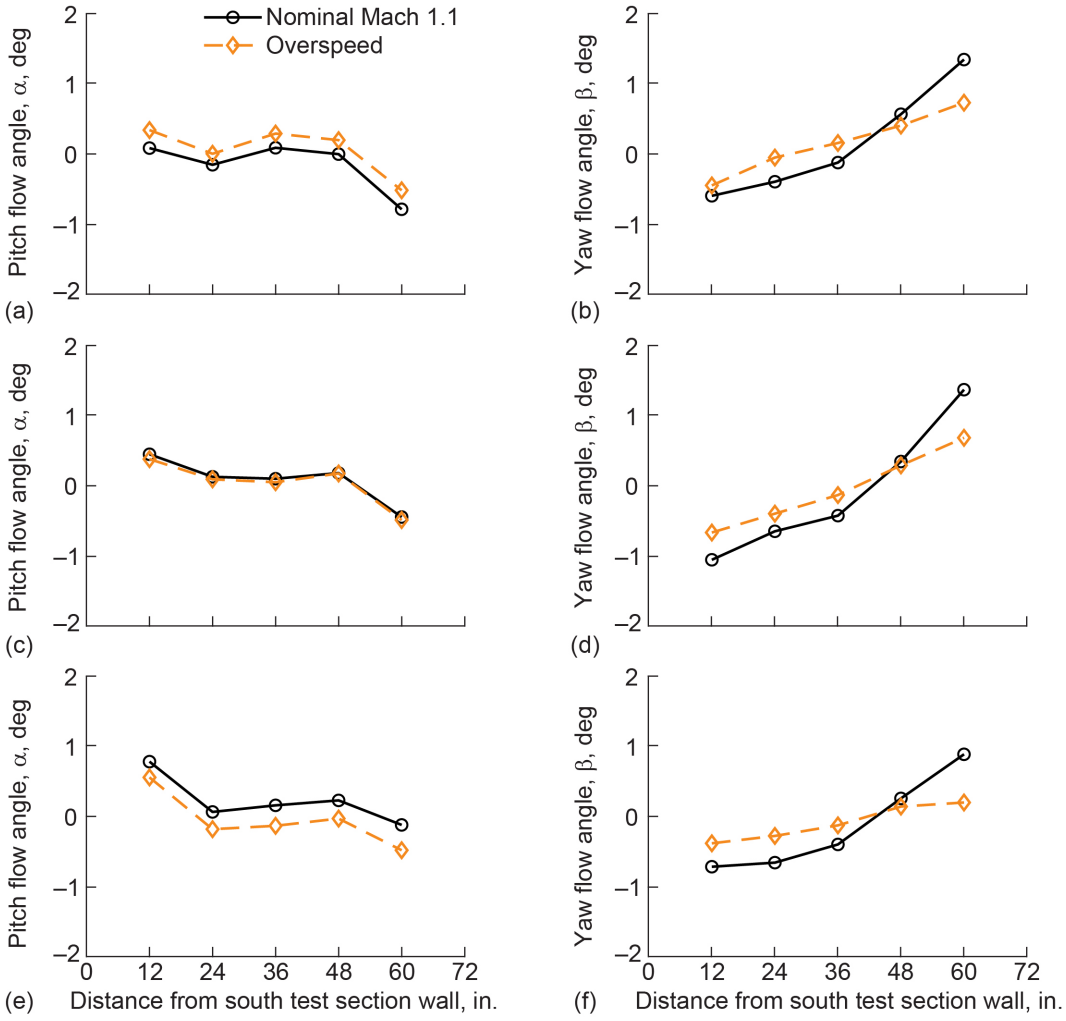

Figure C.10.—Pitch and yaw flow angle profiles in 8- by 6-ft test section at 14-ft test section measurement plane at centerline (CL) and 1 ft above and below CL. Positive pitch flow angle, α, is from floor to ceiling and positive yaw flow angle, β, is from left to right when upstream looking aft. Data acquired during 2019 test section characterization entry at flexwall setting of Mach 1.1. (a) Pitch at CL + 1 ft. (b) Yaw at CL + 1 ft. (c) Pitch at CL. (d) Yaw at CL. (e) Pitch at CL – 1 ft. (f) Yaw at CL – 1 ft.

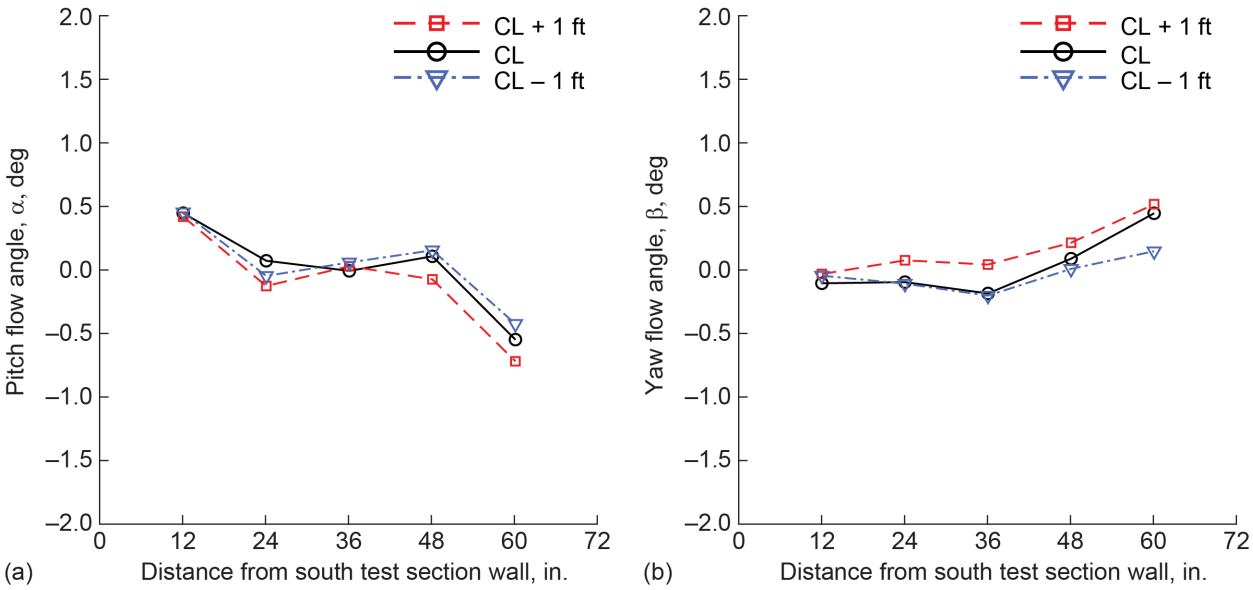

Figure C.11.—Pitch and yaw flow angle profiles in 8- by 6-ft test section at 14-ft test section measurement plane at centerline (CL) and 1 ft above and below CL. Positive pitch flow angle, α, is from floor to ceiling and positive yaw flow angle, β, is from left to right when upstream looking aft. Data acquired during 2019 test section characterization entry at Mach 0.951 (three-drive-motor operation). (a) Pitch. (b) Yaw.

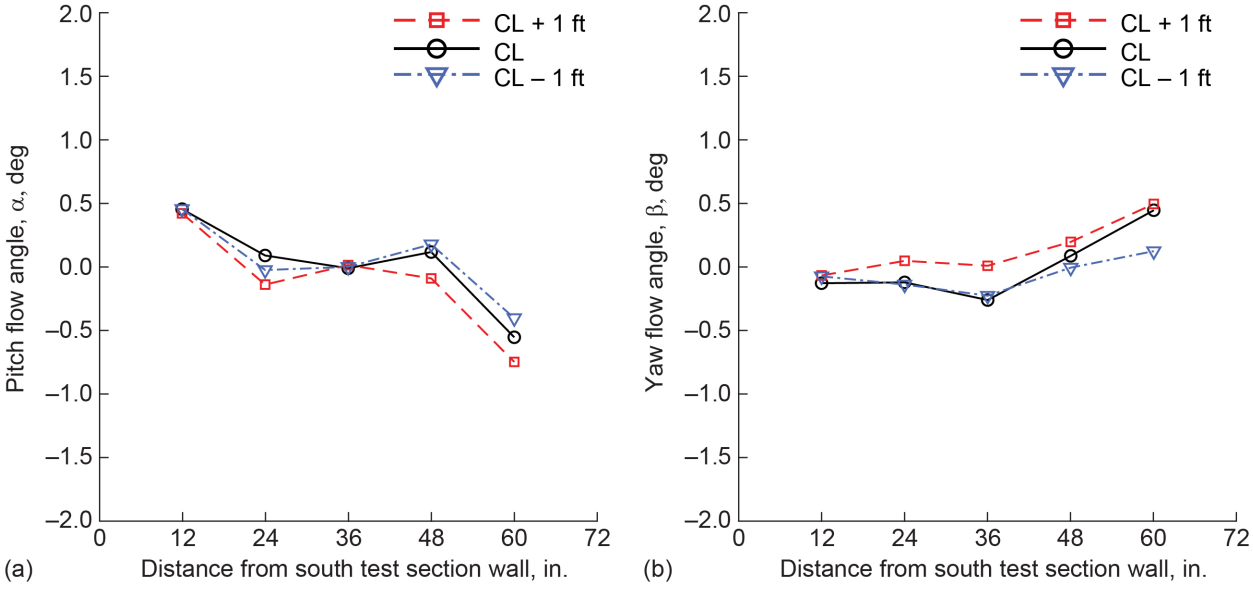

Figure C.12.—Pitch and yaw flow angle profiles in 8- by 6-ft test section at 14-ft test section measurement plane at centerline (CL) and 1 ft above and below CL. Positive pitch flow angle, α, is from floor to ceiling and positive yaw flow angle, β, is from left to right when upstream looking aft. Data acquired during 2019 test section characterization entry at Mach 0.900 (three-drive-motor operation). (a) Pitch. (b) Yaw.

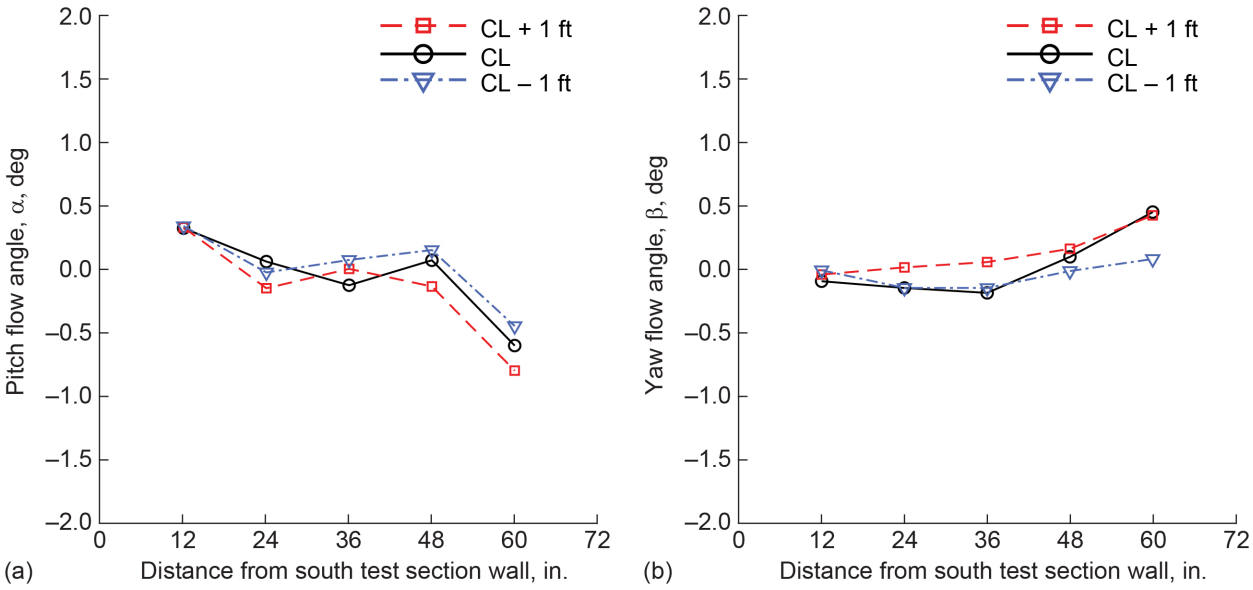

Figure C.13.—Pitch and yaw flow angle profiles in 8- by 6-ft test section at 14-ft test section measurement plane at centerline (CL) and 1 ft above and below CL. Positive pitch flow angle, α, is from floor to ceiling and positive yaw flow angle, β, is from left to right when upstream looking aft. Data acquired during 2019 test section characterization entry at Mach 0.849 (three-drive-motor operation). (a) Pitch. (b) Yaw.

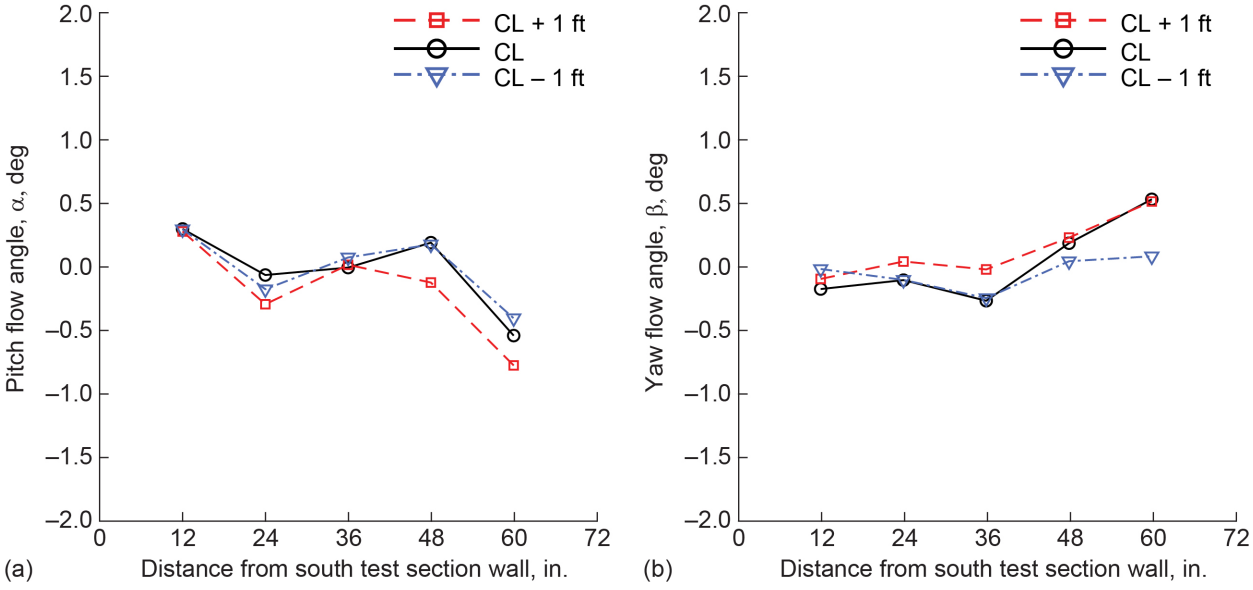

Figure C.14.—Pitch and yaw flow angle profiles in 8- by 6-ft test section at 14-ft test section measurement plane at centerline (CL) and 1 ft above and below CL. Positive pitch flow angle, α, is from floor to ceiling and positive yaw flow angle, β, is from left to right when upstream looking aft. Data acquired during 2019 test section characterization entry at Mach 0.800 (three-drive-motor operation). (a) Pitch. (b) Yaw.

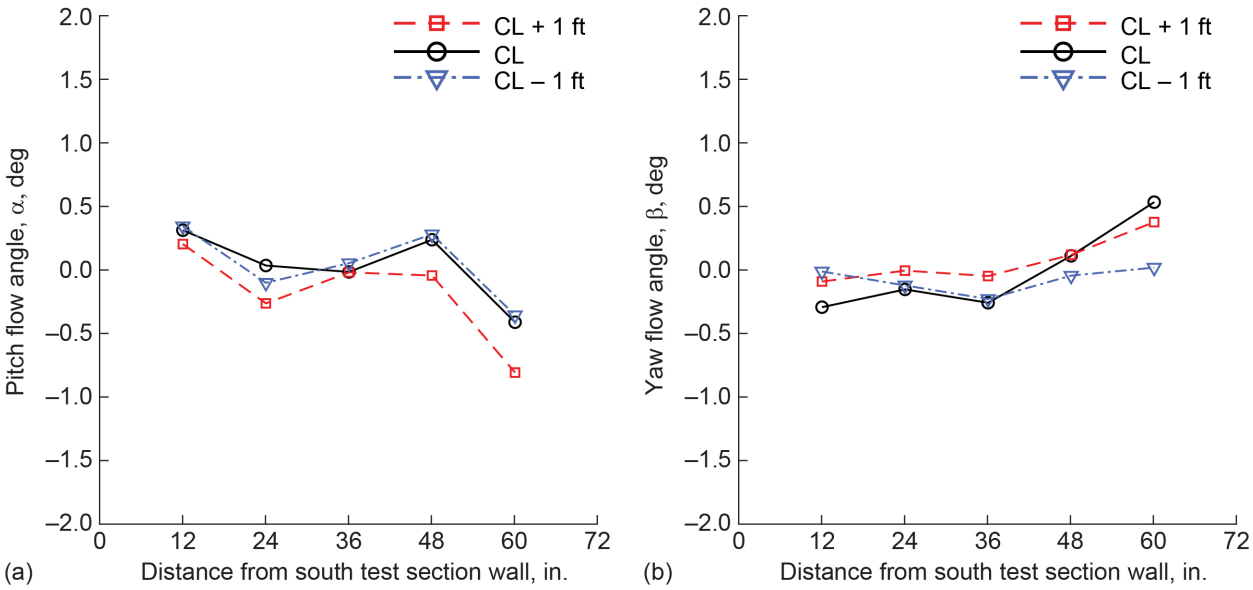

Figure C.15.—Pitch and yaw flow angle profiles in 8- by 6-ft test section at 14-ft test section measurement plane at centerline (CL) and 1 ft above and below CL. Positive pitch flow angle, α, is from floor to ceiling and positive yaw flow angle, β, is from left to right when upstream looking aft. Data acquired during 2019 test section characterization entry at Mach 0.750 (three-drive-motor operation). (a) Pitch. (b) Yaw.

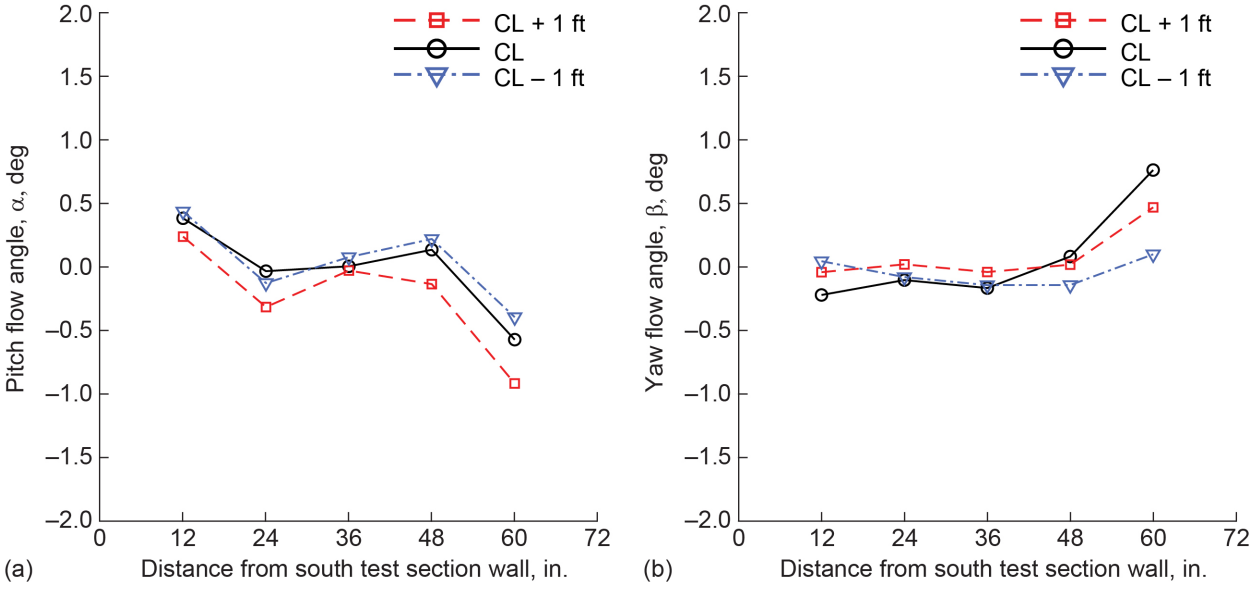

Figure C.16.—Pitch and yaw flow angle profiles in 8- by 6-ft test section at 14-ft test section measurement plane at centerline (CL) and 1 ft above and below CL. Positive pitch flow angle, α, is from floor to ceiling and positive yaw flow angle, β, is from left to right when upstream looking aft. Data acquired during 2019 test section characterization entry at Mach 0.701 (three-drive-motor operation). (a) Pitch. (b) Yaw.

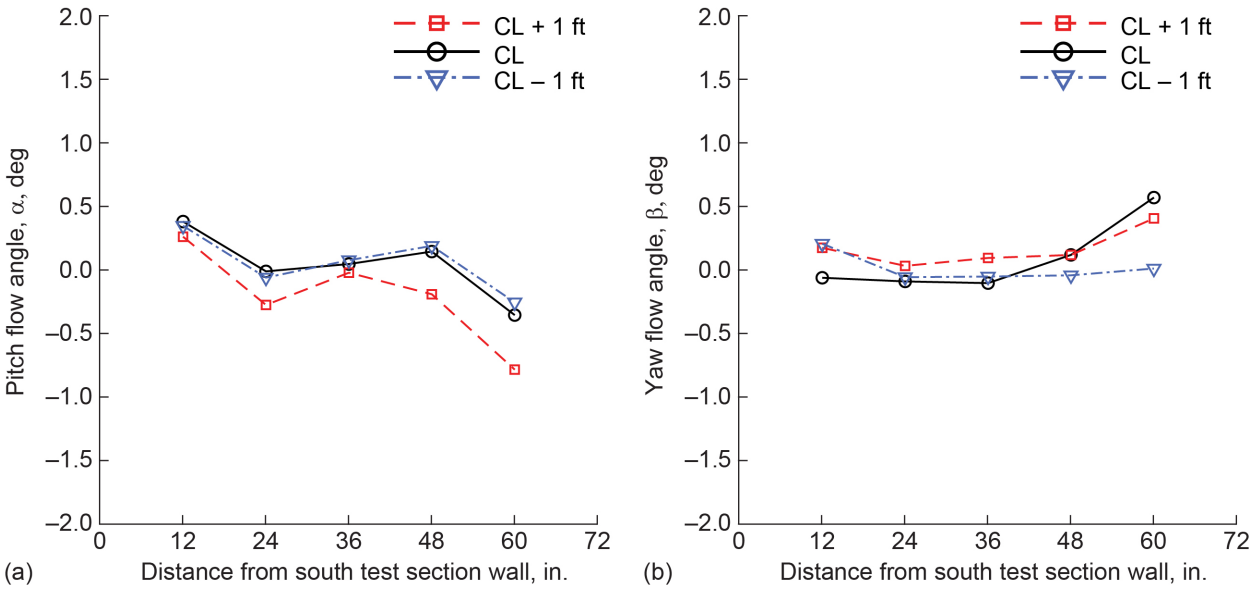

Figure C.17.—Pitch and yaw flow angle profiles in 8- by 6-ft test section at 14-ft test section measurement plane at centerline (CL) and 1 ft above and below CL. Positive pitch flow angle, α, is from floor to ceiling and positive yaw flow angle, β, is from left to right when upstream looking aft. Data acquired during 2019 test section characterization entry at Mach 0.649 (three-drive-motor operation). (a) Pitch. (b) Yaw.

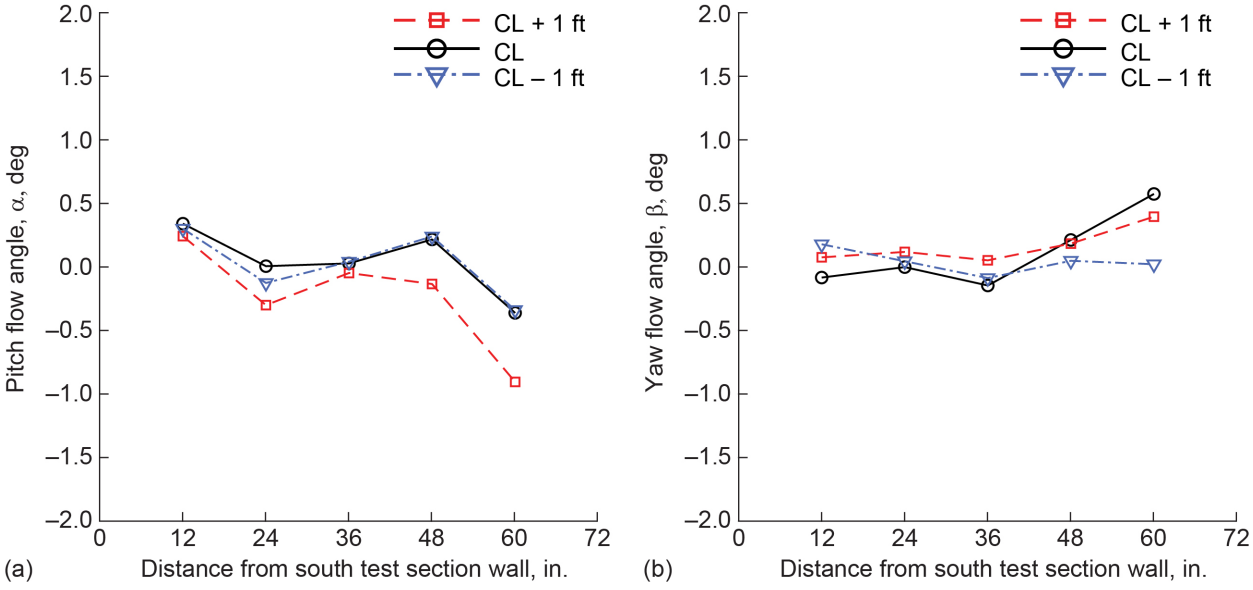

Figure C.18.—Pitch and yaw flow angle profiles in 8- by 6-ft test section at 14-ft test section measurement plane at centerline (CL) and 1 ft above and below CL. Positive pitch flow angle, α, is from floor to ceiling and positive yaw flow angle, β, is from left to right when upstream looking aft. Data acquired during 2019 test section characterization entry at Mach 0.600 (three-drive-motor operation). (a) Pitch. (b) Yaw.

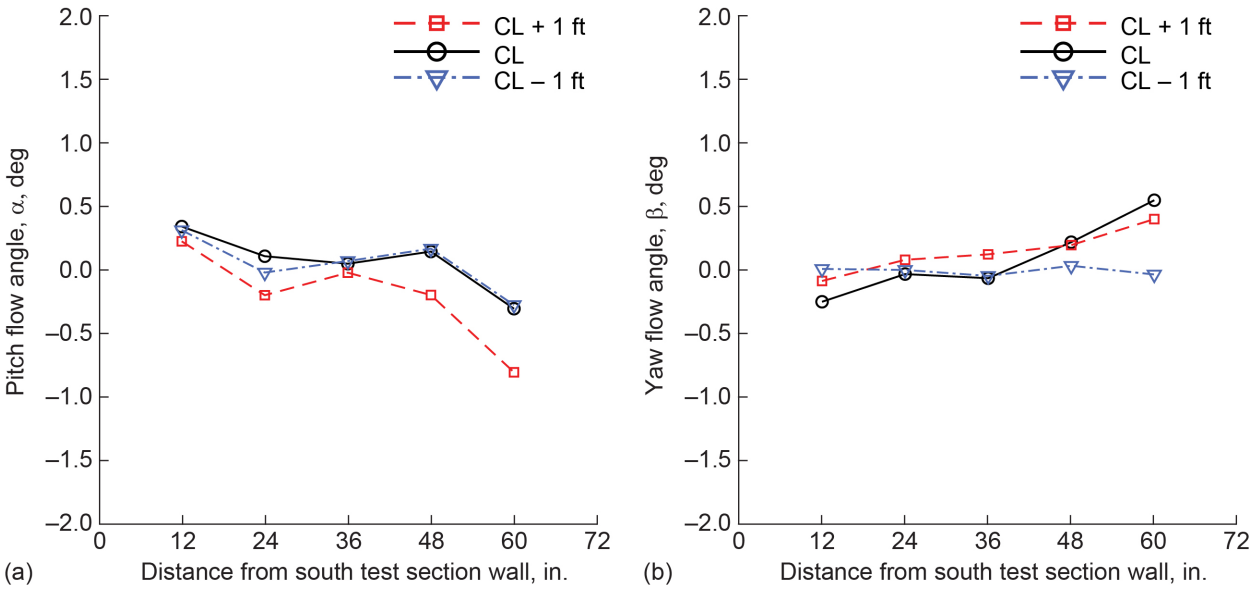

Figure C.19.—Pitch and yaw flow angle profiles in 8- by 6-ft test section at 14-ft test section measurement plane at centerline (CL) and 1 ft above and below CL. Positive pitch flow angle, α, is from floor to ceiling and positive yaw flow angle, β, is from left to right when upstream looking aft. Data acquired during 2019 test section characterization entry at Mach 0.551 (three-drive-motor operation). (a) Pitch. (b) Yaw.

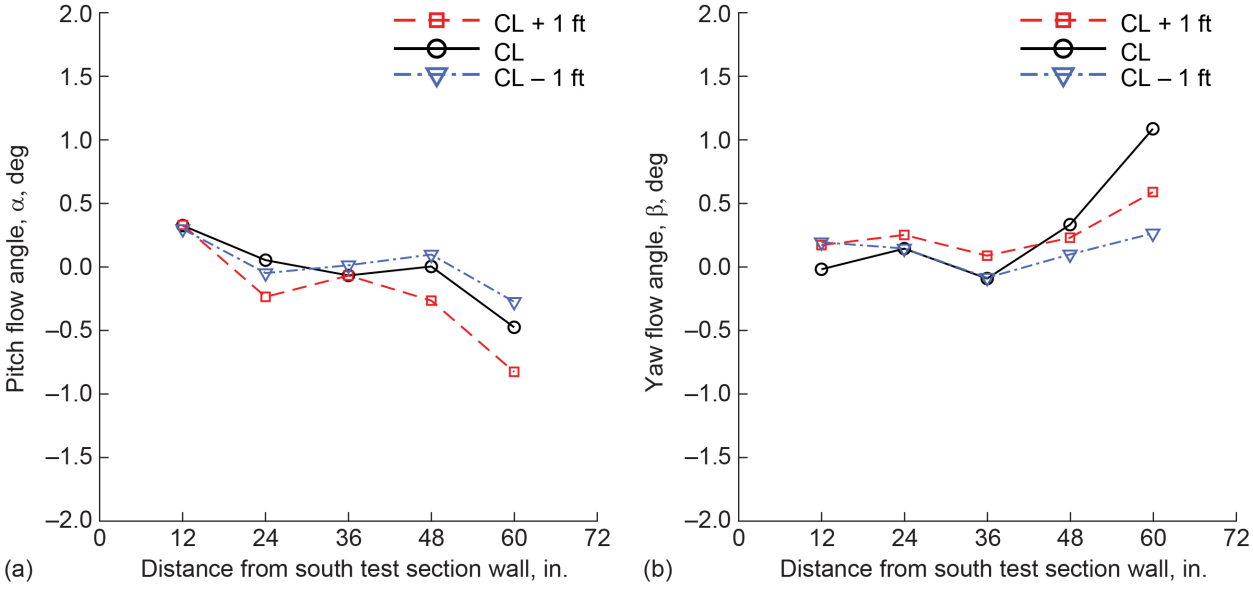

Figure C.20.—Pitch and yaw flow angle profiles in 8- by 6-ft test section at 14-ft test section measurement plane at centerline (CL) and 1 ft above and below CL. Positive pitch flow angle, α, is from floor to ceiling and positive yaw flow angle, β, is from left to right when upstream looking aft. Data acquired during 2019 test section characterization entry at Mach 0.500 (three-drive-motor operation). (a) Pitch. (b) Yaw.

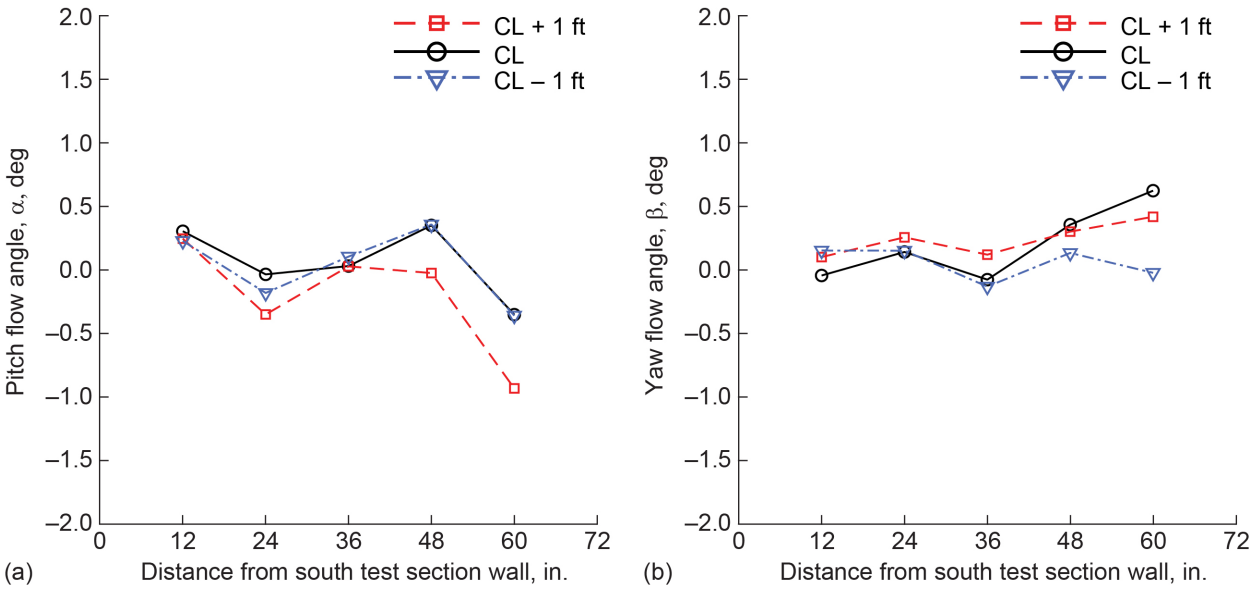

Figure C.21.—Pitch and yaw flow angle profiles in 8- by 6-ft test section at 14-ft test section measurement plane at centerline (CL) and 1 ft above and below CL. Positive pitch flow angle, α, is from floor to ceiling and positive yaw flow angle, β, is from left to right when upstream looking aft. Data acquired during 2019 test section characterization entry at Mach 0.449 (three-drive-motor operation). (a) Pitch. (b) Yaw.

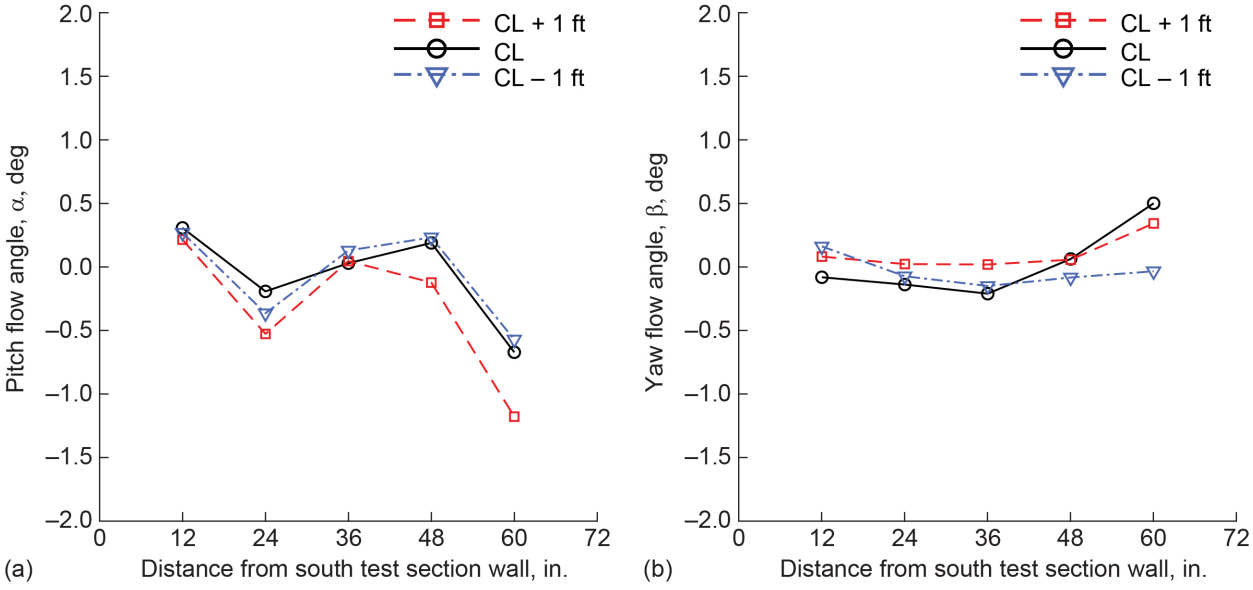

Figure C.22.—Pitch and yaw flow angle profiles in 8- by 6-ft test section at 14-ft test section measurement plane at centerline (CL) and 1 ft above and below CL. Positive pitch flow angle, α, is from floor to ceiling and positive yaw flow angle, β, is from left to right when upstream looking aft. Data acquired during 2019 test section characterization entry at Mach 0.401 (three-drive-motor operation). (a) Pitch. (b) Yaw.

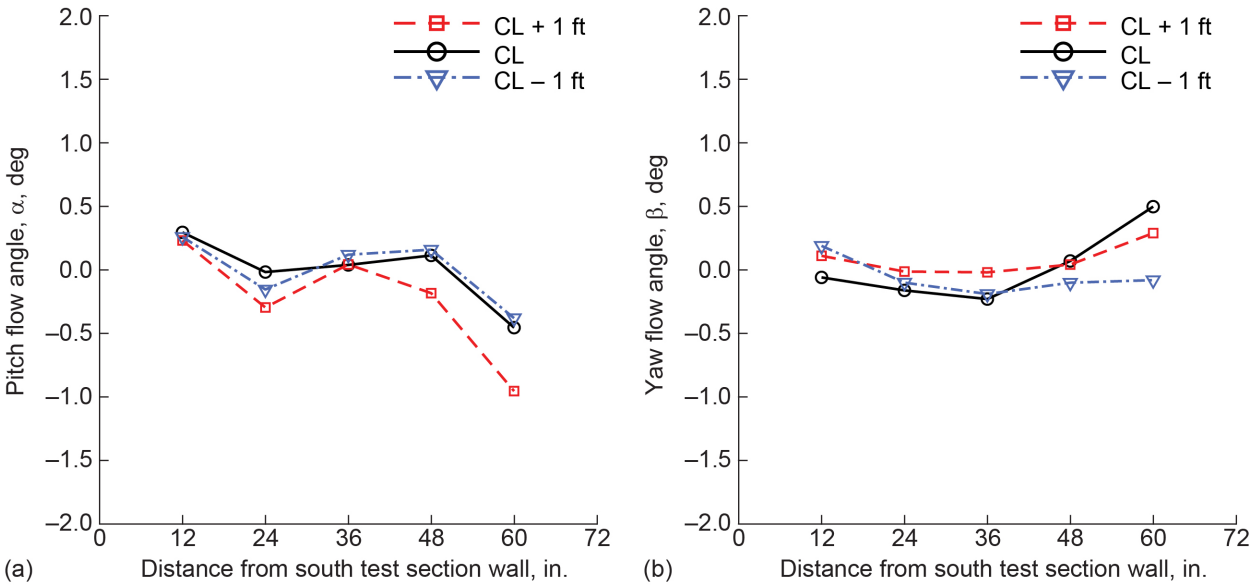

Figure C.23.—Pitch and yaw flow angle profiles in 8- by 6-ft test section at 14-ft test section measurement plane at centerline (CL) and 1 ft above and below CL. Positive pitch flow angle, α, is from floor to ceiling and positive yaw flow angle, β, is from left to right when upstream looking aft. Data acquired during 2019 test section characterization entry at Mach 0.369 (three-drive-motor operation). (a) Pitch. (b) Yaw.

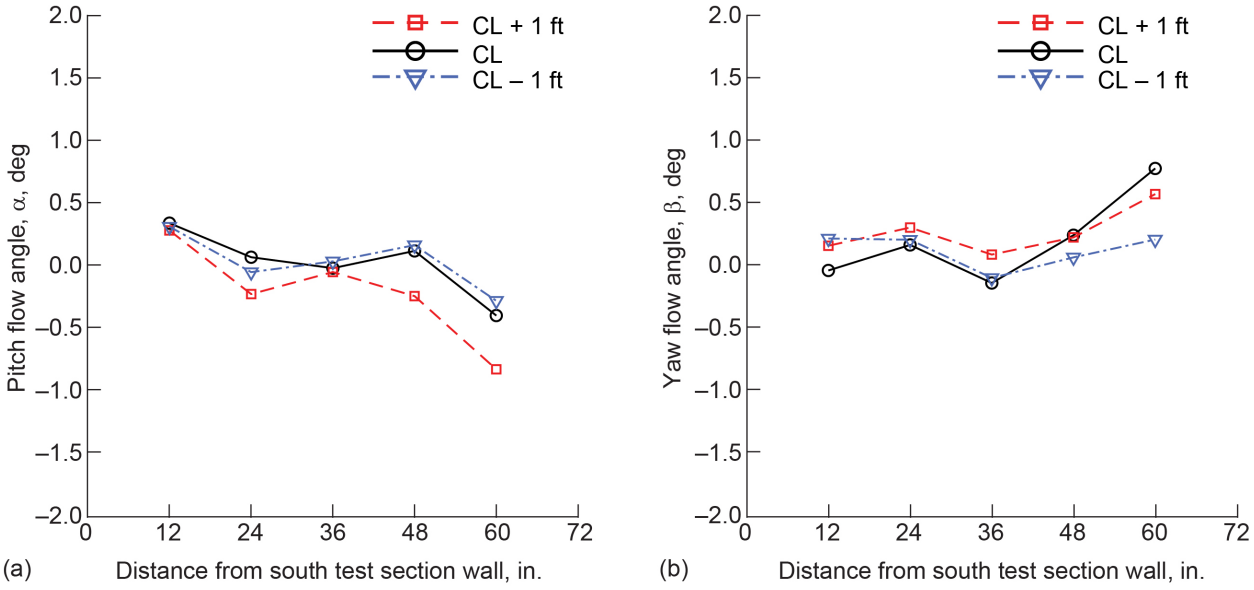

Figure C.24.—Pitch and yaw flow angle profiles in 8- by 6-ft test section at 14-ft test section measurement plane at centerline (CL) and 1 ft above and below CL. Positive pitch flow angle, α, is from floor to ceiling and positive yaw flow angle, β, is from left to right when upstream looking aft. Data acquired during 2019 test section characterization entry at Mach 0.500 (one-drive-motor operation). (a) Pitch. (b) Yaw.

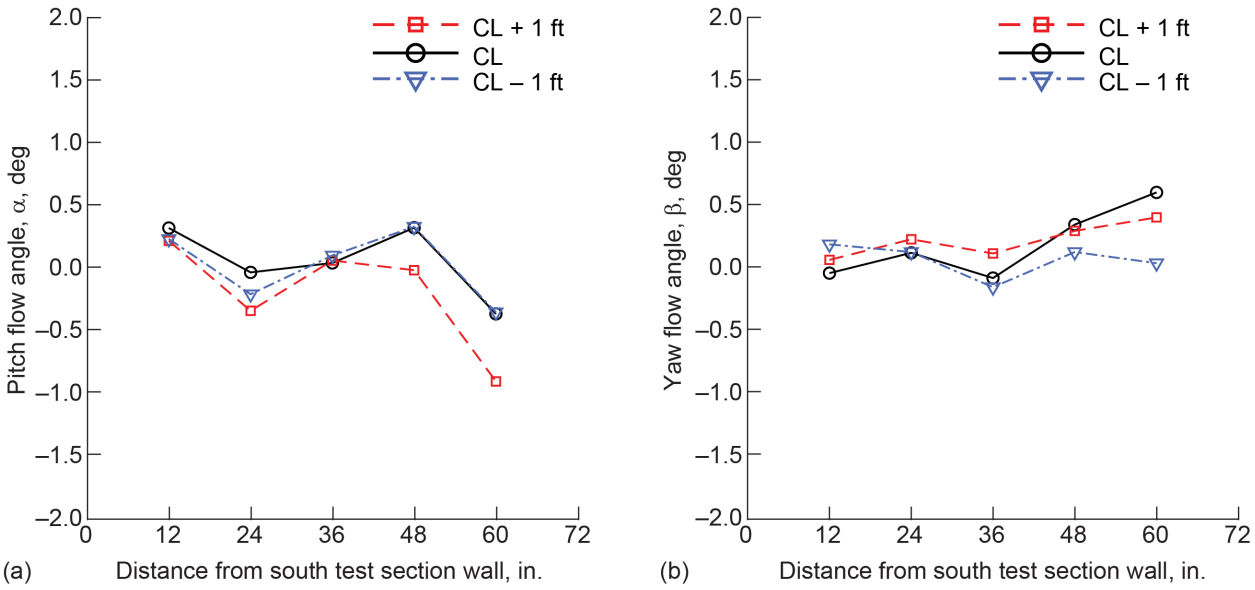

Figure C.25.—Pitch and yaw flow angle profiles in 8- by 6-ft test section at 14-ft test section measurement plane at centerline (CL) and 1 ft above and below CL. Positive pitch flow angle, α, is from floor to ceiling and positive yaw flow angle, β, is from left to right when upstream looking aft. Data acquired during 2019 test section characterization entry at Mach 0.449 (one-drive-motor operation). (a) Pitch. (b) Yaw.

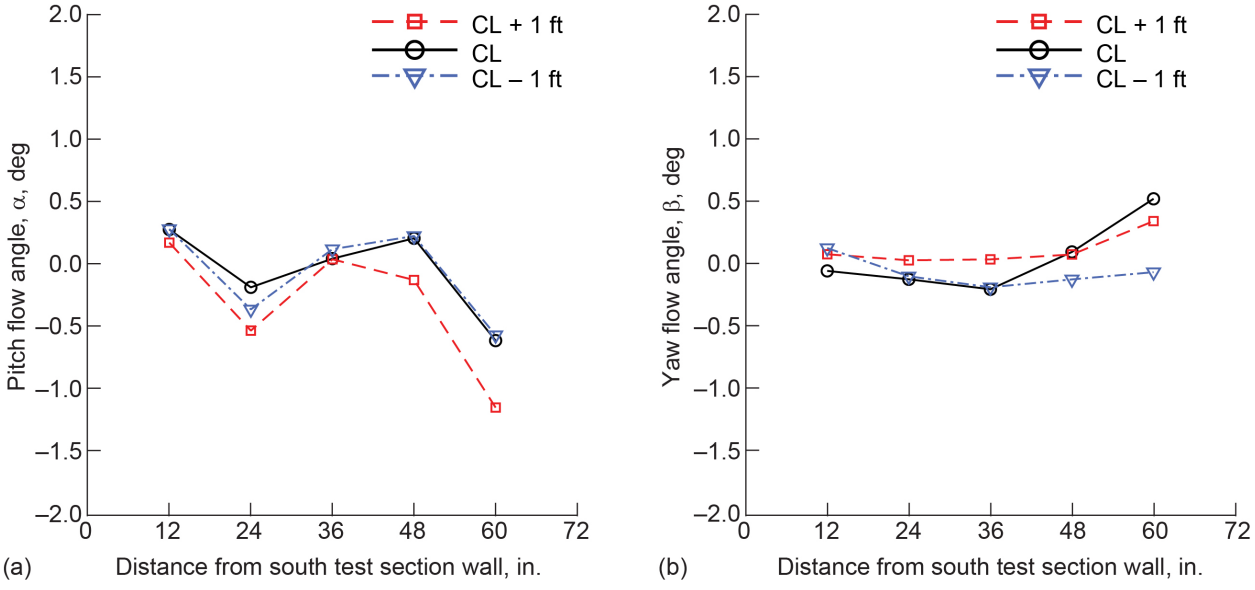

Figure C.26.—Pitch and yaw flow angle profiles in 8- by 6-ft test section at 14-ft test section measurement plane at centerline (CL) and 1 ft above and below CL. Positive pitch flow angle, α, is from floor to ceiling and positive yaw flow angle, β, is from left to right when upstream looking aft. Data acquired during 2019 test section characterization entry at Mach 0.401 (one-drive-motor operation). (a) Pitch. (b) Yaw.

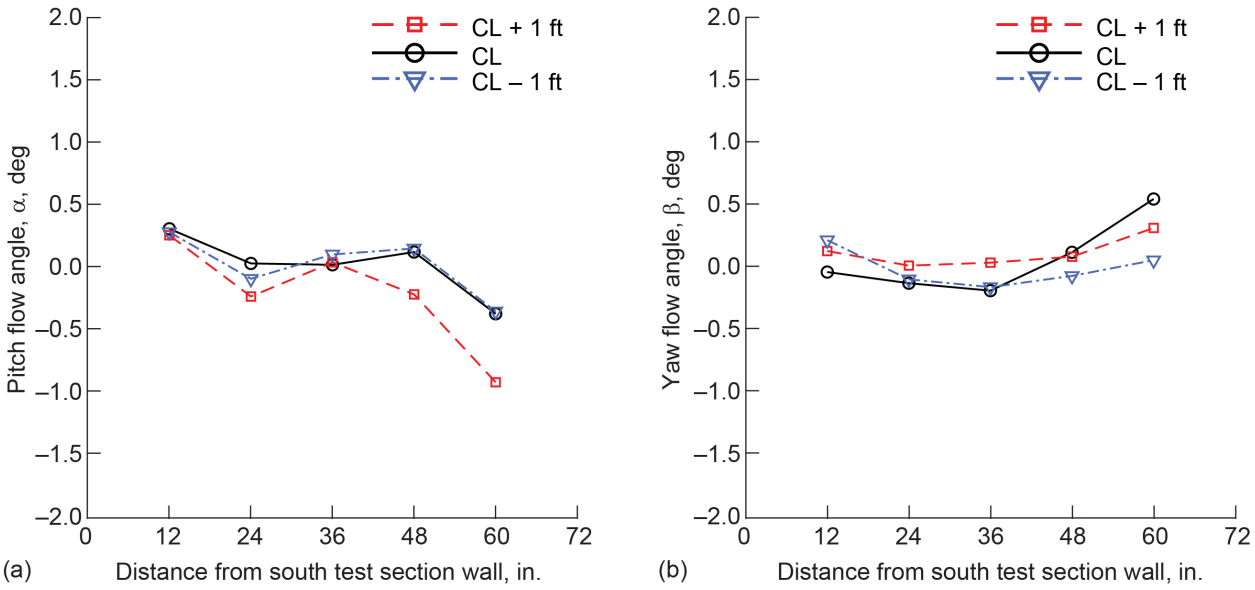

Figure C.27.—Pitch and yaw flow angle profiles in 8- by 6-ft test section at 14-ft test section measurement plane at centerline (CL) and 1 ft above and below CL. Positive pitch flow angle, α, is from floor to ceiling and positive yaw flow angle, β, is from left to right when upstream looking aft. Data acquired during 2019 test section characterization entry at Mach 0.352 (one-drive-motor operation). (a) Pitch. (b) Yaw.

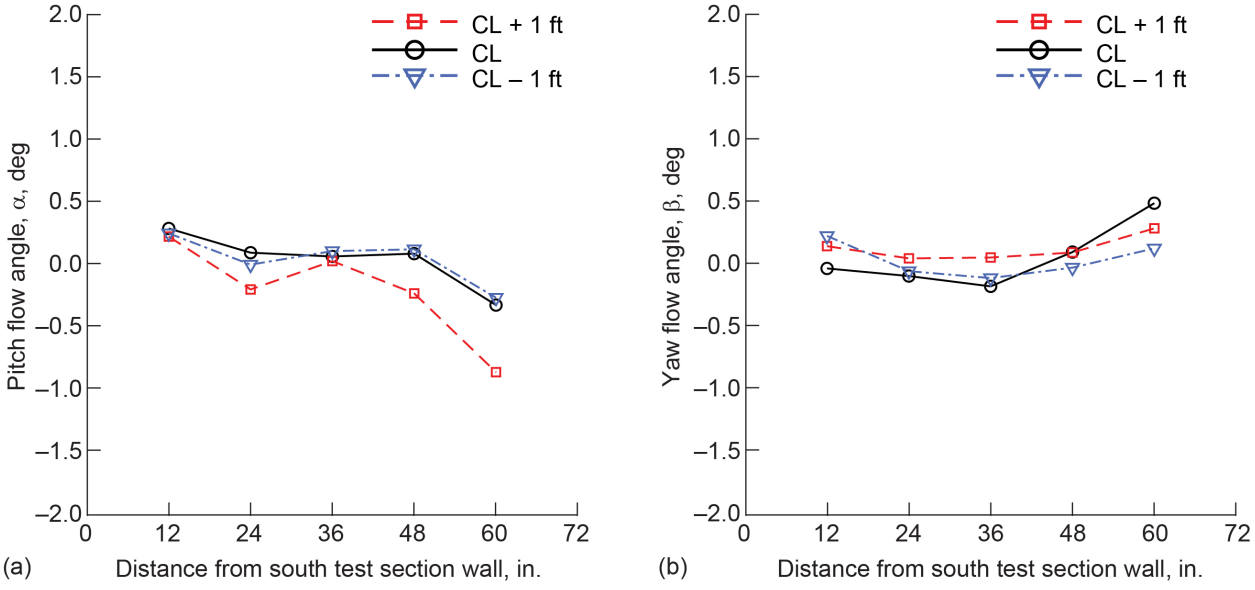

Figure C.28.—Pitch and yaw flow angle profiles in 8- by 6-ft test section at 14-ft test section measurement plane at centerline (CL) and 1 ft above and below CL. Positive pitch flow angle, α, is from floor to ceiling and positive yaw flow angle, β, is from left to right when upstream looking aft. Data acquired during 2019 test section characterization entry at Mach 0.299 (one-drive-motor operation). (a) Pitch. (b) Yaw.

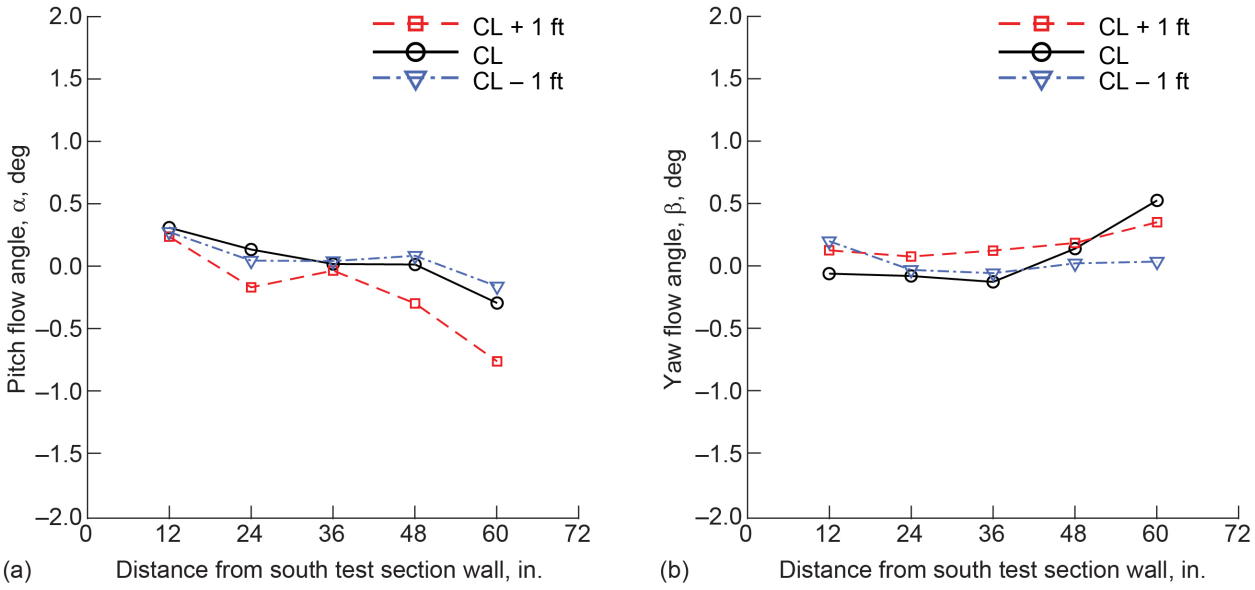

Figure C.29.—Pitch and yaw flow angle profiles in 8- by 6-ft test section at 14-ft test section measurement plane at centerline (CL) and 1 ft above and below CL. Positive pitch flow angle, α, is from floor to ceiling and positive yaw flow angle, β, is from left to right when upstream looking aft. Data acquired during 2019 test section characterization entry at Mach 0.251 (one-drive-motor operation). (a) Pitch. (b) Yaw.

References

1. Johnson, Aaron M.: Flow Quality Survey of the 8- by 6-Foot Supersonic Wind Tunnel (2015 Test) Prior to the 9- by 15-Foot Acoustic Low-Speed Wind Tunnel Acoustic Improvement Modifications. NASA/CR—2018-219880, 2018. http://ntrs.nasa.gov
2. Stephens, Julia, et al.: Uncertainty Analysis of the NASA Glenn 8×6 Supersonic Wind Tunnel. NASA/CR—2016-219411, 2016. http://ntrs.nasa.gov
3. Arrington, E. Allen: Calibration of the NASA Glenn 8- by 6-Foot Supersonic Wind Tunnel (1996 and 1997 Tests). NASA/CR—2012-217270, 2012. http://ntrs.nasa.gov
4. Soeder, Ronald H.: NASA Lewis 8- by 6-Foot Supersonic Wind Tunnel User Manual. NASA TM–105771, 1993. http://ntrs.nasa.gov
5. Arrington, E. Allen; Pickett, Mark T.; and Soeder, Ronald H.: Baseline Calibration of the NASA Lewis Research Center 8- by 6-Foot Supersonic Wind Tunnel (1991 and 1992 Tests). NASA/TM—97-107431, 1998. Available from the NASA STI Program.
6. Ames Aeronautical Laboratory Research Staff: Equations, Tables, and Charts for Compressible Flow. NACA Report 1135, 1953. http://ntrs.nasa.gov
7. Johnson, Aaron M.; and Rinehart, David A: Characterization of the NASA Glenn 8- by 6-Foot Supersonic Wind Tunnel Supersonic Test Section (2020 Test). NASA/CR-20205001889, 2020. http://ntrs.nasa.gov
8. Callahan, Ryan J., et al.: Long-Term Study of Wind-Tunnel Balance Calibration History Using Statistical Process Control. AIAA 2015–3380, 2015.